



NEW PHOTOCHEMICAL METHODS FOR CATALYTIC RADICAL PROCESSES

Wei Zhou

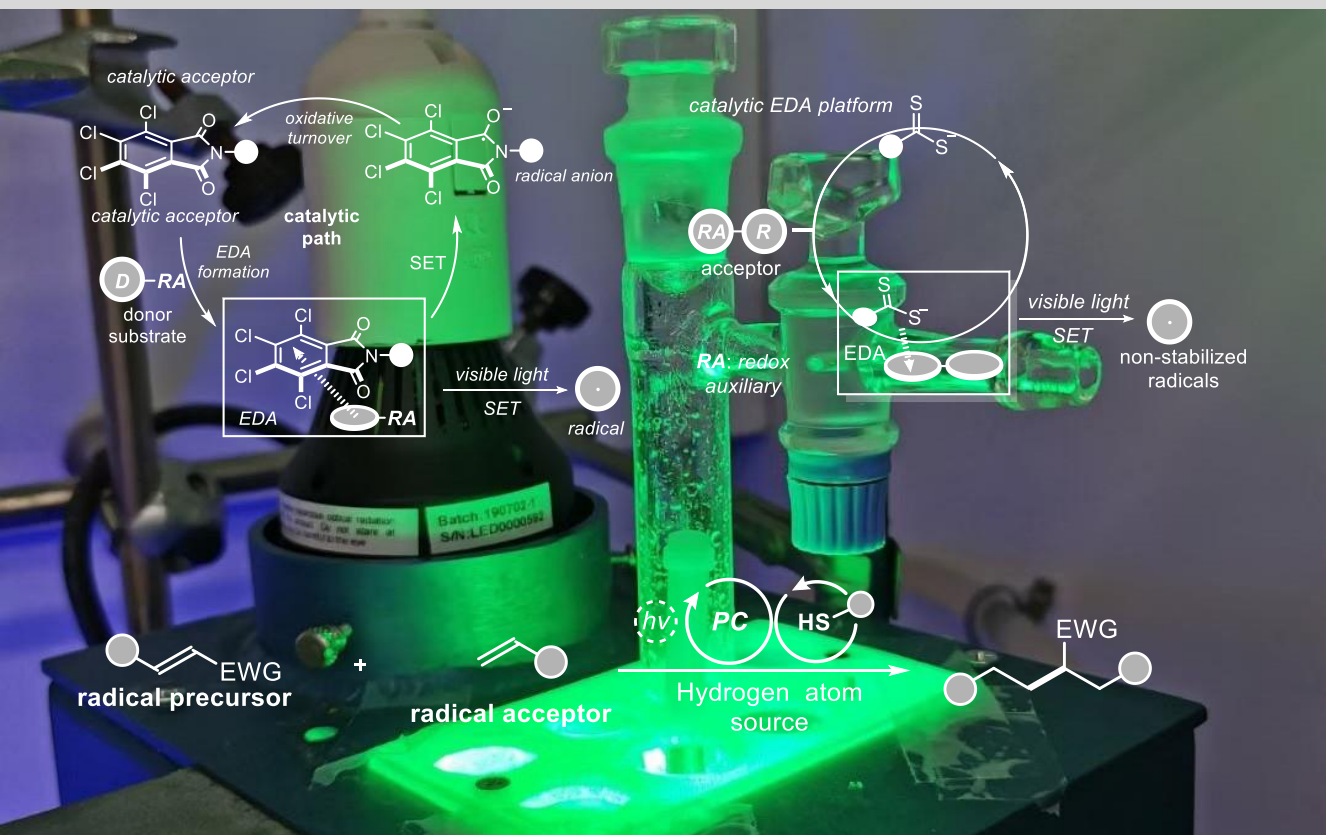
ADVERTIMENT. L'accés als continguts d'aquesta tesi doctoral i la seva utilització ha de respectar els drets de la persona autora. Pot ser utilitzada per a consulta o estudi personal, així com en activitats o materials d'investigació i docència en els termes establerts a l'art. 32 del Text Refós de la Llei de Propietat Intel·lectual (RDL 1/1996). Per altres utilitzacions es requereix l'autorització prèvia i expressa de la persona autora. En qualsevol cas, en la utilització dels seus continguts caldrà indicar de forma clara el nom i cognoms de la persona autora i el títol de la tesi doctoral. No s'autoritza la seva reproducció o altres formes d'explotació efectuades amb finalitats de lucre ni la seva comunicació pública des d'un lloc aliè al servei TDX. Tampoc s'autoritza la presentació del seu contingut en una finestra o marc aliè a TDX (framing). Aquesta reserva de drets afecta tant als continguts de la tesi com als seus resums i índexs.

ADVERTENCIA. El acceso a los contenidos de esta tesis doctoral y su utilización debe respetar los derechos de la persona autora. Puede ser utilizada para consulta o estudio personal, así como en actividades o materiales de investigación y docencia en los términos establecidos en el art. 32 del Texto Refundido de la Ley de Propiedad Intelectual (RDL 1/1996). Para otros usos se requiere la autorización previa y expresa de la persona autora. En cualquier caso, en la utilización de sus contenidos se deberá indicar de forma clara el nombre y apellidos de la persona autora y el título de la tesis doctoral. No se autoriza su reproducción u otras formas de explotación efectuadas con fines lucrativos ni su comunicación pública desde un sitio ajeno al servicio TDR. Tampoco se autoriza la presentación de su contenido en una ventana o marco ajeno a TDR (framing). Esta reserva de derechos afecta tanto al contenido de la tesis como a sus resúmenes e índices.

WARNING. Access to the contents of this doctoral thesis and its use must respect the rights of the author. It can be used for reference or private study, as well as research and learning activities or materials in the terms established by the 32nd article of the Spanish Consolidated Copyright Act (RDL 1/1996). Express and previous authorization of the author is required for any other uses. In any case, when using its content, full name of the author and title of the thesis must be clearly indicated. Reproduction or other forms of for profit use or public communication from outside TDX service is not allowed. Presentation of its content in a window or frame external to TDX (framing) is not authorized either. These rights affect both the content of the thesis and its abstracts and indexes.

New photochemical methods for catalytic radical processes

Wei Zhou (周伟)



UNIVERSITAT ROVIRA I VIRGILI

NEW PHOTOCHEMICAL METHODS FOR CATALYTIC RADICAL PROCESSES

Wei Zhou

UNIVERSITAT ROVIRA I VIRGILI

NEW PHOTOCHEMICAL METHODS FOR CATALYTIC RADICAL PROCESSES

Wei Zhou

Wei Zhou

New photochemical methods for catalytic radical processes

Doctoral Thesis

Supervised by Prof. Paolo Melchiorre

ICIQ – Institut Català d'Investigació Química



UNIVERSITAT
ROVIRA i VIRGILI



Institut
Català
d'Investigació
Química

Tarragona

2023



UNIVERSITAT
ROVIRA i VIRGILI



Prof. Paolo Melchiorre,

Professor at the University of Bologna, Italy, previously Group Leader at ICIQ

STATE

that the present study, entitled “New photochemical methods for catalytic radical processes”,

presented by WEI ZHOU for the award of the degree of Doctor, has been carried out under my supervision at the Institut Català d'Investigació Química (ICIQ).

Tarragona, August 11th, 2023

Doctoral Thesis Supervisor

Prof. Paolo Melchiorre

Acknowledgements

未觉池塘春草梦，阶前梧叶已秋声。

Firstly, I would like to express my deepest gratitude to my supervisor Prof. Paolo Melchiorre for giving me the opportunity to work in his research group for my doctoral studies and for his constant support and guidance during the past four years.

I would also like to thank Prof. Arjan W. Kleij, Prof. Fabio Juliá, and Prof. Giacomo Crisenza for their willingness to be part of my doctoral thesis committee, which I appreciate a lot.

I am grateful for having met so many nice people and amazing scientist in the Melchiorre group during this long journey. Specifically, I want to thank *Eduardo* for introducing me to the EDA chemistry world and the guidance when I just entered the photochemistry field and joined this group, *Davide* for being passionate chemist and funny guy, *Will and Emilien* for “enjoying” the desaturation project together with me, *Shuo* for his help in catalytic acceptor project and our fluent Chinese communication (compared to English) in the Lab, *Igor* for his participation of the olefin coupling project, *Martin* for the correction of my thesis. Thank you also to *Adriana, Laura, Florian*, and other group members (including *Diyuan, Dengke, Xinjun, Vasileios, Eleni, Matteo*) for the moments we had in the lab and outside, for the beers we had together, for every tiny favor you did. Last but not least, I want to thank *Thomas* for the scientific discussion, postdoctoral position talk, proofreading this thesis.

I also want to express my gratitude to *Núria* for the administrative support, and to *Laia* and *Miguel* for their assistance in the lab, and to all the research support units at ICIQ (NMR, mass, chromatography, spectroscopy, and photophysics units).

特别鸣谢奖颁发给张嘉瑜同学，我以前的女盆友，现在的妻子，未来的孩儿他妈，四年来的陪伴和鼓励，使我一直有一个十分轻松愉快的心境，让我在离家万里之外的陌生国度拥有了一个小家，我爱你，宝儿！当然，也要感谢我的老爸老妈，求学二十多年来一直有你们的鼓励和支持，即使家里遭遇巨大变故，你们始终坚定地站在了我的身后，你们辛苦啦！

Finally, I am grateful for the financial support provided by Agencia Estatal de Investigación (PID2019-106278GB-I00), the MCIN/AEI/10.13039/501100011033 (CEX2019-000925-S), and the China Scholarship Council for predoctoral fellowships (Grants CSC201908310093).



European Research Council
Established by the European Commission



List of Publications

Some of the results presented in this thesis have been published:

- De Pedro Beato, E.; Spinnato, D.; **Zhou, W.**; Melchiorre, P. A General Organocatalytic System for Electron Donor–Acceptor Complex Photoactivation and Its Use in Radical Processes. *J. Am. Chem. Soc.* **2021**, 143, 12304–12314.
- **Zhou, W.**; Wu, S.; Melchiorre, P., Tetrachlorophthalimides as Organocatalytic Acceptors for Electron Donor–Acceptor Complex Photoactivation. *J. Am. Chem. Soc.* **2022**, 144, 8914–8919.

UNIVERSITAT ROVIRA I VIRGILI

NEW PHOTOCHEMICAL METHODS FOR CATALYTIC RADICAL PROCESSES

Wei Zhou

Contents

Chapter I: General Overview	1
1.1 Photochemistry.....	1
1.2 Direct excitation of organocatalytic intermediates	5
1.3 Hydrogen atom transfer (HAT).....	7
1.4 General Objectives of the Thesis	10
1.4.1 A catalytic EDA platform with dithiocarbamate-based organocatalysts as donors	11
1.4.2 A catalytic platform with tetrachlorophthalimides as acceptors	12
1.4.3 Reductive cross-coupling of olefins by a radical pathway	12
Chapter II: Catalytic donor	14
2.1 Introduction	14
2.2 Electron donor-acceptor (EDA) complexes.....	18
2.3 Photoreactivity of stoichiometric EDA complexes	23
2.4 Catalytic EDA complexes.....	27
2.5 Target of the Project.....	32
2.5.1 Design plan.....	32
2.6 Results and Discussion.....	34
2.6.1 Developing a Giese-type addition process.....	36
2.6.2 Redox-neutral processes.....	44
2.6.3 Minisci reaction.....	47
2.6.4 Further application of the EDA catalytic system.....	51
2.7 Conclusions	52
2.8 Experimental section.....	52
2.8.1 General information.....	52
2.8.2 Substrate synthesis.....	54
2.8.3 Experimental setups.....	55
2.8.4 Giese addition.....	59
2.8.5 Reduction	70
2.8.6 α -Alkylation of silyl enol ethers.....	75

2.8.7 Minisci reaction.....	87
2.8.8 Trifluoromethylation	96
2.8.9 Amidyl radical.....	97
2.8.10 Large scale reactions	98
2.8.11 Unsuccessful substrates.....	100
2.9 Mechanistic studies.....	100
2.9.1 Control experiments	100
2.9.2 Catalysts' stability experiments	105
2.9.3 UV-Vis spectroscopy.....	107
2.9.4 Transient absorption spectroscopy (TAS).....	108
2.9.5 Cyclic voltammetry measurements.....	109
2.9.6 Quantum yield determination.....	113
Chapter III:Catalytic acceptor	124
3.1 Introduction	124
3.2 Catalytic acceptors in EDA complex photoactivation.....	127
3.3 Target and design of the project.....	130
3.4 Results and discussion.....	131
3.4.1 Developing a Giese addition process.....	131
3.4.2 Developing a Heck-type reaction process.....	135
3.5 Conclusions	139
3.6 Experimental section	140
3.6.1 Synthesis of Substrate and Catalysts.....	141
3.6.2 Experimental Setup	143
3.6.3 Giese Addition.....	145
3.6.4. Heck-type reaction	154
3.6.4 Unsuccessful Substrates.....	166
3.6.5 Mechanistic Studies	166
Chapter IV:Olefin cross-coupling	178
4.1 Introduction	178
4.2 Electron-poor olefins as radical precursors.....	183
4.2.1 β -Radicals from electron-poor olefins.....	185

4.2.2 α -Radicals from electron-poor olefins	187
4.3 Target and design of the project.....	189
4.4 Results and discussion.....	191
4.4.1 Generality of the protocol	192
4.4.2 Mechanistic investigations	195
4.5 Conclusions	197
4.6 Experimental section	198
4.6.1 Experimental Setup	199
4.6.2 General procedures.....	199
4.6.3 Characterization of Products	200
4.6.4 Mechanistic experiments	214
4.6.5. NMR spectra	221
Chapter V: General conclusions	251

Chapter I

General Overview

The research work conducted during my PhD thesis focused on the development of new photochemical methods for the generation of radicals and their use in subsequent transformations. Three distinct photochemical pathways were used to catalytically generate radicals: the photoactivity of catalytic electron-donor acceptor (EDA) complexes; photoredox catalysis; and hydrogen atom transfer (HAT) mechanisms. In this chapter, I will introduce some concepts underlying the field of photochemistry and the different mechanisms available for the photoactivation of organic molecules, mainly focusing on the generation of radicals. Seminal examples will be discussed to highlight how photochemical activation can promote challenging radical-based transformations that are not feasible under thermal conditions. This introduction will provide the context and the background that have motivated my doctoral research.

1.1 Photochemistry

Photochemistry is the branch of chemistry studying the chemical interactions between light and matter,¹ which starts with the absorption of a photon by a molecule. This is corroborated by the Grotthuss–Draper law, a principle of photochemical activation stating that “*only the light absorbed is effective in producing a photochemical change*”.² Behind this statement lies the quantum mechanical description of matter, which was developed by Planck, Stark, Einstein and others³ and elucidated the interaction between light and matter. They proposed that the building unit of light is a ‘quantized’ particle, called “light quantum” or “photon” and that molecules possess quantized energy levels ranging from their low energy ‘ground state’ to a number of higher order excited states. The

¹ Balzani, V.; Ceroni, P.; Juris, A. "Photochemistry and Photophysics: Concepts, Research, Applications" **2014**, *John Wiley & Sons*.

² Rennie, R.; Law J. "A Dictionary of Chemistry" **2016**, *Oxford University Press*.

³ (a) Haar, D. "The old quantum theory" **1967**, *Oxford, New York, Pergamon Press*; (b) Einstein, A. "Über einen die Erzeugung und Verwandlung des Lichtes betreffenden heuristischen Gesichtspunkt" **1905**, *Annalen der Physik*; (c) Lewis, G. N., The Conservation of Photons. *Nature* **1926**, *118*, 874-875.

interaction between photon and matter can only occur if the photon is of *exactly* the same energy as the energy gap between two energy states (ground state and excited state). These states of molecules are described by the wave functions Ψ_f and Ψ_i and the energy of these states are represented by E_f and E_i (excited and ground state, respectively, Figure 1.1b). When a suitable photon is absorbed by a given molecule, an electronically excited state is populated by an electron transition from the highest occupied molecular orbital (HOMO) to the lowest unoccupied molecular orbital (LUMO, Figure 1.1.a).

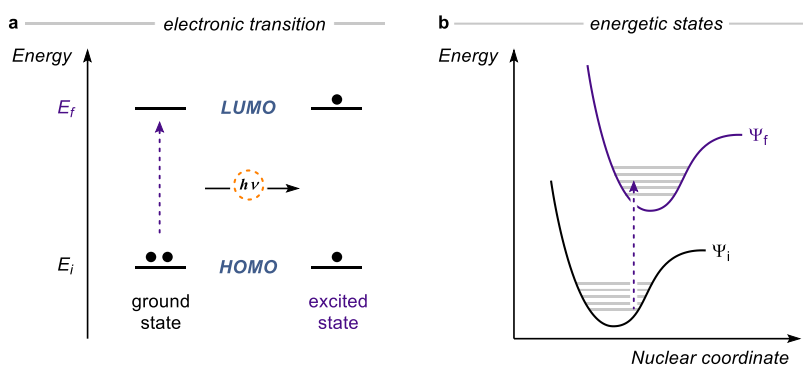


Figure 1.1. a) The energy of the absorbed photon promotes the transition of one electron from the highest occupied orbital (HOMO) to an unoccupied orbital (LUMO) b) Electronic transition from the ground-state Ψ_i to excited-state Ψ_f .

This electronic transition results in the changes of molecule's physical and chemical properties, thus an excited molecule can be considered as a different compound from the ground state.⁴ This difference could be exploited by organic chemists, who endeavor to change the reactivity of molecules by photochemistry, thus achieving transformations not available through thermal activation.⁵

Organic photochemistry was recognized as an independent field in the beginning of the last century,⁶ when Giacomo Ciamician and Paul Silber saw the potential of exploiting sunlight as an inexpensive, abundant, non-toxic and mild alternative to

⁴ Turro N. J., Ramamurthy V., Scaiano J. C. *Modern Molecular Photochemistry of Organic Molecules*. 2010, University Science Books.

⁵ Ravelli, D., Protti, S., Fagnoni, M. Carbon-Carbon Bond Forming Reaction via Photogenerated Intermediates. *Chem. Rev.* 2016, 116, 9850-9913.

⁶ Ciamician, G., Silber, P. Chemische Lichtwirkungen. *Berichte der deutschen chemischen Gesellschaft* 1900, 33, 2911-2913.

achieve the transformations of organic molecules.⁷ However, because most of organic molecules possess a huge HOMO-LUMO energy gap, their photochemical activation requires high-energy UV-light. But such powerful irradiation does not tolerate a wide range of functionality, often leading to inefficient and unselective reactivity, which limits a broad application of photochemistry. An alternative strategy exploits colored *photocatalysts* (**PC**) to promote reactions under *visible-light* irradiation.⁸ These compounds are often transition-metal complexes or organic dyes, which can efficiently absorb photons in the visible light region. The use of these catalysts led to a renaissance of photochemistry initiated by the seminal works from MacMillan,⁹ Yoon,¹⁰ and Stephenson¹¹ in 2008 and 2009. These three reports disclosed the use of tris(bipyridine)ruthenium(II) complex (Ru(bpy)₃²⁺)¹² as a photocatalyst to trigger single-electron transfer (SET) processes upon visible-light activation. A pioneering example was provided by the group of MacMillan. They used the Ru(II) complex as photocatalyst to achieve the stereoselective α -alkylation of aldehydes with alkyl bromides, a sought-after transformation which remained elusive using classic ionic chemistry (Scheme 1.1).⁹

⁷ Ciamician, G. The photochemistry of the future. *Science* **1912**, *36*, 385-394.

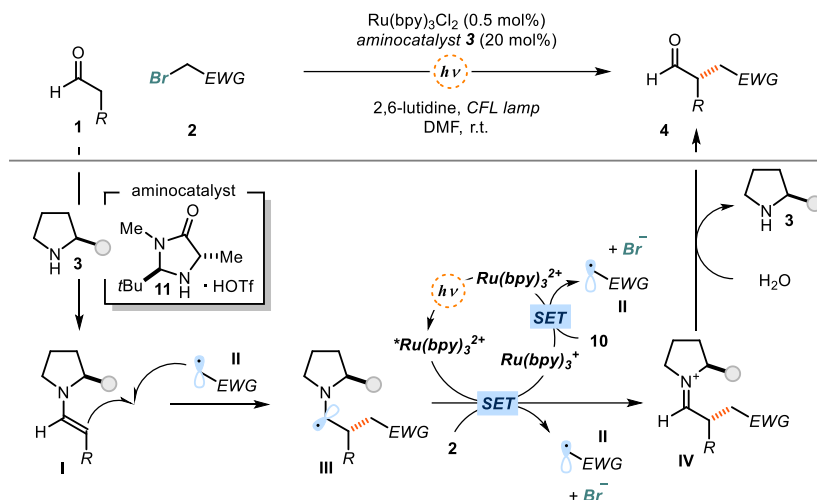
⁸ Yoon, T. P.; Ischay, M. A.; Du, J. "Visible Light Photocatalysis as a Greener Approach to Photochemical Synthesis" *Nat. Chem.* **2010**, *2*, 527-532.

⁹ Nicewicz, D. A.; MacMillan, D. W. C. "Merging Photoredox Catalysis with Organocatalysis: The Direct Asymmetric Alkylation of Aldehydes" *Science* **2008**, *322*, 77-80.

¹⁰ Ischay, M. A.; Anzovino, M. E.; Du, J.; Yoon, T. P. "Efficient Visible Light Photocatalysis of [2+2] Enone Cycloadditions" *J. Am. Chem. Soc.* **2008**, *130*, 12886-12887.

¹¹ Narayanam, J. M. R.; Tucker, J. W.; Stephenson, C. R. J. "Electron-Transfer Photoredox Catalysis: Development of a Tin-Free Reductive Dehalogenation Reaction" *J. Am. Chem. Soc.* **2009**, *131*, 8756-8757.

¹² Paris, J. P.; Brandt, W. W. "Charge Transfer Luminescence of a Ruthenium(II) Chelate" *J. Am. Chem. Soc.* **1959**, *81*, 5001-5002.



Scheme 1.1. Tandem organo-photoredox catalysis for the α -alkylation of aldehydes with electron-poor alkyl bromides.

The mechanism, depicted in Scheme 1.1, proposes the formation of enamine **I**, generated in situ by condensation of aldehyde **1** with the chiral aminocatalyst **3**. Excitation of $[\text{Ru}(\text{bpy})_3]^{2+}$ generated the excited-state complex, which could oxidize a sacrificial amount of enamine **I** via SET, delivering the reduced $[\text{Ru}(\text{bpy})_3]^+$. Then ensuing $\text{Ru}(\text{I})$ complex reduced the alkyl bromide **2** via another SET event, furnishing the target radical **II** upon fragmentation of the bromide anion while regenerating the $[\text{Ru}(\text{bpy})_3]^{2+}$ complex. The electrophilic radical **II** was captured by the electron-rich chiral enamine **I**, forming the new C-C bond and a new stereocenter. The generated α -amino radical **III** could be oxidized by the excited $\text{Ru}(\text{II})$ complex or another equivalent of alkyl bromide **2**¹³ to afford the iminium **IV**, which was then hydrolysed to deliver the enantioenriched product **4** and turnover the organocatalyst **3**.

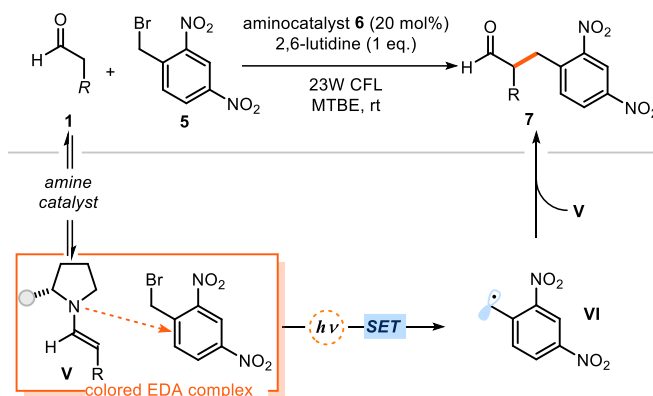
This example highlighted the great potential of *photoredox catalysis* to generate radicals under mild conditions while enabling otherwise difficult synthetic transformations. Since these pioneering work, photoredox catalysis, and by extension light-driven processes, experienced an explosive growth in both academic and industrial settings.¹⁴

¹³ Cismesia, M. A.; Yoon, T. P. Characterizing Chain Processes in Visible Light Photoredox Catalysis. *Chem. Sci.* **2015**, *6*, 5426-5434.

¹⁴ Crisenza, G. E. M.; Melchiorre, P., Chemistry glows green with photoredox catalysis. *Nat. Commun.* **2020**, *11*, 803.

1.2 Direct excitation of organocatalytic intermediates

The use of an external photocatalyst is not the only way to exploit the potential of photocatalysis to generate radical under mild conditions. Our group found that some organocatalytic intermediates are capable of absorbing visible light to access their electronically excited state and triggering the formation of radicals. This ability stems from specific non-covalent aggregations between colorless electron-rich and electron-poor molecules, which can cause a change in the color of the solution and a bathochromic shift of these intermediates in their UV-vis spectra compared to the parent substrates. These aggregates are known as electron donor-acceptor (EDA) complexes.¹⁵ The photoexcitation of EDA complexes can be harnessed to generate radicals and promote useful transformations. For example, our group observed a color change when a colorless enamine **V** (in situ formed from aldehyde **1** and a chiral amine catalyst) was combined with a colorless electron-poor benzyl bromide **5** (Scheme 1.2). This behavior was attributed to the formation of an EDA complex.¹⁶



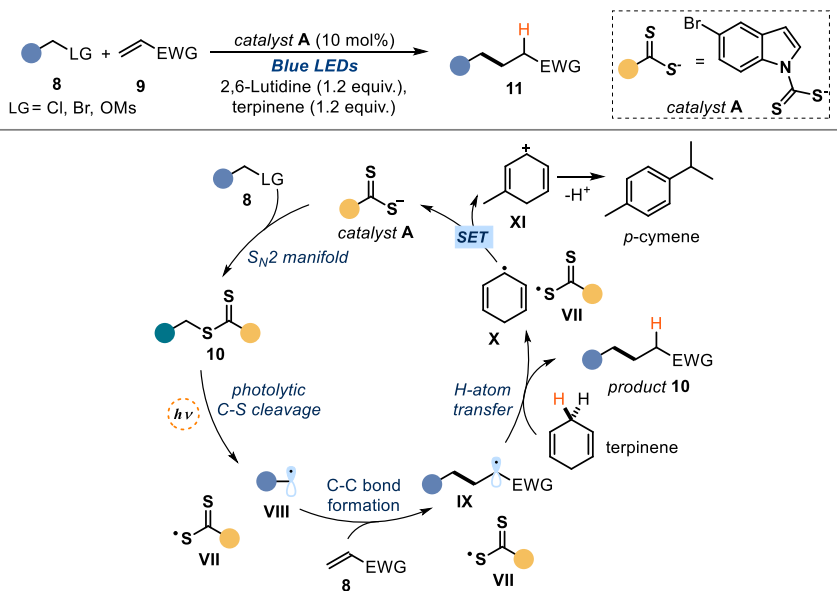
Scheme 1.2. Stereoselective alkylation of aldehydes promoted by the photoactivity of a catalytic EDA complex.

This EDA complex can get excited upon irradiation with visible light, which triggered the fragmentation of the bromide and formation of the benzyl radical **VI**.

¹⁵ Crisenza, G. E. M.; Mazzarella, D.; Melchiorre, P. "Synthetic Methods Driven by the Photoactivity of Electron Donor–Acceptor Complexes" *J. Am. Chem. Soc.* **2020**, *142*, 5461–5476.

¹⁶ Arceo, E.; Jurberg, I. D.; Álvarez-Fernández, A.; Melchiorre, P. "Photochemical Activity of a Key Donor–Acceptor Complex Can Drive Stereoselective Catalytic α -Alkylation of Aldehydes" *Nat. Chem.* **2013**, *5*, 750–756.

The ensuing radical was trapped stereoselectively by the ground-state enamine **V** to ultimately deliver α -benzyl aldehydes **7** with high enantioselectivity. The generation of radicals from organocatalytic intermediates is not restricted to EDA complex formation. Our laboratories have recently developed a photochemical organocatalytic strategy for radical generation that does not rely on the redox properties of the substrate.¹⁷ This approach was realized by implementing the stoichiometric xanthate-based chemistry, developed by Barton¹⁸ and Zard 40 years ago,¹⁹ into a catalytic regime. The strategy required a nucleophilic *dithiocarbamate* organic catalyst **A** decorated with indole-based light absorbing unit (Scheme 1.3). Catalyst **A** could readily activate a wide range of alkyl electrophiles **8** via an S_N2 path to afford the photoactive intermediate **10**. Such intermediate was excited upon irradiation, delivering carbon-centered radical **VIII** and thiyl radical **VII** upon homolytic cleavage of the labile C-S bond.



Scheme 1.3. Photochemical generation of radicals from alkyl electrophiles using a nucleophilic organic catalyst.

¹⁷ Schweitzer-Chaput, B.; Horwitz, M. A.; de Pedro Beato, E.; Melchiorre, P. "Photochemical generation of radicals from alkyl electrophiles using a nucleophilic organic catalyst" *Nat. Chem.* **2019**, *11*, 129–135.

¹⁸ Barton, D. H. R.; McCombie, S. W. "A New Method for the Deoxygenation of Secondary Alcohols" *J. Chem. Soc. Perkin Trans. 1*, **1975**, 1574–1585.

¹⁹ Zard, S. Z. "On the Trail of Xanthates: Some New Chemistry From an Old Functional Group" *Angew. Chem. Int. Ed.* **1997**, *36*, 672–685.

The resulting nucleophilic radical **VIII** was then captured by an electron-poor olefin **9** to generate another electrophilic radical **IX**, which abstracted a hydrogen atom from γ -terpinene to produce the Giese adduct **11** and the radical **X**. The latter intermediate **X** reduced the thiy radical **VII** to regenerate *catalyst A*. This catalytic S_N2-based approach differed from other radical generation strategies since it relied on the electrophilic properties (and not the redox properties or bond-dissociation energies) of the radical precursors.

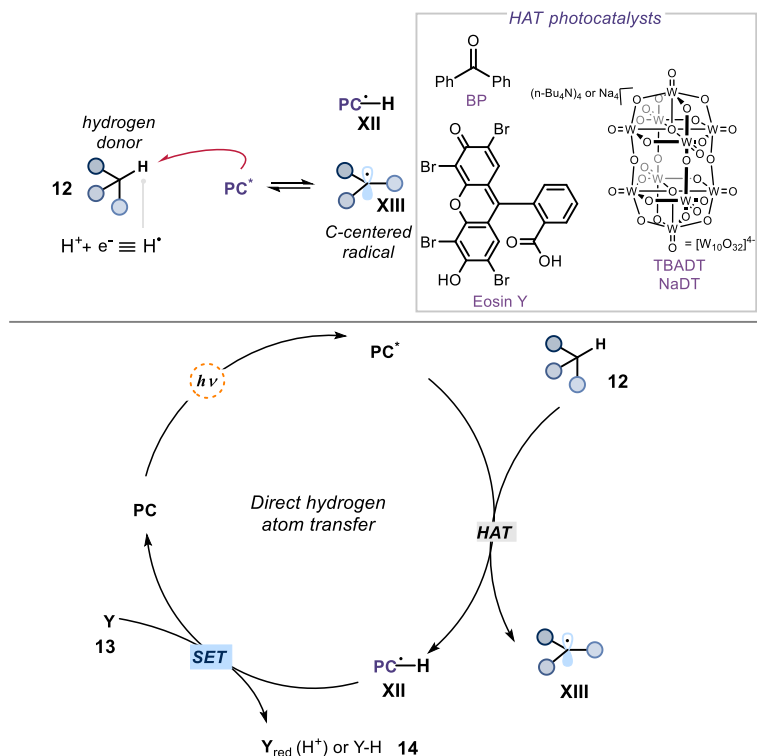
Overall, the works detailed in this section highlighted how the direct excitation of organocatalytic intermediates can be exploited to generate radicals useful for follow up transformations.

1.3 Hydrogen atom transfer (HAT)

Another powerful mechanism to produce radicals is hydrogen atom transfer (HAT). Because of the prevalence of C-H bonds in organic molecules, the most desirable approach is to yield radicals through breaking non-reactive C-H bonds. While transition metal catalysis has gained dominance in the functionalization of C(sp²)-H bonds mostly, the activation C(sp³)-H bonds is more challenging, and the development of methods for their selective manipulations is still in its infancy.²⁰ In this context, HAT has received significant attention, as it tames non-reactive C(sp³)-H bonds to form highly reactive carbon-centered radicals which can engage in a variety of reactions.²¹ In the photochemistry manifold, HAT can be classified in two main approaches: direct hydrogen atom transfer (d-HAT, Scheme 1.4) and indirect hydrogen atom transfer (i-HAT, Scheme 1.5).

²⁰ (a) Goldman, A. S.; Goldberg, K. I. Organometallic C-H Bond Activation: An Introduction. In *Activation and Functionalization of C-H Bonds*; ACS Symposium Series 2004; Vol. 885, pp1-43; (b) Hartwig, J. F.; Larsen, M. A. "Undirected, Homogeneous C-H Bond Functionalization: Challenges and Opportunities" *ACS Cent. Sci.* **2016**, *2*, 281-292.

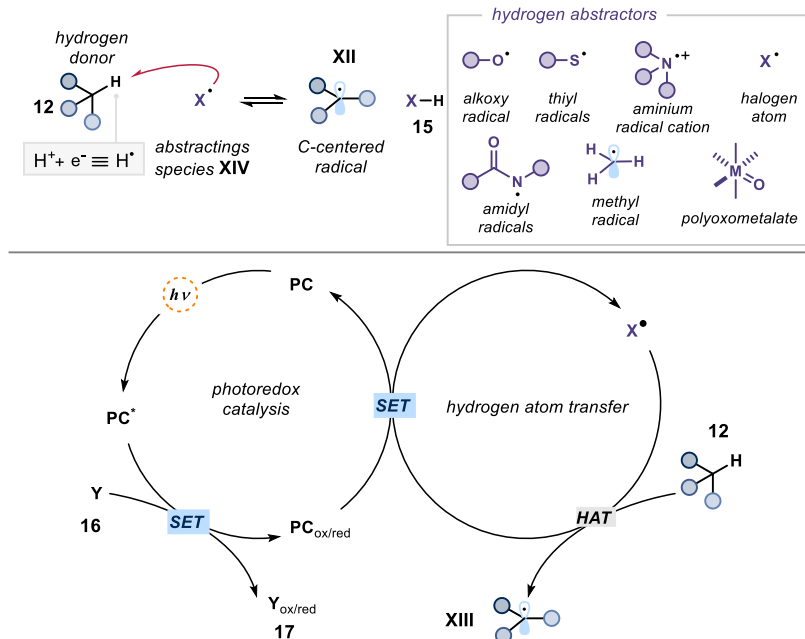
²¹ (a) Capaldo, L.; Ravelli, D. "Hydrogen Atom Transfer (HAT): A Versatile Strategy for Substrate Activation in Photocatalyzed Organic Synthesis" *Enr. J. Org. Chem.* **2017**, 2056-2071 (b) Capaldo, L.; Ravelli, D.; Fagnoni, M. "Direct Photocatalyzed Hydrogen Atom Transfer (HAT) for Aliphatic C-H Bonds Elaboration" *Chem. Rev.* **2022**, *122*, 1875-1924.



Scheme 1.4. Direct photocatalytic hydrogen atom transfer (d-HAT). BP: Benzophenone; Ph: phenyl; TBADT: tetra-*n*-butylammonium decatungstate; NaDT: Sodium decatungstate.

For d-HAT, once a photocatalyst is excited upon light irradiation, it can abstract a hydrogen atom (a $H\cdot$) from alkanes **12** to afford the carbon-center radical **XIII** and the reduced photocatalyst species. To turnover the photocatalyst, an oxidant **13** (**Y** in Scheme 1.4) is also needed. Commonly used HAT photo-activated catalysts are displayed in the grey box in Scheme 1.4, including benzophenone (BP), Eosin Y and decatungstate (DT) salts.

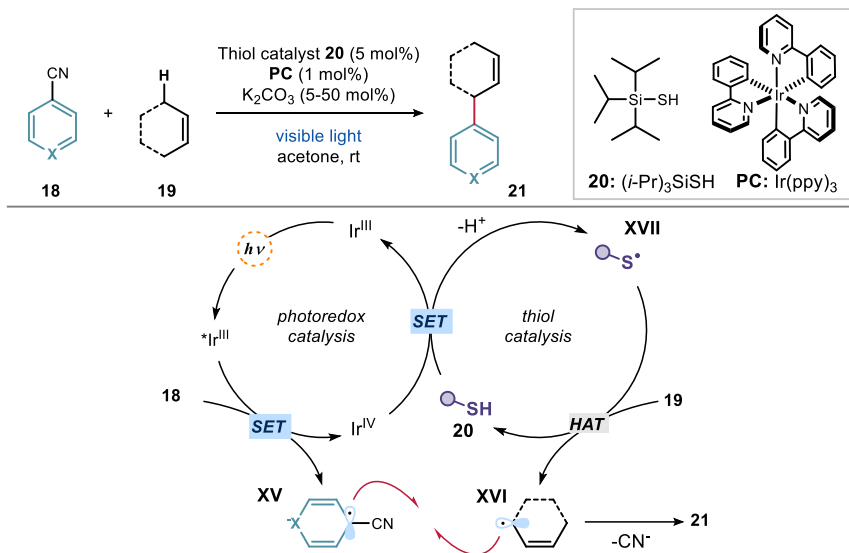
For indirect hydrogen atom transfer (i-HAT, Scheme 1.5), besides the photocatalyst, an external HAT reagent (not shown) is also needed. This reagent can be used to form radical **XIV** (a hydrogen abstractor), which is able to abstract a $H\cdot$ from alkanes **12**, delivering the carbon-center radical **XIII**. In this case, the excited photocatalyst can undergo SET with the HAT reagent to generate the hydrogen abstractor **XIV**. Commonly used hydrogen abstractors are displayed in the grey box in the Scheme 1.5. They are mainly constituted of heteroatom-centered radicals (alkoxy, thiyl, aminium, and amidyl radicals), which are electrophilic abstractors.



Scheme 1.5. Indirect photocatalytic hydrogen atom transfer (i-HAT).

One representative example of indirect HAT was reported by the group of MacMillan (Scheme 1.6).²² In the proposed mechanism, the excited photocatalyst ($\text{Ir}(\text{ppy})_3$) can reduce cyanoarenes **18** to produce the persistent cyanoaryl radical anions **XV** and Ir^{IV} complex. The latter complex can oxidize the HAT catalyst **20** thus turning over the photocatalyst while affording the thiyl radical **XVII**. The latter intermediate could abstract a H \cdot from cyclohexene **19** to regenerate the thiol catalyst **20** and deliver the allylic radical **XVI**. In the last step, radical **XVI** coupled with cyanoaryl radical anions **XV** to provide the allylic arylation product **21**.

²² Cuthbertson, J. D.; MacMillan, D. W. C. The Direct Arylation of Allylic sp^3 C-H Bonds via Organic and Photoredox Catalysis. *Nature* **2015**, *519*, 74-77.



Scheme 1.6. Dual photoredox-thiol arylation of allylic C-H bonds.

1.4 General Objectives of the Thesis

The principal objective of this doctoral thesis was to study and develop new strategies for the photochemical generation of radicals and use them to design radical processes. The two different photochemical activation manifolds discussed previously (EDA complex formation, and photoredox catalysis) were used to generate radicals. In Chapter II and III (Figure 1.2, left), commercially available or easily-prepared molecules (dithiocarbamate and tetrachlorophthalimide) were used as catalytic partners (donor and acceptor catalysts, respectively) to induce EDA complex formation with a variety of radical precursors, eventually generating carbon- and nitrogen-centered radicals upon light excitation. In Chapter IV (Figure 1.2, right), photoredox catalysis was used in concert with HAT catalysis to achieve the reductive coupling of two olefins.

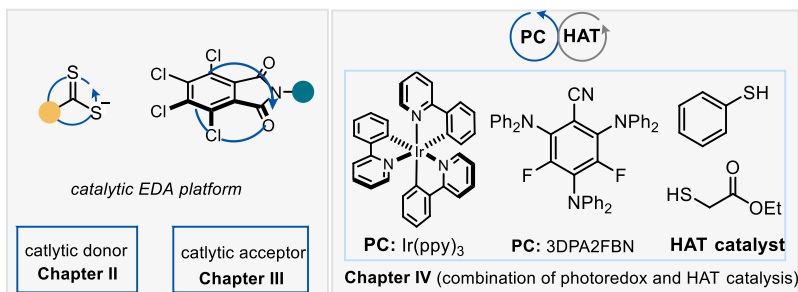
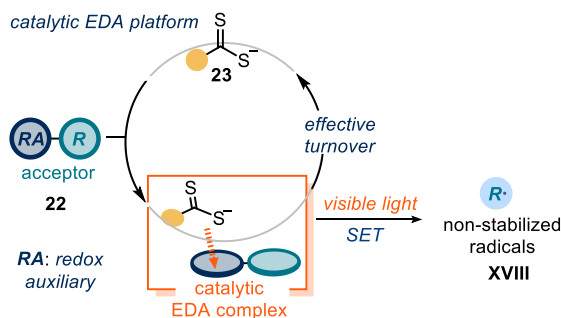


Figure 1.2. General photochemistry tools applied in this thesis.

1.4.1 A catalytic EDA platform with dithiocarbamate-based organocatalysts as donors

In Chapter II, we exploited the electronic properties of dithiocarbamate-based anions **23** to develop a catalytic EDA complex platform, where the organocatalyst **23** acted as the donor. A variety of radical precursors **22** were suitable acceptors for the formation of photoactive EDA complexes, affording non-stabilized radicals **XVIII** upon excitation with blue light (Scheme 1.7).

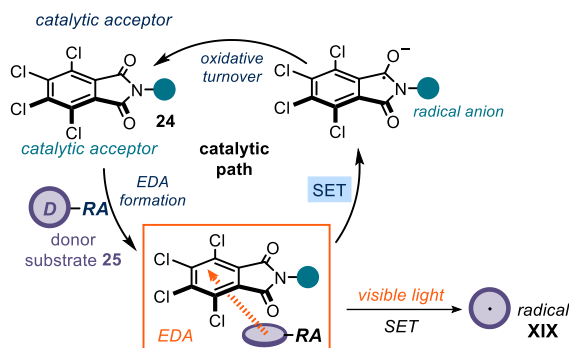


Scheme 1.7. Catalytic EDA platform with dithiocarbamate-based organocatalysts as donors.

The modular nature of the commercially available xanthogenate and dithiocarbamate anion organocatalysts **23** offered a versatile EDA complex catalytic protocol useful for developing mechanistically distinct radical processes, including redox neutral and net-reductive reactions. Mechanistic investigations supported that a closed catalytic cycle was operational, highlighting the ability of the organocatalysts to turnover and iteratively drive every catalytic cycle.

1.4.2 A catalytic platform with tetrachlorophthalimides as acceptors

In chapter III, we report that tetrachlorophthalimide-based compounds **24** can act as effective and general acceptor catalysts for EDA complex activation. These organocatalysts can activate radical precursors **25** bearing different electron-rich redox auxiliaries, including DHPs (1,4-Dihydropyridines), silicates and trifluoroborates. Excitation with visible light granted access to alkyl radicals **XIX** under mild conditions. Importantly, this EDA complex catalytic platform proved flexible enough to promote mechanistically different radical processes, including the first combination with a metal-based catalytic cycle.²³

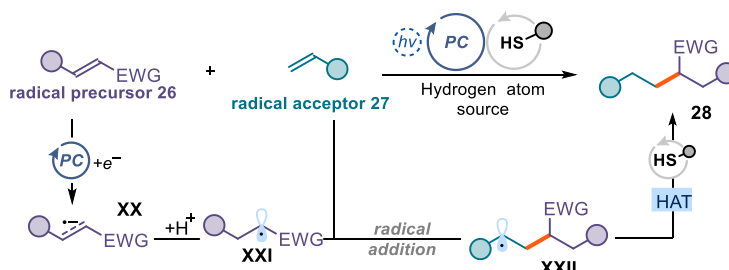


Scheme 1.8. A catalytic acceptor platform for EDA photoactivation.

1.4.3 Reductive cross-coupling of olefins by a radical pathway

Chapter IV details the development of a photochemical protocol based on the combination of photoredox catalysis and HAT catalysis. The protocol accounted for the reduction of electron-poor olefins **26** to generate the radical anion **XX** (Scheme 1.9), which could be protonated to afford radical **XXI**. This intermediate was then intercepted by an electron-rich or electron-neutral olefins **27** via a radical addition path. Ultimately, the generated radical **XXII** was reduced by an external hydrogen donor (thiol) via a HAT path to afford the desired olefin cross-coupling product **28**. Overall, a reductive cross-coupling of two olefins was achieved.

²³ Zhou, W.; Wu, S.; Melchiorre, P., Tetrachlorophthalimides as Organocatalytic Acceptors for Electron Donor–Acceptor Complex Photoactivation. *J. Am. Chem. Soc.* **2022**, *144*, 8914–8919.



Scheme 1.9. Photochemical reductive cross-coupling of olefins.

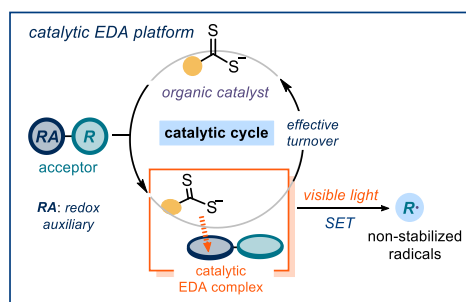
Our method encompasses a variety of olefins as radical precursors, including unsaturated ester, carbonyl, amide, cyano and sulfone, and radical acceptors, such as activated and non-activated olefins.

Chapter II

A General Organocatalytic System for Electron Donor–Acceptor Complex Photoactivation and its Use in Radical Processes

Target

To develop a general catalytic system for electron donor-acceptor (EDA) complex, employing nucleophilic organic catalysts as catalytic donors for the activation of a wide variety of electron-poor radical precursors.



Tool

Using the electronic features of dithiocarbamates and xanthogenates, which we previously used as catalytic nucleophiles, and their potential as donors in a catalytic EDA regime to generate non-stabilized radicals useful for mechanistically distinct radical reactions.¹

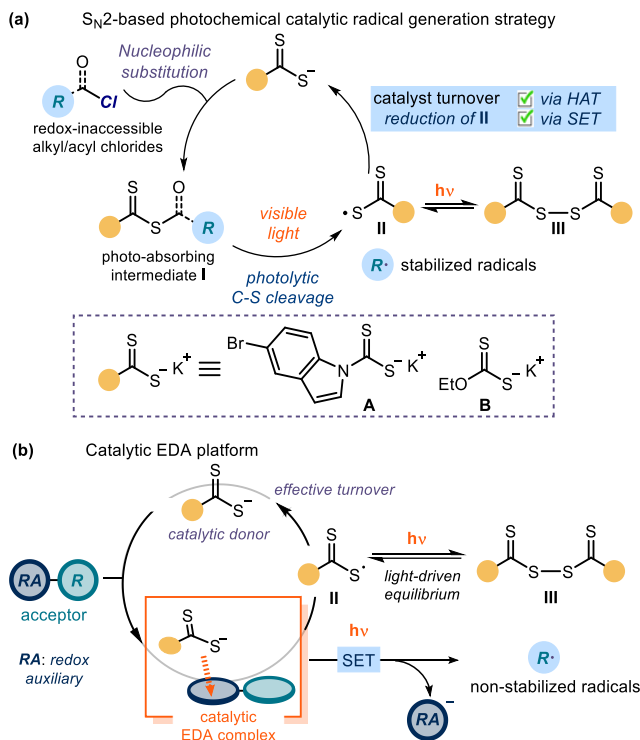
2.1 Introduction

Recently, our laboratory has developed a photochemical catalytic strategy that exploited nucleophilic organocatalysts to generate reactive radicals from simple alkyl (pseudo)halides.² The key of our methodology was the ability of the

¹ The project discussed in this chapter was conducted in collaboration with Dr. Davide Spinnato and Dr. Eduardo de Pedro Beato. I was mainly involved in the discovery and optimization of the Giese addition process and the Minisci reaction while exploring the scope of the Minisci reaction. I have also conducted the mechanistic studies. This work has been published: De Pedro Beato, E.; Spinnato, D.; Zhou, W.; Melchiorre, P. A General Organocatalytic System for Electron Donor–Acceptor Complex Photoactivation and Its Use in Radical Processes. *J. Am. Chem. Soc.* **2021**, *143*, 12304–12314.

² (a) Schweitzer-Chaput, B.; Horwitz, M. A.; de Pedro Beato, E.; Melchiorre, P. Photochemical generation of radicals from alkyl electrophiles using a nucleophilic organic catalyst. *Nat. Chem.* **2019**, *11*, 129–135. (b) Mazzarella, D.; Magagnano, G.; Schweitzer-Chaput, B.; Melchiorre, P. Photochemical Organocatalytic Borylation of Alkyl Chlorides, Bromides, and Sulfonates. *ACS Catal.* **2019**, *9*, 5876–5880. (c) Cuadros, S.; Horwitz, M. A.; Schweitzer-Chaput, B.; Melchiorre,

organocatalyst to promote nucleophilic substitution with alkyl electrophiles to form a photoactive intermediate **I** (Scheme 3.4a). Upon light excitation, the ensuing intermediate **I** could undergo photolytic C-S cleavage to generate the sulfur-centered radical **II** and the corresponding radicals, which engaged in subsequent transformations. Besides developing synthetically useful processes, a detailed mechanistic investigation were also performed.^{2e}



Scheme 2.1. (a) Nucleophilic substitution-based radical generation strategies using catalysts **A** and **B**. (b) Design of a catalytic EDA complex platform where the same catalysts' family serves as catalytic donors. Note that the turnover event would remain identical in the two protocols.

We found that the sulfur-centered radical **II** could dimerize to form the stable intermediate **III**. This dimer could absorb in the visible region, therefore being in

P., A visible-light mediated three-component radical process using dithiocarbamate anion catalysis. *Chem. Sci.* **2019**, *10*, 5484-5488. (d) Spinnato D.; Schweitzer-Chaput B.; Goti G.; M. Ošeka; Melchiorre P., A Photochemical Organocatalytic Strategy for the α -Alkylation of Ketones by using Radicals. *Angew. Chem. Int. Ed.* **2020**, *59*, 9485-9490. (e) de Pedro Beato, E.; Mazzarella, D.; Balletti, M.; Melchiorre, P., Photochemical generation of acyl and carbamoyl radicals using a nucleophilic organic catalyst: applications and mechanism thereof. *Chem. Sci.* **2020**, *11*, 6312-6324.

a light-regulated equilibrium with the progenitor **II**. This dimerization manifold conferred to radical **II** a longer lifetime, thereby enabling an effective catalyst turnover.^{2d,2e} Specifically, we found that the sulfur-centered radical **II** could be readily converted back to the anion state (catalytic active form) in two ways: *i*) via single-electron transfer (SET) from an open-shell intermediate of the catalytic cycle; *ii*) via hydrogen atom transfer (HAT) from an external hydrogen atom donor, such as γ -terpinene.

Based on this knowledge, to overcome the main limitation of our previous approach (namely, the inability to generate non-stabilized radicals), we wondered whether it would be possible to use the same dithiocarbamate catalysts (**A** or **B**, Scheme 2.1) for developing a mechanistically distinct radical generation protocol. We hypothesized that the nucleophilic dithiocarbamate anions could potentially act also as electron-rich *donors* in the formation of photoactive electron donor-acceptor (EDA) complex with a variety of electron-poor radical precursors. Upon excitation, the EDA complex would undergo SET to afford the target radical.³ In this scenario, the generation of radicals would not rely on the electrophilic character of the radical precursor nor on the bond dissociation energy of the C-S bond within **I**, but only on the ability of the catalyst to engage the radical precursor in productive EDA complex formation (Scheme 2.1b). Importantly, the judicious selection of redox-active radical precursors, which would act as acceptors, would allow us to access non-stabilized radicals.

Over the past decade, significant advancements have been made in the generation of radicals using photoredox catalysis and electrochemical processes.^{4,5} These methodologies have enabled radical formation under mild conditions, which helped establishing the synthetic potential of radical transformations as viable alternative to polar processes.⁶ Many existing radical generation methods rely on the use of

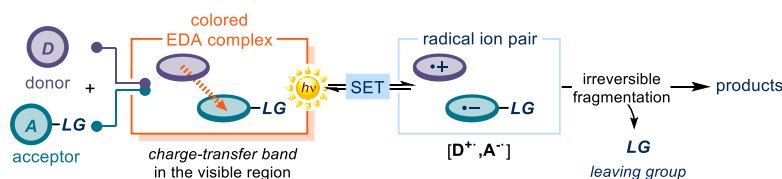
³ Crisenza, G. E. M.; Mazzarella, D.; Melchiorre, P. "Synthetic Methods Driven by the Photoactivity of Electron Donor–Acceptor Complexes" *J. Am. Chem. Soc.* **2020**, *142*, 5461–5476.

⁴ (a) Shaw, M. H.; Twilton, J.; MacMillan, D. W. C. Photoredox Catalysis in Organic Chemistry. *J. Org. Chem.* **2016**, *81*, 6898–6926. (b) Romero, N.; Nicewicz, D. Organic Photoredox Catalysis. *Chem. Rev.* **2016**, *116*, 10075–10166. (c) Matsui, J. K.; Lang, S. B.; Heitz, D. R.; Molander, G. A. Photoredox-mediated routes to radicals: the value of catalytic radical generation in synthetic methods development, *ACS Catal.* **2017**, *7*, 2563–2575.

⁵ Kingston, C.; Palkowitz, M. D.; Takahira, Y.; Vantourout, J. C.; Peters, B. K.; Kawamata, Y.; Baran, P. S. A Survival Guide for the "Electro-curious". *Acc. Chem. Res.* **2020**, *53*, 72–83.

⁶ (a) Blakemore, D. C.; Castro, L.; Churcher, I.; Rees, D. C.; Thomas, A. W.; Wilson, D. M.; Wood, A. Organic synthesis provides opportunities to transform drug discovery. *Nat. Chem.* **2018**, *10*, 383–394. (b) Douglas, J. J.; Sevrin, M. J.; Stephenson, C. R. J., Visible Light

noble metal-based photocatalysts containing iridium (Ir) and ruthenium (Ru).⁷ To address this limitation, researchers have used several organic dyes to replace typical rare metal-based photocatalysts.^{4b} Another mechanistically distinct approach for radical formation involves the formation of photoactive EDA complexes.³ EDA complexes are formed when two or more molecules associate with each other, leading to the generation of new molecular orbitals through re-hybridization of the frontier orbitals of the donor and acceptor partners (specifically, the highest occupied molecular orbital, HOMO, for the donor and the lowest unoccupied molecular orbital, LUMO, for the acceptor).³ Although the individual donor and acceptor components may not absorb visible light themselves, the resulting EDA complex has a smaller HOMO-LUMO gap and often exhibits absorption in the visible light range (Scheme 2.2). When the ground-state EDA complex is irradiated, a direct SET process occurs from the electron-rich donor molecule to the electron-poor acceptor molecule within the complex. This results in a radical ion pair, which can provide access to reactive radicals that subsequently participate in various chemical processes.



Scheme 2.2. Generation of radicals through EDA complex excitation.

Complementary to traditional photocatalyst-dependent processes, the EDA approach allows for the direct engagement of two reactants without the requirement of an external mediator to facilitate SET. The synthetic application of the EDA complex platform, in its most straightforward form, involves the light-driven coupling of two stoichiometric donor and acceptor substrates. In this case, the moieties of the substrates (A and D) will end up in the core of the products, restricting their structural diversity. To enhance the generality and versatility of the method, the EDA complex photochemistry should be implemented within a catalytic regime.

Photocatalysis: Applications and New Disconnections in the Synthesis of Pharmaceutical Agents. *Organic Process Research & Development* **2016**, *20*, 1134-1147. (c) Sambigiagio, C.; Noël, T., Flow Photochemistry: Shine Some Light on Those Tubes! *Trends in Chemistry* **2020**, *2*, 92-106.

⁷ Lee, Y.; Kwon, M. S., Emerging Organic Photoredox Catalysts for Organic Transformations. *Eur. J. Org. Chem.* **2020**, *2020*, 6028-6043.

In this chapter, our efforts to develop a catalytic EDA complex strategy using dithiocarbamate anions as catalytic donors will be discussed. In the following section, I will provide an overview of radical generation methods based on the photoexcitation of EDA complexes.

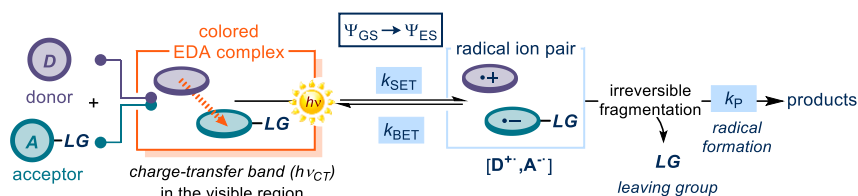
2.2 Electron donor-acceptor (EDA) complexes

The discovery of electron donor-acceptor (EDA) complexes dates back to the last century, when Hildebrand and Glascock found that iodine forms colored solutions in different solvents.⁸ Forty years later, detailed spectroscopic investigations conducted by Benesi and Hildebrand⁹ have conclusively demonstrated that benzene and mesitylene form 1:1 non-covalent complexes with iodine. They attributed the observable color change to ground-state association between the electron-rich aromatic molecule (donor, Lewis basic) and the electron-poor iodine molecule (acceptor, Lewis acidic). Later on, Mulliken proposed a quantum mechanical theory to explain the formation of EDA complexes.¹⁰ More specifically, the association of a donor molecule (**D**) with low ionization potential and an acceptor molecule (**A**) with high electron affinity leads to the formation of a new complex in the ground state (EDA complex, orange box in Scheme 2.3). In this complex, new molecular orbitals arise from the frontier orbitals of **D** and **A** (HOMO/LUMO, respectively), which confer the EDA complex distinct physical properties compared to the separated substrates. The formation of the EDA complex is characterized by the appearance of a charge-transfer band in the absorption spectrum ($h\nu_{CT}$), corresponding to an electronic transition ($\Psi_{GS} \rightarrow \Psi_{ES}$, Ψ = wave-function) between the ground state (Ψ_{GS}) and the excited state (Ψ_{ES}) of the complex. When the EDA complex is excited (Scheme 2.3), the Ψ_{ES} state becomes populated, resulting in an intra-complex SET from the donor (**D**) to the acceptor (**A**). This SET process generates a radical ion pair, characterized by a net charge separation (light blue box).

⁸ Hildebrand, J. H.; Glascock, B. L. "The Color of Iodine Solutions" *J. Am. Chem. Soc.* **1909**, *31*, 26–31.

⁹ Benesi, H. A.; Hildebrand, J. H., A Spectrophotometric Investigation of the Interaction of Iodine with Aromatic Hydrocarbons. *J. Am. Chem. Soc.* **1949**, *71*, 2703-2707.

¹⁰ (a) Mulliken, R. S., Structures of Complexes Formed by Halogen Molecules with Aromatic and with Oxygenated Solvents. *J. Am. Chem. Soc.* **1950**, *72*, 600-608. (b) Mulliken, R. S. Molecular Compounds and their Spectra. II. *J. Am. Chem. Soc.* **1952**, *74*, 811–824. (c) Mulliken, R. S. Molecular Compounds and their Spectra. III. The Interaction of Electron Donors and Acceptors. *J. Phys. Chem.* **1952**, *56*, 801–822.



Scheme 2.3. EDA complex formation and intra-complex SET.

Initial research efforts mainly focused on the physical characterization of EDA complexes.¹¹ Only recently their applications in synthetic organic chemistry has gained more prominence.³ This delay in synthetic application can be attributed to the inherent challenges¹² associated with properties of EDA complexes. One of the major challenges is related to the unproductive back-electron transfer (BET) from the radical ion pair back to the ground-state EDA complex (Scheme 2.3). If the BET process is faster than other processes leading to the formation of reactive radicals and subsequent product generation ($k_{BET} > k_p$, with k being rate constants), the photoactivation of the EDA complex becomes synthetically unproductive. A strategy that addresses this issue involves introducing a suitable leaving group (LG) into the radical anion ($A^{\bullet-}$ in Scheme 2.3). This leaving group can cause an irreversible fragmentation that occurs rapidly enough to compete with the BET process. As a result, the EDA complex would undergo a productive fragmentation, yielding reactive radical intermediates (R^{\bullet}) that can be exploited for further transformation.

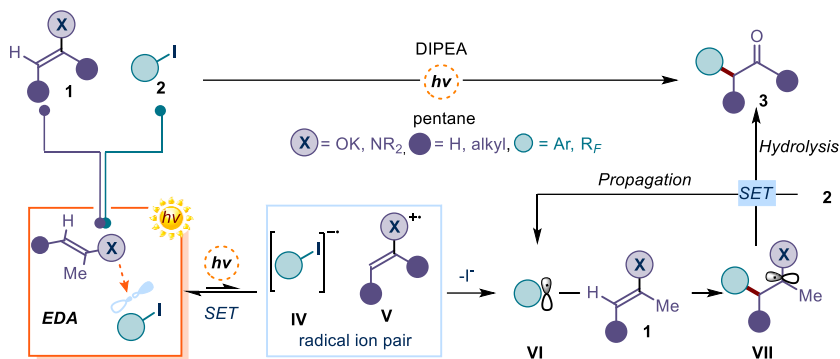
The viability of this approach was demonstrated by seminal contributions in 1970s. For example, Cantacuzene investigated the participation of enamines and enolates **1** as donors in charge-transfer interactions with aryl and perfluoroalkyl iodides **2**,¹³ to form an EDA aggregate (Scheme 2.4). In this study, the iodide functionality present in the acceptor core of compound **2** acted as a suitable leaving group, which

¹¹ (a) Hilinski, E. F.; Masnovi, J. M.; Amatore, C.; Kochi, J. K.; Rentzepis, P. M. Charge-Transfer Excitation of Electron Donor-Acceptor Complexes. Direct Observation of Ion Pairs by Time-Resolved (Picosecond) Spectroscopy. *J. Am. Chem. Soc.* **1983**, *105*, 6167–6168. (b) Singh, J. O.; Anunziata, J. D.; Silber, J. J. $n-\pi$ Electron Donor-Acceptor Complexes. II. Aliphatic Amines with Dinitrobenzenes. *Can. J. Chem.* **1985**, *63*, 903–907.; (d) Rosokha, S. V.; Kochi, J. K. Fresh Look at Electron-Transfer Mechanisms via the Donor/Acceptor Bindings in the Critical Encounter Complex. *Acc. Chem. Res.* **2008**, *41*, 641–653.

¹² Rathore, R.; Kochi, J. K. Donor/Acceptor Organizations and the Electron-Transfer Paradigm for Organic Reactivity. *Adv. Phys. Org. Chem.* **2000**, *35*, 193–318.

¹³ (a) Cantacuzène, D.; Dorme, R., Cetones α perfluorees. *Tetrahedron Letters* **1975**, *16*, 2031–2034.; (b) Cantacuzène, D.; Wakselman, C.; Dorme, R. Condensation of Perfluoroalkyl Iodides with Unsaturated Nitrogen Compounds. *J. Chem. Soc., Perkin Trans. 1* **1977**, 1365–1371.

enabled the fragmentation of the radical anion to productively generate perfluoroalkyl or aryl radical **IV**. In this process, the EDA complex-promoted SET only acted as an initiation event for a chain-propagated reaction. The overall outcome of the photochemical reaction was the perfluoroalkylation/arylation of carbonyl compounds which could not be achieved under thermal activation.

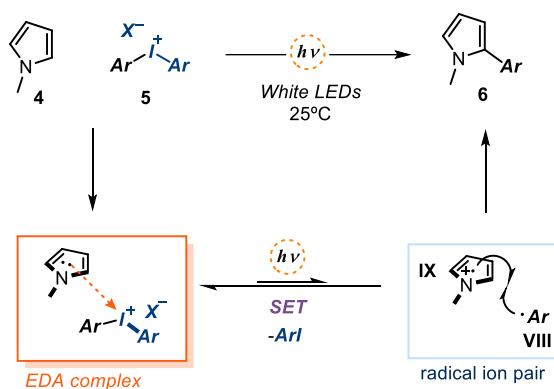


Scheme 2.4. α -Perfluoroalkylation/arylation of carbonyl compounds promoted by light excitation of an EDA complex. Ar: arene; R_f : polyfluoroalkyl.

In the following years, only few synthetic methodologies based on the excitation of EDA complexes were reported.¹⁴ Although these early examples demonstrated the potential of the EDA complex photochemistry as a radical generation strategy, it was only in 2013 that the photoactivity of EDA complexes was recognized as a powerful strategy in visible light-driven radical synthesis and began to emerge as an independent field of research.

¹⁴ (a) Bunnett, J. F.; Sundberg, J. E., Photostimulated arylation of ketone enolate ions by the SRN1 mechanism. *J. Org. Chem.* **1976**, *41*, 1702-1706. (b) Russell, G. A.; Wang, K. Homolytic Alkylation of Enamines by Electrophilic Radicals. *J. Org. Chem.* **1991**, *56*, 3475-3479. (c) Wade, P. A.; Morrison, H. A.; Kornblum, N. The Effect of Light on Electron-Transfer Substitution at a Saturated Carbon Atom. *J. Org. Chem.* **1987**, *52*, 3102-3107. (d) Sankararaman, S.; Haney, W. A.; Kochi, J. K. Annihilation of Aromatic Cation Radicals by Ion-Pair and Radical-Pair Collapse. Unusual Solvent and Salt Effects in the Competition for Aromatic Substitution. *J. Am. Chem. Soc.* **1987**, *109*, 7824-7838. (e) Fukuzumi, S.; Mochida, K.; Kochi, J. K. A Unified Mechanism for Thermal and Photochemical Activation of Charge-Transfer Processes with Organometals. Steric Effects in the Insertion of Tetracyanoethylene. *J. Am. Chem. Soc.* **1979**, *101*, 5961-5972. (f) Gotoh, T.; Padias, A. B.; Hall, J. H. K. An Electron Donor Acceptor Complex and Thermal Triplex as Intermediates in the Cycloaddition Reaction of N-Vinylcarbazole with Dimethyl 2,2-Dicyanoethylene-1,1-dicarboxylate. *J. Am. Chem. Soc.* **1991**, *113*, 1308-1312. (g) Fox, M. A.; Younathan, J.; Fryxell, G. E. Photoinitiation of the SRN1 Reaction by Excitation of Charge-Transfer Complexes. *J. Org. Chem.* **1983**, *48*, 3109-3112.

In 2013, Chatani and coworkers developed a photoredox protocol for arylation of arenes and heteroarenes.¹⁵ When pyrroles were used as substrates (Scheme 2.5), they noticed that mixing of colorless substrates provided a yellow-orange reaction mixture. The product was obtained in comparative yields even when the photocatalyst was excluded. This suggested that a possible EDA aggregation occurred between pyrrole **4** and aryl iodonium salts **5**, which was eventually corroborated by spectroscopic studies. As detailed in Scheme 2.5, photo-activation of the colored EDA aggregate is responsible for irreversible extrusion of the iodide, followed by the formation of radicals **VIII** and **IX**. Upon radical-radical cross-coupling and deprotonation, the arylated product **6** was obtained.



Scheme 2.5. Arylation of pyrrole derivatives promoted by a visible-light absorbing EDA complex.

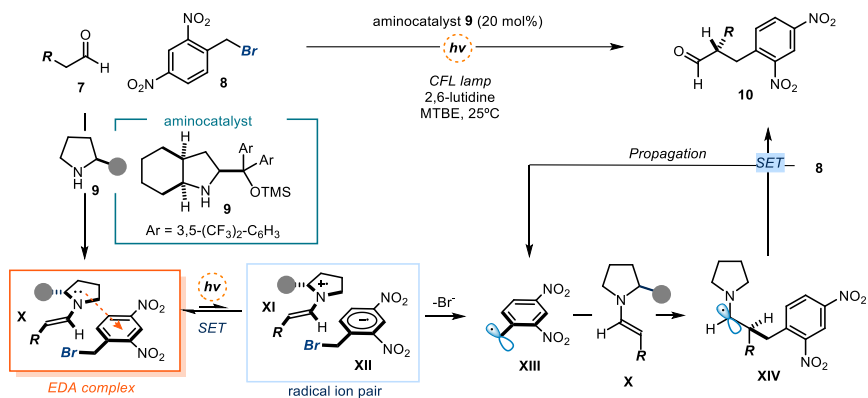
Concomitantly, our research group investigated the enantioselective α -alkylation of aldehydes **7** with electron-deficient alkyl bromides **8** (Scheme 2.).¹⁶ Previous studies have demonstrated the feasibility of this transformation using a photocatalyst to generate the corresponding radicals from substrate **8**.¹⁷ However, when aminocatalyst **9** was used, we observed in a control experiment that no photocatalyst was necessary to achieve the stereoselective transformation with

¹⁵ Tobisu, M.; Furukawa, T.; Chatani, N. Visible Light-mediated Direct Arylation of Arenes and Heteroarenes Using Diaryliodonium Salts in the Presence and Absence of a Photocatalyst. *Chem. Lett.* **2013**, *42*, 1203–1205.

¹⁶ Arceo, E.; Jurberg, I. D.; Álvarez-Fernandez, A.; Melchiorre, P. Photochemical activity of a key donor-acceptor complex can drive stereoselective catalytic α -alkylation of aldehydes. *Nat. Chem.* **2013**, *5*, 750–756.

¹⁷ Nicewicz, D. A.; MacMillan, D. W. C. Merging Photoredox Catalysis with Organocatalysis: The Direct Asymmetric Alkylation of Aldehydes. *Science* **2008**, *322*, 77–80.

halides **8**. Through mechanistic studies, we uncovered the underlying process behind this photocatalyst-free process. After condensation of aldehyde **7** with the chiral aminocatalyst **9**, an electron-rich catalytic enamine intermediate **X** was formed, which associated with the electron-deficient bromides **8**, delivering a colored EDA complex. Upon visible-light irradiation, an intra-complex SET event took place, resulting in the generation of a radical ion pair (**XI** and **XII** in Scheme 2.6, depicted in the light blue box). Importantly, the irreversible fragmentation of **XII** led to the formation of the benzyl radical **XIII**, which would engage another ground-state enamine **X** to afford the α -amino radical **XIV**. Further mechanistic investigations, including quantum yield measurements, revealed that the reaction proceeded through a self-propagating radical chain mechanism.¹⁸ This indicated that the photochemistry of the EDA complex acted as an initiating step for the radical chain process. The propagation step relied on the reduction of the radical precursor **8** by the α -amino radical **XIV**, yielding the enantioenriched product **10**.



Scheme 2.6. Enantioselective alkylation of aldehydes promoted by a visible-light absorbing enamine-based EDA complex.

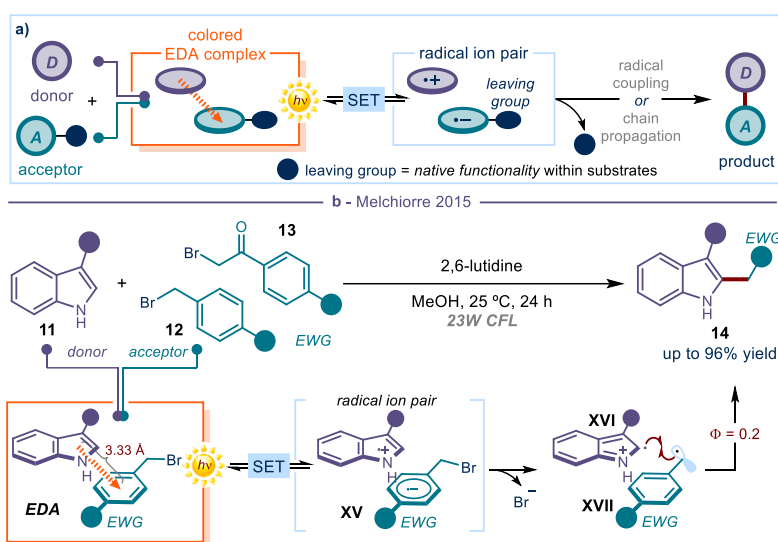
This process offered the first example of EDA complex generated by a *catalytic* donor (the enamine). In addition, since the catalytic enamine donors **X** were chiral, this transformation was the first application of a photoactive EDA complex in stereoselective radical catalysis. This study also showcased the potential of EDA photochemistry in synthetic chemistry, since it allowed chiral enamines to achieve

¹⁸ Bahamonde, A.; Melchiorre, P. Mechanism of the Stereoselective α -Alkylation of Aldehydes Driven by the Photochemical Activity of Enamines. *J. Am. Chem. Soc.* **2016**, *138*, 8019–8030.

radical pathways unavailable to thermal activation.¹⁹ After publication of these two studies, the EDA complex photochemistry regained attention from the synthetic community.

2.3 Photoreactivity of stoichiometric EDA complexes

Recent collective efforts from the synthetic community mainly focused on the most direct application of the EDA complex activation strategy, which involved the light-driven coupling of two substrates, namely a donor and an acceptor (Scheme 2.7a).²⁰



Scheme 2.7. (a) General strategy for the coupling of electron-rich (donor) and electron-poor (acceptor) stoichiometric substrates via EDA complex activation. (b) Photochemical C2-alkylation of indoles enabled by EDA photochemistry.

¹⁹ Silvi, M.; Melchiorre, P. Enhancing the potential of enantioselective organocatalysis with light. *Nature* **2018**, *554*, 41–49.

²⁰ Selected examples of direct coupling between donor and acceptor substrates: (a) Kandukuri, S. R.; Bahamonde, A.; Chatterjee, I.; Jurberg, I. D. *Angew. Chem., Int. Ed.* **2015**, *54*, 1485–1489; (b) Nappi, M.; Bergonzini, G.; Melchiorre, P. *Angew. Chem., Int. Ed.* **2014**, *53*, 4921–4925; (c) Liang, K.; Li, N.; Zhang, Y.; Li, T.; Xia, C. *Chem. Sci.* **2019**, *10*, 3049–3053; (d) Liu, B.; Lim, C.-H.; Miyake, G. M. *J. Am. Chem. Soc.* **2017**, *139*, 13616–13619; (e) Li, G.; Yan, Q.; Gan, Z.; Li, Q.; Dou, X.; Tang, D. *Org. Lett.* **2019**, *21*, 7938–7942. (e) Kandukuri, S. R.; Bahamonde, A.; Chatterjee, I.; Jurberg, I. D.; Escudero-Adán, E. C.; Melchiorre, P., X-Ray Characterization of an Electron Donor–Acceptor Complex that Drives the Photochemical Alkylation of Indoles. *Angew. Chem., Int. Ed.* **2015**, *54*, 1485–1489.

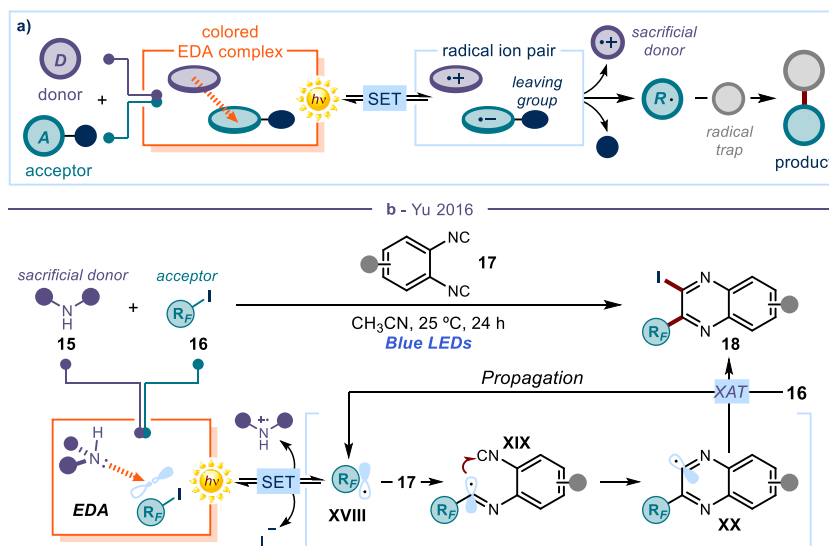
The success of these radical processes rested on the inherent electronic properties of the two substrates, which should be conducive to the formation of a photoactive EDA complex. But in this scenario, the structural components of the substrates that contributed to EDA complex formation eventually became part of the final product. As explained above (Scheme 2.3), a leaving group is generally essential to secure, upon photoinduced SET, an irreversible fragmentation that productively delivering open-shell intermediates, responsible for the formation of the product. Typically, this leaving group is a native functionality, such as halides, incorporated within the structure of one of the substrates. This strategy has been used for the formation of carbon-carbon and carbon-heteroatom bond processes. For example, our research group developed a photochemical strategy for the direct alkylation of 3-substituted indoles **11** with electron-accepting benzyl **12** or phenacyl bromides **13** (Scheme 2.7b).^{20e} The corresponding EDA complex between **11** and **12** was successfully isolated and characterized. Remarkably, the crystallographic analysis showed that the average interplanar distance between the 3-methyl indole and the 2,4-dinitrobenzyl bromide fragments (3.33 Å) is significantly lower than the van der Waals separation for aromatic molecules (3.40 Å),²¹ which was consonant with intermolecular binding forces being at work in the solid state. Irradiation of the EDA complex induced the formation of the radical ion pair **XV**, which evolved into the radicals **XVI** and **XVII** upon extrusion of the bromide anion. The quantum yield determination ($\Phi = 0.2$) implied that a radical combination governed the formation of the C2-alkylated indole **14**.

The methods explained above enable the coupling of two substrates, which are also involved in the EDA complex formation. Therefore, the diversity of the reaction products is somehow restricted by the need to select highly polarized reagents with donor and acceptor properties, which eventually end up in the product scaffold. To overcome this limitation, one strategy is to employ a sacrificial donor, which can aggregate with an electron-poor substrate (acceptor), affording a photoactive EDA complex (Scheme 2.8a). After light-driven SET and expulsion of the leaving group, a radical is generated which then react with an external radical trap. One example of this strategy was developed by Yu and co-workers, who used stoichiometric amounts of secondary amines **15** as a sacrificial donor to form an EDA complex with perfluoroalkyl iodides **16** (scheme 2.8b).²² Visible-light irradiation of the

²¹ Alvarez, S. A Cartography of the van der Waals territories. *Dalton Trans.* **2013**, 42, 8617–8636.

²² Sun, X.; Wang, W.; Li, Y.; Ma, J.; Yu, S. “Halogen-Bond-Promoted Double Radical Isocyanide Insertion under Visible-Light Irradiation: Synthesis of 2-Fluoroalkylated Quinoxalines” *Org. Lett.* **2016**, 18, 4638–4641.

EDA complex enabled the formation the perfluoroalkyl radicals **XVIII**, which was then intercepted by an isocyanide substrate **17** to provide radical **XIX**. Upon cyclization, the heteroaryl radical **XIX** that abstracted an iodine atom from the perfluoroalkyl iodide **16** to form the quinoxaline product **18** while propagating a chain reaction through the generation of a second equivalent of perfluoroalkyl radicals **XVIII**.



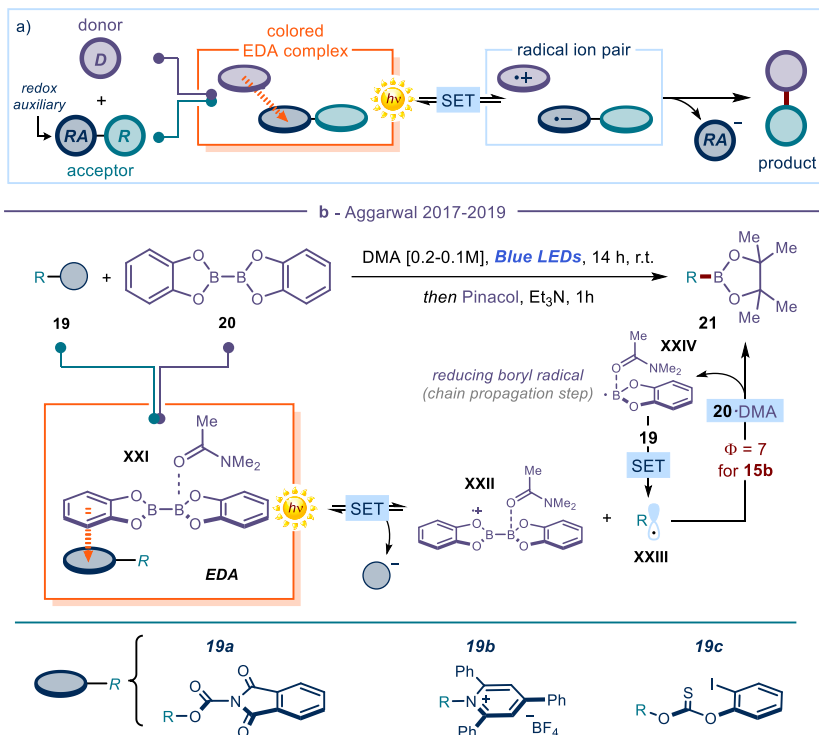
Scheme 2.8. (a) General strategy for EDA complex formation using sacrificial donor; (b) Photochemical generation of perfluoroalkyl radicals for the synthesis of quinoxalines

Another limitation of the EDA complex-based synthetic strategies discussed so far was that at least one substrate must be both electronically biased and bears a fragmenting functionality, which was necessary to form an EDA complex and trigger the fragmentation needed for radical formation. Considering this aspect and the availability of the reagents, generally simple and easily available substrates decorated with native functionalities (mostly halides within acceptors) were used. But the EDA complex formation must be elicited exclusively by the electronic properties of the substrate's main core. This indicated that only highly polarized radicals can be generated. For example, in the previous contribution reported in Scheme 2.8, the electron-poor nature of the perfluoroalkyl fragment within R_FI secured the formation of the EDA complex, while the iodide served as a fragmenting group. The resulting perfluoroalkyl radical was therefore electronically biased (highly electrophilic). In an alternative strategy, which extended the applicability of EDA photochemistry, a substrate was adorned with a

pre-installed activating group, which served as both redox-auxiliary (blue circle in Scheme 2.9a, **RA**) and leaving group. The substrate's main core was not electronically biased, since the EDA complex formation was promoted by the electronic properties of the redox-auxiliary/fragmenting group. The radical arising from the excitation of the EDA complex was therefore electronically unbiased.

Recently, several transformations have been developed by taking advantage of an EDA association between a substrate and a molecule adorned with a redox auxiliary. For example, Aggarwal and coworkers reported photochemical methodologies for the borylation of a wide range of radical precursors **19** (Scheme 2.b).²³ As a general mechanistic proposal, the formation of the EDA complex occurred initially between the redox auxiliary moiety (blue circle in Scheme 2.9b) embedded in the radical precursor **19** and intermediate **XXI**, an adduct formed between a coordinating solvent and bis(catecholato)diboron (B_2cat_2) **20**. *N*-Hydroxyphthalimide (NHPI) esters **19a**, *N*-alkylpyridium salts **19b**, and thionocarbonates **19c** are examples of electron-accepting EDA partners that have been successfully used.

²³ (a) Fawcett, A.; Pradeilles, J.; Wang, Y.; Mutsuga, T.; Myers, E. L.; Aggarwal, V. K. Photoinduced decarboxylative borylation of carboxylic acids. *Science* **2017**, *357*, 283–286. (b) Wu, J.; He, L.; Noble, A.; Aggarwal, V. K. Photoinduced Deaminative Borylation of Alkylamines. *J. Am. Chem. Soc.* **2018**, *140*, 10700–10704. (c) Wu, J.; Bär, R. M.; Guo, L.; Noble, A.; Aggarwal V. K. Photoinduced Deoxygenative Borylations of Aliphatic Alcohols. *Angew. Chem. Int. Ed.* **2019**, *58*, 18830–18834.



Scheme 2.9. (a) General strategy for EDA complex formation using redox auxiliaries; (b) Borylation of alkyl radicals driven by the photoactivity of EDA complexes.

Light-promoted intra-complex charge transfer and rapid fragmentation of the resultant radical anion occurred, affording the desired radical **XXIII**, which was then captured by another molecule of intermediate **XXI** to provide the borylated product. At the same time, the boron-centered radical **XXIV** was formed, which propagated the radical chain by reducing another molecule of radical precursor **19**. Finally, the catecholborane product was converted in situ to the corresponding pinacol boronic ester **21**.

2.4 Catalytic EDA complexes

Previous approaches relied on the use of stoichiometric substrates for EDA complex formation. An important advancement in the field would be to implement

the EDA complex activation strategy within a catalytic regime.^{24,25} Research conducted by our group demonstrated that certain chiral organocatalytic intermediates, such as enamines,²⁶ iminium ions,²⁷ and enolates,²⁸ could participate in catalytic EDA complex formation. These intermediates promoted photochemical radical formation while selectively trapping the resulting open-shell species in a stereocontrolled manner. However, mechanistic studies revealed the dominance of a self-propagating radical chain, indicating that the photoactive EDA complex was only responsible for initiating the process and the electron-rich intermediate could not be regenerated. Therefore, when using a catalytic donor, the most challenging yet essential step for a catalytic protocol would be the effective turnover of the catalyst. This requires a SET reduction of the catalyst radical cation, emerging from the photoactivity of the progenitor EDA complex (Scheme 2.10).

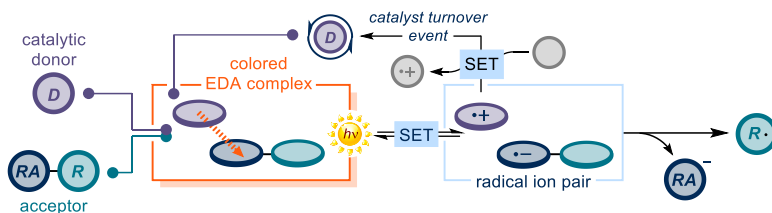
²⁴ (a) Fu, M.-C.; Shang, R.; Zhao, B.; Wang, B.; Fu, Y. Photocatalytic decarboxylative alkylations mediated by triphenylphosphine and sodium iodide. *Science* **2019**, *363*, 1429–1434. (b) Wang, Y.-T.; Fu, M.-C.; Zhao, B.; Shang, R.; Fu, Y. Photocatalytic decarboxylative alkenylation of α -amino and α -hydroxy acid-derived redox active esters by NaI/PPH₃ catalysis. *Chem. Commun.* **2020**, *56*, 2495–2498. (c) Fu, M.-C.; Wang, J. X.; Shang, R. Triphenylphosphine-Catalyzed Alkylative Iododecarboxylation with Lithium Iodide under Visible Light. *Org. Lett.* **2020**, *22*, 8572–8577. (d) Bosque, I.; Bach, T. 3-Acetoxyquinuclidine as Catalyst in Electron Donor-Acceptor Complex-Mediated Reactions Triggered by Visible Light. *ACS Catal.* **2019**, *9*, 9103–9109. (e) McClain, E. J.; Monos, T. M.; Mori, M.; Beatty, J. W.; Stephenson, C. R. J. Design and Implementation of a Catalytic Electron Donor–Acceptor Complex Platform for Radical Trifluoromethylation and Alkylation. *ACS Catalysis* **2020**, *10*, 12636–12641.

²⁵ (a) Quint, V.; Morlet-Savary, F.; Lohier, J.-F.; Lalevée, J.; Gaumont, A.-C.; Lakhdar, S., Metal-Free, Visible Light-Photocatalyzed Synthesis of Benzo[b]phosphole Oxides: Synthetic and Mechanistic Investigations. *J. Am. Chem. Soc.* **2016**, *138*, 7436–7441. (b) Emmanuel, M. A.; Greenberg, N. R.; Oblinsky, D. G.; Hyster, T. K., Accessing non-natural reactivity by irradiating nicotinamide-dependent enzymes with light. *Nature* **2016**, *540*, 414–417. (c) Biegasiewicz, K. F.; Cooper, S. J.; Gao, X.; Oblinsky, D. G.; Kim, J. H.; Garfinkle, S. E.; Joyce, L. A.; Sandoval, B. A.; Scholes, G. D.; Hyster, T. K., Photoexcitation of flavoenzymes enables a stereoselective radical cyclization. *Science* **2019**, *364*, 1166–1169. (d) Clayman, P. D.; Hyster, T. K., Photoenzymatic Generation of Unstabilized Alkyl Radicals: An Asymmetric Reductive Cyclization. *J. Am. Chem. Soc.* **2020**, *142*, 15673–15677. (e) Page, C. G.; Cooper, S. J.; DeHovitz, J. S.; Oblinsky, D. G.; Biegasiewicz, K. F.; Antropow, A. H.; Armbrust, K. W.; Ellis, J. M.; Hamann, L. G.; Horn, E. J.; Oberg, K. M.; Scholes, G. D.; Hyster, T. K., Quaternary Charge-Transfer Complex Enables Photoenzymatic Intermolecular Hydroalkylation of Olefins. *J. Am. Chem. Soc.* **2021**, *143*, 97–102.

²⁶ Arceo, E.; Bahamonde, A.; Bergonzini, G.; Melchiorre, P. Enantioselective direct α -alkylation of cyclic ketones by means of photo-organocatalysis. *Chem. Sci.* **2014**, *5*, 2438–2442.

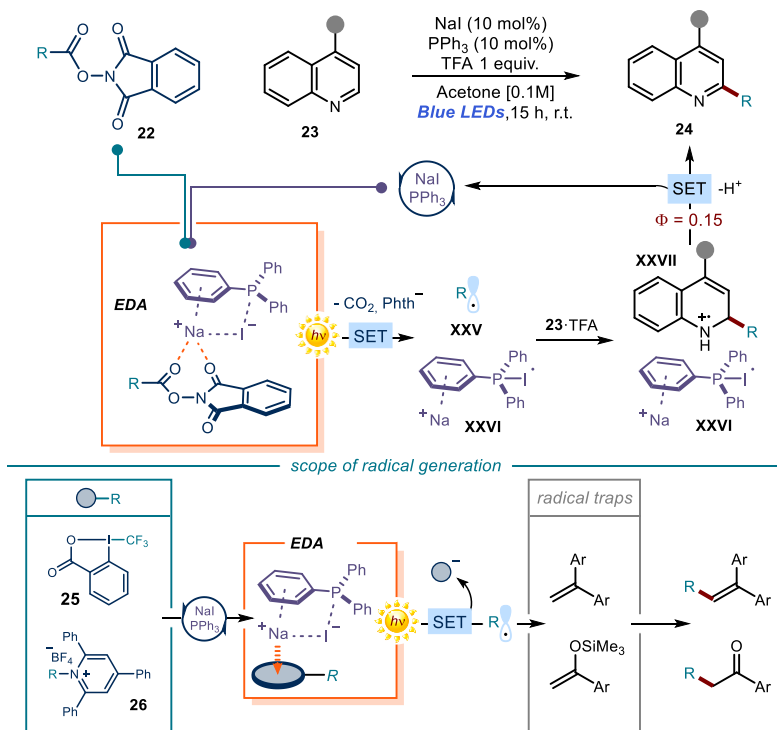
²⁷ Cao, Z.-Y.; Ghosh, T.; Melchiorre, P. Enantioselective radical conjugate additions driven by a photoactive intramolecular iminium-ion-based EDA complex. *Nat. Commun.* **2018**, *9*, 3274.

²⁸ Woźniak, Ł.; Murphy, J. J.; Melchiorre, P. Photo-organocatalytic Enantioselective Perfluoroalkylation of β -Ketoesters. *J. Am. Chem. Soc.* **2015**, *137*, 5678–5681.



Scheme 2.10. EDA complex strategy using a catalytic donor.

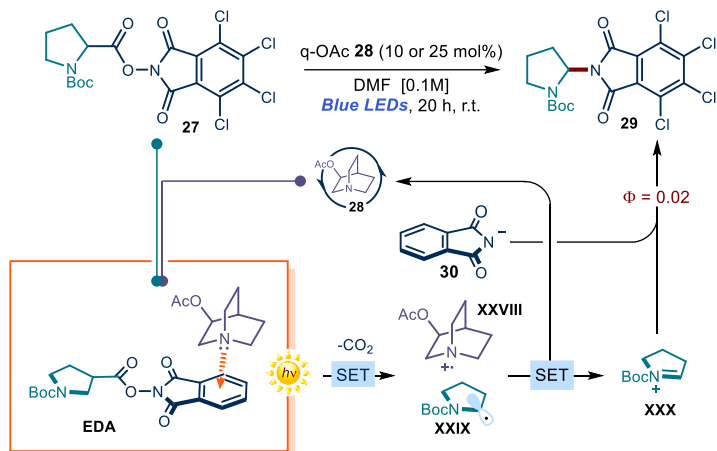
In 2019, Shang, Fu and coworkers developed a general catalytic EDA complex system, in which the donor realized an effective turnover event (scheme 2.11).^{24a} Their study described the combined use of sodium iodide (NaI) and triphenylphosphine (PPh₃) to form a colored EDA complex with NHPI esters **22**. Upon irradiation with blue light, the alkyl radical was generated and efficiently trapped by various substrates. For example, efficient Minisci reaction was promoted between heteroarenes and NHPI esters.



Scheme 2.11. Photocatalytic radical alkylations mediated by the catalytic combination of triphenyl phosphine and sodium iodide.

Initially, radical **XXV** was generated through intra-complex SET driven by irradiation of the three-component EDA complex. Subsequent radical addition to heterocycle **23** occurred in the presence of acid, which led to the formation of radical cation **XXVII**. This could be oxidized by iodine-centered radical **XXVI** to regenerate sodium iodide (NaI) and deliver the C-H functionalized heteroarenes **24**. Triphenylphosphine was crucial for the catalyst turnover owing to its stabilization to the iodine-centered radical by forming the persistent adduct **XXVI**, until it can be turned over via SET to give the iodide anion. A low quantum yield ($\Phi = 0.15$) also confirmed that a closed catalytic cycle was more likely than a chain propagation. Importantly, the system was not limited to NHPI esters **22** but could be also applied to other radical precursors containing electron-deficient moieties, including hypervalent iodine reagents **25** and pyridinium salts **26**. Furthermore, the same NaI/PPh₃ catalytic system could be expanded to other photo-induced transformations, including alkylation of silyl ether and a stereocontrolled version of the Minisci reaction.

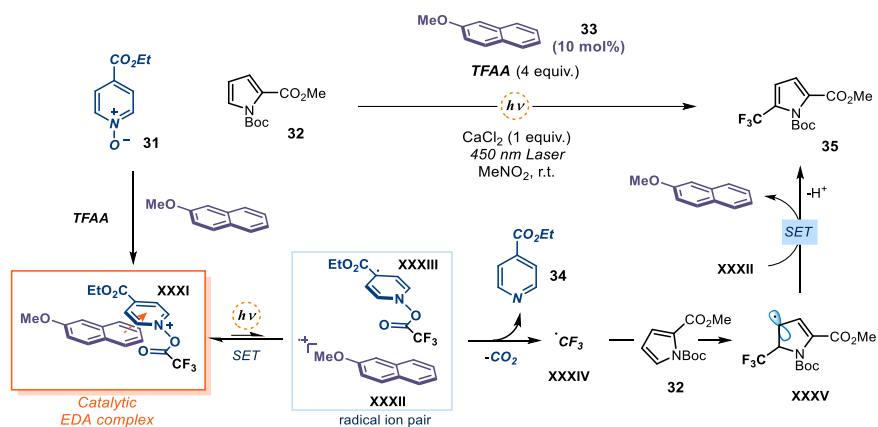
Another example of catalytic donor in an EDA complex photo-activation was reported by Bosque and Bach (Scheme 2.12).^{24d} In their case, 3-acetoxyquinuclidine **28** could be used as a catalytic donor to deliver an EDA complex with electron-poor tetrachlorophthalimide ester **27**. After photoexcitation of the EDA complex, **27** was reduced to provide an α -amino radical **XXIX** and tetrachlorophthalimide anion **30**. Then, another SET took place between α -amino radical **XXIX** and catalyst radical cation **XXVIII**, arising from the intra-complex charge transfer, to regenerate catalyst **28** and produce the iminium ion **XXX**. Eventually, iminium ion **XXX** recombined with the previously liberated tetrachlorophthalimide anion **30** to provide the final product **29**. The low quantum yield value ($\Phi = 0.02$) suggested that a radical chain pathway was insignificant compared to a closed catalytic cycle.



Scheme 2.12. Decarboxylative amination promoted by a catalytic EDA complex.

A crucial aspect for catalysis was the geometrically-constrained structure of the catalyst's quinuclidine core in **24**, which prevented α -deprotonation of the radical cation **XXV** that would lead to the degradation of the catalyst.

A latest example of a catalytic EDA system was reported by Stephenson and coworkers,^{24e} who developed trifluoromethylation of arenes in the absence of a conventional photocatalyst. In their case, pyridinium salt **XXXI** was readily formed in situ from the reaction between trifluoroacetic acid anhydride (TFAA) and *N*-oxide **31** (Scheme 2.13). While **XXXI** had no electron transfer interaction with heterocycle **32**, it formed an EDA aggregate upon the inclusion of a catalytic amount of electron-rich arene **33**. Light irradiation triggered an intra-complex SET to afford radical **XXXIII**, of which the labile N-O bond was cleaved to release trifluoromethyl radical **XXXIV** and pyridine **34** as byproduct. The ensuing radical **XXXIV** was trapped by heteroarene **32**, forging a new C-C bond. Finally, the intermediate **XXXV** was oxidized by the radical cation **XXXII** to regenerate catalyst **33**, providing product **35** after deprotonation.



Scheme 2.13. Catalytic EDA-promoted radical trifluoromethylation of heteroarenes.

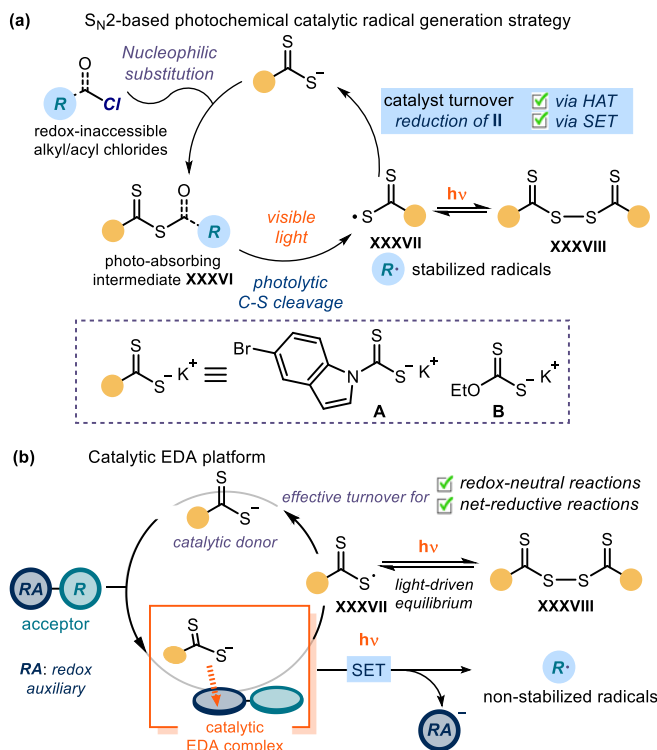
2.5 Target of the Project

The objective of this project was to develop a general catalytic EDA system that can activate various electron-deficient radical precursors using a catalytic donor. The aim is also that the resulting radicals engage in both redox-neutral and net-reductive radical processes, since the established catalytic EDA strategies only can promote redox-neutral processes.^{24a} This project was inspired by our previous research work of dithiocarbamate-based organic catalysts, designed for *nucleophilic* substitution activation.² We wondered whether the electron-rich property of these organocatalysts could be exploited to act as catalytic donors in EDA complex formation. Additionally, we sought to employ mechanistic investigations to determine if a closed catalytic cycle was operative in the developed reactions, providing evidence of the catalysts' ability to turnover and iteratively drive each catalytic cycle.

2.5.1 Design plan

We recently identified a photochemical catalytic strategy that used dithiocarbamates and xanthates as *nucleophilic* organocatalysts to generate radicals from simple alkyl (pseudo)halides (Scheme 2.14a). This methodology capitalized on the ability of the organocatalyst to undergo nucleophilic substitutions with alkyl electrophiles to form a photoactive intermediate **XXXVI** (Scheme 3.44a), which afforded radicals via homolytic cleavage of the weak C-S bond upon light excitation. However, only stabilized radicals (including benzyl, allyl, and radicals bearing either a heteroatom or an electron-withdrawing moiety at the α -position)

could be effectively generated and used in a variety of C-C and C-B bond forming processes.²



Scheme 2.14. (a) Nucleophilic substitution-based radical generation strategies. (b) Design of a catalytic EDA complex platform.

Extensive mechanistic investigation allowed us to elucidate the crucial aspect of this system, namely the mechanism of catalyst turnover. Specifically, we found that the sulfur radical **XXXVII**, which arose from the photolytic cleavage of the C-S bond within intermediate **XXXVI**, readily dimerized to form **XXXVIII**. In our system, there was a light-mediated equilibrium between dimer **XXXVIII** and the progenitor sulfur-centered radical **XXXVII**. Dimer **XXXVIII** was capable of absorbing light in the visible region, which then regenerated the parental radical **XXXVII**. This equilibrium was crucial for effective catalyst turnover because it imparted a longer lifetime to radical **XXXVII**.²⁹ We also demonstrated that the

²⁹ Leifert, D.; Studer, A., The Persistent Radical Effect in Organic Synthesis. *Angew. Chem. Int. Ed.* **2020**, *59*, 74-108.

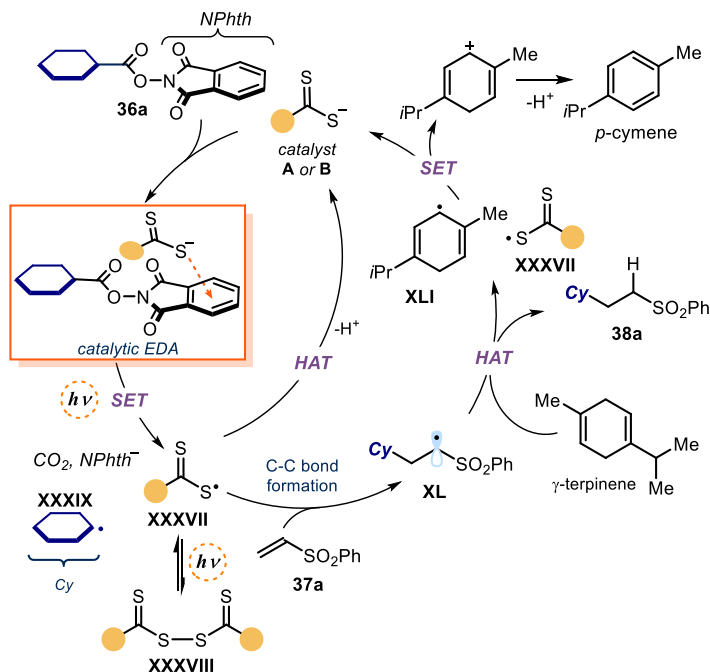
sulfur-centered **XXXVII** could be effectively turned over by either SET or HAT processes (e.g., by using γ -terpinene as the H-donor and/or SET reductant).

Considering that catalyst **A** and **B** could be easily turned over through two possible manifold and their electron-rich nature, we thought these organic catalysts could be used as catalytic donors to form photoactive EDA complex with a variety of electron-poor radical precursors (acceptor in Scheme 2.14b). Synthetically, it would be appealing to develop a general catalytic EDA platform based on the use of commercially available catalysts that enables the generation of a wide range of radicals and to engage them in mechanistically distinct reaction pathways, including reactions (e.g. net-reductive reactions) previously inaccessible by catalytic EDA photochemistry. Furthermore, this goal would significantly expand the synthetic potential and applicability of this family of organocatalysts beyond the S_N2 -based catalytic platform. For example, using radical precursor adorned with a purposely pre-installed electron-poor activating group, which served as both redox-auxiliary (**RA**, blue circle in Scheme 2.14b, which elicits EDA complex formation) and leaving group, would promote formation of previously inaccessible non-stabilized carbon radicals, including primary radicals, and nitrogen-centered radicals.

2.6 Results and Discussion

To assess the viability of the EDA complex catalytic strategy, we selected the reaction between cyclohexyl NHPI ester **36a** (suitable EDA acceptor)^{26a} and vinyl sulfone **37a**, catalyzed by the organic catalysts **A** and **B**. This transformation was chosen as a testbed as it required the formation of a non-stabilized cyclohexyl radical, which was not accessible through our previous S_N2 -based catalytic strategy. The proposed mechanism for the overall process is outlined in Scheme 2.15. Initially, the electron-rich donor catalysts (**A** or **B**) associated with the electron-deficient NHPI substrate **36a**, leading to the formation of a visible-light-absorbing EDA complex, which was feasible considering the tendency of stoichiometric thiolates and dithiocarbonyl anions to serve as donor partners for EDA complexes.³⁰

³⁰ (a) Liu, B.; Lim, C.-H.; Miyake, G. M. Visible-Light-Promoted C–S Cross-Coupling via Intermolecular Charge Transfer. *J. Am. Chem. Soc.* **2017**, *139*, 13616–13619. (b) Yang, M.; Cao, T.; Xu, T.; Liao, S., Visible-Light-Induced Deaminative Thioesterification of Amino Acid Derived Katritzky Salts via Electron Donor–Acceptor Complex Formation. *Org. Lett.* **2019**, *21*, 8673–8678. (c) Li, G.; Yan, Q.; Gan, Z.; Li, Q.; Dou, X.; Yang, D., Photocatalyst-Free Visible-



Scheme 2.15. Mechanistic plan for a net-reductive Giese-type addition manifold catalyzed by the excitation of a catalytic EDA complex; NPhth: phthalimide.

Visible-light irradiation triggered a SET process, generating the sulfur-centered radical **XXXVII** and the reduced NHPI ester, which provided cyclohexyl radical **XXXIX** after facile decarboxylation. **XXXIX** then underwent Giese-type addition to the electron-poor olefin **37a**, forging a new C-C bond and radical **XL**. This electrophilic radical then abstracted a hydrogen atom from a hydrogen atom donor (γ -terpinene) to deliver desired product **38a**. The sequence of these steps, involving the reduction of both the radical precursor **36a** (via SET) and intermediate **XL** (via HAT), characterized a net-reductive process. Crucially for catalyst turnover, the dithiocarbonyl radical **XXXVII** ($E_{ox} = 0.45\text{--}0.75$ V vs. SCE) need to be reduced. Our previous studies established that this reduction can occur through either an SET event from the cyclohexadienyl radical **XLI** ($E_{red} = -0.1$ V vs. SCE) or a HAT pathway from γ -terpinene.

Light-Promoted C(sp²)-S Coupling: A Strategy for the Preparation of S-Aryl Dithiocarbamates. *Org. Lett.* **2019**, *21*, 7938–7942. (d) Sundaravelu, N.; Nandy, A.; Sekar, G., Visible Light Mediated Photocatalyst Free C-S Cross Coupling: Domino Synthesis of Thiochromane Derivatives via Photoinduced Electron Transfer. *Org. Lett.* **2021**, *23*, 3115–3119.

2.6.1 Developing a Giese-type addition process³¹

In initial experiments, we investigated the reaction between NHPI ester **36a** and vinyl sulfone **37a** in dimethylacetamide (DMA) as the solvent.

Table 2.1. Optimization studies.

catalysts used in this study

$E^{ox} = +0.5 \text{ V}$
catalyst A

$E^{ox} = +0.75 \text{ V}$
catalyst B

$E^{ox} = +0.45 \text{ V}$
catalyst C

entry	catalyst	deviation	yield (%) ^a
1	A	none	81
2	B	none	95 (86) ^b
3	C	none	85
4	B	green LED (520 nm)	95
5	B	under air	0
6	B	no light	0
7	none	none	0
8	B	TEMPO (1.5 equiv.)	0

Reactions performed under inert atmosphere on a 0.1 mmol scale at 40 °C for 16 h under illumination by a blue LED strip ($\lambda_{max} = 465 \text{ nm}$, 14 W) using 1.5 equiv. of **36a** and 4 equiv. of γ -terpinene. Redox potentials of the catalysts measured in CH_3CN vs Ag/AgCl , see Experimental section. ^a Yield determined by ¹H NMR analysis of the crude mixture using trimethoxybenzene as the internal standard. ^b Yield of the isolated product **38a**. LED: Light-emitting diode. Cy: cyclohexyl, NPhth: phthalimide.

The reactions were carried out in the presence of γ -terpinene as the hydrogen atom donor (4 equiv.) and 10 mol% of various EDA donor catalysts. Irradiation was provided by a blue LED strip with a wavelength of 460 nm. The performance of three catalysts, namely the bromoindole-containing dithiocarbamate **A**, the more nucleophilic xanthogenate **B**,³² and the dithiocarbamate **C**, was evaluated (Table

³¹ The scope and optimization of the reaction detailed in this section was performed by Dr. Eduardo de Pedro Beato

³² Duan, X.-H.; Maji, B.; Mayr, H., Characterization of the nucleophilic reactivities of thiocarboxylate, dithiocarbonate and dithiocarbamate anions. *Org. Biomol. Chem.* **2011**, *9*, 8046-8050.

2.1). All three catalysts were capable of providing the desired Giese addition product **38a** in good yields (entries 1-3). Catalyst **B**, which offered slightly superior performance and greater accessibility, was selected for further investigations. The modularity of the dithiocarbamate/xanthogenate structure allows for the selection of the most suitable catalyst based on the desired photophysical and chemical properties, thereby providing versatility to the EDA complex catalytic platform.

Interestingly, we also observed that the reaction could be promoted by green light irradiation with a maximum emission wavelength of 520 nm (entry 4). Control experiments confirmed the requirement for both light and the donor catalyst (entries 6 and 7). The addition of TEMPO as a radical scavenger completely inhibited the reactivity (entry 8), and the trapping of the cyclohexyl radical **XXXIX** by TEMPO was observed.

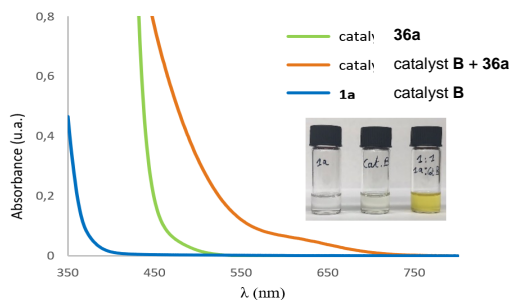


Figure 2.1. Optical absorption spectra, recorded in DMA in 1 cm path quartz cuvettes using a Shimadzu 2401PC UV-vis spectrophotometer, and visual appearance of the separate reaction components and of the colored EDA complex between catalyst **B** and **36a**. [**36a**] = 0.10 M, [catalyst **B**] = 0.01 M.

The formation of an EDA complex between catalyst **B** and NHPI ester **36a** was confirmed through UV/Vis spectroscopic analysis (Figure 2.1). Upon mixing both compounds, the initial colorless solution turned intensely yellow while a bathochromic shift of the absorption spectrum, diagnostic of a ground-state EDA complex, was observed.

In addition, transient absorption spectroscopy (TAS) was performed to directly detect the formation of the xanthy radical **XXXVIIIb**. Laser flash photolysis was performed on a 1:1 mixture of catalyst **B** and ester **36a**. The spectroscopic measurements revealed the existence of a transient species with absorption at 620

nm, consistent with the characteristic line shape of the xanthyl radical **XXXVII**.³³ Its half-lifetime was determined to be 0.1 ± 0.01 ms. This observation provides direct evidence that the photoinduced SET within the EDA complex is the crucial step for radical generation.

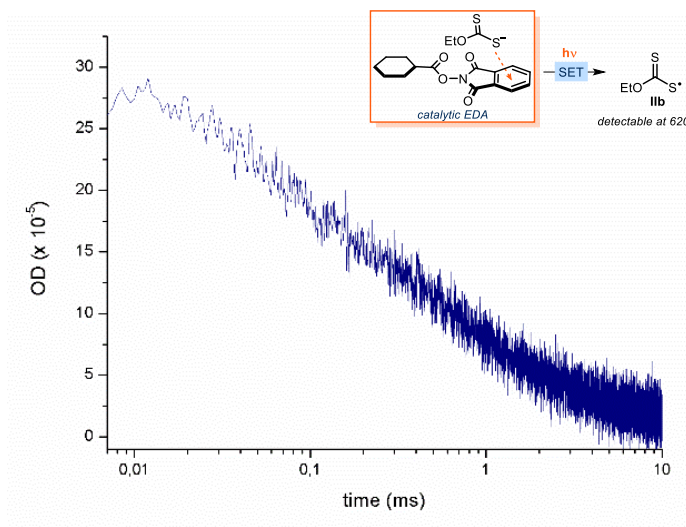


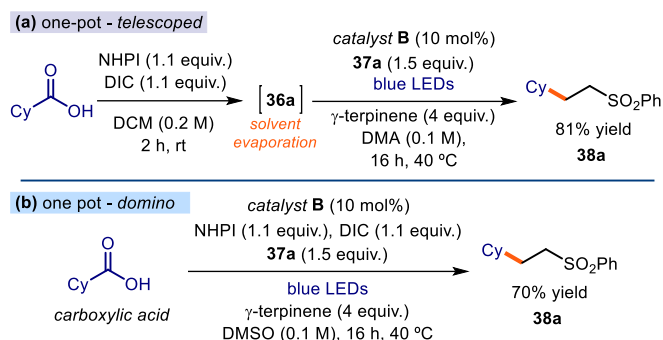
Figure 2.2. Absorption at 620 nm of the transient xanthyl radical **IIb** generated upon 355 nm laser excitation of a 1:1 mixture of **36a** and catalyst **B** 30 mM in DMA.

To gain further insight into the mechanism of the catalytic reaction, we measured the quantum yield (Φ) of the model reaction between **36a** and **37a** catalyzed by catalyst **B**. The measured quantum yield was found to be as low as 0.01 (see experimental section for the details), which indicates that the reaction does not proceed through a radical chain propagation mechanism, supporting the mechanistic scenario depicted in Scheme 2.15. The results align with the original plan of using catalyst **B** as an EDA catalyst, capable of regeneration while driving the formation of radicals in each catalytic cycle.

To enhance the synthetic practicality of this approach, a two-step telescoped sequence was implemented. By synthesizing redox-active ester **36a** in situ, commercial carboxylic acids could be directly used without the need for further purification (Scheme 2.16a). This one-pot telescoped procedure allowed for the direct transformation of a readily available carboxylic acid into product **38a**

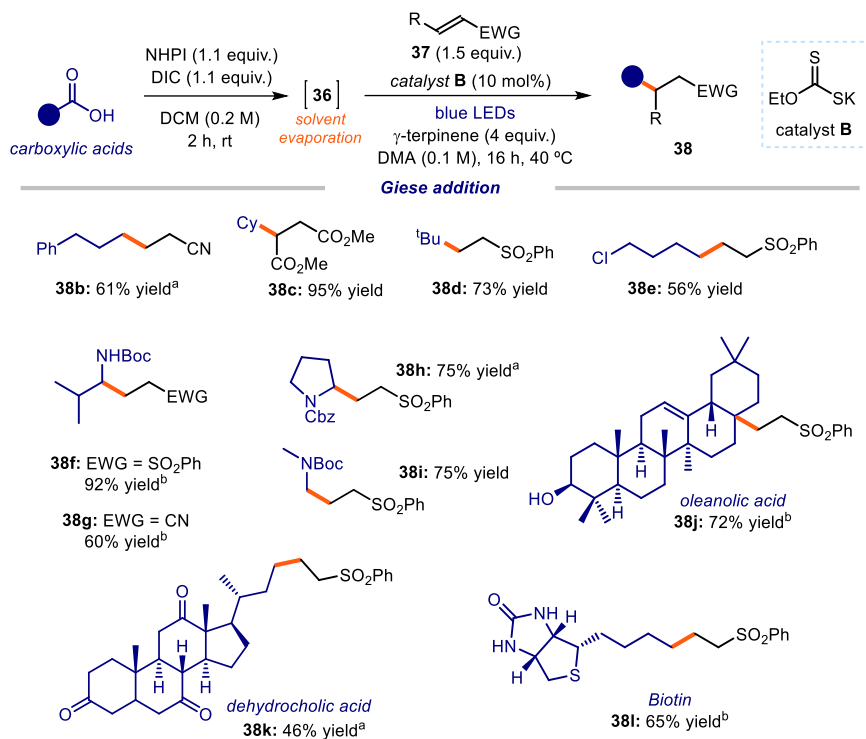
³³ Kaga, A.; Wu, X.; Lim, J. Y. J.; Hayashi, H.; Lu, Y.; Yeow, E. K. L.; Chiba, S., Degenerative xanthate transfer to olefins under visible-light photocatalysis. *Beilstein J. Org. Chem.* **2018**, *14*, 3047-3058.

without the isolation of NHPI ester intermediates **36a** in the process. Furthermore, we aimed to develop a domino protocol where all the reagents of the reaction could be added simultaneously (Scheme 2.16b). These strategies added a synthetically useful dimension to the EDA complex catalytic platform, enabling the direct functionalization of abundant aliphatic carboxylic acids as radical precursors.



Scheme 2.16. (a) One-pot two-step telescoped procedure to functionalize the carboxylic acid; the solvent was evaporated between the two steps. (b) Domino procedure, where all reagents were added at the same time. Yields refer to the isolated product **38a**. DIC: *N,N'*-diisopropylcarbodiimide; NHPI: *N*-(acyloxy)phthalimide; DCM: dichloromethane; Cy: cyclohexyl.

Using the telescoped procedure, we investigated the scope of the decarboxylative Giese-type addition (Scheme 2.17). We found that a wide range of carboxylic acids could be directly functionalized using this approach. Primary (products **38b**, **38e**), secondary (adduct **38c**), and tertiary radicals (product **38d**) were efficiently generated and intercepted by electron-deficient olefins **37** in good to excellent yields. The protocol was found to be compatible with various functional groups, including free alcohols (**38j**) and carbamates (**38f-i**). The selective formation of product **38e** was achieved through EDA aggregation in the presence of an electrophilic alkyl chloride. The method also could be used to access α -amino radicals (**38f-i**). Importantly, we demonstrated the applicability of this method for the direct functionalization of complex, bio-relevant compounds bearing unprotected polar functional groups. Dehydrocholic acid (**38k**), oleanolic acid (**38h**), and biotin (**38l**) were suitable substrates without the need for protection of the functional groups present in the scaffold. Notably, some products (**38g**, **38j**, and **38l**) were successfully obtained using the one-pot domino procedure directly from the carboxylic acid.



Scheme 2.17. EDA complex catalytic strategy for the generation of alkyl radicals from carboxylic acids and their use in decarboxylative Giese addition processes. Reactions performed on 0.2 mmol scale using 1 equiv. of acid; yields of products refer to isolated products **38** after purification; the bold orange bond denotes the newly formed C-C bonds. Unless otherwise indicated, all entries were performed using a telescoped sequence without isolation of the NHPI adduct **36** by simply evaporating the solvent (DCM) after completion of the first step. ^aUsing the preformed NHPI ester **36** as the radical precursor. ^bOne-pot domino procedure according to the conditions in Scheme 2.. NHPI: *N*-Hydroxyphthalimide, DIC: *N,N'*-Diisopropylcarbodiimide, Cbz: carboxybenzyl, EWG: electron-withdrawing group.

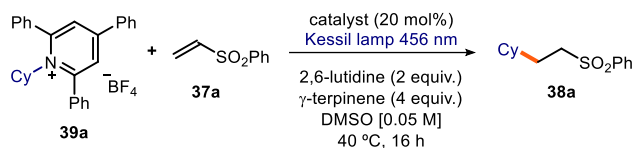
Pyridinium salts **39** also have been reported to engage in EDA complex formation.³⁴ We then investigated the activation of pyridinium salts **39** using the developed conditions (Table 2.2). Catalyst **A** was found to be more effective than catalyst **B** in this case (entry 1 vs. entry 2). This can be justified by the higher stability of catalyst **A** under relatively acidic conditions.³⁵ The results highlighted the significance of modularity in these donor catalysts, which could be tailored for optimal performance matching the different properties of electronically diverse

³⁴ Wu, J.; Grant, P. S.; Li, X.; Noble, A.; Aggarwal, V. K. Catalyst-Free Deaminative Functionalizations of Primary Amines by Photoinduced Single-Electron Transfer. *Angew. Chem., Int. Ed.* **2019**, *58*, 5697–5701.

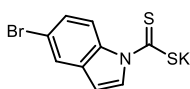
³⁵ As depicted in Scheme 2.16, a proton is released upon aromatization of the resulting cyclohexadienyl carbocation.

radical precursors. Control experiments further confirmed the necessity of both the catalyst (entry 7) and light (entry 6).

Table 2.2. Giese addition with pyridinium salts as radical precursors



catalysts used in this study



catalyst A

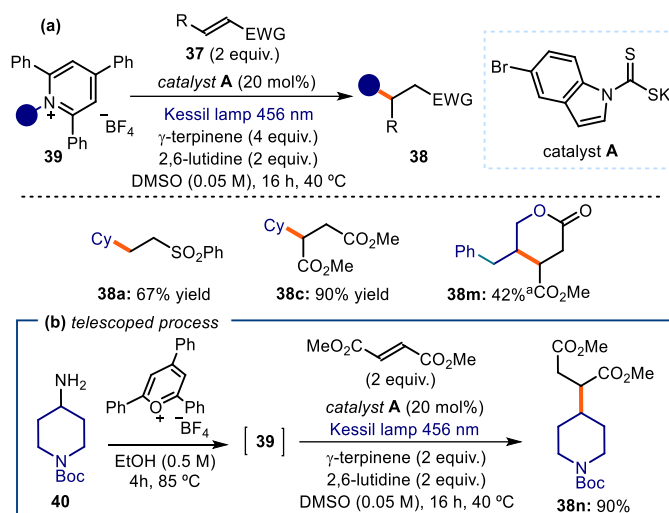


catalyst B

entry	catalyst	deviation	yield (%) ^a
1	A	none	83 (67) ^b
2	B	none	70
3	A	Green light	24
4	B	Green light	20
5	A	under air	0
6	A	no light	0
7	-	no catalyst	0

Reactions performed under inert atmosphere on a 0.1 mmol scale. ^aYield determined by ¹H NMR analysis of the crude mixture using trimethoxybenzene as the internal standard. ^bYield of the isolated product on a 0.2 mmol scale.

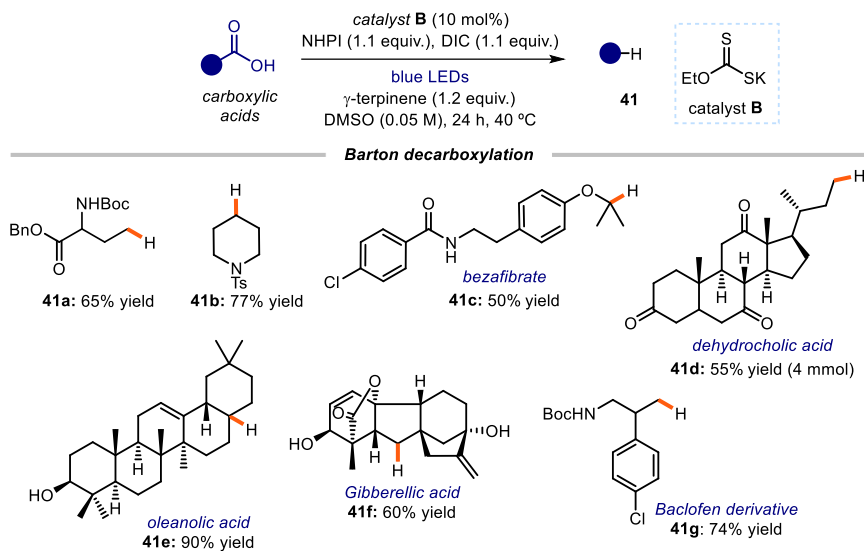
We demonstrated the successful reduction of pyridinium salts **39** using the donor catalyst under blue light irradiation, leading to the generation of non-stabilized secondary alkyl radicals. These radicals were then trapped by electron-deficient olefins **37** to form the desired products (Scheme 2.18a). The efficiency of the method was further highlighted by a one-pot telescoped procedure, where a primary amine **40** was subjected to a reaction with 2,4,6-triphenylpyridinium tetrafluoroborate at 85 °C for 4 hours. The resulting pyridinium salt **39** was directly used in the subsequent photochemical step without further purification, by simply adding the reagents sequentially (Scheme 2.18b).



Scheme 2.18. (a) EDA complex catalytic strategy for the deaminative Giese-type addition processes. ^aProduct **38m** was formed in a 3.8:1 ratio with the regioisomeric five-member ring adduct, see the Experimental section for details. (b) One-pot telescoped procedure for functionalization of amines. Reactions performed on 0.2 mmol scale.

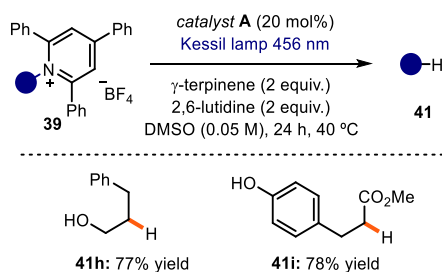
We extended the catalytic protocol to perform a Barton decarboxylation³⁶ process, wherein the EDA complex-based catalytic system generates alkyl radicals that undergo hydrogen atom abstraction (HAT) from γ-terpinene, resulting in defunctionalized reductive products **41**. By implementing a one-pot domino process, the xanthogenate catalyst **B** (10 mol. %) facilitated the decarboxylation of primary (**41a**), secondary (**41b**), and tertiary (**41c**) carboxylic acids. To demonstrate the applicability of this methodology in the reduction of complex bioactive molecules, we used Gibberellic acid (**41f**) and a baclofen derivative (**41g**), which gave the Barton decarboxylation products in 60% and 74% yield, respectively. Furthermore, a large-scale (4 mmol) functionalization of dehydrocholic acid yielded product **41d** in 55% yield, displaying the scalability of this method (Scheme 2.19).

³⁶ (a) Barton, D. H. R.; Crich, D.; Motherwell, W. B. New and Improved Methods for the Radical Decarboxylation of Acids. *J. Chem. Soc., Chem. Commun.* **1983**, 939–941. (b) Barton, D. H. R.; Crich, D.; Motherwell, W. B. The invention of new radical chain reactions. Part VIII. Radical chemistry of thiohydroxamic esters; A new method for the generation of carbon radicals from carboxylic acids. *Tetrahedron* **1985**, *41*, 3901–3924. For a recent application: (c) Qin, T.; Malins, L. R.; Edwards, J. T.; Merchant, R. R.; Novak, A. J. E.; Zhong, J. Z.; Mills, R. B.; Yan, M.; Yuan, C.; Eastgate, M. D.; Baran, P. S. Nickel-Catalyzed Barton Decarboxylation and Giese Reactions: A Practical Take on Classic Transforms. *Angew. Chem., Int. Ed.* **2017**, *56*, 260–265.



Scheme 2.19. EDA complex catalysis for the Barton decarboxylation. (a) Reactions performed on 0.2 mmol scale using a one-pot domino process; yields refer to isolated products **41** after purification; the bold orange bond denotes the newly formed bonds. DIC: *N,N'*-diisopropylcarbodiimide; Boc: *tert*-Butyloxycarbonyl; Bn: benzyl; Ts: *p*-methylphenylsulfonyl.

Finally, this catalytic process could also be applied to a deaminative reduction pathway. Pyridinium salts **39** could be reduced to products **41** in the absence of olefin **37** (Scheme 2.). As previously observed, the indole-based catalyst **A** outperformed **B** and **C** when this type of radical precursors was employed.



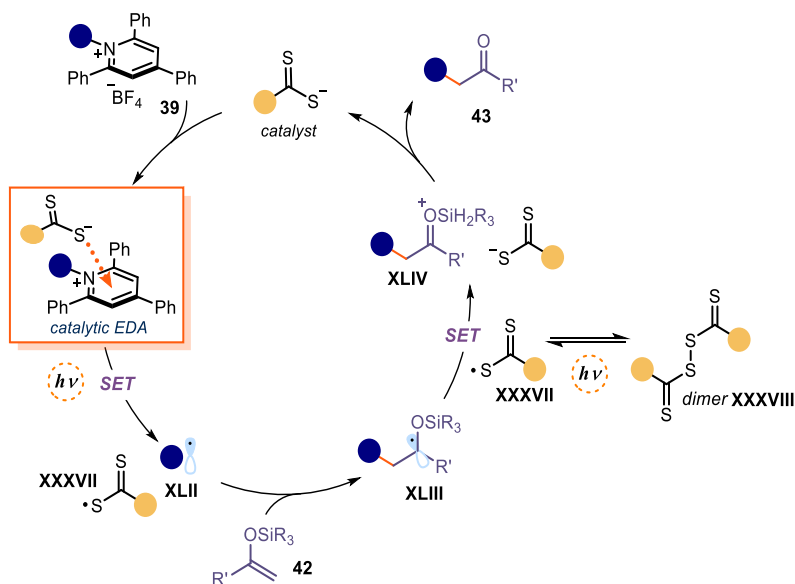
Scheme 2.20. EDA complex catalysis for deaminative reduction.

From a mechanistic standpoint, we measured the quantum yield of these reductive defunctionalization reactions and obtained a value of 0.01, which further supported that a radical chain process was highly unlikely, providing evidence for the ability of the EDA catalytic donor to undergo turnover and facilitate radical formation.

2.6.2 Redox-neutral processes³⁷

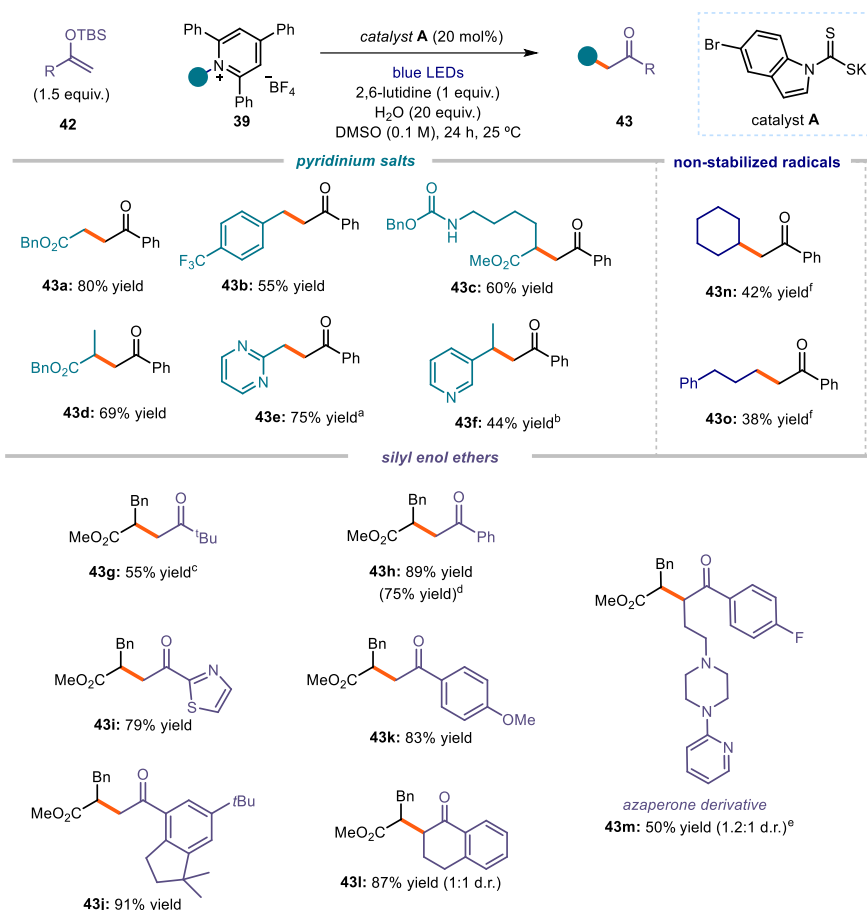
So far, we have used our platform to catalyze net-reductive transformations by using a sacrificial reductant (e.g., γ -terpinene) to turn-over the catalyst. In order to achieve a versatile and general catalytic EDA complex platform, we considered it meaningful to develop a redox-neutral process where one of the intermediates could promote catalyst turnover by reducing the dithiocarbonyl radical **XXXVII** through a SET event. The α -alkylation of silyl enol ethers **42** was identified as a suitable reaction to test this hypothesis. The proposed catalytic cycle, outlined in Scheme 2.21, involved the EDA aggregation of the pyridinium salt **39** with the donor organic catalyst. Under irradiation and subsequent SET, the radical **XLII** was generated. This open-shell species then reacted with the silyl enol ether **42**, leading to the formation of the α -oxy radical **XLIII**. A SET between **XLIII** and the sulfur-centered radical **XXXVII**, which was stabilized by a dimerization mechanism, would regenerate the catalyst and form the oxocarbenium ion **XLIV**. The latter intermediate can undergo hydrolysis to afford the final α -alkylation ketone product **43**. Importantly, the overall sequence involved reduction of the radical precursor **39** and oxidation of intermediate **XLIII**, constituting a redox-neutral process. Unlike previous processes, the effective turnover of the catalyst in this case required an SET between the sulfur radical **XXXVII** and a radical progenitor of the reaction product.

³⁷ The scope and optimization of the reaction detailed in this section was performed by Dr. Davide Spinato.



Scheme 2.21. Mechanistic plan for a redox neutral transformation catalyzed by the excitation of a catalytic EDA complex.

We successfully applied the indole-based dithiocarbamate catalyst **A** in this photochemical alkylation reaction. We chose pyridinium salts **39** as radical precursors because they are readily available from α -amino acid derivatives and can generate electrophilic radicals upon SET (Scheme 2.22). Silyl enol ethers **42** were used as electron-rich olefinic traps. Pyridinium salts **39** leading to primary, benzylic (products **43a**, **43b**), and secondary (product **43c-d**) radicals, were found to be competent substrates. Nitrogen-containing heterocycles were well-tolerated (products **43e-f**). Furthermore, we demonstrated that silyl enol ethers **42** derived aliphatic (product **43g**) ketones also could trap an electrophilic α -ester radical.



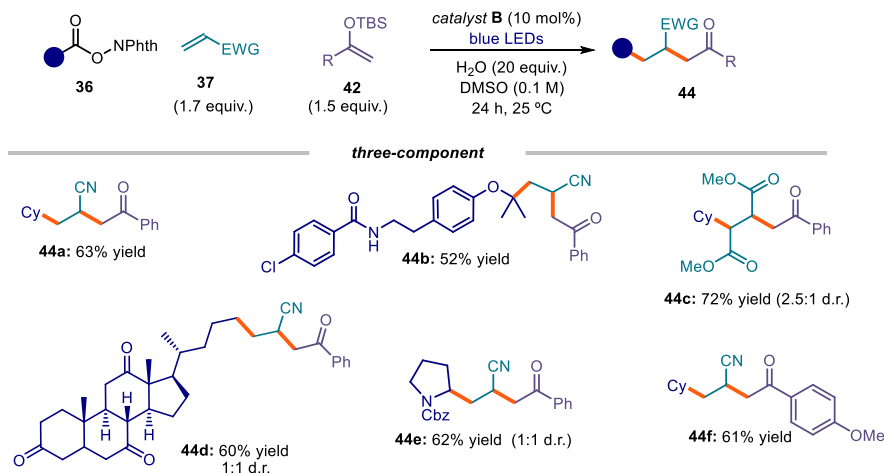
Scheme 2.22. Redox-neutral addition of alkyl radicals to silyl enol ethers under EDA complex catalysis. Reactions performed on 0.2 mmol scale using 2.0 mL of DMSO; yields refer to isolated products **43** after purification; the bold orange bond denotes the newly formed C-C bond. Unless otherwise indicated, all entries were performed at 25 °C. ^a40 °C; ^b60 °C; ^c1:1 mixture of DMSO/DCE used as solvent; ^din the absence of water; ^eusing alkyl *N*-(acyloxy)phthalimides **36** as radical precursors. TBS: *tert*-butyldimethylsilyl.

Various substituted group on the aryl ring, with different electronic or steric profiles (**43h-m**), could be accommodated. Finally, we tested NHPI esters as an alternative radical source, which allowed us to generate non-stabilized primary (**43o**) and secondary radicals (**43n-o**) and construct the corresponding ketone derivatives, although in lower yields due to the polarity mismatch of these electrophilic radicals with the silyl enol ethers.

Considering the different underlying mechanism with respect to previously studied net-reductive transformations, the quantum yield of this redox-neutral process was measured. The reaction leading to product **43h** yielded a low value of $\Phi = 0.02$ (λ

= 460 nm), supporting the mechanism described in Scheme 2.21, where catalyst **A** can undergo both reduction and oxidation processes, enabling effective turnover.

Based on the findings involving non-stabilized radicals, we explored the possibility to make advantage of the polarity mismatch between the reaction partners to develop a three-component reaction (Scheme 2.23). The proposed protocol operated as follows: the nucleophilic radical **XXXVI** formed by EDA activation would selectively react with the electron-poor alkene **33**. The resulting secondary electrophilic radical was then amenable for a second bond-forming event with the electron-rich silyl enol ether **42**, leading to the formation of a three-component coupled product **44**. The turnover of the catalyst in this cascade sequence relied on the same SET pathways depicted in Scheme 2.21. The xanthate catalyst **B** can efficiently catalyze this cascade reaction, providing a straightforward method for accessing structurally complex products **44** from readily available substrates **37** and **42** through an experimentally simple protocol.

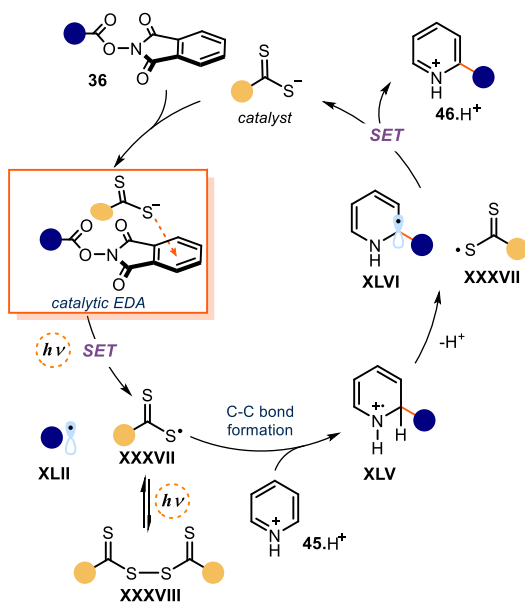


Scheme 2.23. Three-component process under EDA complex catalysis; NPhth: phthalimide.

2.6.3 Minisci reaction

We then aimed to evaluate if our EDA catalytic protocol could be applied to facilitate a redox-neutral transformation that was previously challenging to achieve exploiting the nucleophilicity of our dithiocarbamate-based catalysts. Specifically, we targeted the radical C-H alkylation of heteroarenes, known as the Minisci

reaction.³⁸ This reaction proceeds by the addition of nucleophilic radical **XLII** to a protonated electron-deficient heteroarene **45** to deliver intermediate **XLV**. Then this intermediate would require a final oxidation step for re-aromatization (Scheme 2.24). In the proposed catalytic cycle, the turnover of the catalyst would be promoted by the SET between the sulfur radical **XXXVII** ($E_{ox} = 0.45$ V vs. SCE) and intermediate **XLVI** ($E_{red} = -1.01$ V vs. SCE),³⁹ which should be a thermodynamically favorable process.



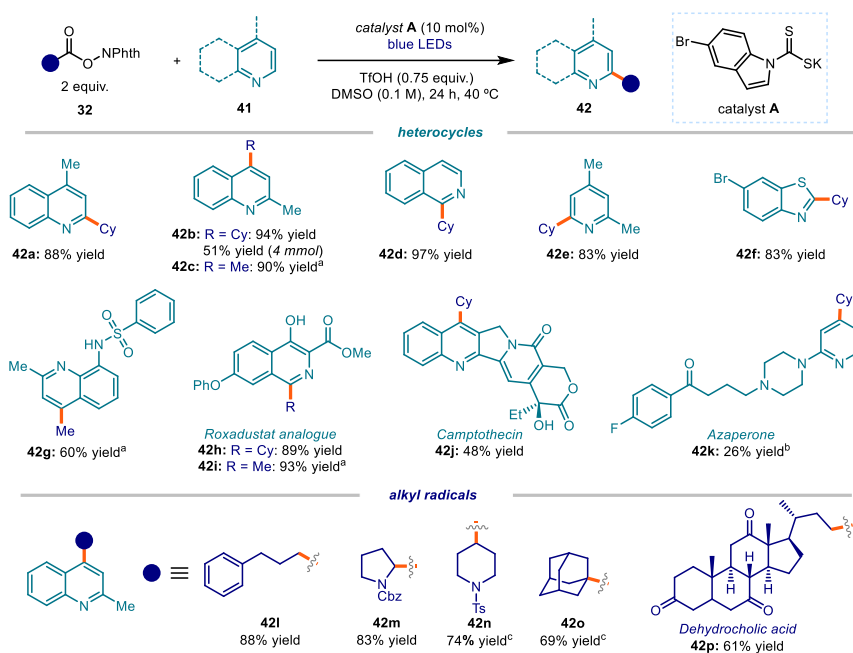
Scheme 2.24. Mechanistic proposal EDA catalyzed Minisci reaction.

This idea was accomplished by using catalyst **A** (10 mol %), which has better stability under the required acidic conditions of the Minisci process compared to catalyst **B**. By employing NHP esters **36** as radical precursors, we achieved the functionalization of heterocyclic aromatics **45** in good yields (Scheme 2.25). The method exhibited a broad applicability, enabling the functionalization of quinolines (products **46a-c**), isoquinolines (**46d**), and pyridines (**46e**). Moreover, the method

³⁸ (a) Minisci, F.; Bernardi, R.; Bertini, F.; Galli, R.; Perchinummo, M., Nucleophilic character of alkyl radicals—VI: A new convenient selective alkylation of heteroaromatic bases. *Tetrahedron* **1971**, *27*, 3575-3579; (b) Proctor, R. S. J.; Phipps, R. J., Recent Advances in Minisci-Type Reactions. *Angew. Chem. Int. Ed.* **2019**, *58*, 13666-13699.

³⁹ Bieszczad, B.; Perego, L. A.; Melchiorre, P., Photochemical C-H Hydroxyalkylation of Quinolines and Isoquinolines. *Angew. Chem. Int. Ed.* **2019**, *58*, 16878-16883.

showcased tolerance towards various functional groups, including protected amines (**46g**) and unprotected alcohols (**46h-j**). To further demonstrate the versatility of our methodology, we applied it to complex molecules such as *Roxadustat*, an intermediate involved in the synthesis of the HIF prolyl-hydroxylase inhibitor (products **46h-i**), the anticancer agent *camptothecin* (**46j**), and the neuroleptic drug *azaperone* (**46k**). By simply changing the solvent of the reaction to *N*-methyl-2-pyrrolidone (NMP), we successfully achieved the methylation of several heterocycles using an acetic acid derivative,⁴⁰ resulting in the formation of adducts **46c**, **46g**, and **46i**.



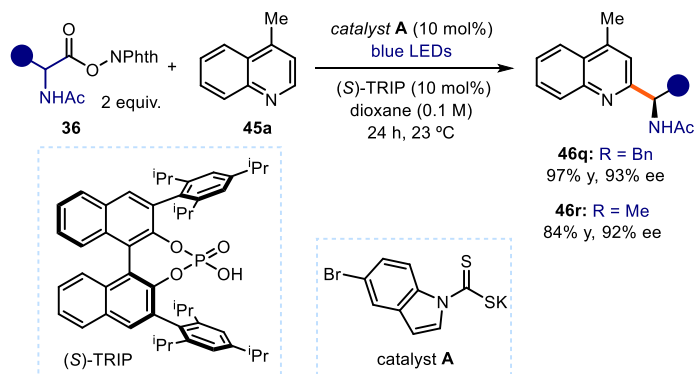
Scheme 2.25. Photochemical catalytic generation of alkyl radicals and their addition to heterocycles. Reactions performed on 0.2 mmol scale using 2.0 mL of DMSO; yields refer to isolated products **46** after purification; the bold orange bond denotes the newly formed C-C bond. ^aPerformed in NMP as solvent; ^b3 equiv. of TfOH; ^cperformed at 60 °C. Cy: cyclohexyl; Ts: tosyl; N-Phth: phthalimide.

⁴⁰ For a review in the importance of methylation in medicinal chemistry: Aynettinova, D.; Callens, M. C.; Hicks, H. B.; Poh, C. Y. X.; Shennan, B. D. A.; Boyd, A. M.; Lim, Z. H.; Leitch, J. A.; Dixon, D. J. Installing the “magic methyl” – C–H methylation in synthesis. *Chem. Soc. Rev.* **2021**, *50*, 5517–5563.

Finally, we demonstrated the successful generation of a variety of primary, secondary, and tertiary carbon-centered radicals from NHPI precursors **32** and their installation within 2-methylquinoline, leading to the formation of products **46l-p**.

The measured quantum yield of <0.01 ($\lambda = 460$ nm) indicated that a radical chain mechanism should not play any role in this catalytic cycle. This observation reinforced the role of donor catalyst **A** in promoting the photochemical generation of alkyl radicals and driving the overall Minisci reaction without the need for external oxidants.

In our efforts to further explore the capabilities of our catalytic EDA system, we then focused on the implementation of an asymmetric radical process (Scheme 2.26). Phipps and coworkers had recently reported an enantioselective version of the Minisci reaction utilizing chiral phosphoric acid catalysis. Prochiral radicals were generated from α -amino acid derivatives of type **36** using an external iridium-based photocatalyst. These radicals were then stereoselectively trapped by heteroarenes **45a** activated by the chiral acid ((*S*)-TRIP).⁴¹ Inspired by this work, we sought to achieve the same transformation by replacing the iridium-based photocatalyst with our EDA donor catalyst **A**. We successfully obtained products **46q** and **46r** in high yields and with excellent stereocontrol.

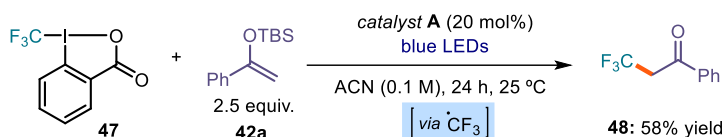


Scheme 2.26. Application in enantioselective radical catalysis; Ac: acetyl; NPhth: phthalimide.

⁴¹ Ermanis, K.; Colgan, A. C.; Proctor, R. S. J.; Hadrys, B. W.; Phipps, R. J.; Goodman, J. M., A Computational and Experimental Investigation of the Origin of Selectivity in the Chiral Phosphoric Acid Catalyzed Enantioselective Minisci Reaction. *J. Am. Chem. Soc.* **2020**, *142*, 21091-21101.

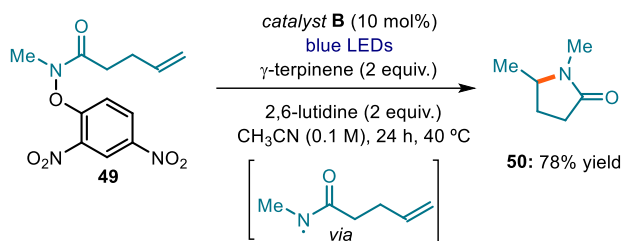
2.6.4 Further application of the EDA catalytic system

We then explored the use of our EDA catalytic radical generation approach for the introduction of trifluoromethyl groups into organic molecules. We used catalyst **A**, the Togni reagent **47** as the EDA complex acceptor, and silyl enol ether **42a** as an efficient trapping agent to achieve the desired transformation (Scheme 2.27). Through the EDA activation of the Togni reagent **47** by catalyst **A**, a trifluoromethyl radical was generated and intercepted by the silyl enol ether **42a**, resulting in the α -trifluoromethyl ketone product **48**.⁴²



Scheme 2.27. Trifluoromethylation of ketones via EDA complex catalysis.

The generation of amidyl radicals using xanthate catalyst **B** was also explored. Specifically, we employed the dinitrophenoxy amide **49** as the radical precursor to generate a transient amidyl radical (Scheme 2.28).⁴³ This amidyl radical then underwent an intramolecular radical cyclization, delivering of the lactam product **50** in high yield.



Scheme 2.28. Amidyl radical formation and cyclization.

⁴² (a) Cheng, Y.; Yu, S. Hydrotrifluoromethylation of Unactivated Alkenes and Alkynes Enabled by an Electron-Donor–Acceptor Complex of Togni’s Reagent with a Tertiary Amine. *Org. Lett.* **2016**, *18*, 2962–2965. (b) Tu, H.-Y.; Zhu, S.; Qing, F.-L.; Chu, L. A four-component radical cascade trifluoromethylation reaction of alkenes enabled by an electron-donor–acceptor complex. *Chem. Commun.* **2018**, *54*, 12710–12713.

⁴³ Davies, J.; Booth, S. G.; Essafi, S.; Dryfe, R. A. W.; Leonori, D. “Visible-Light-Mediated Generation of Nitrogen-Centered Radicals: Metal-Free Hydroimination and Iminohydroxylation Cyclization Reactions” *Angew. Chem. Int. Ed.* **2015**, *54*, 14017–14021.

2.7 Conclusions

In summary, we have successfully developed a versatile catalytic EDA complex system based on our previously designed organic catalysts, where they served as catalytic donors. These catalysts readily formed EDA complexes with a wide range of radical precursors, enabling the generation of both stabilized and non-stabilized alkyl radicals under mild conditions. We have used these generated radicals to design and execute various synthetic transformations. Inspired by the knowledge of our catalyst behavior from previous study, we have developed mechanistically distinct processes, including redox-neutral and net-reductive radical transformations. By quantum yield determination, we have confirmed that these processes proceed via closed catalytic cycles, demonstrating the ability of the EDA catalysts to turnover and drive the radical generation and transformation steps iteratively. The catalysts' stability and high functional group tolerance have been proven advantageous in the direct functionalization of diverse functional groups, such as aliphatic carboxylic acids and amines, as well as in late-stage elaboration of biologically relevant compounds and enantioselective radical catalysis.

2.8 Experimental section

2.8.1 General information

The NMR spectra are available in the published manuscript¹ and are not reported in the present dissertation.

The NMR spectra were recorded at 400 MHz and 500 MHz for ¹H and 100 or 125 MHz for ¹³C. The chemical shift (δ) for ¹H and ¹³C are given in ppm relative to residual signals of the solvents (CHCl₃ @ 7.26 ppm ¹H NMR and 77.16 ppm ¹³C NMR, and tetramethylsilane @ 0 ppm). Coupling constants are given in Hertz. The following abbreviations are used to indicate the multiplicity: s, singlet; d, doublet; q, quartet; m, multiplet; bs, broad signal; app, apparent.

High resolution mass spectra (HRMS) were obtained from the ICIQ HRMS unit on MicroTOF Focus and Maxis Impact (Bruker Daltonics) with electrospray ionization. (ESI). UV-vis measurements were carried out on a Shimadzu UV-2401PC spectrophotometer equipped with photomultiplier detector, double beam optics and D₂ and W light sources or an Agilent Cary60 spectrophotometer. Emission spectra of light sources were recorded on Ocean Optics USB4000 fiber optic spectrometer.

Yields of isolated products refer to materials of >95% purity as determined by ^1H NMR.

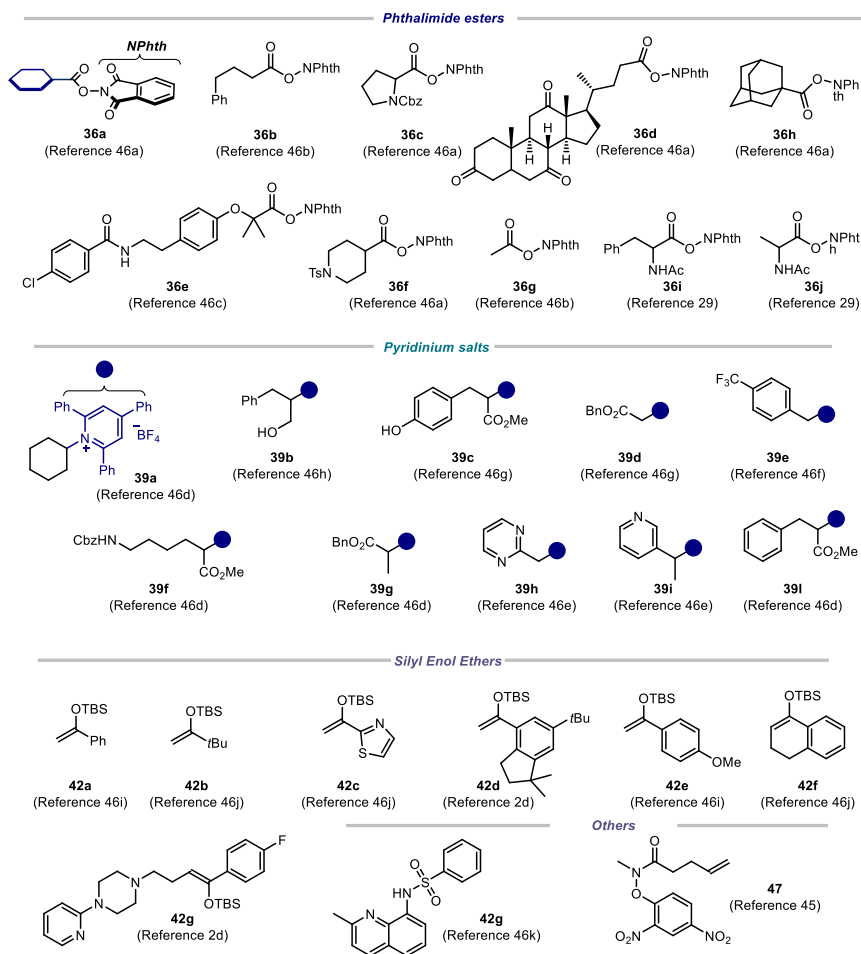
General Procedures. All reactions were set up under an argon atmosphere in oven-dried glassware. Synthesis grade solvents were used as purchased, anhydrous solvents were taken from a commercial SPS solvent dispenser. Chromatographic purification of products was accomplished using forced-flow chromatography (FC) on silica gel (35-70 mesh). For thin layer chromatography (TLC) analysis throughout this work, Merck pre-coated TLC plates (silica gel 60 GF₂₅₄, 0.25 mm) were employed, using UV light as the visualizing agent and an acidic mixture of vanillin or basic aqueous potassium permanganate (KMnO_4) stain solutions, and heat as developing agents. Organic solutions were concentrated under reduced pressure on a Büchi rotatory evaporator.

Determination of Enantiomeric Purity. HPLC analysis on chiral stationary phase was performed on an Agilent 1200-series instrument, employing Daicel Chiralpak IC column.

Materials. Most of the starting materials used in this study are commercial and were purchased in the highest purity available from Sigma-Aldrich, Fluka, Alfa Aesar, Fluorochem, and used as received, without further purifications.

2.8.2 Substrate synthesis

The following substrates were synthesized according to reported procedures (Scheme)⁴⁴



Scheme 2.29. Starting materials synthesized according to known procedures.

⁴⁴ (a) Qin, T.; Malins, L. R.; Edwards, J. T.; Merchant, R. R.; Novak, A. J. E.; Zhong, J. Z.; Mills, R. B.; Yan, M.; Yuan, C.; Eastgate, M. D.; Baran, P. S., Nickel-Catalyzed Barton Decarboxylation and Giese Reactions: A Practical Take on Classic Transforms. *Angew. Chem., Int. Ed.* **2017**, *56*, 260-265. (b) Huihui, K. M. M.; Caputo, J. A.; Melchor, Z.; Olivares, A. M.; Spiewak, A. M.; Johnson, K. A.; DiBenedetto, T. A.; Kim, S.; Ackerman, L. K. G.; Weix, D. J., Decarboxylative Cross-Electrophile Coupling of N-Hydroxyphthalimide Esters with Aryl Iodides. *J. Am. Chem. Soc.* **2016**, *138*, 5016-5019. (c) Ishii, T.; Kakeno, Y.; Nagao, K.; Ohmiya, H., N-Heterocyclic Carbene-Catalyzed Decarboxylative Alkylation of Aldehydes. *J. Am. Chem.*

2.8.3 Experimental setups

2.8.3.1 Set-up 1 - 3D printed reactor with LED strip

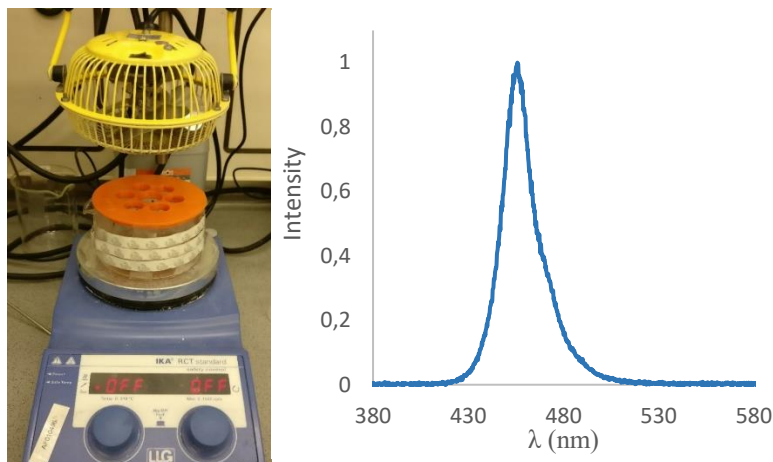


Figure 2.3. Blue LEDs photoreactor used for reactions where temperature control was not needed (*left*). Emission spectrum of the 465 nm LED strip used in this reactor (*right*).

For reactions performed using a blue LED strip as the light source, a 3D-printed photoreactor was used. It consists of a 9 cm diameter crystallizing dish with a 3D printed support of 6 positions, and a hole of 22 mm in the middle to allow ventilation (Figure 2.3, left). A commercial 1-meter LED strip was wrapped around the crystallizing dish, while a fan was used to cool down the reactor (the reaction temperature was measured to be between 35–40 °C). Each of the positions could be used to fit a standard 16 mm diameter vial with a Teflon screw cap. Experiments

Soc. **2019**, *141*, 3854-3858. (d) Klauck F. J. R.; James M. J.; Glorius F., Deaminative Strategy for the Visible-Light-Mediated Generation of Alkyl Radicals. *Angew. Chem., Int. Ed.* **2017**, *56*, 12336-12339. (e) Liao J.; Guan W.; Boscoe B. P.; Tucker J. W.; Tomlin J. W.; Garnsey M. R.; Watson M. P., Transforming Benzylic Amines into Diarylmethanes: Cross-Couplings of Benzylic Pyridinium Salts via C–N Bond Activation. *Org. Lett.* **2018**, *20*, 3030-3033. (f) Xia Q.; Li Y.; Wang X.; Dai P.; Deng H.; Zhang W.-H. Visible Light-Driven α -Alkylation of N-Aryl tetrahydroisoquinolines Initiated by Electron Donor–Acceptor Complexes. *Org. Lett.* **2020**, *22*, 7290-7294. (g) Laroche B.; Tang X.; Archer G.; Di Sanza R.; Melchiorre P., Photochemical Chemoselective Alkylation of Tryptophan-Containing Peptides. *Org. Lett.* **2021**, *23*, 285-289. (h) Lai S.-Z.; Yang Y.-M.; Xu H.; Tang Z.-Y.; Luo Z., Photoinduced Deaminative Coupling of Alkylpyridium Salts with Terminal Arylalkynes. *J. Org. Chem.* **2020**, *85*, 15638-15644. (i) Perrotta D.; Racine S.; Vuilleumier J.; de Nanteuil F.; Waser J., [4 + 2]-Annulations of Aminocyclobutanes. *Org. Lett.* **2015**, *17*, 1030-1033. (j) Li Y.; Liu J.; Zhao S.; Du X.; Guo M.; Zhao W.; Tang X.; Wang G., Copper-Catalyzed Fluoroolefination of Silyl Enol Ethers and Ketones toward the Synthesis of β -Fluoroenones. *Org. Lett.* **2018**, *20*, 917-920. (k) Perez C.; Barkley-Levenson A. M.; Dick B. L.; Glatt P. F.; Martinez Y.; Siegel D.; Momper J. D.; Palmer A. A.; Cohen S. M., Metal-Binding Pharmacophore Library Yields the Discovery of a Glyoxalase 1 Inhibitor. *J. Med. Chem.* **2019**, *62*, 1609-1625.

at 465 nm were conducted using a 1m strip, 14.4W “LEDXON MODULAR 9009083 LED, SINGLE 5050” purchased from Farnell, catalog number 9009083. The emission spectrum of these LEDs is shown in Figure 2.3, right panel.

2.8.3.2 Set-up 2 - Kessil lamp setup

For reactions performed with a Kessil lamp, the irradiation set-up consisted of a 50 W Kessil blue LED lamp (PR160L-456, 100% intensity, 2-3 cm away – Figure 2.4).

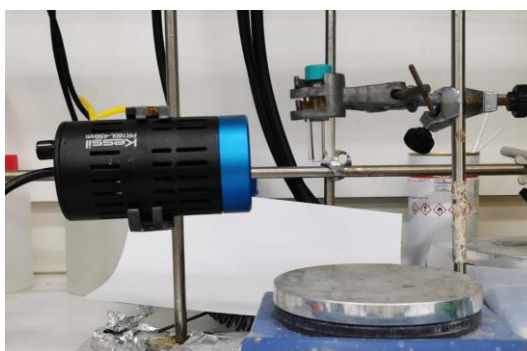


Figure 2.4. Kessil lamp set-up.

2.8.3.3 Set-up 3 - Temperature-controlled 4-position reactor with LED strip

For reactions where temperature control was employed, the photoreactor consisted of a 12.5 cm diameter jar fitted with 4 standard B29 size quickfit-glass joints arranged around a central B29 size joint. A commercial 1-meter LED strip was wrapped around the jar, followed by a layer of aluminium foil and cotton for insulation (Figure 2.5).

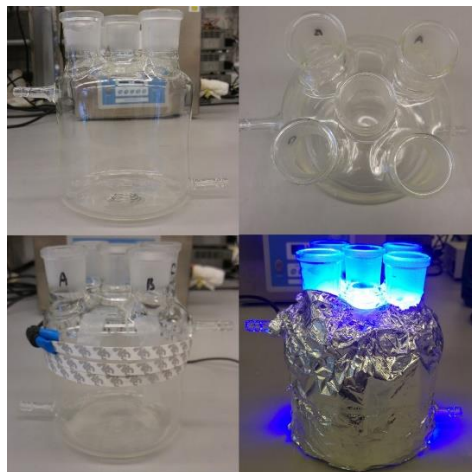


Figure 2.5. Photoreactor used for temperature-controlled reactions - pictures taken at different stages of the set-up assembly.

Each of the joints could be used to fit a standard 16 mm or 25 mm diameter Schlenk tube with a Teflon adaptor (Figure 2.6).



Figure 2.6. Teflon adaptors to use Schlenk tubes in the photoreactor.

An inlet/outlet system provided circulation of liquid (ethylene glycol/water mixture) from a Huber Minichiller 300 inside the jar. This setup allowed the performance of reactions at temperatures ranging from $-20\text{ }^{\circ}\text{C}$ to $80\text{ }^{\circ}\text{C}$ with accurate control of the reaction temperature ($\pm 1^{\circ}\text{C}$, Figure 2.7). In order to maintain consistent illumination between different experiments, only the four external positions were used to perform reactions. The central position was used to monitor the temperature using a thermometer inside another inserted Schlenk tube identical to those used to perform reactions, ensuring that the reaction mixtures were at the desired temperature.

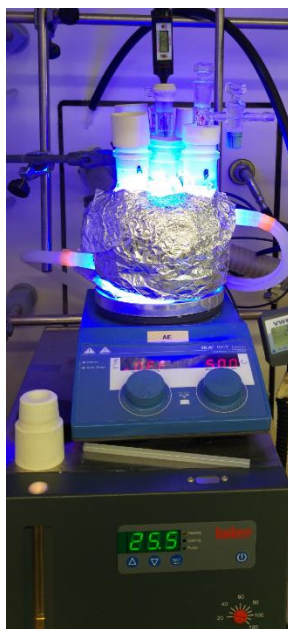


Figure 2.7. Fully assembled temperature-controlled photoreactor in operation.

2.8.3.4 Set-up 4 - Temperature controlled one-position reactor with LED strip

Our photoreactor for the enantioselective version of the Minisci reaction consisted of a consisted of a 4 cm diameter jar fitted with a standard 29 sized ground glass joint. A commercial 1 meter LED strip was wrapped around the jar, followed by a layer of aluminium foil and cotton for insulation. An inlet and an outlet allow the circulation of liquid from a Huber Minichiller 300 inside the jar. This setup allows to perform reactions at temperatures ranging from -20 °C to 80 °C with accurate control of the reaction temperature (± 1 °C). An inlet and an outlet allow the circulation of liquid from a Huber Minichiller 300 inside the jar. This setup allows to perform reactions at temperatures ranging from -20 °C to 80 °C with accurate control of the reaction temperature (± 1 °C, Figure 2.8).

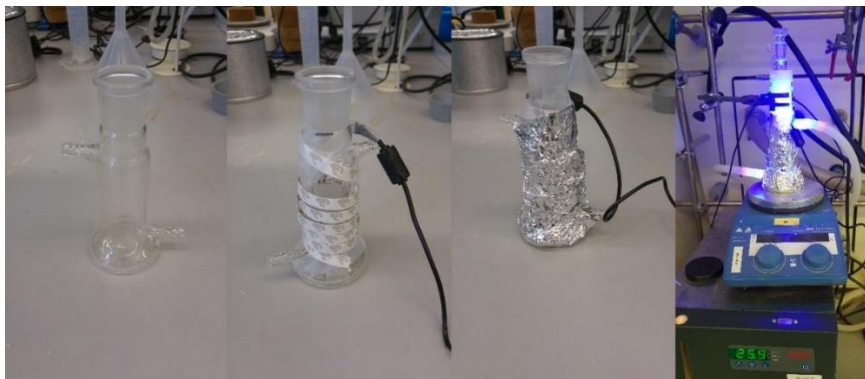
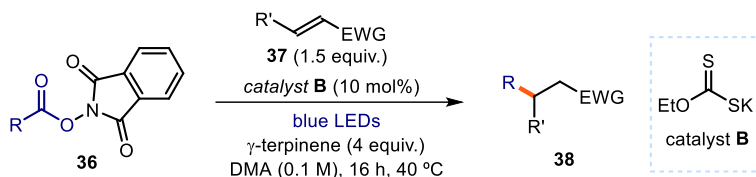


Figure 2.8. Fully assembled controlled temperature photoreactor in operation for enantioselective Minisci reaction.

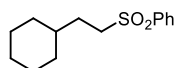
2.8.4 Giese addition

2.8.4.1 General procedure A



Reactions performed using *set-up 1* in Figure 2.3. In an oven dried vial with a Teflon septum screw cap, potassium ethyl xanthogenate **B** (3.2 mg, 0.02 mmol, 0.1 equiv.), *N*-hydroxyphthalimide ester **36** (0.2 mmol, 1 equiv.) and the electron-poor olefin **37** (0.3 mmol, 1.5 equiv., *if solid*), were dissolved in DMA (2 mL, synthesis grade solvent). Then, γ -terpinene (128 μ L, 0.8 mmol, 4 equiv.) was added. The resulting orange mixture was degassed with argon sparging for 60 seconds. If the electron-poor olefin **37** was *liquid*, it was added via syringe after the argon sparging. The vial was then placed in the 3D printed support photoreactor and irradiated under stirring for 16 hours, unless otherwise specified. The mixture was transferred to an extraction funnel, NaOH 1M solution was added, and the organic layer was extracted with DCM. The organic layer was washed with brine twice. The combined organic layers were dried over anhydrous MgSO_4 , filtered, and concentrated to dryness. The crude residue was purified by column chromatography to afford the corresponding product **38** in the stated yield with >95% purity according to ^1H NMR analysis.

2.8.4.2 Characterization of products with general procedure A

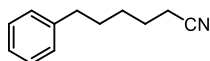


2-(2-(phenylsulfonyl)ethyl)cyclohexane (38a): Synthesized according to General Procedure A using 1,3-dioxoisindolin-2-yl cyclohexanecarboxylate **36a** (54.5 mg, 0.2 mmol, 1 equiv.) and phenyl vinyl sulfone **37a** (50.4 mg, 0.3 mmol, 1.5 equiv.). The crude mixture was purified by flash column chromatography on silica gel (5% AcOEt in hexanes as eluent) to afford **38a** (43.5 mg, 86% yield) as a white solid.

¹H NMR (500 MHz, CDCl₃) δ 7.94 – 7.85 (m, 2H), 7.69 – 7.61 (m, 1H), 7.61 – 7.52 (m, 2H), 3.13 – 3.05 (m, 2H), 1.71 – 1.54 (m, 7H), 1.28 (ddt, *J* = 14.6, 7.5, 3.8 Hz, 1H), 1.23 – 1.06 (m, 3H), 0.92 – 0.76 (m, 2H).

¹³C NMR (126 MHz, CDCl₃) δ 139.4, 133.7, 129.4, 128.2, 54.5, 36.8, 32.9, 29.7, 26.4, 26.1.

Matching reported literature data.⁴⁵

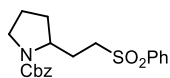


6-phenylhexanenitrile (38b): Synthesized according to General Procedure A using 5 equiv. of γ -terpinene, 1,3-dioxoisindolin-2-yl 4-phenylbutanoate **36b** (62 mg, 0.2 mmol, 1 equiv.) and acrylonitrile **37b** (26.3 μ L, 0.4 mmol, 2 equiv.). The crude mixture was purified by flash column chromatography on silica gel (5% AcOEt in hexanes as eluent) to afford **38b** (21 mg, 61% yield) as a yellow oil.

¹H NMR (400 MHz, CDCl₃) δ 7.33 – 7.24 (m, 2H), 7.23 – 7.14 (m, 3H), 2.64 (t, *J* = 7.6 Hz, 2H), 2.33 (t, *J* = 7.1 Hz, 2H), 1.75 – 1.62 (m, 4H), 1.54 – 1.42 (m, 2H).

¹³C NMR (101 MHz, CDCl₃) δ 142.1, 128.5, 128.5, 126.0, 119.9, 35.7, 30.7, 28.4, 25.4, 17.2.

Matching reported literature data.⁴⁶



Benzyl 2-(2-(phenylsulfonyl)ethyl)pyrrolidine-1-carboxylate (38h): Synthesized according to General Procedure A using 1-benzyl 2-(1,3-dioxoisindolin-2-yl) pyrrolidine-1,2-dicarboxylate **36c** (54.5 mg, 0.2 mmol, 1 equiv.) and phenyl vinyl sulfone **37a** (50.4 mg, 0.3 mmol,

⁴⁵ Chen, X.; Luo, X.; Peng, X.; Guo, J.; Zai, J.; Wang, P., Catalyst-Free Decarboxylation of Carboxylic Acids and Deoxygenation of Alcohols by Electro-Induced Radical Formation. *Chem. Eur. J.* **2020**, *26*, 3226-3230.

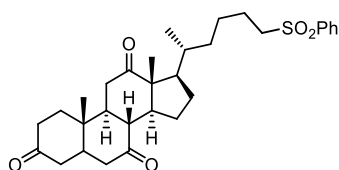
⁴⁶ Bhunia, A.; Bergander, K.; Studer, A., Cooperative Palladium/Lewis Acid-Catalyzed Transfer Hydrocyanation of Alkenes and Alkynes Using 1-Methylcyclohexa-2,5-diene-1-carbonitrile. *J. Am. Chem. Soc.* **2018**, *140*, 16353-16359.

1.5 equiv.). The crude mixture was purified by flash column chromatography on silica gel (20% AcOEt in hexanes as eluent) to afford **38h** (56 mg, 75% yield) as a white solid.

¹H NMR (400 MHz, CDCl₃) mixture of rotamers: δ 7.96 – 7.77 (m, 2H), 7.68 – 7.60 (m, 1H), 7.54 (d, *J* = 7.5 Hz, 2H), 7.40 – 7.20 (m, 5H), 5.05 (d, *J* = 7.6 Hz, 2H), 3.94 (d, *J* = 9.9 Hz, 1H), 3.58 – 3.28 (m, 2H), 3.27 – 2.91 (m, 2H), 2.23 – 1.74 (m, 5H), 1.63 (ddd, *J* = 11.3, 5.5, 3.0 Hz, 1H).

¹³C NMR (101 MHz, CDCl₃) mixture of rotamers: δ 155.5, 139.3, 136.9, 133.8, 129.4, 128.6, 128.1, 127.9, 67.2, 66.9, 56.5, 55.9, 54.0, 53.7, 46.9, 46.5, 31.2, 30.7, 27.9, 23.8, 23.1.

Matching reported literature data.⁴⁷



(5S,8R,9S,10S,13R,14S,17R)-10,13-dimethyl-17-(6-(phenylsulfonyl)hexan-2-yl)dodecahydro-3H-cyclopenta[a]phenanthrene-3,7,12(2H,4H)-trione (38k): Synthesized according to General

Procedure A using 1,3-dioxoisindolin-2-yl 4-((5S,8R,9S,10S,13R,14S,17R)-10,13-dimethyl-3,7,12-trioxohexadecahydro-1H-cyclopenta[a]phenanthren-17-yl)pentanoate **36d** (54.5 mg, 0.2 mmol, 1 equiv.) and phenyl vinyl sulfone **37a** (50.4 mg, 0.3 mmol, 1.5 equiv.). The crude mixture was purified by flash column chromatography on silica gel (50% AcOEt in hexanes as eluent) to afford **38k** (48.0 mg, 46% yield) as a white solid.

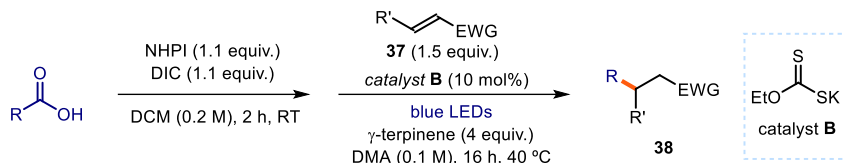
¹H NMR (400 MHz, CDCl₃) δ 7.95 – 7.85 (m, 2H), 7.70 – 7.61 (m, 1H), 7.61 – 7.53 (m, 2H), 3.16 – 3.00 (m, 2H), 2.95 – 2.78 (m, 3H), 2.38 – 2.17 (m, 6H), 2.16 – 2.06 (m, 2H), 2.02 – 1.90 (m, 4H), 1.88 – 1.52 (m, 5H), 1.47 – 1.30 (m, 1H), 1.39 (s, 3H), 1.32 – 1.12 (m, 5H), 1.04 (s, 3H), 0.78 (d, *J* = 6.6 Hz, 3H).

¹³C NMR (101 MHz, CDCl₃) δ 212.1, 209.1, 208.9, 139.4, 133.8, 129.4, 128.2, 57.0, 56.5, 51.9, 49.1, 47.0, 45.8, 45.7, 45.1, 42.9, 38.8, 36.6, 36.2, 35.9, 35.4, 34.9, 28.0, 25.4, 25.3, 23.1, 22.0, 19.0, 12.0.

Matching reported literature data.⁴⁵

⁴⁷ Chu, L.; Ohta, C.; Zuo, Z.; MacMillan, D. W. C., Carboxylic Acids as A Traceless Activation Group for Conjugate Additions: A Three-Step Synthesis of (±)-Pregabalin. *J. Am. Chem. Soc.* **2014**, *136*, 10886-10889.

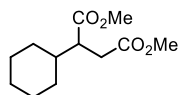
2.8.4.3 General procedure B (one-pot telescoped from carboxylic acids)



Reactions performed using *set-up 1* in Figure 2.3. In an oven dried vial with a Teflon septum screw cap, carboxylic acid (0.2 mmol, 1 equiv.) and *N*-hydroxyphthalimide (NHPI, 35.8 mg, 0.22 mmol, 1.1 equiv.) were dissolved in CH_2Cl_2 (1 mL, HPLC grade) and *N,N'*-diisopropylcarbodiimide (DIC, 34 μL , 0.22 mmol, 1.1 equiv.) was added via syringe. The reaction was stirred at ambient temperature until complete consumption of the carboxylic acid was observed by TLC (usually 1-2 hours). The crude reaction mixture was concentrated under vacuum to obtain the crude NHPI ester, which was used without further purification in the next step.

In the same vial containing the crude NHPI ester, xanthogenate **B** (3.2 mg, 0.02 mmol, 0.1 equiv.) and the electron-poor olefin **37** (0.3 mmol, 1.5 equiv., *if solid*) were dissolved in DMA (2 mL, synthesis grade). Next, γ -terpinene (128 μL , 0.8 mmol, 4 equiv.) was added and the resulting orange mixture was degassed with argon sparging for 60 seconds. If the electron-poor olefin **37** was *liquid*, it was added via syringe after the argon sparging. The vial was then placed in the 3D printed support photoreactor and irradiated under stirring for 16 hours, if not otherwise specified. The mixture was transferred to an extraction funnel, NaOH 1M solution was added and the organic layer was extracted with CH_2Cl_2 . The organic layer was washed with brine twice. The combined organic layers were dried over anhydrous MgSO_4 , filtered, and concentrated to dryness. The crude residue was purified by column chromatography to afford the corresponding product in the stated yield with >95% purity according to ^1H NMR analysis.

2.8.4.4 Characterization of products with general procedure B

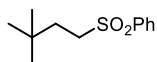


dimethyl 2-cyclohexylsuccinate (38c): Synthesized according to General Procedure B using 2 equiv. of γ -terpinene, cyclohexanecarboxylic acid (25.6 mg, 0.2 mmol, 1 equiv.) and dimethyl fumarate **37c** (43 mg, 0.3 mmol, 1.5 equiv.). The crude mixture was purified by flash column chromatography on silica gel (5% AcOEt in hexanes as eluent) to afford **38c** (44 mg, 95% yield) as a yellow oil.

$^1\text{H NMR}$ (500 MHz, CDCl_3) δ 3.69 (s, 3H), 3.66 (s, 3H), 2.78 – 2.66 (m, 2H), 2.45 (dt, $J = 13.1, 8.9$ Hz, 1H), 1.78 – 1.69 (m, 2H), 1.69 – 1.52 (m, 4H), 1.31 – 1.15 (m, 2H), 1.15 – 1.07 (m, 1H), 1.06 – 0.92 (m, 2H).

$^{13}\text{C NMR}$ (126 MHz, CDCl_3) δ 175.1, 173.1, 51.9, 51.7, 47.2, 40.1, 33.4, 30.8, 30.3, 26.4, 26.3.

Matching reported literature data.⁴⁵

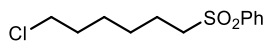


((3,3-dimethylbutyl)sulfonyl)benzene (38d): Synthesized according to General Procedure B using pivalic acid (20.4 mg, 0.2 mmol, 1 equiv.) and phenyl vinyl sulfone **37a** (50.4 mg, 0.3 mmol, 1.5 equiv.). The crude mixture was purified by flash column chromatography on silica gel (7% AcOEt in hexanes as eluent) to afford **38d** (33.0 mg, 73% yield) as a yellow oil.

$^1\text{H NMR}$ (400 MHz, CDCl_3) δ 7.98 – 7.85 (m, 2H), 7.71 – 7.62 (m, 1H), 7.65 – 7.53 (m, 2H), 3.10 – 3.01 (m, 2H), 1.64 – 1.55 (m, 2H), 0.86 (s, 9H).

$^{13}\text{C NMR}$ (101 MHz, CDCl_3) δ 142.1, 128.5, 128.5, 126.0, 119.9, 35.7, 30.7, 28.4, 25.4, 17.2.

Matching reported literature data.⁴⁵



((7-chloroheptyl)sulfonyl)benzene (38e): Synthesized according to General Procedure B using 5-Chlorovaleric acid (27.3 mg, 0.2 mmol, 1 equiv.) and phenyl vinyl sulfone **37a** (50.4 mg, 0.3 mmol, 1.5 equiv.). The crude mixture was purified by flash column chromatography on silica gel (20% DCM in hexanes as eluent) to afford **38e** (29.1 mg, 56% yield) as a white solid.

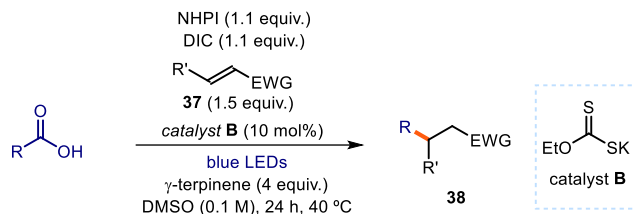
$^1\text{H NMR}$ (400 MHz, CDCl_3) δ 7.95 – 7.88 (m, 2H), 7.69 – 7.64 (m, 1H), 7.61 – 7.55 (m, 2H), 3.50 (t, $J = 6.5$ Hz, 2H), 3.12 – 3.05 (m, 2H), 1.77 – 1.71 (m, 4H), 1.44 – 1.39 (m, 4H).

$^{13}\text{C NMR}$ (101 MHz, CDCl_3) δ 139.3, 133.8, 129.4, 128.2, 56.3, 44.9, 32.2, 29.8, 27.7, 26.4, 22.7.

Matching reported literature data.⁴⁸

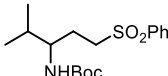
⁴⁸ Li, D.; Ma, T.-K.; Scott, R. J.; Wilden, J. D. Electrochemical radical reactions of alkyl iodides: a highly efficient, clean, green alternative to tin reagents, *Chem. Sci.* **2020**, *11*, 5333-5338.

2.8.4.5 General procedure C (one-pot domino from carboxylic acids)



Reactions performed using **set-up 1** in Figure 2.3. In an oven dried vial with a Teflon septum screw cap, carboxylic acid (0.2 mmol, 1 equiv.), *N*-hydroxyphthalimide ($NHPI$, 35.8 mg, 0.22 mmol, 1.1 equiv.), xanthogenate catalyst **B** (3.2 mg, 0.02 mmol, 0.1 equiv.), and the electron-poor olefin **37** (0.3 mmol, 1.5 equiv., *if solid*) were dissolved in DMSO (2 mL) and *N,N'*-diisopropylcarbodiimide (DIC , 34 μ L, 0.22 mmol, 1.1 equiv.) was added via syringe. Next, γ -terpinene (128 μ L, 0.8 mmol, 4 equiv.) was added and the resulting orange mixture was degassed with argon sparging for 60 seconds. If the electron-poor olefin **37** were *liquid*, it was added via syringe after the argon sparging. The vial was then placed in the 3D printed support photoreactor and irradiated under stirring for 24 hours, unless otherwise specified. The mixture was transferred to an extraction funnel, $NaOH$ 1M solution was added and the organic layer was extracted with CH_2Cl_2 . The organic layer was washed with brine twice. The combined organic layers were dried over anhydrous $MgSO_4$, filtered, and concentrated to dryness. The crude residue was purified by column chromatography to afford the corresponding product in the stated yield with >95% purity according to 1H NMR analysis.

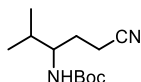
2.8.4.6 Characterization of products with general procedure C

 **tert-butyl (4-methyl-1-(phenylsulfonyl)pentan-3-yl)carbamate (38f)**: Synthesized according to General Procedure C using NMP as solvent, L-valine (43.5 mg, 0.2 mmol, 1 equiv.) and phenyl vinyl sulfone **37a** (50.4 mg, 0.3 mmol, 1.5 equiv.). The crude mixture was purified by flash column chromatography on silica gel (25% AcOEt in hexanes as eluent) to afford **38f** (63 mg, 92% yield) as a white solid.

1H NMR (500 MHz, $CDCl_3$) δ 7.93 – 7.88 (m, 2H), 7.69 – 7.63 (m, 1H), 7.57 (dd, $J = 8.4, 7.1$ Hz, 2H), 4.32 (d, $J = 10.1$ Hz, 1H), 3.42 (td, $J = 10.4, 4.8$ Hz, 1H), 3.15 (ddd, $J = 9.1, 6.1, 1.7$ Hz, 2H), 1.93 (tdd, $J = 12.1, 7.4, 3.4$ Hz, 1H), 1.82 – 1.61 (m, 2H), 1.40 (s, 9H), 0.87 (dd, $J = 10.0, 6.8$ Hz, 6H).

$^{13}\text{C NMR}$ (126 MHz, CDCl_3) δ 156.1, 139.4, 133.9, 129.5, 128.1, 79.7, 54.7, 54.1, 32.8, 28.5, 25.9, 19.2, 17.8.

Matching reported literature data.⁴⁹



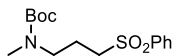
tert-butyl (1-cyano-4-methylpentan-3-yl)carbamate (38g):

Synthesized according to General Procedure C using 5 equiv. of γ -terpinene, L-valine (43.5 mg, 0.2 mmol, 1 equiv.) and acrylonitrile **37b** (26.3 μL , 0.4 mmol, 2 equiv.). The crude mixture was purified by flash column chromatography on silica gel (15% AcOEt in hexanes as eluent) to afford **38g** (27 mg, 60% yield) as a yellow oil.

$^1\text{H NMR}$ (400 MHz, CDCl_3) δ 4.34 (d, $J = 9.9$ Hz, 1H), 3.45 (tdd, $J = 10.4, 5.5, 3.4$ Hz, 1H), 2.49 – 2.30 (m, 2H), 1.90 (td, $J = 11.7, 9.8, 5.5$ Hz, 1H), 1.72 (dt, $J = 13.0, 6.5$ Hz, 1H), 1.62 (td, $J = 15.0, 14.5, 9.7$ Hz, 1H), 1.44 (s, 9H), 0.91 (dd, $J = 10.4, 6.8$ Hz, 6H).

$^{13}\text{C NMR}$ (101 MHz, CDCl_3) δ 156.1, 119.9, 79.7, 55.4, 32.5, 29.4, 28.5, 19.2, 17.9, 14.7.

Matching reported literature data.⁴⁹



tert-butyl methyl(3-(phenylsulfonyl)propyl)carbamate (38i):

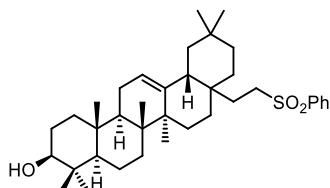
Synthesized according to General Procedure C using *N*-(tert-butoxycarbonyl)-*N*-methylglycine (38 mg, 0.2 mmol, 1 equiv.) and phenyl vinyl sulfone **37a** (50.4 mg, 0.3 mmol, 1.5 equiv.). The crude mixture was purified by flash column chromatography on silica gel (20% AcOEt in hexanes as eluent) to afford **38i** (47 mg, 75% yield) as a yellow oil.

$^1\text{H NMR}$ (400 MHz, CDCl_3) mixture of rotamers: δ 7.94 – 7.86 (m, 2H), 7.70 – 7.62 (m, 1H), 7.57 (dd, $J = 8.3, 6.8$ Hz, 2H), 3.29 (t, $J = 6.8$ Hz, 2H), 3.11 – 2.99 (m, 2H), 2.79 (s, 3H), 1.99 – 1.87 (m, 2H), 1.40 (s, 9H).

$^{13}\text{C NMR}$ (101 MHz, CDCl_3) mixture of rotamers: δ 155.9, 139.2, 133.9, 129.5, 128.1, 79.9, 53.9, 47.4, 34.3, 28.5, 21.0.

⁴⁹ Yoshimi, Y.; Masuda, M.; Mizunashi, T.; Nishikawa, K.; Maeda, K.; Koshida, N.; Itou, T.; Morita, T.; Hatanaka, M., Inter- and Intramolecular Addition Reactions of Electron-Deficient Alkenes with Alkyl Radicals, Generated by SET-Photochemical Decarboxylation of Carboxylic Acids, Serve as a Mild and Efficient Method for the Preparation of γ -Amino Acids and Macrocyclic Lactones. *Org. Lett.* **2009**, *11*, 4652-4655.

HRMS: calculated for $C_{15}H_{23}NNaO_4S$ ($M+Na^+$): 336.1240, found 336.1236 (+1.2 ppm).



**(3S,4aR,6aR,6bS,12aR,14aR,14bR)-
4,4,6a,6b,11,11,14b-heptamethyl-8a-(2-
(phenylsulfonyl)ethyl)-**

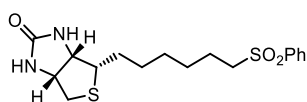
1,2,3,4,4a,5,6,6a,6b,7,8,8a,9,10,11,12,12a,14,14a,14b-icosahydricen-3-ol

(38j): Synthesized according to General Procedure C using NMP as solvent, oleanolic acid (91 mg, 0.2 mmol, 1 equiv) and phenyl vinyl sulfone **37a** (50.4 mg, 0.3 mmol, 1.5 equiv.). The crude mixture was purified by flash column chromatography on silica gel (40% AcOEt in hexanes as eluent) to afford **38j** (84 mg, 72% yield) as light-yellow solid.

¹H NMR (400 MHz, $CDCl_3$) δ 7.90 – 7.84 (m, 2H), 7.67 – 7.59 (m, 1H), 7.58 – 7.50 (m, 2H), 5.15 (t, $J = 3.6$ Hz, 1H), 3.19 (dd, $J = 10.7, 4.8$ Hz, 1H), 3.01 (dtd, $J = 37.9, 13.5, 4.3$ Hz, 2H), 2.01 – 1.76 (m, 7H), 1.66 (t, $J = 13.5$ Hz, 1H), 1.62 – 1.36 (m, 7H), 1.37 – 1.26 (m, 3H), 1.23 – 1.11 (m, 4H), 1.09 (s, 3H), 1.02 (dd, $J = 13.7, 2.1$ Hz, 1H), 0.97 (s, 3H), 0.94 – 0.90 (m, 1H), 0.88 (s, 3H), 0.85 (s, 3H), 0.82 (s, 3H), 0.77 (s, 3H), 0.68 (dd, $J = 11.5, 1.9$ Hz, 1H), 0.60 (s, 3H).

¹³C NMR (101 MHz, $CDCl_3$) δ 143.6, 139.3, 133.6, 129.4, 128.1, 123.1, 79.0, 55.2, 51.6, 47.6, 46.9, 46.5, 41.6, 39.7, 38.9, 38.7, 37.0, 34.7, 34.3, 33.2, 32.9, 32.5, 31.9, 31.0, 29.8, 28.2, 27.3, 26.1, 25.5, 23.6, 23.3, 18.4, 16.5, 15.7, 15.6.

Matching reported literature data.⁴⁵



**(3aS,4S,6aR)-4-(6-
(phenylsulfonyl)hexyl)tetrahydro-1H-
thieno[3,4-d]imidazol-2(3H)-one (38l):**

Synthesized according to General Procedure C using 4 mL of DMSO, biotin (49 mg, 0.2 mmol, 1 equiv.) and phenyl vinyl sulfone **37a** (50.4 mg, 0.3 mmol, 1.5 equiv.). The crude mixture was purified by flash column chromatography on silica gel (2-5% MeOH in DCM as eluent) to afford **38l** (48 mg, 65% yield) as a yellow oil.

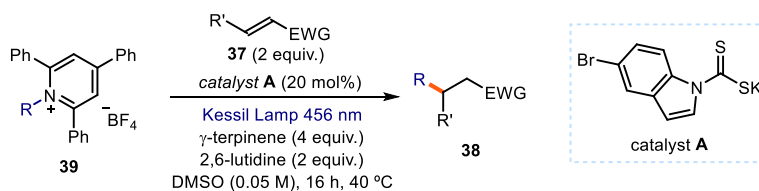
¹H NMR (500 MHz, Methanol- d_4) δ 7.99 – 7.89 (m, 2H), 7.77 – 7.70 (m, 1H), 7.72 – 7.58 (m, 2H), 4.53 – 4.46 (m, 1H), 4.29 (ddd, $J = 12.2, 7.9, 4.5$ Hz, 1H), 3.24 – 3.19 (m, 2H), 3.19 – 3.14 (m, 1H), 2.92 (dt, $J = 12.7, 5.1$ Hz, 1H), 2.70 (dd, $J =$

12.7, 4.4 Hz, 1H), 1.66 (tdd, $J = 15.3, 8.3, 4.4$ Hz, 3H), 1.53 (ddd, $J = 16.8, 8.8, 5.5$ Hz, 1H), 1.45 – 1.27 (m, 6H).

^{13}C NMR (101 MHz, CDCl_3) δ 164.5, 139.2, 133.8, 129.4, 128.1, 62.4, 60.8, 56.1, 55.8, 40.6, 31.4, 31.0, 28.8, 28.7, 28.4, 27.9, 22.7, 22.5, 14.1.

HRMS: calculated for $\text{C}_{17}\text{H}_{24}\text{N}_2\text{NaO}_3\text{S}_2$ ($\text{M}+\text{Na}^+$): 391.1120, found 391.1121 (–0.3 ppm).

2.8.4.7 General procedure D (using pyridinium salts)



Reactions performed using *set-up 2* in Figure 2.4. In an oven dried vial, with a Teflon septum screw cap, dithiocarbamate **A** (12.4 mg, 0.04 mmol, 0.2 equiv.), pyridinium salt **39** (0.2 mmol, 1 equiv.) and the electron-poor olefin **37** (0.4 mmol, 2 equiv.), were dissolved in DMSO (4 mL). Then, γ -terpinene (128 μL , 0.8 mmol, 4 equiv.) and 2,6-lutidine (46 μL , 0.4 mmol, 2 equiv.) were added. The resulting orange mixture was degassed with argon sparging for 60 seconds. The vial was then placed at 2–3 cm of a 50 W Kessil blue LED lamp and irradiated under stirring for 16 hours. The mixture was transferred to an extraction funnel, NaHCO_3 sat. solution was added and the organic layer was extracted with EtOAc. The organic layer was washed with brine twice. The combined organic layers were dried over anhydrous MgSO_4 , filtered, and concentrated to dryness. The crude residue was purified by column chromatography to afford the corresponding product in the stated yield with >95% purity according to ^1H NMR analysis.

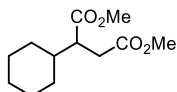
2.8.4.8 Characterization of products with general procedure D

((2-cyclohexylethyl)sulfonyl)benzene (**38a**): Synthesized according to General Procedure D using 1-cyclohexyl-2,4,6-triphenylpyridin-1-ium tetrafluoroborate **39a** (95 mg, 0.2 mmol, 1 equiv.) and phenyl vinyl sulfone **37a** (67 mg, 0.4 mmol, 2 equiv.). The crude mixture was purified by flash column chromatography on silica gel (10% AcOEt in hexanes as eluent) to afford **38a** (34 mg, 67% yield) as a white solid.

$^1\text{H NMR}$ (500 MHz, CDCl_3) δ 7.94 – 7.85 (m, 2H), 7.69 – 7.61 (m, 1H), 7.61 – 7.52 (m, 2H), 3.13 – 3.05 (m, 2H), 1.71 – 1.54 (m, 7H), 1.28 (ddt, $J = 14.6, 7.5, 3.8$ Hz, 1H), 1.23 – 1.06 (m, 3H), 0.92 – 0.76 (m, 2H).

$^{13}\text{C NMR}$ (126 MHz, CDCl_3) δ 139.4, 133.7, 129.4, 128.2, 54.5, 36.8, 32.9, 29.7, 26.4, 26.1.

Matching reported literature data.⁴⁵



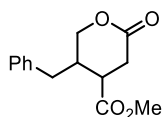
dimethyl 2-cyclohexylsuccinate (38c): Synthesized according to General Procedure D using 2 equiv. of γ -terpinene, 1-cyclohexyl-2,4,6-triphenylpyridin-1-ium tetrafluoroborate **39a**

(95 mg, 0.2 mmol, 1 equiv.) and dimethyl fumarate **37c** (57 mg, 0.4 mmol, 2 equiv.). The crude mixture was purified by flash column chromatography on silica gel (5% AcOEt in hexanes as eluent) to afford **38c** (41 mg, 90% yield) as a yellow oil.

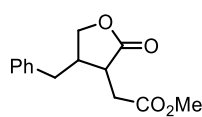
$^1\text{H NMR}$ (400 MHz, CDCl_3) δ 3.69 (s, 3H), 3.66 (s, 3H), 2.78 – 2.66 (m, 2H), 2.45 (dt, $J = 13.1, 8.9$ Hz, 1H), 1.78 – 1.69 (m, 2H), 1.69 – 1.52 (m, 4H), 1.31 – 1.15 (m, 2H), 1.15 – 1.07 (m, 1H), 1.06 – 0.92 (m, 2H).

$^{13}\text{C NMR}$ (126 MHz, CDCl_3) δ 175.1, 173.1, 51.9, 51.7, 47.2, 40.1, 33.4, 30.8, 30.3, 26.4, 26.3.

Matching reported literature data.⁴⁵



33m



33m'

methyl 5-benzyl-2-oxotetrahydro-2H-pyran-4-carboxylate (38m): Synthesized

according to General Procedure D using 2 equiv. of γ -terpinene, 1-(1-hydroxy-3-phenylpropan-2-yl)-2,4,6-triphenylpyridin-1-ium tetrafluoroborate **39b** (106 mg, 0.2 mmol, 1 equiv.) and dimethyl fumarate **37c** (57 mg, 0.4 mmol, 2 equiv.). The crude mixture was purified by flash column chromatography on silica gel (10% AcOEt in hexanes as eluent) to afford an unseparable mixture of regioisomers **38m/38m'** (**3.8:1**) (27 mg, 54% yield) as a yellow oil. Corrected yield for **38m** (42% yield)

Products formed upon intramolecular esterification promoted by the acidic conditions delivered by the silica during purification.

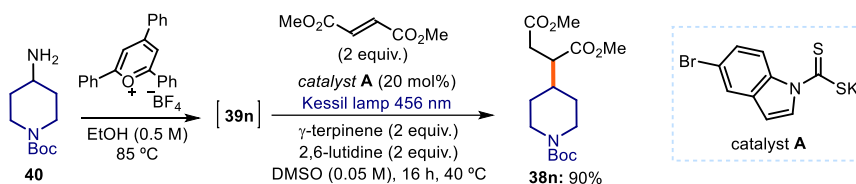
$^1\text{H NMR}$ (400 MHz, CDCl_3) mixture of regioisomers δ 7.35 – 7.28 (m, 2.5H), 7.28 – 7.21 (m, 1.25H), 7.19 – 7.10 (m, 2.5H), 4.35 – 4.28 (m, 1H), 4.14 – 4.06 (m,

0.5H), 3.96 – 3.88 (m, 1H), 3.74 (s, 0.75H), 3.69 (s, 3H), 3.31 – 3.23 (m, 0.25H), 3.05 – 2.85 (m, 1.5H), 2.85 – 2.66 (m, 3.25H), 2.63 (d, $J = 10.2$ Hz, 0.25H), 2.61 – 2.55 (m, 2H), 2.34 (dd, $J = 13.7, 11.9$ Hz, 0.25H).

^{13}C NMR (101 MHz, CDCl_3) mixture of regioisomers: δ 177.8, 171.6, 137.8, 129.1, 129.0, 129.0, 128.7, 127.1, 126.9, 71.4, 70.1, 52.3, 52.2, 42.4, 42.0, 40.8, 39.7, 38.4, 33.6, 33.3, 30.2, 29.8.

HRMS: calculated for $\text{C}_{14}\text{H}_{16}\text{NaO}_4$ ($\text{M}+\text{Na}^+$): 271.0941, found 271.0939 (+0.7 ppm).

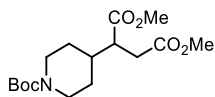
2.8.4.9 General procedure E (telescoped reaction from amine)



Reactions performed using *set-up 2* in Figure 2.4. In an oven dried vial, with a Teflon septum screw cap, primary amine (0.22 mmol, 1.1 equiv.) and 2,4,6-triphenylpyrylium tetrafluoroborate (79.2 mg, 0.2 mmol, 1 equiv.) were dissolved in ethanol (0.4 mL, HPLC grade). The reaction was stirred at 80 °C for 4 hours. In the same vial without evaporating the solvent, dithiocarbamate **A** (12.4 mg, 0.04 mmol, 0.2 equiv.), electron-poor olefin **37** (0.4 mmol, 2 equiv.), DMSO (4 mL), γ -terpinene (64 μL , 0.4 mmol, 2 equiv.) and 2,6-lutidine (46 μL , 0.4 mmol, 2 equiv.) were added sequentially. The resulting orange mixture was degassed with argon sparging for 60 seconds. The vial was then placed at 2-3 cm of a 50 W Kessil blue LED lamp and irradiated under stirring for 16 hours. The mixture was transferred to an extraction funnel, saturated aqueous NaHCO_3 was added, and the organic layer extracted with EtOAc. The organic layer was washed with brine twice. The combined organic layers were dried over anhydrous MgSO_4 , filtered, and concentrated to dryness. The crude residue was purified by column chromatography to afford the corresponding product in the stated yield with >95% purity according to ^1H NMR analysis.

A control experiment without catalyst **A** delivered no conversion of the pyridinium salt upon irradiation.

2.8.4.10 Characterization of products with general procedure E



dimethyl 2-(1-(tert-butoxycarbonyl)piperidin-4-yl)succinate (38n): Synthesized according to General

Procedure E using 2 equiv. of γ -terpinene, *tert*-butyl 4-aminopiperidine-1-carboxylate (40 mg, 0.2 mmol, 1 equiv.) and dimethyl fumarate **37c** (57 mg, 0.4 mmol, 2 equiv.). The crude mixture was purified by flash column chromatography on silica gel (0-40% AcOEt in hexanes as eluent) to afford **38n** (59 mg, 90% yield) as a yellow oil.

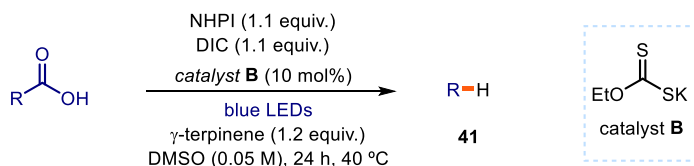
$^1\text{H NMR}$ (400 MHz, CDCl_3) δ 4.12 (d, $J = 13.3$ Hz, 2H), 3.70 (s, 3H), 3.66 (s, 3H), 2.81 – 2.68 (m, 2H), 2.63 (tt, $J = 13.0, 3.0$ Hz, 2H), 2.52 – 2.41 (m, 1H), 1.73 (tdd, $J = 12.3, 6.1, 3.6$ Hz, 1H), 1.57 (ddt, $J = 23.3, 13.0, 3.0$ Hz, 2H), 1.44 (s, 9H), 1.34 – 1.15 (m, 2H).

$^{13}\text{C NMR}$ (126 MHz, CDCl_3) δ 174.7, 172.9, 155.1, 79.9, 52.2, 46.6, 44.2, 38.7, 33.6, 33.6, 29.9, 29.7, 28.8, 28.8.

HRMS: calculated for $\text{C}_{16}\text{H}_{27}\text{NNaO}_6$ ($\text{M}+\text{Na}^+$): 352.1731, found 352.1726. (+1.4 ppm).

2.8.5 Reduction

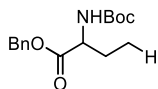
2.8.5.1 General procedure F (Barton decarboxylation)



Reactions performed using *set-up 1* in Figure 2.3. In an oven dried vial, with a Teflon septum screw cap, carboxylic acid (0.2 mmol, 1 equiv.), *N*-hydroxyphthalimide (NHPI, 35.8 mg, 0.22 mmol, 1.1 equiv.) and xanthogenate **B** (3.2 mg, 0.02 mmol, 0.1 equiv.) were dissolved in DMSO (4 mL) and *N,N'*-diisopropylcarbodiimide (DIC, 34 μL , 0.22 mmol, 1.1 equiv.) was added via syringe. Then, γ -terpinene (38 μL , 0.24 mmol, 1.2 equiv.) was added. The resulting orange mixture was degassed with argon sparging for 60 seconds. The vial was then placed in the 3D printed support photoreactor and irradiated under stirring for 24 hours, unless otherwise specified. The mixture was transferred to an extraction funnel, NaOH 1M solution was added and the organic layer was extracted with CH_2Cl_2 . The organic layer was washed with brine twice. The combined organic

layers were dried over anhydrous MgSO_4 , filtered, and concentrated to dryness. The crude residue was purified by column chromatography to afford the corresponding product in the stated yield with >95% purity according to ^1H NMR analysis.

2.8.5.2 Characterization of products with general procedure F



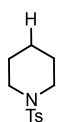
benzyl (S)-2-((tert-butoxycarbonyl)amino)butanoate (41a):

Synthesized according to General Procedure F using (S)-5-(benzyloxy)-4-((tert-butoxycarbonyl)amino)-5-oxopentanoic acid (67 mg, 0.2 mmol, 1 equiv.). The crude mixture was purified by flash column chromatography on silica gel (25% AcOEt in hexanes as eluent) to afford **41a** (38 mg, 65% yield) as a yellow oil.

^1H NMR (400 MHz, CDCl_3) δ 7.41 – 7.28 (m, 5H), 5.24 – 5.10 (m, 2H), 5.04 (d, J = 8.3 Hz, 1H), 4.30 (t, J = 7.1 Hz, 1H), 1.93 – 1.80 (m, 1H), 1.69 (dt, J = 14.2, 7.2 Hz, 1H), 1.44 (s, 9H), 0.90 (t, J = 7.5 Hz, 3H).

^{13}C NMR (101 MHz, CDCl_3) δ 172.8, 155.5, 135.6, 128.7, 128.5, 128.4, 79.9, 67.1, 54.8, 28.5, 26.1, 9.7.

Matching reported literature data.^{44a}

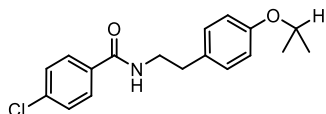


1-tosylpiperidine (41b): Synthesized according to General Procedure F using 1-tosylpiperidine-4-carboxylic acid (57 mg, 0.2 mmol, 1 equiv.). The crude mixture was purified by flash column chromatography on silica gel (10% AcOEt in hexanes as eluent) to afford **41b** (37 mg, 77% yield) as a white solid.

^1H NMR (500 MHz, CDCl_3) δ 7.66 – 7.60 (m, 2H), 7.34 – 7.28 (m, 2H), 2.99 – 2.93 (m, 4H), 2.42 (s, 3H), 1.63 (p, J = 5.9 Hz, 4H), 1.40 (tt, J = 8.2, 4.7 Hz, 2H).

^{13}C NMR (126 MHz, CDCl_3) δ 143.4, 133.5, 129.7, 127.8, 47.1, 25.3, 23.7, 21.6.

Matching reported literature data.^{44a}



4-chloro-N-(4-isopropoxyphenethyl)benzamide (41c):

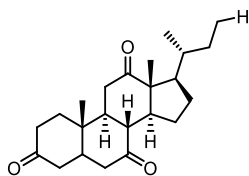
Synthesized according to General Procedure F using Bezafibrate (72 mg, 0.2 mmol, 1 equiv.).

The crude mixture was purified by flash column chromatography on silica gel (25% AcOEt in hexanes as eluent) to afford **41c** (32 mg, 50% yield) as a white solid.

¹H NMR (400 MHz, CDCl₃) mixture of rotamers: δ 7.65 – 7.59 (m, 2H), 7.37 (dd, *J* = 8.6, 2.0 Hz, 2H), 7.15 – 7.04 (m, 2H), 6.89 – 6.79 (m, 2H), 6.13 (s, 1H), 4.52 (p, *J* = 6.1 Hz, 1H), 3.67 (qd, *J* = 6.7, 6.3, 3.7 Hz, 2H), 2.85 (t, *J* = 6.9 Hz, 2H), 1.33 (d, *J* = 6.1 Hz, 6H).

¹³C NMR (101 MHz, CDCl₃) mixture of rotamers: δ 166.6, 156.8, 137.8, 133.1, 130.6, 130.0, 129.9, 129.0, 128.4, 116.3, 115.8, 70.1, 41.5, 34.8, 22.2.

HRMS: calculated for C₁₆H₁₈ClN₄NaO (M+Na⁺): 340.1061, found 340.1075 (+4.1 ppm).



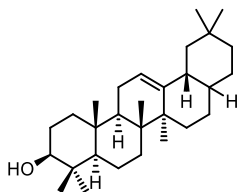
(5*S*,8*R*,9*S*,10*S*,13*R*,14*S*,17*R*)-17-(sec-butyl)-10,13-dimethyldodecahydro-3H-cyclopenta[*a*]phenanthrene-3,7,12(2*H*,4*H*)-trione (41d): Synthesized according to General Procedure F using dehydrocholic acid (81 mg, 0.2 mmol, 1 equiv.).

The crude mixture was purified by flash column chromatography on silica gel (30% AcOEt in hexanes as eluent) to afford **41d** (37 mg, 51% yield) as a light-yellow solid.

¹H NMR (400 MHz, CDCl₃) δ 2.96 – 2.80 (m, 3H), 2.39 – 2.17 (m, 6H), 2.13 (dd, *J* = 12.5, 4.8 Hz, 2H), 2.09 – 1.90 (m, 4H), 1.85 (td, *J* = 11.2, 7.0 Hz, 1H), 1.68 – 1.56 (m, 2H), 1.52 – 1.44 (m, 1H), 1.40 (s, 3H), 1.35 – 1.20 (m, 3H), 1.20 – 1.10 (m, 1H), 1.07 (s, 3H), 0.85 (dd, *J* = 15.9, 6.9 Hz, 6H).

¹³C NMR (101 MHz, CDCl₃) δ 212.2, 209.2, 208.9, 57.0, 52.0, 49.2, 47.0, 45.7, 45.6, 45.1, 42.9, 38.8, 37.6, 36.6, 36.2, 35.4, 28.0, 27.8, 25.4, 22.1, 18.6, 12.0, 11.0.

Matching reported literature data.^{44a}



(3*S*,4*aR*,6*aR*,6*bS*,12*aR*,14*aR*,14*bR*)-4,4,6*a*,6*b*,11,11,14*b*-heptamethyl-1,2,3,4,4*a*,5,6,6*a*,6*b*,7,8,8*a*,9,10,11,12,12*a*,14,14*a*,14*b*-icosahydricen-3-ol (41e): Synthesized according to General Procedure F using oleanolic acid (91 mg, 0.2

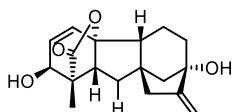
mmol, 1 equiv). The crude mixture was purified by flash column chromatography on silica gel (15% AcOEt in hexanes as eluent) to afford **41e** (74 mg, 90% yield) as white solid.

¹H NMR (400 MHz, CDCl₃) δ 5.19 (t, *J* = 3.7 Hz, 1H), 3.22 (ddz, *J* = 11.0, 5.0 Hz, 1H), 2.34 (dt, *J* = 13.7, 4.8 Hz, 1H), 1.91 – 1.83 (m, 2H), 1.83 – 1.75 (m, 1H), 1.74 – 1.65 (m, 2H), 1.65 – 1.58 (m, 4H), 1.5 – 1.54 (m, 2H), 1.50 – 1.31 (m, 6H), 1.29

– 1.17 (m, 4H), 1.11 (d, $J = 0.9$ Hz, 3H), 1.08 – 1.04 (m, 1H), 1.02 – 0.96 (m, 4H), 0.93 (s, 3H), 0.89 (s, 3H), 0.87 (s, 6H), 0.79 (s, 3H), 0.77 – 0.70 (m, 1H).

$^{13}\text{C NMR}$ (101 MHz, CDCl_3) δ 146.1, 121.2, 79.2, 55.4, 47.9, 45.1, 42.6, 41.1, 39.3, 38.9, 38.6, 37.3, 35.9, 33.8, 33.8, 33.2, 31.3, 31.2, 29.9, 28.3, 28.1, 27.4, 25.2, 24.0, 23.5, 22.4, 18.6, 17.6, 15.8, 15.5.

Matching reported literature data.^{44a}



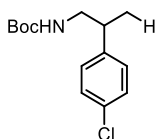
(1S,2S,4aR,4bR,7S,9aR,10aR)-2,7-dihydroxy-1-methyl-8-methylene-1,2,4b,5,6,7,8,9,10,10a-decahydro-4a,1-(epoxymethano)-7,9a-

methanobenzo[a]azulen-13-one (41f): Synthesized according to General Procedure F using gibberellic acid (69 mg, 0.2 mmol, 1 equiv.). The crude mixture was purified by flash column chromatography on silica gel (40% AcOEt in hexanes as eluent) to afford **41f** (36 mg, 60% yield) as a white solid.

$^1\text{H NMR}$ (400 MHz, Acetone- d_6) δ 6.34 (dd, $J = 9.3, 0.9$ Hz, 1H), 5.85 (dd, $J = 9.3, 3.7$ Hz, 1H), 5.16 (td, $J = 2.5, 1.1$ Hz, 1H), 4.81 (tt, $J = 2.1, 1.0$ Hz, 1H), 4.56 – 4.50 (m, 1H), 4.01 (dd, $J = 6.4, 3.6$ Hz, 1H), 3.71 (s, 1H), 2.85 – 2.74 (m, 1H), 2.40 (q, $J = 2.0$ Hz, 2H), 2.03 – 2.00 (m, 1H), 1.91 (dd, $J = 13.6, 8.2$ Hz, 1H), 1.87 – 1.80 (m, 2H), 1.79 – 1.65 (m, 3H), 1.61 (dd, $J = 13.6, 11.0$ Hz, 1H), 1.53 – 1.47 (m, 1H), 1.21 (s, 3H).

$^{13}\text{C NMR}$ (101 MHz, Acetone- d_6) δ 179.6, 160.6, 134.0, 133.3, 105.7, 92.8, 78.9, 70.2, 54.5, 52.3, 50.2, 48.2, 45.9, 40.1, 36.4, 30.2, 17.6, 15.2.

HRMS: calculated for $\text{C}_{18}\text{H}_{22}\text{NaO}_4$ ($\text{M}+\text{Na}^+$): 325.1410, found 325.1400 (–3.3 ppm).



tert-butyl (2-(4-chlorophenyl)propyl)carbamate (41g):

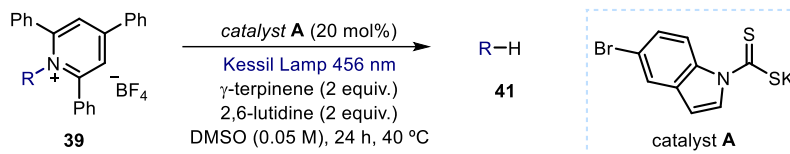
Synthesized according to General Procedure F using 4-((*tert*-butoxycarbonyl)amino)-3-(4-chlorophenyl)butanoic acid (63 mg, 0.2 mmol, 1 equiv.). The crude mixture was purified by flash column chromatography on silica gel (10% AcOEt in hexanes as eluent) to afford **41g** (40 mg, 74% yield) as colorless oil.

$^1\text{H NMR}$ (400 MHz, CDCl_3) δ 7.34 – 7.20 (m, 2H), 7.17 – 7.07 (m, 2H), 4.41 (s, 1H), 3.35 (s, 1H), 3.15 (dd, $J = 13.6, 8.3$ Hz, 1H), 2.91 (q, $J = 7.1$ Hz, 1H), 1.41 (s, 9H), 1.24 (d, $J = 7.0$ Hz, 3H).

^{13}C NMR (101 MHz, CDCl_3) δ 156.0, 142.9, 132.4, 129.8, 128.8, 128.8, 128.6, 47.4, 39.8, 28.5, 28.5, 19.2, 1.2.

Matching reported literature data.⁵⁰

2.8.5.3 General procedure G (deaminative reduction)



Reactions performed using *set-up 2* in Figure 2.4. In an oven dried vial, with a Teflon septum screw cap, dithiocarbamate **A** (12.4 mg, 0.04 mmol, 0.2 equiv.) and pyridinium salt **39** (0.2 mmol, 1 equiv.) were dissolved in DMSO (4 mL). Then, γ -terpinene (64 μL , 0.4 mmol, 2 equiv.) and 2,6-lutidine (46 μL , 0.4 mmol, 2 equiv.) were added. The resulting orange mixture was degassed with argon sparging for 60 seconds. The vial was then placed at 2-3 cm of a 50 W Kessil blue LED lamp and irradiated under stirring for 16 hours. The mixture was transferred to an extraction funnel, NaHCO_3 sat. solution was added and the organic layer was extracted with EtOAc. The organic layer was washed with brine twice. The combined organic layers were dried over anhydrous MgSO_4 , filtered, and concentrated to dryness. The crude residue was purified by column chromatography to afford the corresponding product in the stated yield with >95% purity according to ^1H NMR analysis.

2.8.5.4 Characterization of products with general procedure G

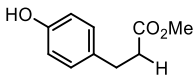
3-phenylpropan-1-ol (41h): Synthesized according to General Procedure G using 1-(1-hydroxy-3-phenylpropan-2-yl)-2,4,6-triphenylpyridin-1-ium tetrafluoroborate **39b** (106 mg, 0.2 mmol, 1 equiv.). The crude mixture was purified by flash column chromatography on silica gel (15% AcOEt in pentane as eluent) to afford **41h** (21 mg, 77% yield) as a colorless oil.

⁵⁰ Steiman, T. J.; Liu, J.; Mengiste, A.; Doyle, A. G., Synthesis of β -Phenethylamines via Ni/Photoredox Cross-Electrophile Coupling of Aliphatic Aziridines and Aryl Iodides. *J. Am. Chem. Soc.* **2020**, *142*, 7598-7605.

$^1\text{H NMR}$ (400 MHz, CDCl_3) δ 7.33 – 7.26 (m, 2H), 7.23 – 7.17 (m, 3H), 3.68 (t, J = 6.4 Hz, 2H), 2.72 (dd, J = 8.7, 6.8 Hz, 2H), 1.96 – 1.85 (m, 2H).

$^{13}\text{C NMR}$ (101 MHz, CDCl_3) δ 141.9, 128.6, 128.5, 126.0, 62.4, 34.4, 32.2.

Matching reported literature data.⁵¹

 **methyl 3-(4-hydroxyphenyl)propanoate (41i):** Synthesized according to General Procedure G using 1-(3-(4-hydroxyphenyl)-1-methoxy-1-oxopropan-2-yl)-2,4,6-triphenylpyridin-1-ium tetrafluoroborate **39c** (115 mg, 0.2 mmol, 1 equiv.). The crude mixture was purified by flash column chromatography on silica gel (0-40% AcOEt in hexanes as eluent) to afford **41i** (28 mg, 78% yield) as a colorless oil.

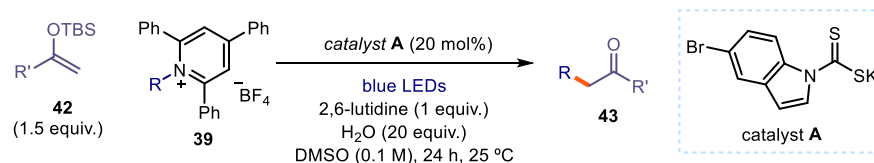
$^1\text{H NMR}$ (400 MHz, CDCl_3) δ 7.04 (d, J = 8.4 Hz, 2H), 6.79 – 6.71 (m, 2H), 5.74 (s, 1H), 3.67 (s, 3H), 2.88 (t, J = 7.7 Hz, 2H), 2.61 (dd, J = 9.0, 6.5 Hz, 2H).

$^{13}\text{C NMR}$ (101 MHz, CDCl_3) δ 174.1, 154.4, 132.4, 129.5, 115.5, 51.9, 36.2, 30.2.

Matching reported literature data.⁵²

2.8.6 α -Alkylation of silyl enol ethers

2.8.6.1 General procedure H



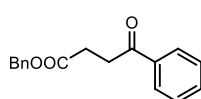
Reactions performed using *set-up 3* in Figure 2.7. In an oven dried vial with a Teflon septum screw cap, silyl enol ether **42** (0.3 mmol, 1.5 equiv.) was dissolved in DMSO (2 mL), followed by addition of 2,6-lutidine (23 μL , 0.2 mmol, 1.0 equiv.), pyridinium salt **39** (0.2 mmol, 1.0 equiv.), catalyst **A** (12.4 mg, 0.04 mmol, 0.2 equiv.) and water (4.0 mmol, 20 equiv.). The resulting orange mixture was degassed by bubbling argon for 60 seconds. The vial was then placed in the

⁵¹ Vechorkin, O.; Proust, V.; Hu, X., Functional Group Tolerant Kumada–Corriu–Tamao Coupling of Nonactivated Alkyl Halides with Aryl and Heteroaryl Nucleophiles: Catalysis by a Nickel Pincer Complex Permits the Coupling of Functionalized Grignard Reagents. *J. Am. Chem. Soc.* **2009**, *131*, 9756–9766.

⁵² Percec, V.; Peterca, M.; Sienkowska, M. J.; Ilies, M. A.; Aqad, E.; Smidrkal, J.; Heiney, P. A., Synthesis and Retrostructural Analysis of Libraries of AB3 and Constitutional Isomeric AB2 Phenylpropyl Ether-Based Supramolecular Dendrimers. *J. Am. Chem. Soc.* **2006**, *128*, 3324–3334.

irradiation setup, maintained at a temperature of 25 °C (25-26 °C measured in the central well), and the reaction was stirred for 24 hours under continuous irradiation from a blue LED strip, unless otherwise stated. The crude mixture was diluted with EtOAc and brine was added. The layers were separated, and the aqueous layer extracted with EtOAc (×3). The combined organic fractions were dried over anhydrous MgSO₄, filtered, and concentrated to dryness. The crude residue was purified by column chromatography on silica gel to afford the corresponding product in the stated yield with >95% purity according to ¹H NMR analysis.

2.8.6.2 Characterization of products with general procedure H

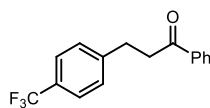


Benzyl 4-oxo-4-phenylbutanoate (43a): Prepared according to General Procedure H using *set-up 2* (75% intensity). 2,6-lutidine (46 μL, 0.4 mmol, 2 equiv.), *tert*-butyldimethyl((1-phenylvinyl)oxy)silane **42a** (70 mg, 0.4 mmol, 2 equiv.) and 1-(2-(benzyloxy)-2-oxoethyl)-2,4,6-triphenylpyridin-1-ium tetrafluoroborate **39d** (109 mg, 0.2 mmol, 1 equiv.). Flash column chromatography (hexanes/EtOAc 95:5) to afford product **43a** as an off-white oil (43 mg, 80% yield).

¹H NMR (300 MHz, CDCl₃) δ 8.03 – 7.94 (m, 2H), 7.56 (m, 1H), 7.46 (m, 2H), 7.40 – 7.23 (m, 5H), 5.15 (s, 3H), 3.34 (t, *J* = 6.6 Hz, 2H), 2.83 (t, *J* = 6.6 Hz, 2H).

¹³C NMR (75 MHz, CDCl₃) δ 198.2, 172.9, 136.7, 136.0, 133.4, 128.8, 128.7, 128.4, 128.2, 66.7, 33.5, 28.43.

Matching reported literature data.⁵³



1-phenyl-3-(4-(trifluoromethyl)phenyl)propan-1-one (43b): Prepared according to General Procedure H using *tert*-butyldimethyl((1-phenylvinyl)oxy)silane **42a** (70 mg, 0.3 mmol,) and 2,4,6-triphenyl-1-(4-(trifluoromethyl)benzyl)pyridin-1-ium tetrafluoroborate **39e** (111 mg, 0.2 mmol). Time of irradiation: 24 hours at 25 °C. Flash column chromatography (Toluene) to afford product **43b** as a white solid (35 mg, 55% yield).

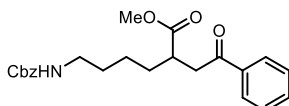
⁵³ Dong S.; Wu G.; Yuan X.; Zou C.; Ye J., Visible-light photoredox catalyzed hydroacylation of electron-deficient alkenes: carboxylic anhydride as an acyl radical source. *Org. Chem. Front.* **2017**, *4*, 2230-2234.

¹H NMR (300 MHz, CDCl₃) δ 7.97 – 7.90 (m, 2H), 7.59 – 7.50 (m, 3H), 7.48 – 7.44 (m, 2H), 7.41 – 7.35 (m, 2H), 3.33 (t, *J* = 7.5 Hz, 2H), 3.15 (t, *J* = 7.5 Hz, 2H).

¹³C NMR (75 MHz, CDCl₃) δ 198.2, 145.5, 136.8, 136.8, 133.4, 129.1, 128.8, 128.7, 128.1, 125.4 (q, *J* = 3.9 Hz), 124.5 (q, *J* = 270 Hz), 39.9, 29.9.

¹⁹F NMR (376 MHz, CDCl₃) δ –62.49.

Matching reported literature data.⁵⁴



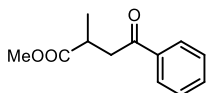
Methyl 6-(((benzyloxy)carbonyl)amino)-2-(2-oxo-2-phenylethyl)hexanoate (43c): Prepared according to General Procedure H using *tert*-butyldimethyl((1-phenylvinyl)oxy)silane **42a** (70 mg, 0.3 mmol) and (±)-1-(6-(((benzyloxy)carbonyl)amino)-1-methoxy-1-oxohexan-2-yl)-2,4,6-

triphenylpyridin-1-ium tetrafluoroborate **39f** (135 mg, 0.2 mmol). Flash column chromatography (hexanes/EtOAc 7:3 to 1:1) to afford product **43c** as a yellowish oil (53 mg, 67% yield).

¹H NMR (400 MHz, CDCl₃) δ 7.99 – 7.93 (m, 2H), 7.60 – 7.54 (m, 1H), 7.49 – 7.44 (m, 2H), 7.36 – 7.30 (m, 5H), 5.09 (s, 2H), 4.76 (s, 1H), 3.69 (s, 3H), 3.56 – 3.34 (m, 1H), 3.20 (q, *J* = 6.7 Hz, 2H), 3.15 – 2.99 (m, 2H), 1.77 – 1.50 (m, 5H), 1.39 (m, 1H).

¹³C NMR (101 MHz, CDCl₃) δ 198.2, 176.1, 156.5, 136.8, 136.7, 133.4, 128.8, 128.7, 128.3, 128.2, 66.8, 52.0, 40.9, 40.6, 40.3, 31.9, 29.9, 24.5.

HRMS: calculated for C₂₃H₂₇NNaO₅ (M+Na⁺): 420.1781, found 420.1771 (+2.3 ppm).



Benzyl 2-methyl-4-oxo-4-phenylbutanoate (43d):

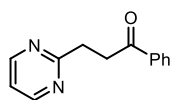
Prepared according to General Procedure H using *tert*-butyldimethyl((1-phenylvinyl)oxy)silane **42a** (70 mg, 0.3 mmol) and (±)-1-(1-(benzyloxy)-1-oxopropan-2-yl)-2,4,6-triphenylpyridin-1-ium tetrafluoroborate **39g** (111 mg, 0.2 mmol). Time of irradiation: 24 hours at 25 °C. Flash column chromatography (hexanes/EtOAc 98:2 to 90:10) to afford product **43d** as a yellowish oil (39 mg, 69% yield).

⁵⁴ Ding B.; Zhang Z.; Liu Y.; Sugiya M.; Imamoto T.; Zhang W., Chemoselective Transfer Hydrogenation of α,β-Unsaturated Ketones Catalyzed by Pincer-Pd Complexes Using Alcohol as a Hydrogen Source. *Org. Lett.* **2013**, *15*, 3690-3693.

¹H NMR (300 MHz, CDCl₃) δ 8.07 – 7.88 (m, 2H), 7.72 – 7.53 (m, 1H), 7.53 – 7.42 (m, 2H), 7.35 (m, 5H), 5.22 – 5.09 (dd, *J* = 16.5 Hz, 12.4 Hz, 2H), 3.52 (dd, *J* = 17.5 Hz, 7.8 Hz, 1H), 3.22 (m, 1H), 3.06 (dd, *J* = 17.5 Hz, 5.5 Hz, 1H), 1.32 (d, *J* = 7.1 Hz, 3H).

¹³C NMR (75 MHz, CDCl₃) δ 198.1, 175.9, 136.8, 136.2, 133.3, 128.7, 128., 128.2, 128.2, 128.2, 66.5, 42.0, 35.2, 17.4.

Matching reported literature data.⁵³

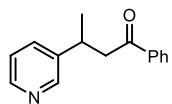


1-phenyl-3-(pyrimidin-2-yl)propan-1-one (43e): Prepared according to General Procedure H at 40 °C using *tert*-butyldimethyl((1-phenylvinyl)oxy)silane **42a** (70 mg, 0.3 mmol) and 2,4,6-triphenyl-1-(pyrimidin-2-ylmethyl)pyridin-1-ium tetrafluoroborate **39h** (98 mg, 0.2 mmol). Flash column chromatography (hexanes/EtOAc 7:3) to afford product **43e** as a yellowish oil (32 mg, 75% yield).

¹H NMR (300 MHz, CDCl₃) δ 8.66 (d, *J* = 4.9 Hz, 2H), 8.25 – 7.88 (m, 2H), 7.61 – 7.52 (m, 1H), 7.51 – 7.39 (m, 2H), 7.13 (t, *J* = 4.9 Hz, 1H), 3.66 – 3.55 (m, 2H), 3.46 (m, 2H).

¹³C NMR (75 MHz, CDCl₃) δ 199.0, 170., 157.1, 137.1, 133.2, 128.7, 128.3, 118.8, 36.2, 33.1.

HRMS: calculated for C₁₃H₁₃N₂O (M+H⁺): 213.1022, found 213.1020 (+1.0 ppm).

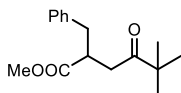


1-phenyl-3-(pyridin-3-yl)butan-1-one (43f): Prepared according to General Procedure H at 60 °C using *tert*-butyldimethyl((1-phenylvinyl)oxy)silane **42a** (70 mg, 0.3 mmol) and (±)-2,4,6-triphenyl-1-(1-(pyridin-3-yl)ethyl)pyridin-1-ium tetrafluoroborate **39i** (100 mg, 0.2 mmol). Flash column chromatography (hexanes/EtOAc 8:2) to afford product **43f** as a yellowish oil (20 mg, 44% yield).

¹H NMR (400 MHz, CDCl₃) δ 8.52 (d, *J* = 4.9, 1H), 8.04 – 7.91 (m, 2H), 7.64 (td, *J* = 7.7 Hz, 1.9 Hz, 1H), 7.58 – 7.49 (m, 1H), 7.48 – 7.37 (m, 2H), 7.30 (d, *J* = 7.8 Hz, 1H), 7.13 (m, 1H), 3.82 – 3.60 (m, 2H), 3.25 (dd, *J* = 16.4 Hz, 5.6 Hz, 1H), 1.40 (d, *J* = 6.8 Hz, 3H).

¹³C NMR (101 MHz, CDCl₃) δ 199.3, 164.9, 148.7, 137.3, 133.1, 128.6, 128.3, 123.0, 121.7, 45.0, 37.2, 21.2.

HRMS: calculated for C₁₅H₁₆NO (M+H⁺): 226.1226, found 226.1222 (+1.8 ppm).

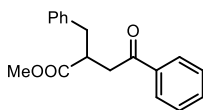
**Methyl 2-benzyl-5,5-dimethyl-4-oxohexanoate (43g):**

Prepared according to General Procedure H with *set-up 2* (75% intensity) and solvent system DMSO/DCE (1:1). 2,6-Lutidine (47 μ L, 0.4 mmol, 2.0 equiv.), methyl 2-benzyl-5,5-dimethyl-4-oxohexanoate **42b** (119 mg, 0.5 mmol) and (\pm)-1-(1-methoxy-1-oxo-3-phenylpropan-2-yl)-2,4,6-triphenylpyridin-1-ium tetrafluoroborate **39I** (111 mg, 0.2 mmol). Flash column chromatography (Hexanes/EtOAc from 98:2 to 96:4) to afford product **43g** as a yellow oil (33 mg, 63% yield).

$^1\text{H NMR}$ (400 MHz, CDCl_3) δ 7.31 – 7.26 (m, 2H), 7.24 – 7.19 (m, 1H), 7.17 – 7.10 (m, 2H), 3.63 (s, 3H), 3.21 – 3.09 (m, 1H), 3.01 (dd, $J = 13.6$ Hz, 6.6 Hz, 1H), 2.93 (dd, $J = 18.1$, 8.9 Hz, 1H), 2.73 (dd, $J = 13.6$ Hz, 8.3 Hz, 1H), 2.52 (dd, $J = 18.1$ Hz, 4.6 Hz, 1H), 1.10 (s, 9H).

$^{13}\text{C NMR}$ (101 MHz, CDCl_3) δ 214.2, 175.6, 138.8, 129.1, 128.6, 126.7, 51.9, 44.1, 42.1, 37.93, 37.9, 26.5.

HRMS: calculated for $\text{C}_{18}\text{H}_{21}\text{O}_3$ ($\text{M}+\text{H}^+$): 285.1485, found 285.1475 (+3.5 ppm).

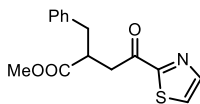
**Methyl 2-benzyl-4-oxo-4-phenylbutanoate (43h):**

Prepared according to General Procedure H using *tert*-butyldimethyl((1-phenylvinyl)oxy)silane **42a** (70 mg, 0.3 mmol) and (\pm)-1-(1-methoxy-1-oxo-3-phenylpropan-2-yl)-2,4,6-triphenylpyridin-1-ium tetrafluoroborate **39I** (111 mg, 0.2 mmol). Flash column chromatography (hexanes/EtOAc 92:8) to afford product **43h** as a yellowish oil (50 mg, 89% yield).

$^1\text{H NMR}$ (400 MHz, CDCl_3) δ 7.93 – 7.87 (m, 2H), 7.59 – 7.50 (m, 1H), 7.43 (dd, $J = 8.4$ Hz, 7.0 Hz, 2H), 7.34 – 7.16 (m, 5H), 3.67 (s, 3H), 3.47 – 3.32 (m, 2H), 3.12 (dd, $J = 13.6$ Hz, 6.0 Hz, 1H), 3.05 – 2.99 (m, 1H), 2.85 (dd, $J = 13.6$, 8.1 Hz, 1H).

$^{13}\text{C NMR}$ (101 MHz, CDCl_3) δ 198.2, 175.4, 133.4, 129.2, 128.7, 128.7, 128.2, 126.8, 52.1, 42.4, 39.5, 38.0.

HRMS: calculated for $\text{C}_{18}\text{H}_{18}\text{NaO}_3$ ($\text{M}+\text{Na}^+$): 305.1148, found 305.1142 (+2.0 ppm).

**Methyl 2-benzyl-4-oxo-4-(thiazol-2-yl)butanoate (43i):**

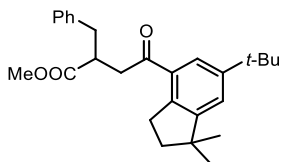
Prepared according to General Procedure H using 2-(1-((*tert*-butyldimethylsilyloxy)vinyl)thiazole **42c** (73 mg, 0.3 mmol) and (\pm)-1-(1-methoxy-1-oxo-3-phenylpropan-2-yl)-2,4,6-triphenylpyridin-1-ium tetrafluoroborate **39I** (111 mg, 0.2 mmol). Flash column chromatography

(Hexanes/Acetone 95:5) to afford product **43i** as a yellowish solid (46 mg, 79% yield).

¹H NMR (300 MHz, CDCl₃) δ 7.98 (d, *J* = 3.0 Hz, 1H), 7.65 (d, *J* = 3.0 Hz, 1H), 7.33 – 7.26 (m, 2H), 7.23 – 7.18 (m, 3H), 3.76 – 3.58 (m, 4H), 3.40 – 3.30 (m, 1H), 3.26 – 3.10 (m, 2H), 2.84 (dd, *J* = 13.6, 8.6 Hz, 1H).

¹³C NMR (75 MHz, CDCl₃) δ 192.0 (C), 174.9 (C), 166.7 (C), 144.9 (CH), 138.5 (C), 129.2 (CH), 128.7 (CH), 126.8 (CH), 126.4 (CH), 52.1 (CH₃), 42.3 (CH), 39.5 (CH₂), 38.0 (CH₂).

HRMS: calculated for C₁₅H₁₅NNaO₃S (M+Na⁺): 312.0665, found 312.0665 (+0.0 ppm).



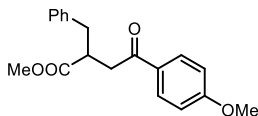
Methyl 2-benzyl-4-(6-(tert-butyl)-1,1-dimethyl-2,3-dihydro-1H-inden-4-yl)-4-oxobutanoate (43j):

Prepared according to General Procedure H using tert-butyl((1-(6-(tert-butyl)-1,1-dimethyl-2,3-dihydro-1H-inden-4-yl)vinyl)oxy)dimethylsilane **42d** (108 mg, 0.3 mmol) and (±)-1-(1-methoxy-1-oxo-3-phenylpropan-2-yl)-2,4,6-triphenylpyridin-1-ium tetrafluoroborate **39i** (111 mg, 0.2 mmol). Flash column chromatography (Hexanes/EtOAc 98:2) to afford product **43j** as a yellowish oil (74 mg, 91% yield).

¹H NMR (400 MHz, CDCl₃) δ 7.62 (d, *J* = 1.8 Hz, 1H), 7.33 – 7.26 (m, 3H), 7.24 – 7.17 (m, 3H), 3.66 (s, 3H), 3.47 – 3.22 (m, 2H), 3.14 – 3.07 (m, 3H), 3.05 – 2.97 (m, 1H), 2.84 (dd, *J* = 13.5, 7.9 Hz, 1H), 1.94 – 1.87 (m, 2H), 1.33 (s, 9H), 1.24 (d, *J* = 2.6 Hz, 6H).

¹³C NMR (101 MHz, CDCl₃) δ 200.2, 175.6, 154.5, 150.1, 141.2, 138.9, 133.3, 129.2, 128.6, 126.7, 124.0, 123.5, 52.0, 43.6, 42.6, 41.6, 41.5, 38.1, 34.9, 31.6, 30.88, 28.9.

HRMS: calculated for C₂₇H₃₄NaO₃ (M+Na⁺): 429.2400, found 429.2409 (+2.1 ppm).



Methyl 2-benzyl-4-(4-methoxyphenyl)-4-oxobutanoate (43k):

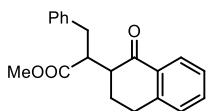
Prepared according to General Procedure H using tert-butyl((1-(4-methoxyphenyl)vinyl)oxy)dimethylsilane **42e** (80 mg, 0.3 mmol) and (±)-1-(1-methoxy-1-oxo-3-phenylpropan-2-yl)-2,4,6-triphenylpyridin-1-ium tetrafluoroborate **39i** (111 mg, 0.2 mmol). Flash column chromatography

(Hexanes/EtOAc 93:7) to afford product **43k** as an off-white solid (52 mg, 83% yield).

¹H NMR (400 MHz, CDCl₃) δ 7.88 (d, *J* = 9.0 Hz, 2H), 7.32 – 7.27 (m, 2H), 7.24 – 7.17 (m, 3H), 6.90 (d, *J* = 9.0 Hz, 2H), 3.86 (s, 3H), 3.66 (s, 3H), 3.44 – 3.26 (m, 2H), 3.10 (dd, *J* = 13.6, 5.9 Hz, 1H), 2.97 (d, *J* = 12.9 Hz, 1H), 2.84 (dd, *J* = 13.6, 7.9 Hz, 1H).

¹³C NMR (101 MHz, CDCl₃) δ 196.7, 175.6, 163.7, 138.7, 130.4, 129.9, 129.2, 128.7, 126.8, 113.8, 55.6, 52.0, 42.4, 39.2, 38.0.

HRMS: calculated for C₂₇H₃₄NaO₃ (M+Na⁺): 429.2400, found 429.2409 (–2.1 ppm).



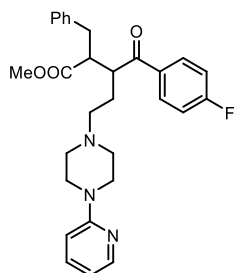
Methyl 2-benzyl-4-(6-(tert-butyl)-1,1-dimethyl-2,3-dihydro-1H-inden-4-yl)-4-oxobutanoate (43l): Prepared according to General Procedure H using tert-butyl((3,4-

dihydronaphthalen-1-yl)oxy)dimethylsilane **42f** (104 mg, 0.4 mmol) and (±)-1-(1-methoxy-1-oxo-3-phenylpropan-2-yl)-2,4,6-triphenylpyridin-1-ium tetrafluoroborate **39l** (111 mg, 0.2 mmol). Flash column chromatography (Hexanes/EtOAc from 95:5 to 85:15) to afford product **43l** as an off-green solid (50 mg, 81% yield, 1:1 dr).

¹H NMR (300 MHz, CDCl₃) (1:1 mixture of diastereoisomers) δ 8.02 (ddd, *J* = 9.7, 7.8, 1.5 Hz, 1H), 7.54 – 7.39 (m, 1H), 7.35 – 7.26 (m, 3H), 7.26 – 7.14 (m, 4H), 3.66 – 3.60 (m, 0.4 H), 3.59 (s, 1.1 H), 3.57 (s, 1.8 H), 3.47 – 3.38 (m, 0.6 H), 3.26 – 3.17 (m, 0.5H), 3.05 – 2.75 (m, 4H), 2.66 – 2.58 (m, 0.7H), 2.19 – 2.32 (m, 1H), 1.94 – 1.87 (m, 1H).

¹³C NMR (75 MHz, CDCl₃) (1:1 mixture of diastereoisomers) δ 197.8, 175.3, 174.3, 143.9, 143.7, 139.9, 139.3, 133.7, 133.5, 132.6, 129.2, 129.0, 128.8, 128.8, 128.7, 128.5, 127.7, 127.7, 126.9, 126.8, 126.6, 126.5, 51.80, 50.3, 48.7, 47.3, 46.1, 35.4, 34.7, 29.6, 29.2, 26.1, 25.4.

HRMS: calculated for C₂₀H₂₀NaO₃ (M+Na⁺): 331.1305, found 331.1289 (+4.8 ppm).



Methyl 2-benzyl-3-(4-fluorobenzoyl)-5-(4-(pyridin-2-yl)piperazin-1-yl)pentanoate (43m): Prepared according to General Procedure H using (*Z*)-1-(4-((*tert*-butyldimethylsilyl)oxy)-4-(4-fluorophenyl)but-3-en-1-yl)-4-(pyridin-2-yl)piperazine **42g** (133 mg, 0.3 mmol) and (\pm)-1-(1-methoxy-1-oxo-3-phenylpropan-2-yl)-2,4,6-triphenylpyridin-1-ium tetrafluoroborate **39I** (111 mg, 0.2

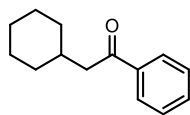
mmol), no water is added into the reaction mixture. Flash column chromatography (Hexanes/Acetone from 7:3 to 1:1) to afford product **43m** as an off-white solid (49 mg, 50% yield, 1.2:1 dr).

$^1\text{H NMR}$ (500 MHz, CDCl_3) δ 8.14 (m, 1H), 8.05 – 7.97 (m, 2H), 7.47 – 7.39 (m, 1H), 7.25 – 7.14 (m, 4H), 7.13 – 7.04 (m, 5H), 6.62 – 6.51 (m, 2H), 3.95 – 3.82 (m, 1H), 3.49 (s, 1H), 3.44 (s, 2H), 3.28 (t, $J = 44.1$ Hz, 4H), 3.12 – 3.04 (m, 1H), 2.80 – 2.61 (m, 1H), 2.34 (d, $J = 37.0$ Hz, 6H), 2.13 (ddd, $J = 13.9, 10.4, 6.4$ Hz, 1H), 1.99 (s, 1H), 1.70 (s, 1H)

$^{13}\text{C NMR}$ (126 MHz, CDCl_3) 1:1 mixture of diastereoisomer δ 200.5, 200.1, 174.5, 174.4, 159.5, 148.1, 148.1, 138.8, 138.6, 137.6, 137.6, 135.1, 134.0, 131.2, 131.2, 131.1, 131.0, 129.0, 128.9, 128.6, 128.5, 126.7, 126.7, 115.9, 115.9, 115.8, 115.7, 113.5, 113.4, 107.2, 107.1, 56.1, 55.9, 52.8, 52.6, 51.8, 51.6, 51.4, 49.2, 45.9, 45.6, 44.9, 44.8, 37.2, 34.7.

$^{19}\text{F NMR}$ (376 MHz, CDCl_3) 1:1 mixture of diastereoisomer δ -105.4 (s, 1F), -105.6 (s, 1F).

HRMS: calculated for $\text{C}_{29}\text{H}_{33}\text{FN}_3\text{O}_3$ ($\text{M}+\text{H}^+$): 490.2500, found 490.2500 (0.0 ppm).



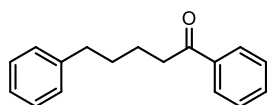
Methyl 2-benzyl-5,5-dimethyl-4-oxohexanoate (43n):

Prepared according to General Procedure H with *set-up 1* and no 2,6-Lutidine. *tert*-butyldimethyl((1-phenylvinyl)oxy)silane **42a** (70 mg, 0.3 mmol) and 1,3-dioxoisindolin-2-yl cyclohexanecarboxylate **36a** (54.5 mg, 0.2 mmol, 1 equiv.). Flash column chromatography (Hexanes/EtOAc from 100:0 to 98:2) to afford product **43n** as a yellow oil (17 mg, 42% yield).

$^1\text{H NMR}$ (400 MHz, CDCl_3) δ 7.98 – 7.92 (m, 2H), 7.58 – 7.51 (m, 1H), 7.49 – 7.42 (m, 2H), 2.82 (d, $J = 6.8$ Hz, 2H), 2.04 – 1.93 (m, 1H), 1.80 – 1.73 (m, 2H), 1.73 – 1.61 (m, 2H), 1.34 – 1.23 (m, 3H), 1.22 – 1.14 (m, 1H), 1.07 – 0.96 (m, 2H).

$^{13}\text{C NMR}$ (101 MHz, CDCl_3) δ 200.5, 137.6, 133.0, 128.7, 128.3, 46.4, 34.7, 33.6, 26.4, 26.3.

Matching reported literature data.⁵⁵



Methyl 2-benzyl-5,5-dimethyl-4-oxohexanoate

(43o): Prepared according to General Procedure H with *set-up 1* and no 2,6-Lutidine. *tert*-butyldimethyl((1-phenylvinyl)oxy)silane **42a** (70 mg, 0.3 mmol) and 1,3-dioxoisindolin-2-yl 4-phenylbutanoate **36b** (62 mg, 0.2 mmol, 1 equiv.). Flash column chromatography (Hexanes/EtOAc from 100:0 to 98:2) to afford product **43o** as a yellow oil (18 mg, 38% yield).

¹H NMR (400 MHz, CDCl₃) δ 7.97 – 7.92 (m, 2H), 7.59 – 7.52 (m, 1H), 7.49 – 7.42 (m, 2H), 7.31 – 7.21 (m, 2H), 7.19 (dt, *J* = 8.0, 1.8 Hz, 3H), 2.99 (t, *J* = 7.2 Hz, 2H), 2.67 (t, *J* = 7.5 Hz, 2H), 1.83 – 1.76 (m, 2H), 1.76 – 1.68 (m, 2H).

¹³C NMR (101 MHz, CDCl₃) δ 200.4, 142.4, 137.2, 133.1, 128.7, 128.5, 128.5, 128.2, 125.9, 38.5, 35.9, 31.2, 29.8, 24.1.

Matching reported literature data.⁵⁶

2.8.6.3 General procedure I (three-component reaction)



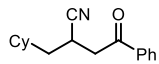
Reactions performed using *set-up 1* in Figure 2.3. In an oven dried vial, with a Teflon septum screw cap, silyl enol ether **42** (0.3 mmol, 1.5 equiv.) was dissolved in DMSO (2 mL), then NHPI ester **36** (0.2 mmol, 1.0 equiv.) was added, followed by catalyst **B** (3.2 mg, 0.02 mmol, 0.1 equiv.), electron-poor olefin **37** (0.34 mmol, 1.7 equiv.) and water (4.0 mmol, 20 equiv.). The resulting orange mixture was degassed by bubbling argon for 60 seconds. The vial was then placed in the 3D printed support photoreactor and irradiated under stirring for 24 hours, unless otherwise specified. The crude mixture was diluted with EtOAc and brine was added. The combined organic fractions were dried over anhydrous MgSO₄ and concentrated to dryness. The crude residue was purified by column

⁵⁵ Kong, W.; Yu, C.; An, H.; Song, Q., Photoredox-Catalyzed Decarboxylative Alkylation of Silyl Enol Ethers To Synthesize Functionalized Aryl Alkyl Ketones. *Org. Lett.* **2018**, *20*, 349-352.

⁵⁶ Zheng, Y.-L.; Xie, P.-P.; Daneshfar, O.; Houk, K. N.; Hong, X.; Newman, S. G., Direct Synthesis of Ketones from Methyl Esters by Nickel-Catalyzed Suzuki–Miyaura Coupling. *Angew. Chem. Int. Ed.* **2021**, *60* (24), 13476-13483.

chromatography on silica gel to afford the corresponding product in the stated yield with >95% purity according to ^1H NMR analysis.

2.8.6.4 Characterization of products with general procedure I



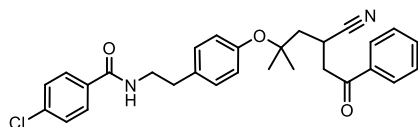
2-(cyclohexylmethyl)-4-oxo-4-phenylbutanenitrile (44a):

Prepared according to General Procedure I using *tert*-butyldimethyl((1-phenylvinyl)oxy)silane **42a** (63 mg, 0.24 mmol), 1,3-dioxoisindolin-2-yl cyclohexanecarboxylate **36a** (55 mg, 0.2 mmol), and acrylonitrile **37b** (22 μL , 0.34 mmol). Flash column chromatography (hexanes/EtOAc 94:6) to afford product **44a** as an off-white solid (31 mg, 61% yield).

^1H NMR (300 MHz, CDCl_3) δ 8.04 – 7.86 (m, 2H), 7.72 – 7.59 (m, 1H), 7.52 – 7.45 (m, 2H), 3.52 – 3.30 (m, 2H), 3.30 – 3.13 (m, 1H), 1.89 (d, $J = 12.9$ Hz, 1H), 1.83 – 1.57 (m, 6H), 1.49 – 1.40 (m, 1H), 1.24 – 1.08 (m, 2H), 1.06 – 0.83 (m, 3H).

^{13}C NMR (75 MHz, CDCl_3) δ 195.5, 136.1, 134.0, 129.0, 128.2, 122.3, 41.5, 39.9, 35.7, 33.8, 32.2, 26.5, 26.2, 26.0, 24.0.

HRMS: calculated for $\text{C}_{17}\text{H}_{21}\text{NNaO}$ ($\text{M}+\text{Na}^+$): 278.1515, found 278.1511 (+1.4 ppm).



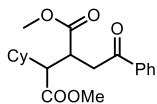
4-chloro-N-(4-((4-cyano-2-methyl-6-oxo-6-phenylhexan-2-yl)oxy)phenethyl)benzamide (44b):

Prepared according to General Procedure I using *tert*-butyldimethyl((1-phenylvinyl)oxy)silane **42a** (63 mg, 0.24 mmol), 1,3-dioxoisindolin-2-yl 2-(4-(2-(4-chlorobenzamido)ethyl)phenoxy)-2-methylpropanoate **36e** (101 mg, 0.2 mmol), and acrylonitrile **37b** (22 μL , 0.34 mmol). Flash column chromatography (hexanes/EtOAc from 7:3 to 1:1) to afford product **44b** as a yellowish fluffy solid (51 mg, 52% yield).

^1H NMR (300 MHz, CDCl_3) δ 8.05 – 7.86 (m, 2H), 7.64 (d, $J = 8.4$ Hz, 3H), 7.57 – 7.46 (m, 2H), 7.42 – 7.38 (m, 2H), 7.14 (d, $J = 8.4$ Hz, 2H), 6.98 (d, $J = 8.4$ Hz, 2H), 6.09 (s, 1H), 3.74 – 3.61 (m, 3H), 3.57 – 3.37 (m, 2H), 2.90 (t, $J = 6.9$ Hz, 2H), 2.23 (dd, $J = 14.2, 9.2$ Hz, 1H), 1.99 (dd, $J = 14.2, 3.8$ Hz, 1H), 1.44 (s, 3H), 1.40 (s, 3H).

^{13}C NMR (75 MHz, CDCl_3) δ 195.8, 166.5, 153.4, 136.1, 134.2, 134.0, 133.5, 129.6, 129.0, 128.4, 128.2, 124.3, 79.2, 44.8, 42.3, 35.0, 27.1, 26.2, 21.9.

HRMS: calculated for $\text{C}_{29}\text{H}_{29}\text{ClN}_2\text{NaO}_3$ ($\text{M}+\text{Na}^+$): 511.1759, found 511.1759 (+0.0 ppm).

**Dimethyl 2-cyclohexyl-3-(2-oxo-2-phenylethyl)succinate**

(44c): Prepared according to General Procedure I using *tert*-butyldimethyl((1-phenylvinyl)oxy)silane **42a** (63 mg, 0.24 mmol), 1,3-dioxoisindolin-2-yl cyclohexanecarboxylate **36a** (55 mg, 0.2 mmol), and dimethylfumarate **37c** (43 mg, 0.3 mmol). Flash column chromatography (hexanes/EtOAc 88:12) to afford the two separable diastereoisomeric products **44c** (major diastereoisomer) and **44c'** (minor diastereoisomer) as off-white solids (d.r. 1:2.5, 50 mg, 72% yield).

Spectroscopic data for 44c:

¹H NMR (300 MHz, CDCl₃) δ 8.05 – 7.86 (m, 2H), 7.63 – 7.52 (m, 1H), 7.52 – 7.45 (m, 2H), 3.69 (s, 3H), 3.67 (s, 3H), 3.67 – 3.59 (m, 1H), 3.46– 2.94 (m, 2H), 2.71 (dd, *J* = 8.7, 5.6 Hz, 1H), 1.81 – 1.59 (m, 6H), 1.22 – 1.17 (m, 2H), 1.09 – 0.77 (m, 3H).

¹³C NMR (75 MHz, CDCl₃) δ 198.3, 174.7, 173.8, 136.7, 133.4, 128.7, 128.3, 52.6, 52.3, 51.7, 39.8, 37.4, 36.6, 31.1, 30.4, 26.3, 26.3, 26.2.

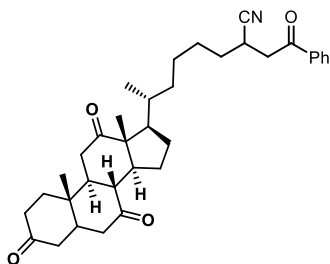
HRMS: calculated for C₂₀H₂₆NaO₅ (M+Na⁺): 369.1677, found 369.1672 (+1.4 ppm).

Spectroscopic data for 44c':

¹H NMR (300 MHz, CDCl₃) δ 8.01 – 7.94 (m, 2H), 7.61 – 7.54 (m, 1H), 7.50 – 7.42 (m, 2H), 3.68 (s, 3H), 3.68 (s, 3H), 3.58 – 3.47 (m, 2H), 3.24 – 3.10 (m, 1H), 2.66 – 2.55 (m, 1H), 1.96 (m, 1H), 1.80 – 1.64 (m, 6H), 1.07 – 0.85 (m, 5H).

¹³C NMR (75 MHz, CDCl₃) δ 197.9, 174.2, 173.9, 136.8, 133.4, 128.8, 128.2, 53.4, 52.2, 51.7, 39.3, 38.1, 37.4, 31.1, 30.9, 26.4, 26.4.

HRMS: calculated for C₂₀H₂₆NaO₅ (M+Na⁺): 369.1677, found 369.1672 (+1.4 ppm).

**6-((5S,8R,9S,10S,13R,14S,17R)-10,13-dimethyl-3,7,12-trioxohexadecahydro-1H-cyclopenta[a]phenanthren-17-yl)-2-(2-oxo-2-phenylethyl)heptanenitrile** (**44d**):

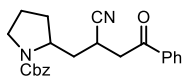
Prepared according to General Procedure I using *tert*-butyldimethyl((1-phenylvinyl)oxy)silane **42a** (63 mg, 0.24 mmol), 1,3-dioxoisindolin-2-yl 4-((5S,8R,9S,10S,13R,14S,17R)-10,13-dimethyl-3,7,12-trioxohexadecahydro-1H-cyclopenta[a]phenanthren-17-yl)pentanoate **36d** (110 mg, 0.2 mmol), and

acrylonitrile **37b** (22 μ L, 0.340 mmol). Flash column chromatography (hexanes/EtOAc 1:1) to afford product **44d** as a white solid (64 mg, 60% yield).

$^1\text{H NMR}$ (300 MHz, CDCl_3) δ 8.03 – 7.89 (m, 2H), 7.72 – 7.57 (m, 1H), 7.53 – 7.45 (m, 2H), 3.63 – 3.15 (m, 3H), 2.99 – 2.75 (m, 3H), 2.39 – 1.80 (m, 14H), 1.77 – 1.43 (m, 6H), 1.40 (s, 3H), 1.35 – 1.16 (m, 3H), 1.07 (s, 3H), 0.86 (dd, $J = 6.4$, 2.0 Hz, 3H).

$^{13}\text{C NMR}$ (75 MHz, CDCl_3) δ 212.0, 209.1, 208.8, 195.3, 135.9, 133.9, 128.9, 128.1, 121.9, 56.9, 51.8, 49.0, 46.9, 45.8, 45.6, 45.0, 42.8, 40.9, 40.8, 38.7, 36.5, 36.0, 36.0, 35.3, 34.8, 32.4, 29.7, 27.9, 26.4, 26.3, 25.2, 24.5, 24.4, 21.9, 19.0, 18.9, 11.9.

HRMS: calculated for $\text{C}_{34}\text{H}_{43}\text{NNaO}_4$ ($\text{M}+\text{Na}^+$): 552.3081, found 552.3084 (–0.5 ppm).



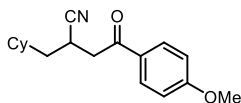
Benzyl 2-(2-cyano-4-oxo-4-phenylbutyl)pyrrolidine-1-carboxylate (44e): Prepared according to General Procedure I

using *tert*-butyldimethyl((1-phenylvinyl)oxy)silane **42a** (63 mg, 0.240 mmol), 1-benzyl 2-(1,3-dioxoisindolin-2-yl) pyrrolidine-1,2-dicarboxylate **36c** (55 mg, 0.2 mmol), and acrylonitrile **37b** (22 μ L, 0.34 mmol). Flash column chromatography (hexanes/acetone 7:3) to afford product **44e** as a reddish oil (47 mg, 62% yield, 1:1 dr).

$^1\text{H NMR}$ (400 MHz, CDCl_3) (1:1 mixture of diastereoisomers) δ 8.01 – 7.79 (m, 2H), 7.68 – 7.59 (m, 1H), 7.50 (t, $J = 7.6$ Hz, 2H), 7.46 – 7.30 (m, 5H), 5.26 – 5.10 (m, 2H), 4.24 – 3.96 (m, 1H), 3.57 – 3.19 (m, 5H), 2.15 – 2.04 (m, 1H), 2.02 – 1.65 (m, 5H).

$^{13}\text{C NMR}$ (101 MHz, CDCl_3) (1:1 mixture of diastereoisomers) δ 195.3, 194.8, 155.3, 136.8, 136.8, 133.8, 128.8, 128.5, 128.1, 127.8, 123.7, 122.0, 121.1, 66.9, 66.8, 56.2, 55.6, 55.3, 46.4, 41.0, 40.7, 36.9, 36.5, 36.0, 32.5, 30.6, 30.3, 29.7, 24.3, 23.9, 23.4, 23.0.

HRMS: calculated for $\text{C}_{23}\text{H}_{24}\text{N}_2\text{NaO}_3$ ($\text{M}+\text{Na}^+$): 399.1679, found 399.1682 (–0.75 ppm).



2-(cyclohexylmethyl)-4-(4-methoxyphenyl)-4-oxobutanenitrile (44f): Prepared according to General Procedure I using *tert*-butyl((1-(4-

methoxyphenyl)vinyl)oxy)dimethylsilane **42e** (65 mg, 0.24 mmol), 1,3-dioxoisindolin-2-yl cyclohexanecarboxylate **36a** (55 mg, 0.2 mmol), and

acrylonitrile **37b** (22 μ L, 0.34 mmol). Flash column chromatography (hexanes/acetone 88:12) to afford product **44f** as an off-white solid (31 mg, 61% yield).

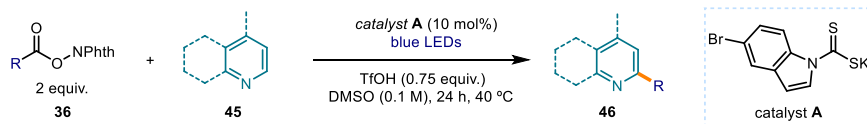
$^1\text{H NMR}$ (300 MHz, CDCl_3) δ 7.93 (d, J = 8.9 Hz, 2H), 6.95 (d, J = 8.9 Hz, 2H), 3.88 (s, 3H), 3.42 – 3.29 (m, 2H), 3.21 – 3.10 (m, 1H), 1.88 (d, J = 12.8 Hz, 1H), 1.77 – 1.58 (m, 7H), 1.23 – 1.10 (m, 2H), 1.00 – 0.79 (m, 3H).

$^{13}\text{C NMR}$ (75 MHz, CDCl_3) δ 193.9, 164.2, 130.5.0, 129.2, 122.4, 114.1, 55.7, 41.1, 39.9, 35.7, 33.8, 32.2, 26.5, 26.2, 26.0, 24.0.

HRMS: calculated for $\text{C}_{18}\text{H}_{23}\text{NNaO}_2$ ($\text{M}+\text{Na}^+$): 308.1630, found 308.1621 (+2.9 ppm).

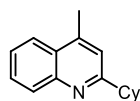
2.8.7 Minisci reaction

2.8.7.1 General procedure J



Reactions performed using *set-up 1* in Figure 2.3. In an oven dried vial, with a Teflon septum screw cap, heteroarene **45** (0.2 mmol, 1.0 equiv.) and trifluoromethanesulfonic acid (13.3 μ L, 0.15 mmol, 0.75 equiv.) were dissolved in DMSO (2 ml). Then, NHPI ester **36** (0.4 mmol, 2 equiv.) and catalyst **A** (6.2 mg, 0.02 mmol, 0.1 equiv.) were added. The resulting yellow mixture was degassed with argon sparging for 60 seconds. The vial was placed in the 3D printed photoreactor and irradiated under stirring for 24 hours, unless otherwise specified. The mixture was transferred to an extraction funnel, NaHCO_3 sat. solution was added and the organic layer was extracted with EtOAc. The organic layer was washed with brine twice. The combined organic layers were dried over anhydrous MgSO_4 , filtered, and concentrated to dryness. The crude residue was purified by column chromatography to afford the corresponding product in the stated yield with >95% purity according to $^1\text{H NMR}$ analysis.

2.8.7.2 Characterization of products with general procedure J



2-Cyclohexyl-4-methylquinoline (46a): Synthesized according to General

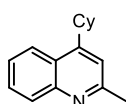
Procedure J using 1,3-dioxoisindolin-2-yl cyclohexanecarboxylate **36a** (109 mg, 0.4 mmol, 2 equiv.) and 4-methylquinoline **45a** (26.4 μ L, 0.2 mmol, 1 equiv.). The crude mixture was purified by flash column

chromatography on silica gel (10% EtOAc in hexane as eluent) to afford **46a** (39.6 mg, 88% yield) as a yellow oil.

$^1\text{H NMR}$ (400 MHz, CDCl_3) δ 8.28 (s, 1H), 7.98 – 7.96 (m, 1H), 7.74 – 7.70 (m, 1H), 7.57 – 7.53 (m, 1H), 7.23 (s, 1H), 3.15 – 3.10 (m, 1H), 2.73 (s, 3H), 2.06 – 2.01 (m, 2H), 1.89 (dt, $J = 13.0, 3.3$ Hz, 2H), 1.83 – 1.76 (m, 1H), 1.63 (qd, $J = 12.3, 3.0$ Hz, 2H), 1.49 (qt, $J = 12.8, 3.0$ Hz, 2H), 1.38 – 1.30 (m, 1H).

$^{13}\text{C NMR}$ (101 MHz, CDCl_3) δ 166.0, 130.2, 128.1, 127.1, 126.3, 123.8, 120.3, 46.5, 32.9, 26.5, 26.1, 19.3.

Matching reported literature data.⁵⁷

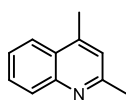


4-Cyclohexyl-2-methylquinoline (46b): Synthesized according to General Procedure J using 1,3-dioxoisindolin-2-yl cyclohexanecarboxylate **36a** (109 mg, 0.4 mmol, 2 equiv.) and 2-methylquinoline **45b** (27.1 μL , 0.2 mmol, 1.0 equiv.). The crude mixture was purified by flash column chromatography on silica gel (10% EtOAc in hexane as eluent) to afford **46b** (42.3 mg, 94% yield) as a yellow oil.

$^1\text{H NMR}$ (400 MHz, CDCl_3) δ 8.05 (t, $J = 9.8$ Hz, 2H), 7.67 - 7.63 (m, 1H), 7.51 – 7.47 (m, 1H), 7.17 (s, 1H), 3.32 – 3.27 (ddd, $J = 11.4, 8.3, 3.4$ Hz, 1H), 2.73 (s, 3H), 2.05 – 1.90 (m, 4H), 1.88 - 1.83 (m, 1H), 1.61 – 1.48 (m, 4H), 1.40 – 1.31 (m, 4H).

$^{13}\text{C NMR}$ (101 MHz, CDCl_3) δ 158.8, 153.8, 147.9, 129.4, 129.1, 125.5, 125.3, 123.0, 118.5, 39.0, 33.7, 27.1, 26.5, 25.5.

Matching reported literature data.⁵⁷



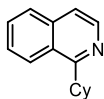
2,4-Dimethylquinoline (46c): Synthesized according to General Procedure J using 1,3-dioxoisindolin-2-yl acetate **36g** (82.1 mg, 0.4 mmol, 2 equiv.) and 2-methylquinoline **45b** (27.1 μL , 0.2 mmol, 1.0 equiv.) in NMP (2 ml) for 48 hours. The crude mixture was purified by flash column chromatography on silica gel (20% CH_2Cl_2 in MeOH as eluent) to afford **46c** (28.3 mg, 90% yield) as a colorless oil.

⁵⁷ McCallum, T.; Barriault, L., Direct alkylation of heteroarenes with unactivated bromoalkanes using photoredox gold catalysis. *Chem. Sci.* **2016**, 7, 4754-4758.

$^1\text{H NMR}$ (400 MHz, CDCl_3) δ 8.09 (dt, $J = 8.5, 0.9$ Hz, 1H), 7.89 – 7.85 (m, 1H), 7.72 (ddd, $J = 8.4, 6.9, 1.4$ Hz, 1H), 7.54 (ddd, $J = 8.3, 6.9, 1.3$ Hz, 1H), 6.98 (s, 1H), 2.86 (s, 3H), 2.73 (s, 3H).

$^{13}\text{C NMR}$ (101 MHz, CDCl_3) δ 159.2, 148.6, 129.9, 129.7, 126.4, 124.1, 123.4, 122.1, 29.8, 25.6.

Matching reported literature data.⁵⁸

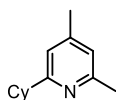


1-Cyclohexylisoquinoline (46d): Synthesized according to General Procedure J using 1,3-dioxoisindolin-2-yl cyclohexanecarboxylate **36a** (109 mg, 0.4 mmol, 2 equiv.) and isoquinoline **45c** (25.8 mg, 0.2 mmol, 1.0 equiv.). The crude mixture was purified by flash column chromatography on silica gel (10% EtOAc in hexane as eluent) to afford **46d** (40.9 mg, 97% yield) as a colorless oil.

$^1\text{H NMR}$ (400 MHz, CDCl_3) δ 8.50 (d, $J = 5.8$ Hz, 1H), 8.25 (d, $J = 8.5$ Hz, 1H), 7.83 (d, $J = 8.3$ Hz, 1H), 7.72 – 7.66 (m, 1H), 7.63 – 7.59 (ddd, $J = 8.3, 6.9, 1.4$ Hz, 1H), 7.53 (d, $J = 5.8$ Hz, 1H), 3.58 (tt, $J = 11.6, 3.2$ Hz, 1H), 2.05 – 1.78 (m, 7H), 1.61 – 1.37 (m, 3H).

$^{13}\text{C NMR}$ (101 MHz, CDCl_3) δ 165.7, 141.1, 136.8, 130.3, 127.8, 127.3, 126.4, 125.1, 119.4, 41.6, 32.7, 27.0, 26.3.

Matching reported literature data.⁵⁷



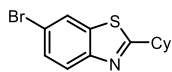
2-Cyclohexyl-4,6-dimethylpyridine (46e): Synthesized according to General Procedure J using 1,3-dioxoisindolin-2-yl acetate **36a** (109 mg, 0.4 mmol, 2 equiv) and 2,4-dimethylpyridine **45d** (23.1 μL , 0.2 mmol, 1.0 equiv.). The crude mixture was purified by flash column chromatography on silica gel (10% EtOAc in hexane as eluent) to afford **46e** (31.3 mg, 83% yield) as a colorless oil.

$^1\text{H NMR}$ (400 MHz, CDCl_3) δ 6.80 (s, 2H), 2.71 (dd, $J = 8.5, 4.8$ Hz, 1H), 2.50 (s, 3H), 2.29 (s, 3H), 1.95 (dd, $J = 13.4, 3.0$ Hz, 2H), 1.86 – 1.79 (m, 2H), 1.78 – 1.70 (m, 1H), 1.51 – 1.36 (m, 4H), 1.33 – 1.25 (m, 1H).

$^{13}\text{C NMR}$ (101 MHz, CDCl_3) δ 165.8, 157.0, 122.0, 118.6, 44.1, 33.3, 26.7, 26.3, 23.1, 21.2.

⁵⁸ Zidan, M.; Morris, A. O.; McCallum, T.; Barriault, L., The Alkylation and Reduction of Heteroarenes with Alcohols Using Photoredox Catalyzed Hydrogen Atom Transfer via Chlorine Atom Generation. *Eur. J. Org. Chem.* **2020**, 1453-1458.

Matching reported literature data.⁵⁷

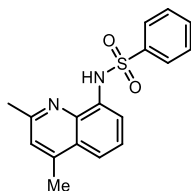


6-Bromo-2-cyclohexylbenzo[d]thiazole (46f): Synthesized according to General Procedure J using 1,3-dioxoisindolin-2-yl cyclohexanecarboxylate **36a** (109 mg, 0.4 mmol, 2 equiv.) and 6-bromo-1,3-benzothiazole **45e** (42.8 mg, 0.2 mmol, 1.0 equiv.). The crude mixture was purified by flash column chromatography on silica gel (10% AcOEt in hexane as eluent) to afford **46f** (49.1 mg, 83% yield) as a white solid.

¹H NMR (500 MHz, CDCl₃) δ 7.96 (d, *J* = 2.0 Hz, 1H), 7.81 (d, *J* = 8.7 Hz, 1H), 7.53 (dd, *J* = 8.7, 2.0 Hz, 1H), 3.07 (tt, *J* = 11.6, 3.6 Hz, 1H), 2.22 – 2.15 (m, 2H), 1.88 (dp, *J* = 10.6, 3.5 Hz, 2H), 1.76 (dtt, *J* = 13.1, 3.4, 1.5 Hz, 1H), 1.69 – 1.57 (m, 2H), 1.50 – 1.37 (m, 2H), 1.32 (tt, *J* = 12.5, 3.5 Hz, 1H).

¹³C NMR (126 MHz, CDCl₃) δ 178.3, 152.1, 136.4, 129.4, 124.2, 123.8, 118.2, 43.5, 33.5, 26.1, 25.9.

Matching reported literature data.⁵⁸

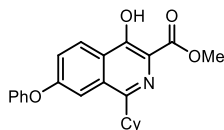


N-(2,4-Dimethylquinolin-8-yl) benzenesulfonamide (46g): Synthesized according to General Procedure J using 1,3-dioxoisindolin-2-yl acetate **36g** (82.1 mg, 0.4 mmol, 2.0 equiv.) and 2-((4-((7-chloro-2-methylquinolin-4-yl) amino) pentyl) (ethyl) amino) ethan-1-ol **45f** (59.7 mg, 0.2 mmol, 1.0 equiv.) in NMP (2 ml, 0.1 M) for 48 hours. The crude mixture was purified by flash column chromatography on silica gel (20% CH₂Cl₂ in MeOH as eluent) to afford **46g** (37.5 mg, 60% yield) as a white solid.

¹H NMR (300 MHz, CDCl₃) δ 9.48 (s, 1H), 8.01 – 7.91 (m, 2H), 7.80 (dd, *J* = 7.3, 1.5 Hz, 1H), 7.53 – 7.36 (m, 5H), 6.98 (s, 1H), 2.82 (s, 3H), 2.70 (s, 3H).

¹³C NMR (101 MHz, CDCl₃) δ 176.0, 158.0, 139.6, 138.2, 134.0, 133.0, 129.1, 127.4, 126.7, 124.2, 116.7, 115.4, 29.1, 25.3.

HRMS: calculated for C₁₇H₁₆N₂NaO₂S (M+Na⁺): 335.3762, found: 335.3768.



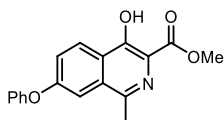
Methyl 1-cyclohexyl-4-hydroxy-7-phenoxyisoquinoline-3-carboxylate (46h): Synthesized according to General Procedure J using 1,3-dioxoisindolin-2-yl cyclohexanecarboxylate **36a** (109 mg, 0.4 mmol, 2.0 equiv.) and Roxadustat analogue **45g** (59.1 mg, 0.2 mmol, 1.0

equiv.). The crude mixture was purified by flash column chromatography on silica gel (50% EtOAc in hexane as eluent) to afford **46h** (67.1 mg, 89% yield) as a white solid.

¹H NMR (400 MHz, CDCl₃) δ 8.41 (d, *J* = 9.1 Hz, 1H), 7.62 (d, *J* = 2.4 Hz, 1H), 7.49 – 7.41 (m, 3H), 7.27 – 7.21 (m, 1H), 7.17 – 7.10 (m, 2H), 4.08 (s, 3H), 3.18 (tt, *J* = 11.6, 3.3 Hz, 1H), 1.99 – 1.85 (m, 4H), 1.86 – 1.71 (m, 3H), 1.51 – 1.31 (m, 3H).

¹³C NMR (101 MHz, CDCl₃) δ 171.8, 159.0, 156.1, 155.4, 155.4, 131.4, 130.3, 126.2, 124.6, 124.2, 121.9, 119.8, 119.0, 111.4, 53.0, 41.9, 32.2, 26.8, 26.2.

HRMS: calculated for C₂₃H₂₄NO₄ (M+H⁺): 378.1700, found: 378.1702.

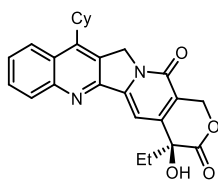


Methyl 4-hydroxy-1-methyl-7-phenoxyisoquinoline-3-carboxylate (46i): Synthesized according to General Procedure J using 1,3-dioxoisindolin-2-yl acetate **36g** (82.1 mg, 0.4 mmol, 2.0 equiv.) and Roxadustat analogue **45g** (59.1 mg, 0.2 mmol, 1.0 equiv.) in NMP (2 ml) for 48 hours. The crude mixture was purified by flash column chromatography on silica gel (50% EtOAc in hexane as eluent) to afford **46i** (57.5 mg, 93% yield) as a white solid.

¹H NMR (300 MHz, CDCl₃) δ 11.83 (s, 1H), 8.44 (d, *J* = 9.1 Hz, 1H), 7.53 – 7.43 (m, 3H), 7.38 (m, 1H), 7.29 (tt, *J* = 6.4, 1.2 Hz, 1H), 7.16 – 7.09 (m, 2H), 4.04 (s, 3H), 2.71 (s, 3H).

¹³C NMR (101 MHz, CDCl₃) δ 175.4, 160.1, 156.4, 155.2, 147.5, 130.7, 130.5, 126.7, 125.4, 124.2, 122.4, 120.4, 119.1, 108.6, 53.0, 30.0.

Matching reported literature data.⁵⁹



(S)-11-Cyclohexyl-4-ethyl-4-hydroxy-1,12-dihydro-14H-pyrano [3',4':6,7] indolizino [1,2-b] quinoline-3,14(4H)-dione (46j): Synthesized according to General Procedure using J 1,3-dioxoisindolin-2-yl cyclohexanecarboxylate **36a** (109 mg, 0.4 mmol, 2 equiv.) and Camptothecin **45h** (69.7 mg, 0.2 mmol, 1.0 equiv.). The crude mixture was

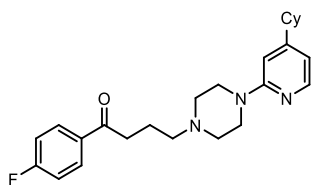
⁵⁹ Wei, W.; Wang, L.; Bao, P.; Shao, Y.; Yue, H.; Yang, D.; Yang, X.; Zhao, X.; Wang, H., Metal-Free C(sp²)-H/N-H Cross-Dehydrogenative Coupling of Quinoxalinones with Aliphatic Amines under Visible-Light Photoredox Catalysis. *Org. Lett.* **2018**, *20*, 7125-7130.

purified by flash column chromatography on silica gel (5% CH₂Cl₂ in MeOH as eluent) to afford **46j** (41,3 mg, 48% yield) as a white solid.

¹H NMR (400 MHz, CDCl₃) δ 8.27 – 8.15 (d, *J* = 8.4 Hz, 2H), δ 7.76 (t, *J* = 7.5 Hz, 1H), 7.66 - 7.61 (m, 2H), 5.74 (d, *J* = 16.3 Hz, 1H), 5.39 (s, 2H), 5.29 (d, *J* = 16.3 Hz, 1H), 3.95 (s, 1H), 3.61 (s, 1H), 2.06 – 1.82 (m, 8H), 1.66 – 1.53 (m, 3H), 1.46 (t, *J* = 12.7 Hz, 1H), 1.03 (t, *J* = 7.4 Hz, 3H).

¹³C NMR (101 MHz, CDCl₃) δ 174.1, 157.7, 150.4, 148.8, 130.9, 130.0, 127.8, 127.1, 118.5, 97.9, 72.9, 66.5, 50.8, 31.9, 31.8, 29.8, 27.1, 26.1, 8.0.

Matching reported literature data.⁶⁰



4-(4-(4-Cyclohexylpyridin-2-yl) piperazin-1-yl)-1-(4-fluorophenyl) butan-1-one (46k):

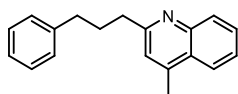
Synthesized according to General Procedure J using 1,3-dioxoisindolin-2-yl cyclohexanecarboxylate **36a** (109 mg, 0.4 mmol, 2.0 equiv.) and Azaperone **45i** (65.5 mg, 0.2 mmol, 1.0 equiv.). The crude mixture was purified by flash column chromatography on silica gel (50% EtOAc in hexane as eluent) to afford **46k** (21.3 mg, 26% yield) as a white solid.

¹H NMR (400 MHz, Acetone-*d*₆) δ 8.15 – 8.07 (m, 2H), 7.46 (dd, *J* = 8.4, 7.3 Hz, 1H), 7.30 – 7.24 (m, 2H), 6.63 (d, *J* = 8.4 Hz, 1H), 6.54 (d, *J* = 7.4 Hz, 1H), 3.65 – 3.53 (m, 4H), 3.19 (t, *J* = 6.9 Hz, 2H), 3.00 – 2.90 (m, 5H), 2.52 (tt, *J* = 11.8, 3.4 Hz, 1H), 2.15 – 2.07 (m, 2H), 1.83 – 1.28 (m, 10H).

¹³C NMR (101 MHz, Acetone-*d*₆) δ 198.7, 165.1, 159.5, 138.7, 131.8, 131.7, 116.4, 116.2, 111.1, 105.1, 58.1, 53.5, 47.1, 45.1, 36.4, 33.5, 30.6, 27.3, 26.9.

¹⁹F NMR (376 MHz, Acetone-*d*₆) δ –108.12.

HRMS: calculated for C₂₅H₃₃FN₃O (M+H⁺): 410.2602, found 410.2595 (–1.7 ppm).



4-Methyl-2-(3-phenylpropyl)quinoline (46l):

Synthesized according to General Procedure J using 1,3-dioxoisindolin-2-yl 4-phenylbutanoate **36b** (123 mg, 0.4 mmol, 2.0 equiv.) and 4-methylquinoline **45a** (26.4 μL, 0.2 mmol, 1.0 equiv.). The

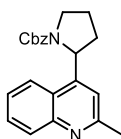
⁶⁰ Li, G.-X.; Morales-Rivera, C. A.; Wang, Y.; Gao, F.; He, G.; Liu, P.; Chen, G., Photoredox-mediated Minisci C–H alkylation of N-heteroarenes using boronic acids and hypervalent iodine. *Chem. Sci.* **2016**, *7*, 6407-6412.

crude mixture was purified by flash column chromatography on silica gel (10% EtOAc in hexane as eluent) to afford **46l** (46.0 mg, 88% yield) as a white solid.

$^1\text{H NMR}$ (400 MHz, CDCl_3) δ 8.11 – 8.03 (m, 1H), 7.95 (dd, $J = 8.3, 1.4$ Hz, 1H), 7.68 (ddd, $J = 8.4, 6.9, 1.4$ Hz, 1H), 7.51 (ddd, $J = 8.2, 6.9, 1.3$ Hz, 1H), 7.33 – 7.26 (m, 2H), 7.26 – 7.15 (m, 3H), 7.13 (d, $J = 1.1$ Hz, 1H), 3.03 – 2.95 (m, 2H), 2.79 – 2.71 (m, 2H), 2.67 (d, $J = 1.0$ Hz, 3H), 2.21 – 2.10 (m, 2H).

$^{13}\text{C NMR}$ (101 MHz, CDCl_3) δ 162.3, 147.7, 144.6, 142.3, 129.4, 129.3, 128.6, 128.4, 126.9, 125.9, 125.7, 123.7, 122.2, 38.8, 35.9, 31.7, 18.8.

HRMS: calculated for $\text{C}_{19}\text{H}_{20}\text{N}$ ($\text{M}+\text{H}^+$): 262.1586, found 262.1590 (+1.5 ppm).



Benzyl 2-(2-methylquinolin-4-yl)pyrrolidine-1-carboxylate

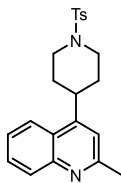
(46m): Synthesized according to General Procedure J using 1-benzyl 2-(1,3-dioxoisindolin-2-yl) pyrrolidine-1,2-dicarboxylate **36c** (157 mg, 0.4 mmol, 2 equiv.) and 2-methylquinoline **45b** (27.1 μL , 0.2

mmol, 1.0 equiv.). The crude mixture was purified by flash column chromatography on silica gel (30% EtOAc in hexane as eluent) to afford **46m** (57.3 mg, 83% yield) as a yellow oil.

$^1\text{H NMR}$ (400 MHz, CDCl_3) mixture of rotamers: δ 8.08 (t, $J = 9.5$ Hz, 1H), 7.92 (dd, $J = 8.8, 4.0$ Hz, 1H), 7.67 (dt, $J = 12.4, 7.6$ Hz, 1H), 7.50 (t, $J = 7.5$ Hz, 1H), 7.44 – 7.28 (m, 2H), 7.11 (dt, $J = 14.7, 7.2$ Hz, 2H), 6.98 (d, $J = 3.3$ Hz, 1H), 6.85 (d, $J = 7.4$ Hz, 1H), 5.76 – 5.61 (m, 1H), 5.18 (s, 1H), 5.10 – 4.83 (m, 1H), 3.82 (td, $J = 9.5, 8.2, 3.1$ Hz, 1H), 3.77 – 3.62 (m, 1H), 2.67 (d, $J = 26.7$ Hz, 3H), 2.59 – 2.40 (m, 1H), 2.00 – 1.79 (m, 3H).

$^{13}\text{C NMR}$ (101 MHz, CDCl_3) mixture of rotamers: δ 158.8, 158.6, 154.9, 149.3, 148.6, 148.0, 136.9, 136.5, 129.5, 129.3, 128.6, 128.3, 128.2, 128.1, 127.8, 127.4, 125.8, 124.1, 124.0, 123.0, 122.8, 117.6, 117.3, 67.2, 66.7, 58.1, 57.5, 47.6, 47.3, 34.2, 33.2, 25.5, 23.7, 23.0.

HRMS: calculated for $\text{C}_{22}\text{H}_{23}\text{N}_2\text{O}_2$ ($\text{M}+\text{H}^+$): 347.1754, found 347.1760 (-1.7 ppm).



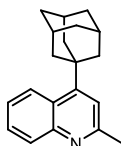
2-Methyl-4-(1-tosylpiperidin-4-yl)quinoline (46n): Synthesized according to General Procedure J using 1,3-dioxoisindolin-2-yl 1-tosylpiperidine-4-carboxylate **36f** (171 mg, 0.4 mmol, 2.0 equiv.) and 2-methylquinoline **45b** (27.1 μL , 0.2 mmol, 1.0 equiv.) using *set-up 4* at 60 $^{\circ}\text{C}$. The crude mixture was purified by flash column

chromatography on silica gel (30% EtOAc in hexane as eluent) to afford **46n** (56.2 mg, 74% yield) as a white solid.

¹H NMR (400 MHz, CDCl₃) δ 8.04 (dd, *J* = 8.5, 1.3 Hz, 1H), 7.85 (dd, *J* = 8.5, 1.4 Hz, 1H), 7.74 – 7.67 (m, 2H), 7.63 (ddd, *J* = 8.3, 6.8, 1.4 Hz, 1H), 7.43 (ddd, *J* = 8.3, 6.8, 1.3 Hz, 1H), 7.36 (d, *J* = 2.0 Hz, 2H), 7.12 (s, 1H), 4.08 – 3.96 (m, 2H), 3.20 (tt, *J* = 11.5, 3.8 Hz, 1H), 2.71 (s, 3H), 2.47 (m, 5H), 2.07 – 1.85 (m, 4H).

¹³C NMR (101 MHz, CDCl₃) δ 159.0, 150.3, 148.2, 143.8, 133.1, 129.9, 129.8, 129.2, 127.9, 125.8, 124.8, 122.2, 118.6, 47.0, 36.4, 31.8, 25.5, 21.7.

HRMS: calculated for C₂₂H₂₅N₂O₂S (M+H⁺): 381.1627, found 381.1631 (+1.1 ppm).

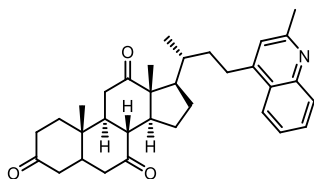


4-((3S)-Adamantan-1-yl)-2-methylquinoline (46o): Synthesized according to General Procedure J using 1,3-dioxoisindolin-2-yl (3*r*,5*r*,7*r*)-adamantane-1-carboxylate **36h** (130 mg, 0.4 mmol, 2 equiv.) and 2-methylquinoline **45b** (27.1 μL, 0.2 mmol, 1.0 equiv.) using *set-up 4* at 60 °C. The crude mixture was purified by flash column chromatography on silica gel (10% EtOAc in hexane as eluent) to afford **46o** (38.2 mg, 69% yield) as a white solid.

¹H NMR (400 MHz, CDCl₃) δ 8.62 (d, *J* = 8.8 Hz, 1H), 8.35 (s, 1H), 7.69 (ddd, *J* = 8.3, 6.8, 1.3 Hz, 1H), 7.52 (ddd, *J* = 8.5, 6.8, 1.5 Hz, 1H), 7.28 (s, 1H), 2.85 (s, 3H), 2.29 – 2.28 (m, 6H), 2.23 - 2.22 (m, 3H), 1.89 (t, *J* = 3.1 Hz, 6H).

¹³C NMR (101 MHz, CDCl₃) δ 159.5, 130.1, 126.3, 125.4, 125.3, 119.7, 42.3, 39.3, 36.9, 29.1.

HRMS: calculated for C₂₀H₂₄N (M+H⁺): 278.1897, found 278.1903 (+2.2 ppm).



(8*R*,9*S*,10*S*,13*R*,14*S*,17*R*)-10,13-dimethyl-17-((*R*)-4-(2-methylquinolin-4-yl)butan-2-yl)dodecahydro-3H-cyclopenta[*a*]phenanthrene-3,7,12(2*H*,4*H*)-trione (46p): Synthesized according to General

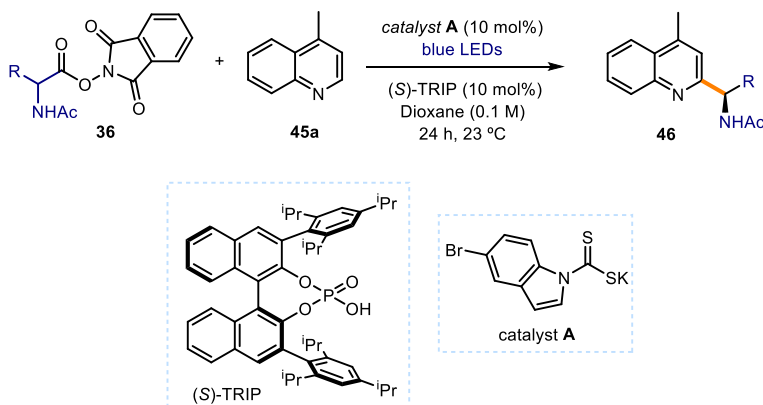
Procedure J using Dehydrocholic acid NHPI ester **36d** (219 mg, 0.4 mmol, 2.0 equiv.) and 2-methylquinoline **45b** (27.1 μL, 0.2 mmol, 1.0 equiv.). The crude mixture was purified by flash column chromatography on silica gel (30% EtOAc in hexane as eluent) to afford **46p** (70.0 mg, 61% yield) as a white solid.

¹H NMR (400 MHz, CDCl₃) δ 8.12 (d, *J* = 8.4 Hz, 1H), 7.96 (dd, *J* = 8.5, 1.4 Hz, 1H), 7.67 (ddd, *J* = 8.4, 6.9, 1.4 Hz, 1H), 7.51 (ddd, *J* = 8.2, 6.9, 1.3 Hz, 1H), 7.14 (s, 1H), 3.15 (ddd, *J* = 13.7, 11.7, 5.0 Hz, 1H), 2.96 – 2.85 (m, 4H), 2.74 (s, 3H), 2.41 – 1.22 (m, 19H), 1.39 (s, 3H), 1.08 (s, 3H), 1.05 (d, *J* = 6.6 Hz, 3H).

^{13}C NMR (101 MHz, CDCl_3) δ 212.1, 209.1, 208.8, 158.4, 150.6, 146.9, 129.7, 128.6, 126.0, 125.9, 123.4, 121.8, 57.0, 51.9, 49.1, 46.9, 45.7, 45.6, 45.1, 42.9, 38.7, 36.6, 36.5, 36.3, 36.1, 35.4, 29.5, 27.9, 25.2, 24.8, 22.0, 19.2, 12.0.

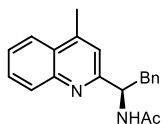
HRMS: calculated for $\text{C}_{33}\text{H}_{42}\text{NO}_3$ ($\text{M}+\text{H}^+$): 500.3157, found: 500.3159 (+0.4 ppm).

2.8.7.3 General procedure K (enantioselective variant)



Reactions performed using *set-up 4* in Figure 2.8. In an oven dried vial, with a Teflon septum screw cap, 4-methylquinoline (26.4 μL , 0.2 mmol, 1.0 equiv.) and chiral phosphoric acid (S)-TRIP (7.5 mg, 0.01 mmol, 5 mol%) were dissolved in dioxane (2 ml). Then, NHPI ester **36** (0.4 mmol, 2 equiv.) and catalyst **A** (6.2 mg, 0.02 mmol, 0.1 equiv.) were added. The resulting yellow mixture was degassed with argon sparging for 60 seconds. The vial was placed in the one-position photoreactor with temperature control and irradiated under stirring for 24 hours, unless otherwise specified. The solvent was evaporated, and the residue purified by column chromatography to afford the corresponding product in the stated yield with >95% purity according to ^1H NMR analysis.

2.8.7.4 Characterization of products with general procedure K (enantioselective variant)

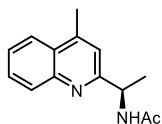


(R)-N-(1-(4-methylquinolin-2-yl)-2-phenylethyl) acetamide (46q): Synthesized according to General Procedure K using 1,3-dioxoisindolin-2-yl acetylphenylalaninate **36i** (140 mg, 0.4 mmol) and 4-methylquinoline **45a** (26.4 μ L, 0.2 mmol). The crude mixture was purified by flash column chromatography on silica gel (40% EtOAc in hexane as eluent) to afford **46q** (60.0 mg, 97% yield) as a white solid.

¹H NMR (400 MHz, CDCl₃) δ 8.05 (dt, J = 8.5, 0.9 Hz, 1H), 7.96 (ddd, J = 8.3, 1.5, 0.6 Hz, 1H), 7.70 (ddd, J = 8.4, 6.9, 1.5 Hz, 1H), 7.59 – 7.51 (m, 1H), 7.27 (s, 1H), 7.18 – 7.13 (m, 3H), 6.99 – 6.92 (m, 2H), 6.82 (d, J = 1.2 Hz, 1H), 5.39 (td, J = 7.7, 5.4 Hz, 1H), 3.35 (dd, J = 13.3, 5.4 Hz, 1H), 3.17 (dd, J = 13.3, 7.9 Hz, 1H), 2.59 (d, J = 0.9 Hz, 3H), 2.07 (s, 3H).

¹³C NMR (101 MHz, CDCl₃) δ 169.6, 158.9, 147.1, 144.9, 137.3, 129.8, 129.5, 129.4, 128.2, 127.6, 126.6, 126.3, 124.00, 121.7, 55.6, 42.3, 23.7, 18.9.

Matching reported literature data. **Error! Bookmark not defined.**



(R)-N-(1-(4-methylquinolin-2-yl) ethyl) acetamide (46r): Synthesized according to General Procedure K using 1,3-dioxoisindolin-2-yl acetylalaninate **36j** (110 mg, 0.4 mmol) and 4-methylquinoline **45a** (26.4 μ L, 0.2 mmol). The crude mixture was purified by flash column chromatography on silica gel (40% AcOEt in hexane as eluent) to afford **46r** (38.3 mg, 84% yield) as a white solid.

¹H NMR (400 MHz, CDCl₃) δ 8.08 (dt, J = 8.1, 1.0 Hz, 1H), 7.98 (ddd, J = 8.3, 1.5, 0.7 Hz, 1H), 7.71 (ddd, J = 8.4, 6.9, 1.4 Hz, 1H), 7.56 (ddd, J = 8.3, 6.9, 1.3 Hz, 1H), 7.51 (s, 1H), 7.17 (d, J = 1.1 Hz, 1H), 5.21 (p, J = 6.8 Hz, 1H), 2.70 (d, J = 1.0 Hz, 3H), 2.11 (s, 3H), 1.54 (d, J = 6.8 Hz, 3H).

¹³C NMR (101 MHz, CDCl₃) δ 169.6, 160.7, 146.9, 145.8, 129.6, 129.3, 127.6, 126.4, 123.9, 120.5, 50.1, 23.74, 22.8, 19.0.

Matching reported literature data. **Error! Bookmark not defined.**

2.8.8 Trifluoromethylation



Reactions performed using **set-up 3** in Figure 2.7. In an oven dried vial with a Teflon septum screw cap, silyl enol ether **42a** (117 mg, 0.5 mmol, 2.5 equiv.) was dissolved in MeCN (2 mL), then the Togni reagent **47** (105 mg (60% Wt) 0.2 mmol, 1.0 equiv.), catalyst **A** (6.2 mg, 0.02 mmol, 0.1 equiv.). The resulting orange mixture was degassed bubbling argon for 60 seconds. The vial was then placed in the irradiation setup, maintained at a temperature of 25 °C (25-26 °C measured in the central well), and the reaction, unless otherwise stated, was stirred for 24 hours under continuous irradiation from a blue LED strip. The crude mixture was diluted with AcOEt and brine was added. The combined organic fractions were dried over anhydrous MgSO₄, filtered, and concentrated to dryness. The crude mixture was purified by flash column chromatography on silica gel (Hexane/AcOEt) to afford **48** (22 mg, 58% yield) as a yellow oil.

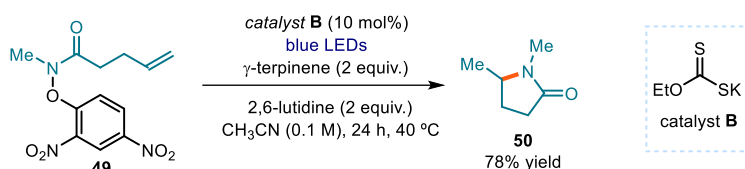
¹H NMR (300 MHz, CDCl₃) δ 8.01 – 7.91 (m, 2H), 7.69 – 7.61 (m, 1H), 7.60 – 7.46 (m, 3H), 3.82 (q, *J* = 10.0 Hz, 2H).

¹⁹F NMR (376 MHz, CDCl₃) δ –62.11.

¹³C NMR (126 MHz, CDCl₃) δ 135.7, 134.2, 128.9, 128.4, 124.7, 42.2.

Matching reported literature data.⁶¹

2.8.9 Amidyl radical



Reactions performed using **set-up 1** in Figure 2.3. In an oven dried vial, with a Teflon septum screw cap, **49** (29 mg, 0.1 mmol, 1 equiv.) and catalyst **B** (1.6 mg, 0.01 mmol, 0.1 equiv.) were dissolved in CH₃CN (1 mL), then 2,6-lutidine (23 μ L, 0.2 mmol, 2.0 equiv.) was added, followed by γ -terpinene (32 μ L, 0.2 mmol, 2 equiv.). The resulting orange mixture was degassed with argon sparging for 60 seconds. The vial was then placed in the 3D printed support photoreactor and irradiated under stirring for 16 hours. The crude mixture was concentrated to

⁶¹ Jacquet J.; Cheaib K.; Ren Y.; Vezin H.; Orio M.; Blanchard S.; Fensterbank L.; Desage El Murr M., Circumventing Intrinsic Metal Reactivity: Radical Generation with Redox-Active Ligands. *Chem. Eur. J.* **2017**, *23*, 15030-15034.

dryness. Trichloroethylene was added as internal standard (9 μL , 0.1 mmol, 1.0 equiv) and NMR yield was determined by ^1H NMR in CDCl_3 matching reported literature data. **Error! Bookmark not defined.**

2.8.10 Large scale reactions

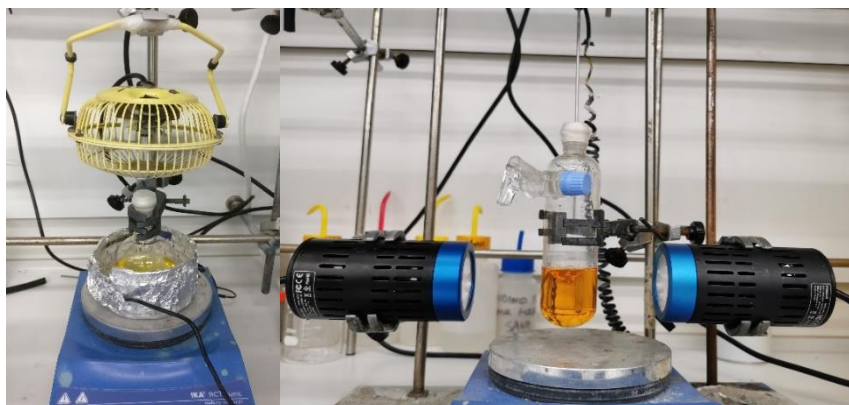
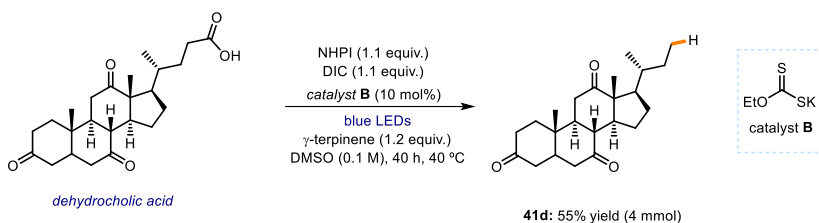


Figure 2.9. Scale-up set-ups. Barton decarboxylation (left). Minisci reaction (right).

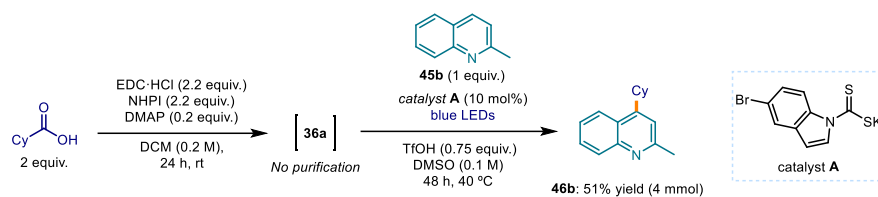
2.8.10.1 Barton decarboxylation



Using set-up in Figure 2.9 (left). In a 100 mL round bottom flask with a Teflon cap, dehydrocholic acid (1,62 g, 4 mmol, 1 equiv.), *N*-hydroxyphthalimide (NHPI, 716 mg, 4.4 mmol, 1.1 equiv.), and xanthogenate catalyst A (64 mg, 0.4 mmol, 0.1 equiv.) were dissolved in DMSO (40 mL), and *N,N'*-diisopropylcarbodiimide (DIC, 760 μL , 4.4 mmol, 1.1 equiv.) was added via syringe. Then, γ -terpinene (760 μL , 4.8 mmol, 1.2 equiv.) was added. The resulting orange mixture was degassed with nitrogen sparging for 5 min. The round bottom flask was then irradiated for 40 hours with a 1-meter 14W blue LED strip and cooled with a fan to keep the temperature between 30 and 35 $^{\circ}\text{C}$ (see Figure 2.9, left). The mixture was transferred to an extraction funnel, NaOH 1M solution was added and the organic layer was extracted with CH_2Cl_2 . The organic layer was dried over anhydrous

MgSO₄, filtered, and concentrated to dryness. The crude residue was purified by chromatography on silica gel (10% AcOEt in hexanes) to afford 800 mg of product **41d** (2.2 mmol, 55% yield) as an off white solid. NMR analysis was consistent with product synthesized in the small scale process.

2.8.10.2 Minisci reaction



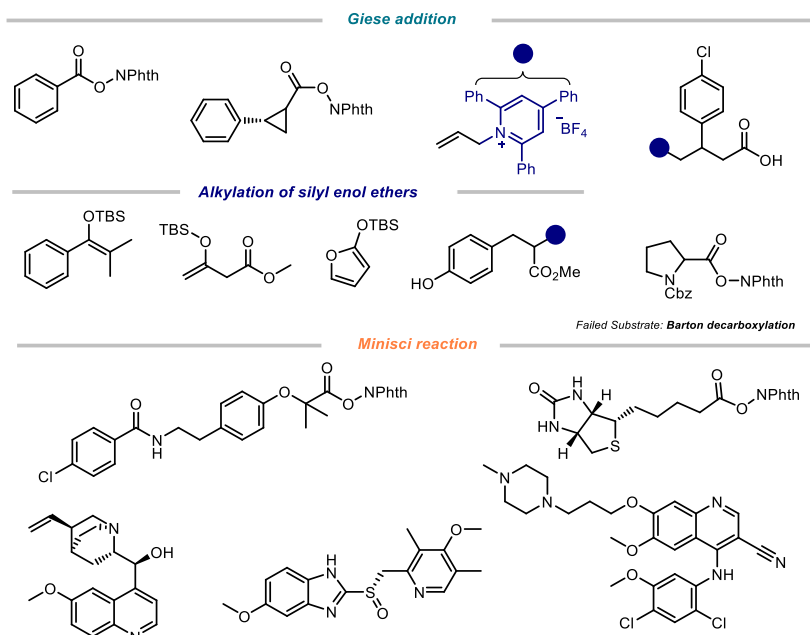
Using set-up in Figure 2.9 (right). In a 100 mL round bottom flask, cyclohexanecarboxylic acid (1.03 g, 8 mmol, 2 equiv.), EDC·HCl (1.69 g, 8.8 mmol, 2.2 equiv.), DMAP (97.7 mg, 0.8 mmol, 0.2 equiv.), and *N*-hydroxyphthalimide (1.44 g, 8.8 mmol, 2.2 equiv.) were dissolved in CH₂Cl₂ (20 mL). The reaction was stirred at ambient temperature for 24 hours. The mixture was transferred to an extraction funnel, NaHCO₃ sat. solution was added and the organic layer was extracted with CH₂Cl₂. The organic phase was concentrated to dryness under vacuum to obtain the crude NHPI ester, which was used without further purification in the next step.

In a 100 mL Schlenk flask with a Teflon septum, the crude NHPI ester was dissolved in DMSO (40 mL). Then, 2-methylquinoline (540 μL, 4.00 mmol, 1.0 equiv.), trifluoromethanesulfonic acid (265 μL, 3.00 mmol, 0.75 equiv.) and catalyst **A** (124 mg, 0.40 mmol, 0.1 equiv.) were added. The resulting orange mixture was degassed with nitrogen sparging for 5 minutes. The Schlenk flask was irradiated with stirring for 48 hours using two 50 W Kessil blue LED lamp (one PR160L-456 and one PR160L-427, 100% intensity, 4-5 cm away) (see

Figure 2.9. Scale-up set-ups. Barton decarboxylation (left). Minisci reaction (right).

Figure 2.9, right). The mixture was transferred to an extraction funnel, NaHCO₃ sat. solution was added and the organic layer was extracted with CH₂Cl₂. The organic layer was dried over anhydrous MgSO₄, filtered, and concentrated to dryness. The crude residue was purified by chromatography on silica gel (10% AcOEt in hexanes) to afford 459 mg of product **46b** (2.04 mmol, 51% yield) as a yellowish oil. NMR analysis was consistent with product synthesized in the small scale process.

2.8.11 Unsuccessful substrates



Scheme 2.30. Unsuccessful substrates that offered poor yields (ranging from 0 to <20%).

2.9 Mechanistic studies

2.9.1 Control experiments

2.9.1.1 Experiments with green light

For the reactions performed under green light irradiation, an EvoluChem™ P303-30-1 LEDs (18 W, $\lambda_{\text{max}} = 520 \text{ nm}$) was used. The reaction temperature was measured to be between 25 °C and 30 °C using the setup depicted in Figure 2.10).

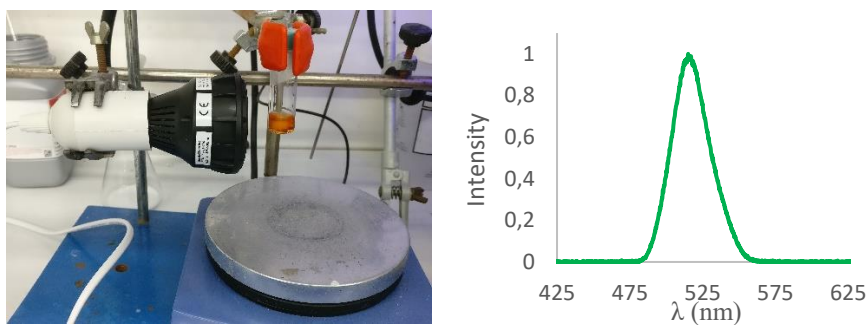
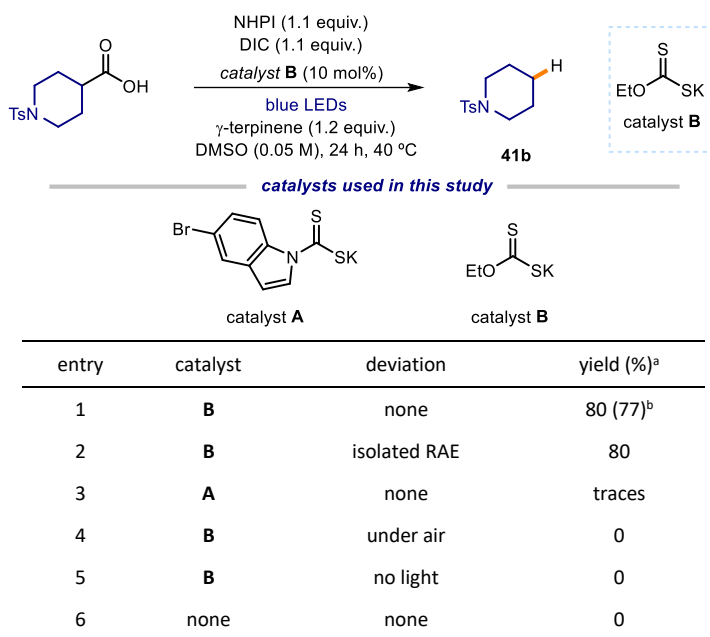


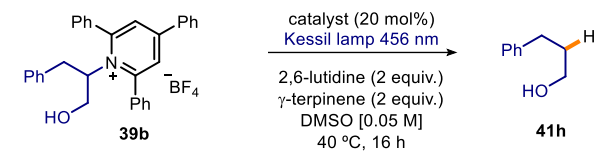
Figure 2.10. Reaction set-up for green light irradiation (*left*). Emission spectrum of the 520 nm EvoluChem™ P303-30-1 LEDs used in this reactor (*right*).

2.9.1.2 Optimization studies

Table 2.3. Barton decarboxylation.

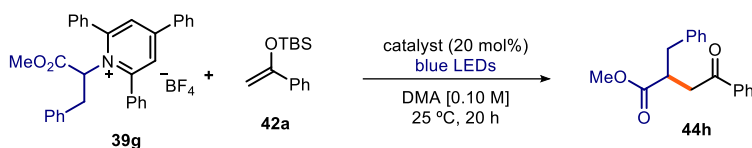


Reactions performed using *set-up 1* in Figure 2.3.

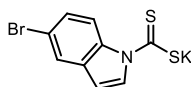
Table 2.4. Deamination with pyridinium salts as radical precursors.

entry	catalyst	deviation	yield (%) ^a
1	A	none	95 (78) ^b
2	A	under air	0
3	A	no light	0
4	none	none	0

Reactions performed using *set-up 2* in Figure 2.4.

Table 2.5. α -alkylation of silyl enol ethers.

catalysts used in this study



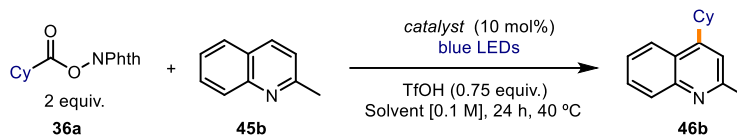
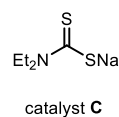
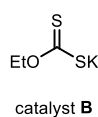
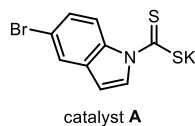
catalyst A



catalyst B

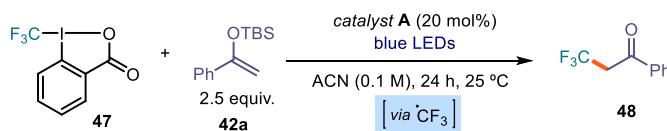
entry	catalyst	Base	deviation	yield (%) ^a
1	A	-	none	16
2	A	2,6-lutidine (1 equiv.)	none	95 (89%) ^b
3	B	2,6-lutidine (1 equiv.)	none	80
4	B	2,6-lutidine (1 equiv.)	Green light	45
5	A	2,6-lutidine (1 equiv.)	cat. 10 mol%	62
6	A	2,6-lutidine (1 equiv.)	under air	0
7	A	2,6-lutidine (1 equiv.)	no light	0
8	none	2,6-lutidine (1 equiv.)	none	0

Reactions performed using *set-up 3* in Figure 2.7.

Table 2.6. Minisci reaction.**catalysts used in this study**

entry	catalyst	Solvents	deviation	yield (%) ^a
1	A	DMSO	TFA	82
2	B	DMSO	TFA	0
3	C	DMSO	TFA	0
6	A	DMSO	none	97(95) ^b
8	A	DMSO	Green light	8
9	A	DMSO	No acid	0
10	A	DMSO	No light	0
11	A	DMSO	under air	0
12	none	DMSO	none	0

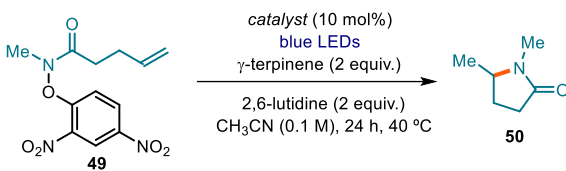
Reactions performed using *set-up 2* in Figure 2.4.

Table 2.7. Trifluoromethylation of silyl enol ethers.

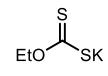
entry	catalyst	Base	deviation	yield (%) ^a
1	A	-	Acetone	21
2	A	-	none	63(58%) ^b
3	A	2,6-lutidine (1 equiv.)	none	62
4	B	-	none	22
5	C	-	none	27
6	-	-	No catalyst	0

Reactions performed using *set-up 3* in Figure 2.7.

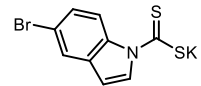
Table 2.8. Amidyl radical cyclization



catalysts used in this study



catalyst **A**

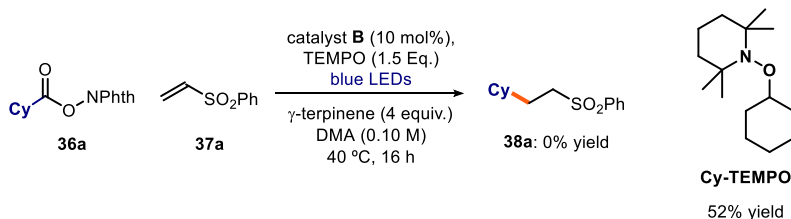


catalyst **B**

entry	catalyst	deviation	yield (%) ^a
1	A	None	86
2	B	None	78
3	A	No base	60
4	B	No base	50
5	A	Under air	0
6	A	No light	0
7	none	None	0

Reactions performed using set-up 1 in Figure 2.3.

2.9.1.3 TEMPO trapping experiment



Reactions performed using set-up 1 in Figure 2.3. In an oven dried vial with a Teflon septum screw cap, potassium ethyl xanthogenate **B** (1.6 mg, 0.01 mmol, 0.1 equiv.), NHPI ester **36a** (0.1 mmol, 27.3 mg, 1 equiv.), 2,2,6,6-tetramethylpiperidine 1-oxyl (TEMPO, 0.15 mmol, 23.5 mg, 1.5 equiv.) and **37a** (0.15 mmol, 25.2 mg, 1.5 equiv.) were dissolved in DMA (1 mL). Then, γ-terpinene (64 μL, 0.4 mmol, 4 equiv.) was added. The resulting orange mixture was degassed by argon sparging for 60 seconds. The vial was then placed in the 3D printed support photoreactor (Figure 2.3) and irradiated under stirring for 16 hours. The

mixture was transferred to an extraction funnel, brine was added and the organic layer was extracted with EtOAc. The organic layer was dried over anhydrous MgSO_4 , filtered, and concentrated to dryness. The crude residue was then purified by column chromatography (2% EtOAc in hexanes) to afford the corresponding **Cy-TEMPO** adduct in 52% yield. No product corresponding with giese addition was detected in the crude NMR or during the purification.

$^1\text{H NMR}$ (500 MHz, CDCl_3) δ 3.68 – 3.64 (m, 1H), 2.07 (brs, 2H), 1.76 (brs, 2H), 1.57 – 1.54 (m, 2H), 1.48 – 1.45 (m, 4H), 1.31 – 1.06 (m, 19H).

$^{13}\text{C NMR}$ (126 MHz, CDCl_3) δ 81.7, 59.6, 40.3, 32.9, 26.0, 25.1, 17.3.

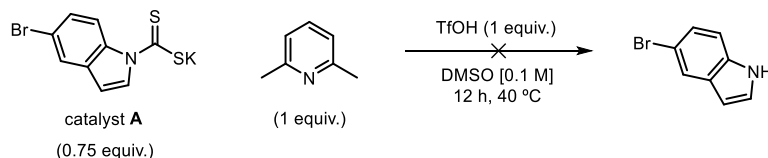
Characterization data matching data reported in the literature.⁶²

2.9.2 Catalysts' stability experiments

During the course of our investigation into the EDA complex system, we realized stability of the catalyst under reaction conditions was often the reason one of the catalyst greatly out-performed the other in some transformations.

In general, the potassium ethyl xanthate catalyst **B** is a suitable EDA donor catalyst when no protonated organic based is present in the mixture, we believed this is due to decomposition of the catalyst promoted by the pyridinium salt. On the other hand, indole-based dithiocarbamate anion catalyst **A** seems to be more stable to acidic media, and it does not undergo decomposition when faced with the same pyridinium salts. In order to test this hypothesis, we conducted the following experiments. These experiments provide an explanation on why the Minisci reaction is completely shut down when employing catalyst **B**.

- Catalyst A:



⁶² Tobisu M.; Koh K.; Furukawa T.; Chatani N., Modular Synthesis of Phenanthridine Derivatives by Oxidative Cyclization of 2-Isocyanobiphenyls with Organoboron Reagents. *Angew. Chem., Int. Ed.* **2012**, *51*, 11363-11366.

In an oven dried vial with a Teflon septum screw cap, 2,6-lutidine (0.1 mmol, 12 μL) was added followed by triflic acid (0.1 mmol, 8.9 μL). The resulting pyridinium salt was then dissolved in 1 mL of d^6 -DMSO, followed by the addition of catalyst **A** (23.3 mg, 0.075 mmol). The mixture was stirred overnight and the crude mixture was analyzed by ^1H NMR. Catalyst **A** showed no degradation to the corresponding indole (see Figure 2.11).

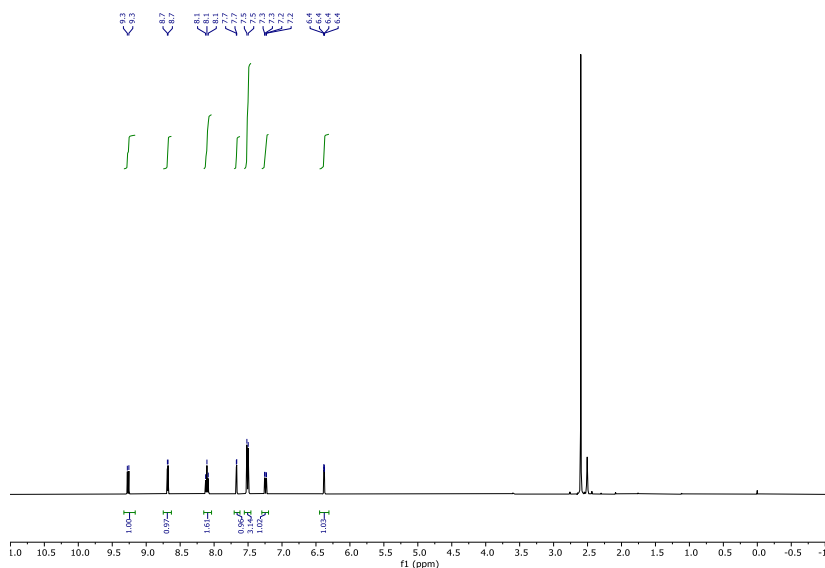
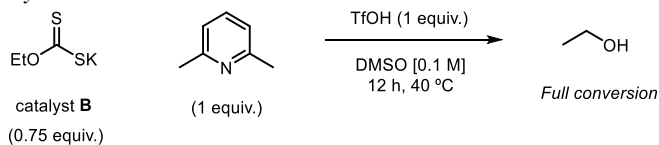


Figure 2.11. ^1H NMR analysis to evaluate catalyst **A** stability.

- Catalyst **B**:



In an oven dried vial with a Teflon septum screw cap, 2,6-lutidine (0.1 mmol, 12 μL) was added followed by triflic acid (0.1 mmol, 8.9 μL). The resulting pyridinium salt was then dissolved in 1 mL of d^6 -DMSO, followed by the addition of catalyst **B** (12 mg, 0.075 mmol). The mixture was left stirring overnight and the crude mixture is analyzed by ^1H NMR. Catalyst **B** showed complete degradation to ethanol (Figure 2.12).

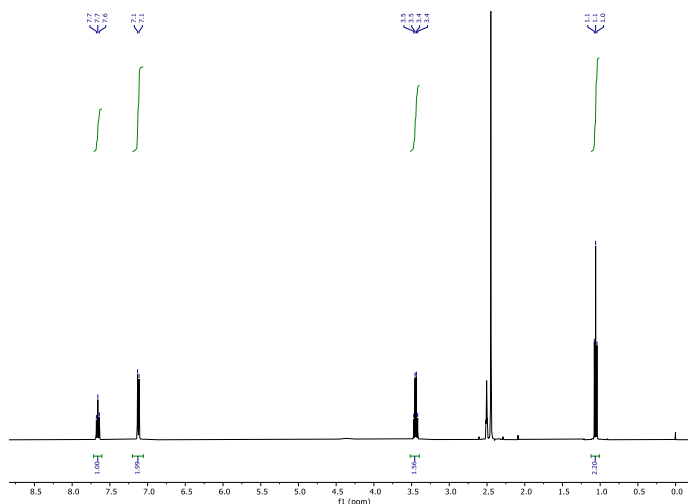


Figure 2.12. ^1H NMR analysis to evaluate catalyst **B** stability.

2.9.3 UV-Vis spectroscopy

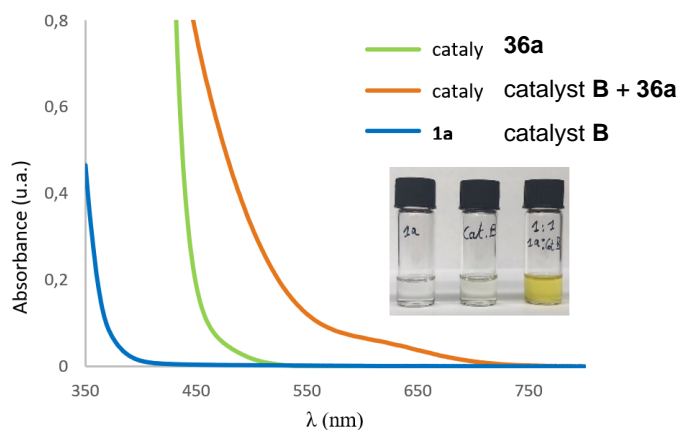


Figure 2.13. Optical absorption spectra, recorded in DMA in 1 cm path quartz cuvettes using a Shimadzu 2401PC UV-vis spectrophotometer, and visual appearance of the separate reaction components and of the colored EDA complex between catalyst **B** and **36a**. $[\mathbf{36a}] = 0.10$ M, $[\text{catalyst } \mathbf{B}] = 0.01$ M.

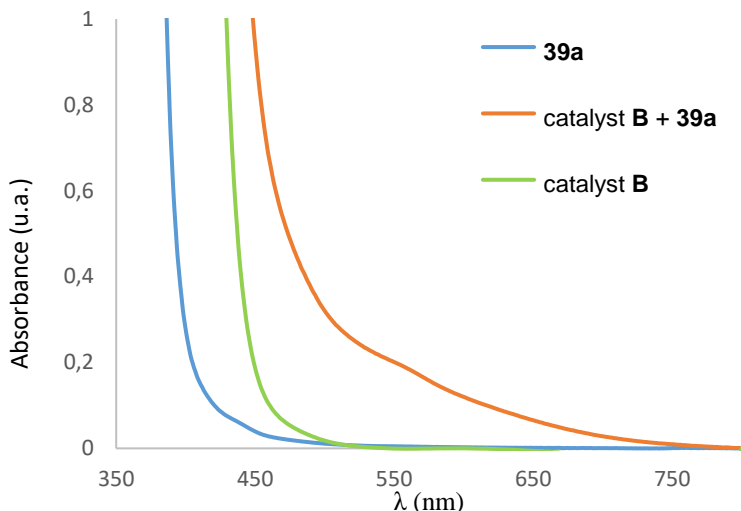


Figure 2.14. Optical absorption spectra, recorded in DMA in 1 cm path quartz cuvettes using a Shimadzu 2401PC UV–vis spectrophotometer of the separate reaction components and of the colored EDA complex between catalyst **B** and **39a**. [**39a**] = 0.10 M, [catalyst **B**] = 0.01 M.

2.9.4 Transient absorption spectroscopy (TAS)

Studies with microsecond transient absorption spectroscopy (TAS) were performed using an excitation source of NdYAG (neodymium-doped yttrium aluminium garnet) Opolette laser with an optical parametric oscillator (OPO) system that allows variable wavelength excitation from 400 -1800 nm, pulse width of 6 ns, up to 2 mJ of energy from OPO output with fiber optic coupled, and high energy output from direct NdYAG harmonics 355 (20 mJ, 5 ns) and 532 (45mJ, 6 ns). The system is completed with 150 W tungsten lamp as probe; 2 monochromators Minuteman MM151; Si amplified photodetector module for VIS; DSPDAU high speed data rate recorder and interface software from RAMDSP. Laser intensity for the chosen wavelength was 355 nm – 1.30 mJ.

We selected a logarithmic time scale suitable for clearly showing the decay of the transient species in the samples. The characteristics of the detected transient species match literature data.^{Error! Bookmark not defined.}^{Error! Bookmark not defined.}

In a typical transient absorption spectroscopy experiment, solutions in DMA of a mixture of **36a** and catalyst **B** was prepared under an argon atmosphere and transferred into a screw-top 3.0 mL quartz cuvette for measurement. Upon irradiation with the appropriated wavelength, the decay of absorption at 620 nm of the transient xanthyl radical **IIIb** was recorded. Irradiation at 420 nm and 460 nm

of the sample also provided signal absorbing at 620 nm, but in a much lower intensity and higher noise.

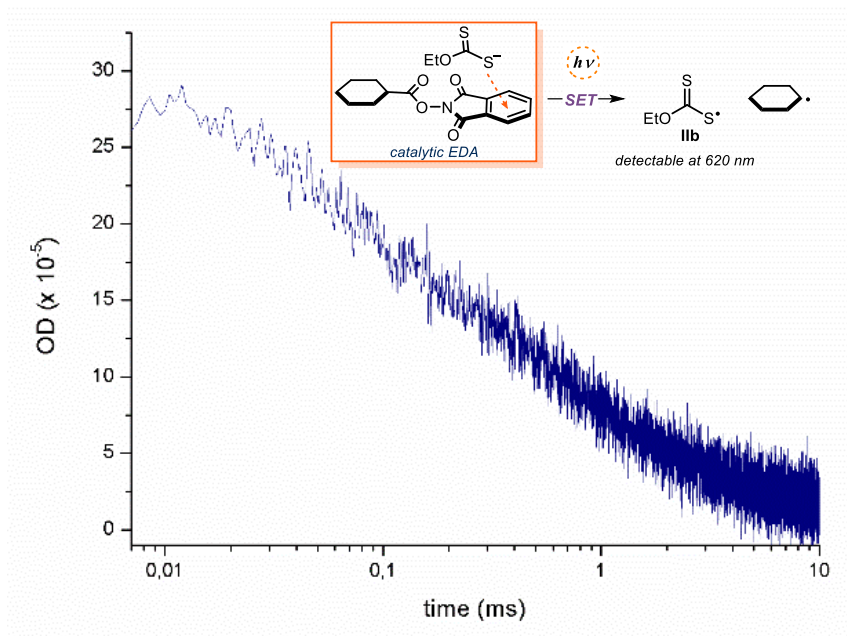


Figure 2.15. Absorption at 620 nm of the transient xanthyl radical **IIb** (blue line) generated upon 355 nm laser excitation of a 1:1 mixture of 32a and catalyst B 30 mM in DMA. Note logarithmic scale for time. ΔOD : optical density variation.

2.9.5 Cyclic voltammetry measurements

For all cyclic voltammetry (CV) measurements, a glassy carbon disk electrode (diameter 3 mm) was used as the working electrode. A silver wire coated with AgCl immersed in a 3.5 M aqueous solution of KCl and separated from the analyte by a fritted glass disk was employed as the reference electrode. A Pt wire counter-electrode completed the electrochemical setup. The scan rate used in each CV experiment is indicated case by case.

Potentials are quoted with the following notation: E_p^C refers to the cathodic peak potential, E_p^A refers to the anodic peak potential, while the E^{red} value describes the electrochemical properties of the referred compound.

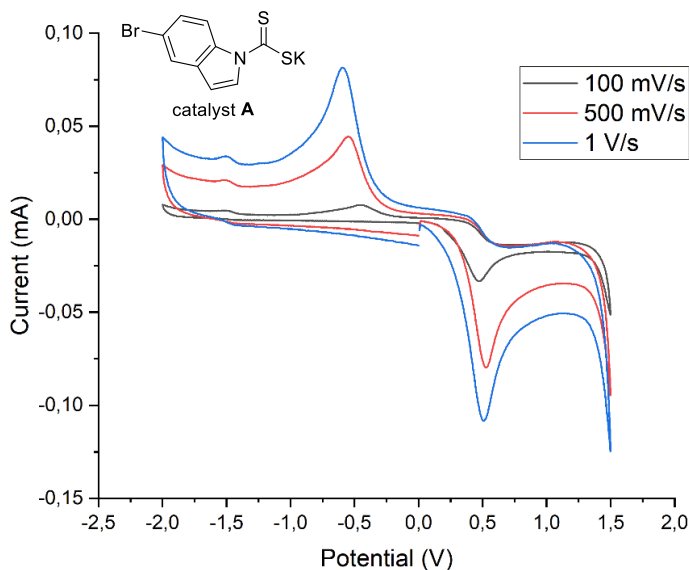


Figure 2.16. Cyclic voltammogram for catalyst **A** [0.02 M] in [0.1 M] TBAPF₆ in CH₃CN. Measurement started by oxidation from 0 to +1.5 V, followed by reduction from +1.5 V to -2.0 V, and finishing at 0 V. Glassy carbon electrode working electrode, Ag/AgCl (KCl 3.5 M) reference electrode, Pt wire auxiliary electrode. Two irreversible peaks observed increasing with sweep rate.

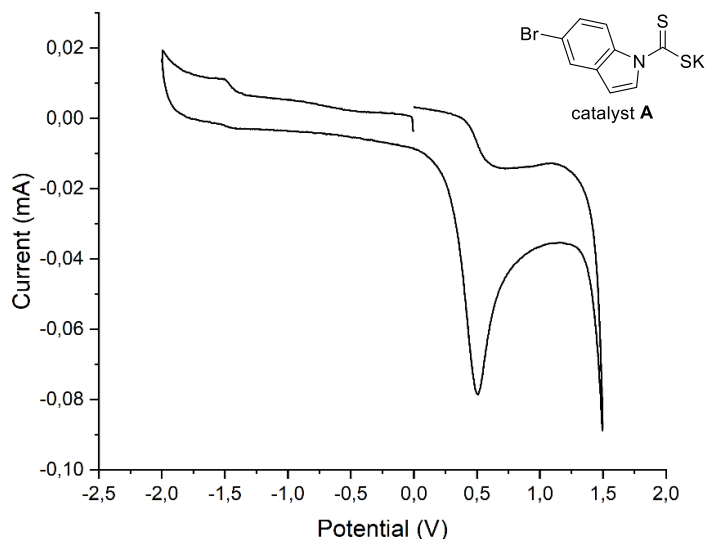


Figure 2.17. Cyclic voltammogram for catalyst **A** [0.02M] in [0.1 M] TBAPF₆ in CH₃CN. Measurement started by reduction from 0 to -2.0 V, followed by oxidation from -2.0 V to +1.5 V, and finishing at 0 V. Glassy carbon electrode working electrode, Ag/AgCl (KCl 3.5 M) reference electrode, Pt wire auxiliary electrode. Only one irreversible peak observed. Sweep rate: 500 mV/s.

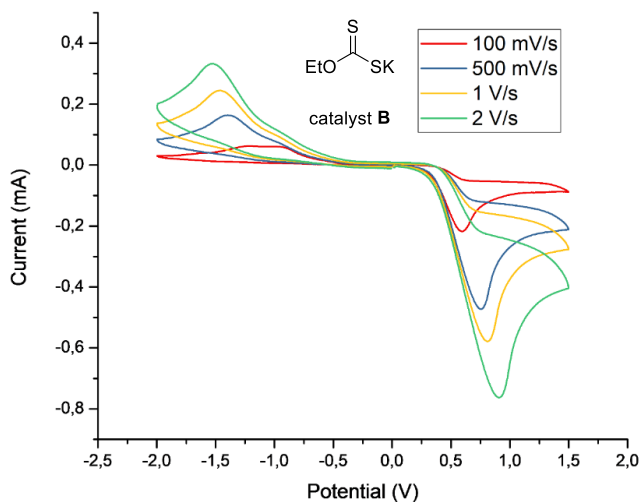


Figure 2.18. Cyclic voltammogram for catalyst **B** [0.02 M] in [0.1 M] TBAPF₆ in CH₃CN. Measurement started by oxidation from 0 to +1.5 V, followed by reduction from +1.5 V to -2.0 V, and finishing at 0 V. Glassy carbon electrode working electrode, Ag/AgCl (KCl 3.5 M) reference electrode, Pt wire auxiliary electrode. Two irreversible peaks observed increasing with sweep rate.

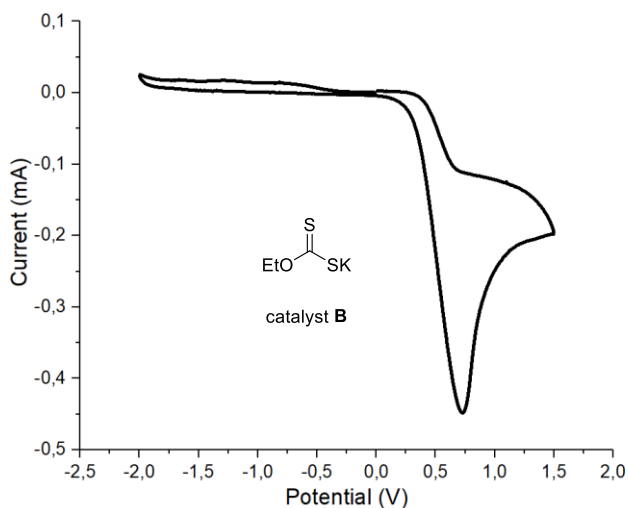


Figure 2.19. Cyclic voltammogram for catalyst **B** [0.02M] in [0.1 M] TBAPF₆ in CH₃CN. Measurement started by reduction from 0 to -2.0 V, followed by oxidation from -2.0 V to +1.5 V, and finishing at 0 V. Glassy carbon electrode working electrode, Ag/AgCl (KCl 3.5 M) reference electrode, Pt wire auxiliary electrode. Only one irreversible peak observed. Sweep rate: 500 mV/s.

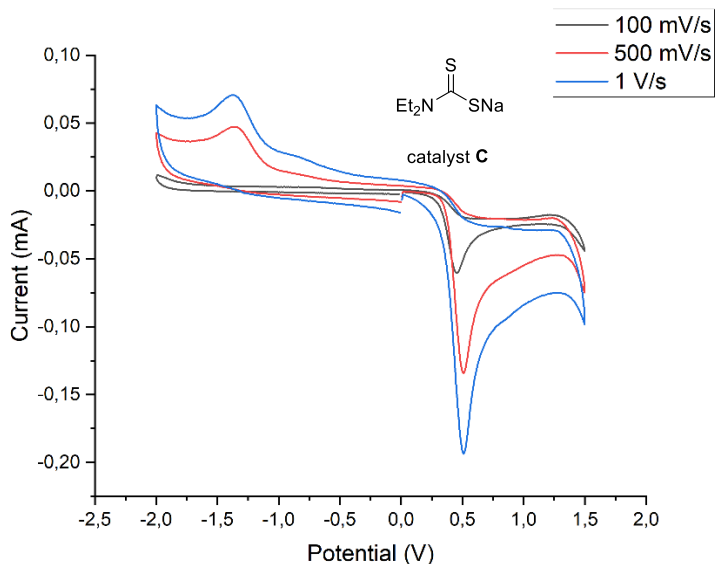


Figure 2.20. Cyclic voltammogram for catalyst **C** [0.02 M] in [0.1 M] TBAPF₆ in CH₃CN. Measurement started by oxidation from 0 to +1.5 V, followed by reduction from +1.5 V to -2.0 V, and finishing at 0 V. Glassy carbon electrode working electrode, Ag/AgCl (KCl 3.5 M) reference electrode, Pt wire auxiliary electrode. Two irreversible peaks observed increasing with sweep rate.

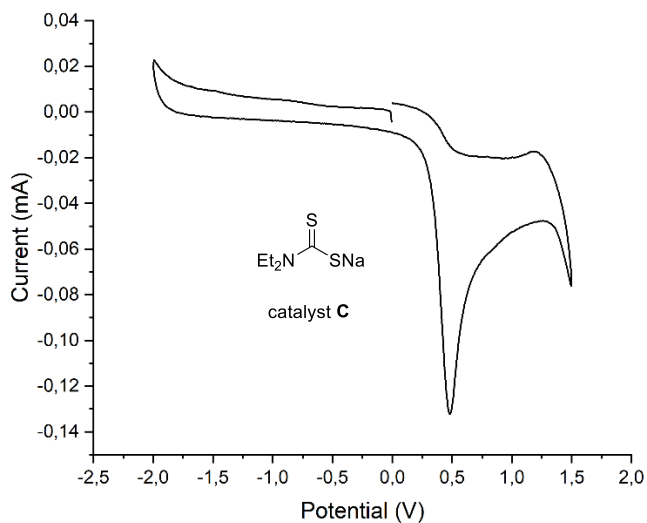


Figure 2.21. Cyclic voltammogram for catalyst **C** [0.02M] in [0.1 M] TBAPF₆ in CH₃CN. Measurement started by reduction from 0 to -2.0 V, followed by oxidation from -2.0 V to +1.5 V, and finishing at 0 V. Glassy carbon electrode working electrode, Ag/AgCl (KCl 3.5 M) reference electrode, Pt wire auxiliary electrode. Only one irreversible peak observed. Sweep rate: 500 mV/s.

2.9.6 Quantum yield determination

2.9.6.1 Giese addition

A ferrioxalate actinometer solution was prepared by following the Hammond variation of the Hatchard and Parker procedure outlined in the Handbook of Photochemistry.⁶³ The ferrioxalate actinometer solution measures the decomposition of ferric ions to ferrous ions, which are complexed by 1,10-phenanthroline and monitored by UV/Vis absorbance at 510 nm. The moles of iron-phenanthroline complex formed are related to moles of photons absorbed. The following solutions were prepared and stored in a dark laboratory (red light):

1. Potassium ferrioxalate solution: 294.8 mg of potassium ferrioxalate (commercially available from Alfa Aesar) and 139 μL of sulfuric acid (96%) were added to a 50 mL volumetric flask, and filled to the mark with water (HPLC grade).
2. Phenanthroline solution: 0.2% by weight of 1,10-phenanthroline in water (100 mg in 50 mL volumetric flask).
3. Buffer solution: 2.47 g of NaOAc and 0.5 mL of sulfuric acid (96%) were added to a 50 mL volumetric flask and filled to the mark with water (HPLC grade).

The actinometry measurements were done as follows:

1. 1 mL of the actinometer solution was added to a Schlenk tube (diameter = 12 mm). The Schlenk tube was placed in one of the positions of the 3D printed reactor (Figure 2.3). The solution was irradiated at 460 nm. This procedure was repeated 4 times, quenching the solutions after different time intervals: 1 s, 2 s, 4 s, and 8 s.
2. Then 1 mL of the model reaction following general procedure A with **36a** (0.10 mmol) and **37a** as substrates was placed in a Schlenk tube, degassed via argon bubbling, placed in the irradiation set up and irradiated for 15 minutes. This procedure was performed a total of four times with different irradiation times (30 min, 45 min, 60 min).
3. After irradiation, the actinometer solutions were removed and placed in a 10 mL volumetric flask containing 0.5 mL of 1,10-phenanthroline solution and 2 mL of buffer solution. These flasks were filled to the mark with water (HPLC grade).
4. The UV-Vis spectra of the complexed actinometer samples were recorded for each time interval. The absorbance of the complexed actinometer solution was monitored at 510 nm.

The moles of Fe^{2+} formed for each sample is determined using Beers' Law (Eq. 1):

$$\text{Mols of Fe(II)} = V_1 \times V_3 \times \Delta A(510 \text{ nm}) / 10^3 \times V_2 \times l \times \epsilon(510 \text{ nm}) \text{ (Eq. 1)}$$

⁶³ Murov, S. L. Ed. *Handbook of Photochemistry* (Marcel Dekker, New York, 1973).

where V_1 is the irradiated volume (1 mL), V_2 is the aliquot of the irradiated solution taken for the determination of the ferrous ions (1 mL), V_3 is the final volume after complexation with phenanthroline (10 mL), l is the optical path-length of the irradiation cell (1 cm), $\Delta A(510 \text{ nm})$ is the optical difference in absorbance between the irradiated solution and the one stored in the dark, $\epsilon(510 \text{ nm})$ is the extinction coefficient the complex $\text{Fe}(\text{phen})_3^{2+}$ at 510 nm ($11100 \text{ L mol}^{-1} \text{ cm}^{-1}$). The moles of Fe^{2+} formed (x) are plotted as a function of time (t). The slope of this line was correlated to the moles of incident photons by unit of time ($q_0 \text{ n,p}$) by the use of the following Equation 2:

$$\Phi(\lambda) = \frac{dx/dt}{q_0 \text{ n,p}} [1 - 10^{-A(\lambda)}] \quad (\text{Eq. 2})$$

where dx/dt is the rate of change of a measurable quantity (spectral or any other property), the quantum yield (Φ) for Fe^{2+} at 458 nm is 1.1,⁶⁴ $[1 - 10^{-A(\lambda)}]$ is the ratio of absorbed photons by the solution, and $A(\lambda)$ is the absorbance of the actinometer at the wavelength used to carry out the experiments (460 nm). The absorbance at 460 nm $A(460)$ was measured using a Shimadzu 2401PC UV-Vis spectrophotometer in a 10 mm path quartz cuvette, obtaining an absorbance of 0.183. $q_0 \text{ n,p}$, which is the photon flux, was determined to be 5.3×10^{-7} .

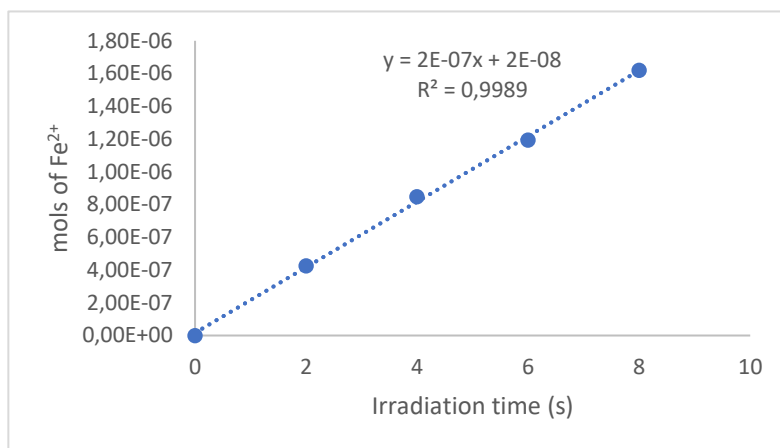


Figure 2.14. Plot of mols of Fe^{2+} formed vs irradiation time. Slope of the line correlates to the moles of incident photons by unit of time.

The moles of product **38a** formed for the model reaction were determined by GC measurement (FID detector) using 1,3,5-trimethoxybenzene as internal standard.

⁶⁴ Holubov C. A.; Langford C. H., Wavelength and temperature dependence in the photolysis of the chemical actinometer, potassium trisoxalatoferate(III), at longer wavelengths. *Inorg. Chim. Acta.* **1981**, 53, 59-60.

The moles of product per unit of time are related to the number of photons absorbed.

The photons absorbed are correlated to the number of incident photons by the use of Equation 1. According to this, if we plot the moles of product (y) versus the moles of incident photons ($q_0 n, p \cdot dt$), the slope is equal to: $\Phi \cdot (1 - 10^{-A(460 \text{ nm})})$, where Φ is the quantum yield to be determined and $A(460 \text{ nm})$ is the absorption of the reaction under study. $A(460 \text{ nm})$ was measured using a Shimadzu 2401PC UV-Vis spectrophotometer in 10 mm path quartz. An absorbance of 0.049 was determined for the model reaction mixture (1:4 dilution). The quantum yield (Φ)_{cat.} of the photochemical transformation was measured to be 0.01.

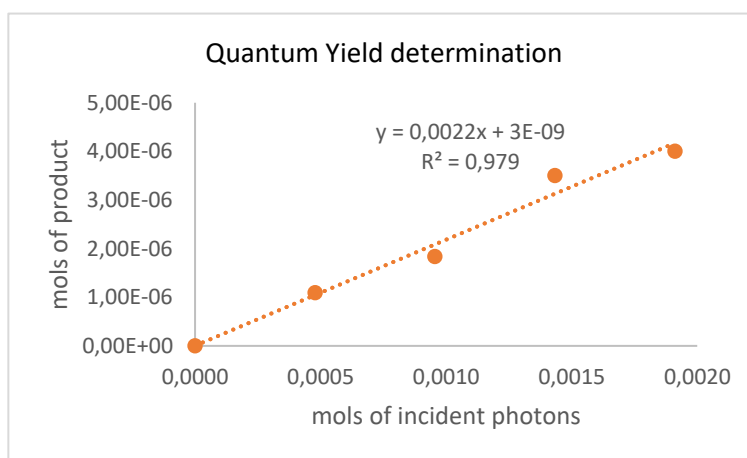


Figure 2.15. Plot of mols of incident photons vs mols of product formed. Slope of the line correlates to quantum yield of the photochemical transformation.

2.9.6.2 Barton decarboxylation

A ferrioxalate actinometer solution was prepared by following the Hammond variation of the Hatchard and Parker procedure outlined in the Handbook of Photochemistry.⁶³ The ferrioxalate actinometer solution measures the decomposition of ferric ions to ferrous ions, which are complexed by 1,10-phenanthroline and monitored by UV/Vis absorbance at 510 nm. The moles of iron-phenanthroline complex formed are related to moles of photons absorbed. The following solutions were prepared and stored in a dark laboratory (red light):

1. Potassium ferrioxalate solution: 294.8 mg of potassium ferrioxalate (commercially available from Alfa Aesar) and 139 μL of sulfuric acid (96%) were added to a 50 mL volumetric flask and filled to the mark with water (HPLC grade).

2. Phenanthroline solution: 0.2% by weight of 1,10-phenanthroline in water (100 mg in 50 mL volumetric flask).

3. Buffer solution: 2.47 g of NaOAc and 0.5 mL of sulfuric acid (96%) were added to a 50 mL volumetric flask and filled to the mark with water (HPLC grade).

The actinometry measurements were done as follows:

1. 1 mL of the actinometer solution was added to a Schlenk tube (diameter = 12 mm). The Schlenk tube was placed in one of the positions of the 3D printed reactor (Figure 2.3). The solution was irradiated at 460 nm. This procedure was repeated 4 times, quenching the solutions after different time intervals: 1 s, 2 s, 4 s, and 8 s.
2. Then 1 mL of the model reaction following general procedure F starting from isolated **36f** (0.10 mmol) as substrate was placed in a Schlenk tube, degassed via argon bubbling, placed in the irradiation set up and irradiated for 15 minutes. This procedure was performed a total of four times with different irradiation times (30 min, 60 min, 120 min).
3. After irradiation, the actinometer solutions were removed and placed in a 10 mL volumetric flask containing 0.5 mL of 1,10-phenanthroline solution and 2 mL of buffer solution. These flasks were filled to the mark with water (HPLC grade).
4. The UV-Vis spectra of the complexed actinometer samples were recorded for each time interval. The absorbance of the complexed actinometer solution was monitored at 510 nm.

The moles of Fe²⁺ formed for each sample is determined using Beers' Law (Eq. 1):

$$\text{Mols of Fe(II)} = V_1 \times V_3 \times \Delta A(510 \text{ nm}) / 10^3 \times V_2 \times l \times \epsilon(510 \text{ nm}) \quad (\text{Eq. 1})$$

where V_1 is the irradiated volume (1 mL), V_2 is the aliquot of the irradiated solution taken for the determination of the ferrous ions (1 mL), V_3 is the final volume after complexation with phenanthroline (10 mL), l is the optical path-length of the irradiation cell (1 cm), $\Delta A(510 \text{ nm})$ is the optical difference in absorbance between the irradiated solution and the one stored in the dark, $\epsilon(510 \text{ nm})$ is the extinction coefficient the complex Fe(phen)_3^{2+} at 510 nm (11100 L mol⁻¹ cm¹). The moles of Fe²⁺ formed (x) are plotted as a function of time (t). The slope of this line was correlated to the moles of incident photons by unit of time (q_0 n,p) by the use of the following Equation 2:

$$\Phi(\lambda) = dx/dt \cdot q_{n,p} / [1 - 10^{-A(\lambda)}] \quad (\text{Eq. 2})$$

where dx/dt is the rate of change of a measurable quantity (spectral or any other property), the quantum yield (Φ) for Fe²⁺ at 458 nm is 1.1,64 [1-10^{-A(λ)}] is the ratio

of absorbed photons by the solution, and $A(\lambda)$ is the absorbance of the actinometer at the wavelength used to carry out the experiments (460 nm). The absorbance at 460 nm $A(460)$ was measured using a Shimadzu 2401PC UV-Vis spectrophotometer in a 10 mm path quartz cuvette, obtaining an absorbance of 0.183. $q_{n,p}^0$, which is the photon flux, was determined to be 5.2×10^{-7} .

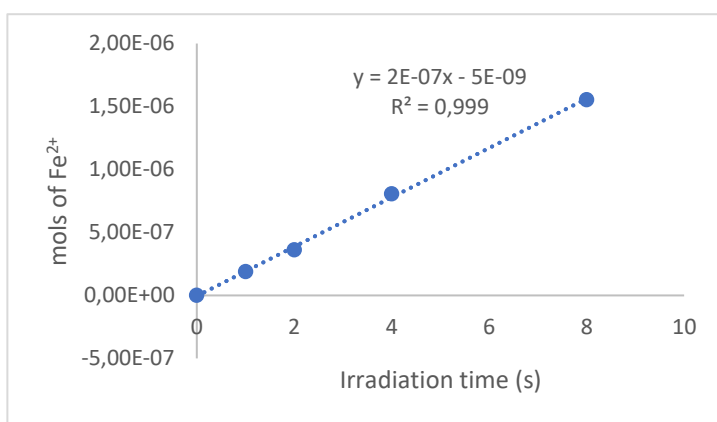


Figure 2.16. Plot of moles of Fe^{2+} formed vs irradiation time. Slope of the line correlates to the moles of incident photons by unit of time.

The moles of product **41b** formed for the model reaction were determined by GC measurement (FID detector) using 1,3,5-trimethoxybenzene as internal standard. The moles of product per unit of time are related to the number of photons absorbed.

The photons absorbed are correlated to the number of incident photons by the use of Equation 1. According to this, if we plot the moles of product (y) versus the moles of incident photons ($q_0 n,p \cdot dt$), the slope is equal to: $\Phi \cdot (1 - 10^{-A(460 \text{ nm})})$, where Φ is the quantum yield to be determined and $A(460 \text{ nm})$ is the absorption of the reaction under study. $A(460 \text{ nm})$ was measured using a Shimadzu 2401PC UV-Vis spectrophotometer in 10 mm path quartz. An absorbance of 0.052 was determined for the model reaction mixture. The quantum yield (Φ)_{cat.} of the photochemical transformation was measured to be 0.01.

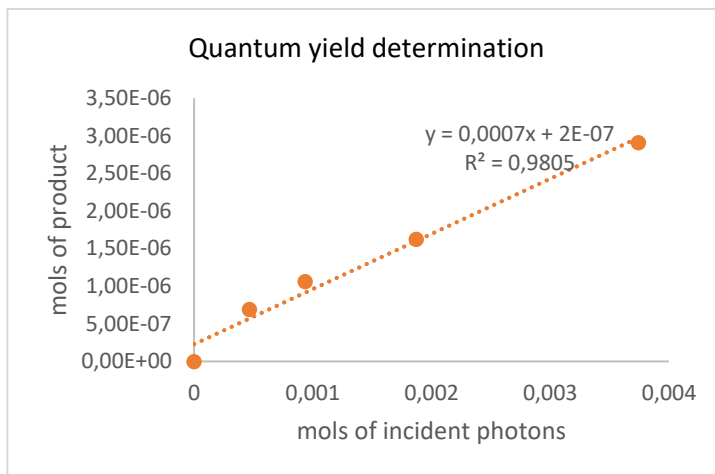


Figure 2.17. Plot of moles of incident photons vs moles of product formed. Slope of the line correlates to quantum yield of the photochemical transformation.

2.9.6.3 Alkylation enol ethers

A ferrioxalate actinometer solution was prepared by following the Hammond variation of the Hatchard and Parker procedure outlined in the Handbook of Photochemistry.⁶³ The ferrioxalate actinometer solution measures the decomposition of ferric ions to ferrous ions, which are complexed by 1,10-phenanthroline and monitored by UV/Vis absorbance at 510 nm. The moles of iron-phenanthroline complex formed are related to moles of photons absorbed. The following solutions were prepared and stored in a dark laboratory (red light):

1. Potassium ferrioxalate solution: 294.8 mg of potassium ferrioxalate (commercially available from Alfa Aesar) and 139 μL of sulfuric acid (96%) were added to a 50 mL volumetric flask and filled to the mark with water (HPLC grade).
2. Phenanthroline solution: 0.2% by weight of 1,10-phenanthroline in water (100 mg in 50 mL volumetric flask).
3. Buffer solution: 2.47 g of NaOAc and 0.5 mL of sulfuric acid (96%) were added to a 50 mL volumetric flask, and filled to the mark with water (HPLC grade).

The actinometry measurements were done as follows:

1. 1 mL of the actinometer solution was added to a Schlenk tube (diameter = 12 mm). The Schlenk tube was placed in a single HP LED 1.5 cm away from the light source (irradiance 10 mW/cm^2).¹² The solution was irradiated at 460 nm. This procedure was repeated 4 times, quenching the solutions after different time intervals: 5 s, 10 s, 20 s, and 40 s.

2. Then 1 mL of the model reaction following general procedure H with **39a** (0.10 mmol) and **42i** as substrates was placed in a Schlenk tube, degassed via argon bubbling, placed in the irradiation set up and irradiated for 15 minutes. This procedure was performed a total of four times with different irradiation times (30 min, 50 min, 70 min).
3. After irradiation, the actinometer solutions were removed and placed in a 10 mL volumetric flask containing 0.5 mL of 1,10-phenanthroline solution and 2 mL of buffer solution. These flasks were filled to the mark with water (HPLC grade).
4. The UV-Vis spectra of the complexed actinometer samples were recorded for each time interval. The absorbance of the complexed actinometer solution was monitored at 510 nm.

The moles of Fe^{2+} formed for each sample is determined using Beers' Law (Eq. 1):

$$\text{Mols of Fe(II)} = V_1 \times V_3 \times \Delta A(510 \text{ nm}) / 10^3 \times V_2 \times l \times \epsilon(510 \text{ nm}) \quad (\text{Eq. 1})$$

where V_1 is the irradiated volume (1 mL), V_2 is the aliquot of the irradiated solution taken for the determination of the ferrous ions (1 mL), V_3 is the final volume after complexation with phenanthroline (10 mL), l is the optical path-length of the irradiation cell (1 cm), $\Delta A(510 \text{ nm})$ is the optical difference in absorbance between the irradiated solution and the one stored in the dark, $\epsilon(510 \text{ nm})$ is the extinction coefficient the complex $\text{Fe}(\text{phen})_3^{2+}$ at 510 nm (11100 L mol⁻¹ cm¹). The moles of Fe^{2+} formed (x) are plotted as a function of time (t). The slope of this line was correlated to the moles of incident photons by unit of time (q_0 n,p) by the use of the following Equation 2:

$$\Phi(\lambda) = dx/dt \cdot q_{n,p} / q_0 [1 - 10^{-A(\lambda)}] \quad (\text{Eq. 2})$$

where dx/dt is the rate of change of a measurable quantity (spectral or any other property), the quantum yield (Φ) for Fe^{2+} at 458 nm is 1.1,64 $[1 - 10^{-A(\lambda)}]$ is the ratio of absorbed photons by the solution, and $A(\lambda)$ is the absorbance of the actinometer at the wavelength used to carry out the experiments (460 nm). The absorbance at 460 nm $A(460)$ was measured using a Shimadzu 2401PC UV-Vis spectrophotometer in a 10 mm path quartz cuvette, obtaining an absorbance of 0.148. $q_{n,p}^0$, which is the photon flux, was determined to be 1.18×10^{-7} .

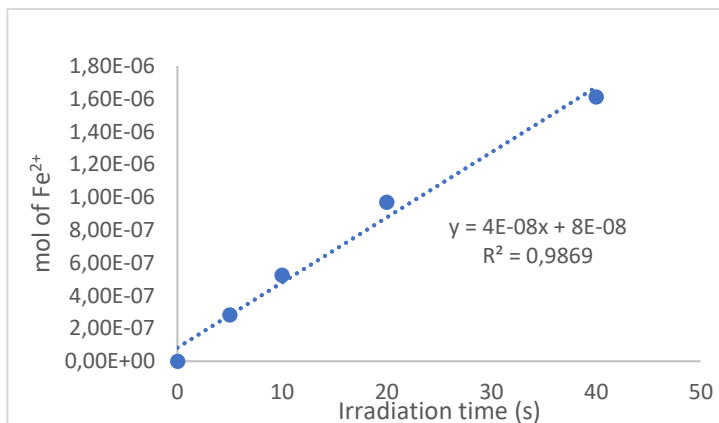


Figure 2.18. Plot of mols of Fe²⁺ formed vs irradiation time. Slope of the line correlates to the moles of incident photons by unit of time.

The moles of product **43h** formed for the model reaction were determined by GC measurement (FID detector) using 1,3,5-trimethoxybenzene as internal standard. The moles of product per unit of time are related to the number of photons absorbed.

The photons absorbed are correlated to the number of incident photons by the use of Equation 1. According to this, if we plot the moles of product (y) versus the moles of incident photons ($q_0 n_p \cdot dt$), the slope is equal to: $\Phi \cdot (1 - 10^{-A(460 \text{ nm})})$, where Φ is the quantum yield to be determined and $A(460 \text{ nm})$ is the absorption of the reaction under study.

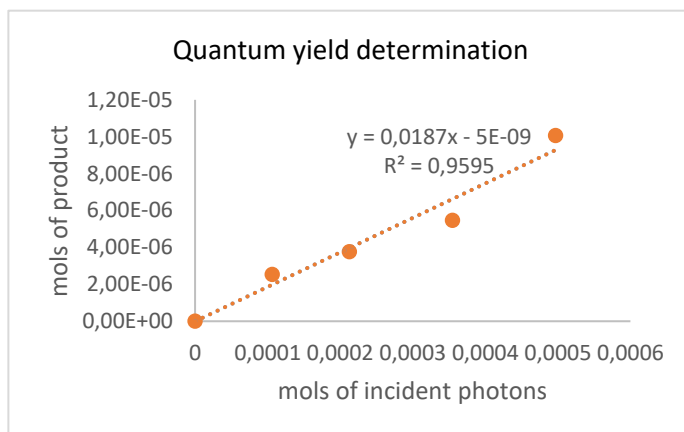


Figure 2.19. Plot of mols of incident photons vs mols of product formed. Slope of the line correlates to quantum yield of the photochemical transformation.

A(460 nm) was measured using a Shimadzu 2401PC UV-Vis spectrophotometer in 10 mm path quartz. An absorbance of 0.018 was determined for the model reaction mixture (1:100 dilution). The quantum yield (Φ)_{cat.} of the photochemical transformation was measured to be 0.02.

2.9.6.4 Minisci reaction

A ferrioxalate actinometer solution was prepared by following the Hammond variation of the Hatchard and Parker procedure outlined in the Handbook of Photochemistry.⁶³ The ferrioxalate actinometer solution measures the decomposition of ferric ions to ferrous ions, which are complexed by 1,10-phenanthroline and monitored by UV/Vis absorbance at 510 nm. The moles of iron-phenanthroline complex formed are related to moles of photons absorbed. The following solutions were prepared and stored in a dark laboratory (red light):

1. Potassium ferrioxalate solution: 294.8 mg of potassium ferrioxalate (commercially available from Alfa Aesar) and 139 μ L of sulfuric acid (96%) were added to a 50 mL volumetric flask, and filled to the mark with water (HPLC grade).
2. Phenanthroline solution: 0.2% by weight of 1,10-phenanthroline in water (100 mg in 50 mL volumetric flask).
3. Buffer solution: 2.47 g of NaOAc and 0.5 mL of sulfuric acid (96%) were added to a 50 mL volumetric flask, and filled to the mark with water (HPLC grade).

The actinometry measurements were done as follows:

1. 1 mL of the actinometer solution was added to a Schlenk tube (diameter = 12 mm). The Schlenk tube was placed in one of the position of the 3D printed reactor (Figure 2.3). The solution was irradiated at 460 nm. This procedure was repeated 4 times, quenching the solutions after different time intervals: 1 s, 2 s, 4 s, and 8 s.
2. Then 1 mL of the model reaction following general procedure J with **36a** (0.10 mmol) and 2-methylquinoline **45b** as substrates was placed in a Schlenk tube, degassed via argon bubbling, placed in the irradiation set up and irradiated for 60 minutes. This procedure was performed a total of four times with different irradiation times (90 min, 120 min, 150 min).
3. After irradiation, the actinometer solutions were removed and placed in a 10 mL volumetric flask containing 0.5 mL of 1,10-phenanthroline solution and 2 mL of buffer solution. These flasks were filled to the mark with water (HPLC grade).

4. The UV-Vis spectra of the complexed actinometer samples were recorded for each time interval. The absorbance of the complexed actinometer solution was monitored at 510 nm.

The moles of Fe^{2+} formed for each sample is determined using Beers' Law (Eq. 1):

$$\text{Mols of Fe(II)} = V_1 \times V_3 \times \Delta A(510 \text{ nm}) / 10^3 \times V_2 \times l \times \epsilon(510 \text{ nm}) \quad (\text{Eq. 1})$$

where V_1 is the irradiated volume (1 mL), V_2 is the aliquot of the irradiated solution taken for the determination of the ferrous ions (1 mL), V_3 is the final volume after complexation with phenanthroline (10 mL), l is the optical path-length of the irradiation cell (1 cm), $\Delta A(510 \text{ nm})$ is the optical difference in absorbance between the irradiated solution and the one stored in the dark, $\epsilon(510 \text{ nm})$ is the extinction coefficient the complex $\text{Fe}(\text{phen})_3^{2+}$ at 510 nm (11100 L mol⁻¹ cm⁻¹). The moles of Fe^{2+} formed (x) are plotted as a function of time (t). The slope of this line was correlated to the moles of incident photons by unit of time ($q_{n,p}^0$) by the use of the following Equation 2:

$$\Phi(\lambda) = dx/dt \cdot q_{n,p}^0 [1 - 10^{-A(\lambda)}] \quad (\text{Eq. 2})$$

where dx/dt is the rate of change of a measurable quantity (spectral or any other property), the quantum yield (Φ) for Fe^{2+} at 458 nm is 1.1,64 $[1 - 10^{-A(\lambda)}]$ is the ratio of absorbed photons by the solution, and $A(\lambda)$ is the absorbance of the actinometer at the wavelength used to carry out the experiments (460 nm). The absorbance at 460 nm $A(460)$ was measured using a Shimadzu 2401PC UV-Vis spectrophotometer in a 10 mm path quartz cuvette, obtaining an absorbance of 0.183. $q_{n,p}^0$, which is the photon flux, was determined to be 4.68×10^{-7} .

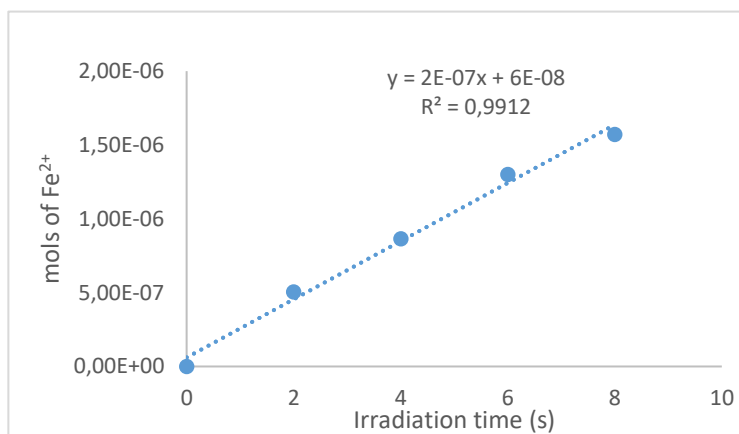


Figure 2.20. Plot of mols of Fe^{2+} formed vs irradiation time. Slope of the line correlates to the moles of incident photons by unit of time.

The moles of product **46b** formed for the model reaction were determined by GC measurement (FID detector) using 1,3,5-trimethoxybenzene as internal standard. The moles of product per unit of time are related to the number of photons absorbed.

The photons absorbed are correlated to the number of incident photons by the use of Equation 1. According to this, if we plot the moles of product (y) versus the moles of incident photons ($q_0 n \cdot dt$), the slope is equal to: $\Phi \cdot (1 - 10^{-A(460 \text{ nm})})$, where Φ is the quantum yield to be determined and $A(460 \text{ nm})$ is the absorption of the reaction under study. $A(460 \text{ nm})$ was measured using a Shimadzu 2401PC UV-Vis spectrophotometer in 10 mm path quartz. An absorbance of 0.174 was determined for the model reaction mixture (1:10 dilution). The quantum yield (Φ_{cat}) of the photochemical transformation was measured to be 0.0003.

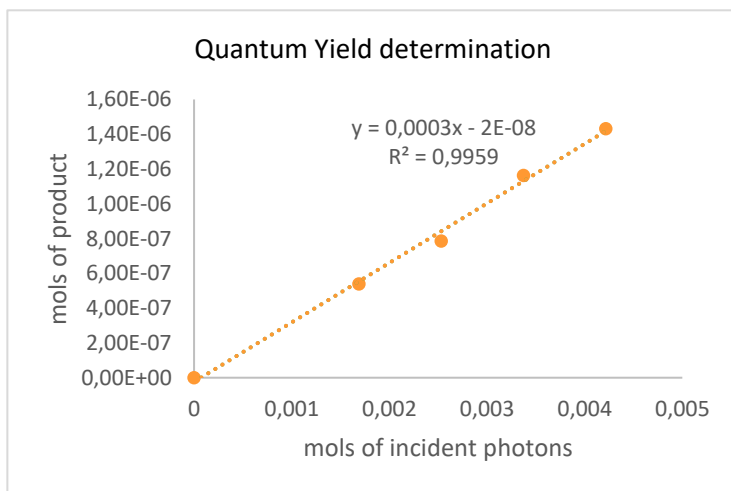


Figure 2.21. Plot of mols of incident photons vs mols of product formed. Slope of the line correlates to quantum yield of the photochemical transformation.

Chapter III

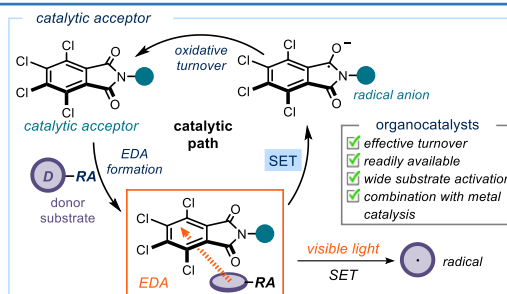
Tetrachlorophthalimides as Organocatalytic Acceptors for Electron Donor–Acceptor Complex Photoactivation

Target

To develop a general and modular class of electron-acceptor organocatalysts that can readily form photoactive electron donor–acceptor (EDA) complexes with a variety of radical precursors.

Tools

Tendency of tetrachlorophthalimides to act as suitable acceptors in a catalytic EDA regime. Use of these organocatalysts to activate a variety of radical precursors not amenable to previous EDA catalytic methods, thus developing radical transformations.¹



3.1 Introduction

The previous chapter detailed the development of a class of electron-donor organocatalysts suitable for electron-donor acceptor (EDA) complex activation, by which we have succeeded in expanding the strategy's synthetic efficiency.² The protocol relied on electron-rich dithiocarbamate and xanthogenate donor catalysts suitable for EDA complex formation with electron-poor radical precursors adorned

¹ The project discussed in this chapter was conducted in collaboration with Shuo Wu. I was involved in the discovery of the catalysts and optimization of the reactions and investigated the scope of the Giese reaction and Heck-type reaction. I also conducted the mechanistic studies. This work has been published: Zhou, W.; Wu, S.; Melchiorre, P., Tetrachlorophthalimides as Organocatalytic Acceptors for Electron Donor–Acceptor Complex Photoactivation. *J. Am. Chem. Soc.* **2022**, *144*, 8914–8919.

² De Pedro Beato, E.; Spinnato, D.; Zhou, W.; Melchiorre, P. A General Organocatalytic System for Electron Donor–Acceptor Complex Photoactivation and Its Use in Radical Processes. *J. Am. Chem. Soc.* **2021**, *143*, 12304–12314.

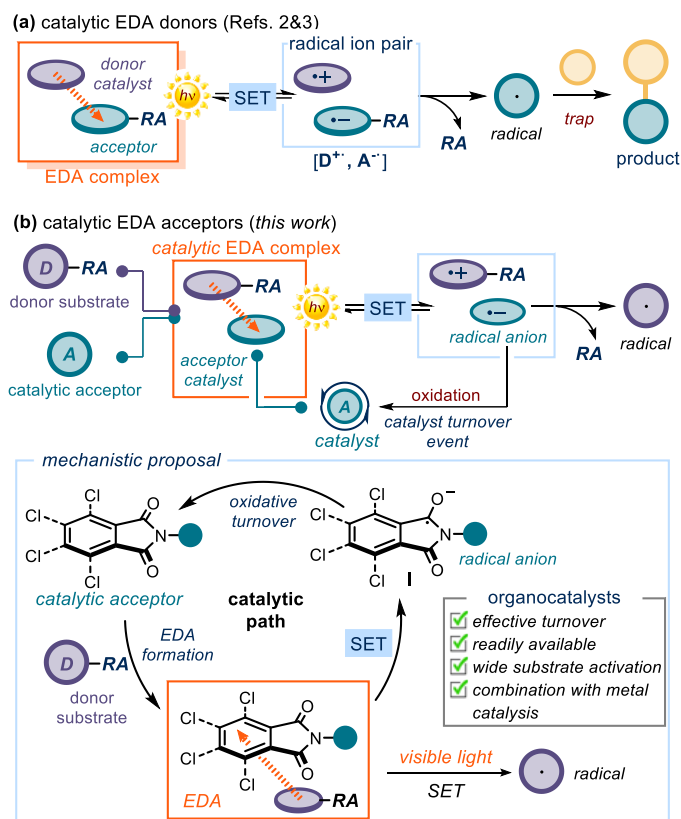
with a suitable redox auxiliary. A photoinduced single-electron transfer (SET) enabled the generation of radicals that could engage in a variety of bond-forming processes. In addition to our strategy, researchers have also reported a few protocols using electron donor catalysts³ for EDA complex photoactivation (for a detailed discussion, see section 2.4). In contrast, the use of electron-deficient catalytic acceptors for EDA complex formation and radical formation is far more limited. A few recent reports confirmed the feasibility of such strategy,⁴ but those catalysts were found to activate only specific radical precursors and were therefore limited to selected transformations.

We therefore focused on the development of a general strategy for EDA complex catalysis based on catalytic acceptors, suitable for activating multiple classes of electron-rich substrates not amenable to previous EDA catalytic protocols (Scheme 3.1). The crucial step for an effective catalyst turnover would require SET oxidation of the catalyst radical anion (blue circle in Scheme 3.1b), arising from the photoactivity of the progenitor EDA complex. Cognizant of the tendency of

³ (a) Fu, M.-C.; Shang, R.; Zhao, B.; Wang, B.; Fu, Y, Photocatalytic decarboxylative alkylations mediated by triphenylphosphine and sodium iodide. *Science* **2019**, *363*, 1429–1434. (b) Bosque, I.; Bach, T. 3-Acetoxyquinuclidine as Catalyst in Electron Donor-Acceptor Complex-Mediated Reactions Triggered by Visible Light. *ACS Catal.* **2019**, *9*, 9103–9109. (c) McClain, E. J.; Monos, T. M.; Mori, M.; Beatty, J. W.; Stephenson, C. R. J. Design and Implementation of a Catalytic Electron Donor–Acceptor Complex Platform for Radical Trifluoromethylation and Alkylation. *ACS Catal.* **2020**, *10*, 12636–12641. (d) Fu, M.-C.; Wang, J. X.; Shang, R. Triphenylphosphine-Catalyzed Alkylative Iododecarboxylation with Lithium Iodide under Visible Light. *Org. Lett.* **2020**, *22*, 8572–8577. For photochemical enzymatic processes that use co-factors as catalytic donors in EDA complexes, see: (e) Emmanuel, M. A.; Greenberg, N. R.; Oblinsky, D. G.; Hyster, T. K., Accessing non-natural reactivity by irradiating nicotinamide-dependent enzymes with light. *Nature* **2016**, *540*, 414–417. (f) Page, C. G.; Cooper, S. J.; DeHovitz, J. S.; Oblinsky, D. G.; Biegasiewicz, K. F.; Antropow, A. H.; Armbrust, K. W.; Ellis, J. M.; Hamann, L. G.; Horn, E. J.; Oberg, K. M.; Scholes, G. D.; Hyster, T. K., Quaternary Charge-Transfer Complex Enables Photoenzymatic Intermolecular Hydroalkylation of Olefins. *J. Am. Chem. Soc.* **2021**, *143*, 97–102. (g) Liu, C.; Shen, N.; Shang, R., Photocatalytic decarboxylative alkylation of silyl enol ether and enamide with N-(acyloxy)phthalimide using ammonium iodide. *Org. Chem. Front.* **2021**, *8*, 4166–4170. (h) Wang, G.-Z.; Fu, M.-C.; Zhao, B.; Shang, R., Photocatalytic decarboxylative alkylations of C(sp³)-H and C(sp²)-H bonds enabled by ammonium iodide in amide solvent. *Sci. China: Chem.*, **2021**, *64*, 439–444. (i) Fuse, H.; Irie, Y.; Fuki, M.; Kobori, Y.; Kato, K.; Yamakata, A.; Higashi, M.; Mitsunuma, H.; Kanai, M., Identification of a Self-Photosensitizing Hydrogen Atom Transfer Organocatalyst System. *J. Am. Chem. Soc.*, **2022**, *144*, 6566–6574.

⁴ (a) Morack, T.; Mück-Lichtenfeld, C.; Gilmour, R. Bioinspired Radical Stetter Reaction: Radical Umpolung Enabled by Ion-Pair Photocatalysis. *Angew. Chem., Int. Ed.* **2019**, *58*, 1208–1212. (b) Aramaki, Y.; Imaizumi, N.; Hotta, M.; Kumagai, J.; Ooi, T., Exploiting single-electron transfer in Lewis pairs for catalytic bond-forming reactions. *Chem. Sci.* **2020**, *11*, 4305–4311. (c) Runemark, A.; Sundén, S. Aerobic Oxidative EDA Catalysis: Synthesis of Tetrahydroquinolines Using an Organocatalytic EDA Active Acceptor. *J. Org. Chem.* **2022**, *87*, 1457–1469.

(tetrachloro)phthalimides to act as electron-poor redox auxiliaries for stoichiometric EDA complex formation,⁵ we surmised that these fragments could ensure i) effective EDA complex formation upon ground-state aggregation with electron-rich substrates, and ii) effective turnover, upon SET oxidation of the ensuing radical anion of type **I** (see the mechanistic inset in scheme 3.1b).



Scheme 3.4. (a) Donor catalysts for EDA complex catalysis. (b) Design of a catalytic acceptor platform for EDA complex photoactivation.

In this chapter, the conceptual development and synthetic implementation of a general and modular class of electron-acceptor organocatalysts for EDA complex

⁵ Selected applications of phthalimides and tetrachlorophthalimides as redox auxiliaries for EDA complex formation: (a) Candish, L.; Teders, M.; Glorius, F., Transition-Metal-Free, Visible-Light-Enabled Decarboxylative Borylation of Aryl N-Hydroxyphthalimide Esters *J. Am. Chem. Soc.* **2017**, *139*, 7440–7443. (b) Li, Y.; Zhang, J.; Li, D.; Chen, Y., Metal-Free C(sp³)-H Allylation via Aryl Carboxyl Radicals Enabled by Donor–Acceptor Complex. *Org. Lett.* **2018**, *20*, 3296–3299. (c) Le Saux, E.; Zanini, M.; Melchiorre, P. Photochemical Organocatalytic Benzoylation of Allylic C–H Bonds. *J. Am. Chem. Soc.* **2022**, *144*, 1113–1118. See also ref. 3a and 3b.

photoactivation will be described. We found that readily available tetrachlorophthalimide catalysts can easily form photoactive EDA complexes with a variety of electron-rich radical precursors that, upon irradiation with visible light, enable radical transformations and regeneration of the catalyst to close the catalytic cycle. In the following section, relevant examples of catalytic EDA complex platforms will be discussed, mainly focusing on the use of catalytic electron acceptors.

3.2 Catalytic acceptors in EDA complex photoactivation

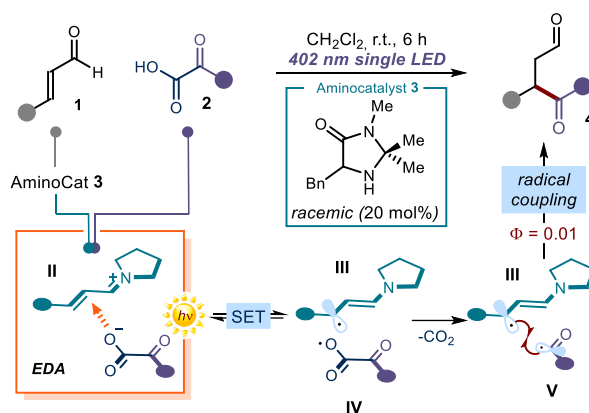
Excitation of photoactive EDA complexes is an effective way to generate radicals without the reliance on exogenous photocatalysts.⁶ Research conducted by different groups, including ours, demonstrated that electron-rich organocatalytic intermediates⁷ and catalysts^{2,3} could act as catalytic donors in EDA complex formation (for a detailed discussion see section 2.4 in the previous chapter). In sharp contrast, a general system for EDA photoactivation based on catalytic acceptors still remains underdeveloped (Scheme 3.1b). Only a few previous studies have used electron-poor catalysts to participate in EDA complex formation.⁴

The first example of a catalytic acceptor to participate in EDA interactions was reported in 2018 by the Gilmour group.^{4a} In their case (Scheme 3.2), EDA complex formation occurred between an α -ketocarboxylic acid **2** and a catalytic iminium ion

⁶ Selected applications of stoichiometric EDA complexes: (a) Sankararaman, S.; Haney, W. A.; Kochi, J. K. Annihilation of Aromatic Cation Radicals by Ion-Pair and Radical-Pair Collapse. Unusual Solvent and Salt Effects in the Competition for Aromatic Substitution. *J. Am. Chem. Soc.* **1987**, *109*, 7824–7838. (b) Russell, G. A.; Wang, K. Homolytic Alkylation of Enamines by Electrophilic Radicals. *J. Org. Chem.* **1991**, *56*, 3475–3479. (c) Tobisu, M.; Furukawa, T.; Chatani, N. Visible Light-mediated Direct Arylation of Arenes and Heteroarenes Using Diaryliodonium Salts in the Presence and Absence of a Photocatalyst. *Chem. Lett.* **2013**, *42*, 1203–1205. (d) Kandukuri, S. R.; Bahamonde, A.; Chatterjee, I.; Jurberg, I. D.; Escudero-Adán, E. C.; Melchiorre, P. X-Ray Characterization of an Electron Donor-Acceptor Complex Drives the Photochemical Alkylation of Indoles. *Angew. Chem., Int. Ed.* **2015**, *54*, 1485–1489. (e) Liu, B.; Lim, C.-H.; Miyake, G. M. Visible-Light-Promoted C–S Cross-Coupling via Intermolecular Charge Transfer. *J. Am. Chem. Soc.* **2017**, *139*, 13616–13619. (f) Lübbsmeyer, M.; Mackay, E. G.; Raycroft, M. A. R.; Elfert, J.; Pratt, D. A.; Studer, A. Base-Promoted C–C Bond Activation Enables Radical Allylation with Homoallylic Alcohols. *J. Am. Chem. Soc.* **2020**, *142*, 2609–2616.

⁷ (a) Arceo, E.; Bahamonde, A.; Bergonzini, G.; Melchiorre, P. Enantioselective direct α -alkylation of cyclic ketones by means of photo-organocatalysis. *Chem. Sci.* **2014**, *5*, 2438–2442. (b) Cao, Z.-Y.; Ghosh, T.; Melchiorre, P. Enantioselective radical conjugate additions driven by a photoactive intramolecular iminium-ion-based EDA complex. *Nat. Commun.* **2018**, *9*, 3274. (c) Woźniak, Ł.; Murphy, J. J.; Melchiorre, P. Photo-organocatalytic Enantioselective Perfluoroalkylation of β -Ketoesters. *J. Am. Chem. Soc.* **2015**, *137*, 5678–5681.

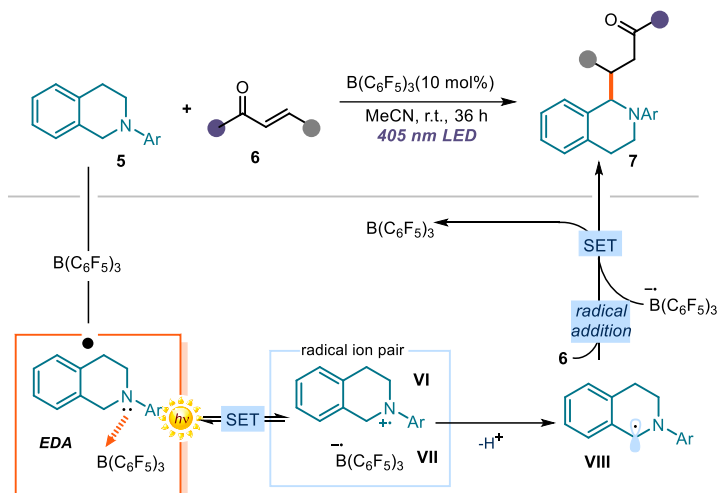
intermediate **II**, which was generated in situ from the condensation of enals **1** and a racemic aminocatalyst **3**. Upon photoexcitation, the EDA complex underwent intra-complex charge transfer to deliver radicals **III** and **IV**. Concomitant release of CO₂ from **IV** provided the acyl radical **V**, which coupled with the β -enaminy radical **III**. Hydrolysis of the resulting enamine enabled catalyst turnover while affording racemic 1,4-dicarbonyl compound **4** as the final product. This closed catalytic cycle was supported by the low quantum yield ($\Phi = 0.01$) of the overall process. Overall, this reaction offered the radical version of the Stetter reaction, enabling the selective conversion of α,β -unsaturated aldehydes into 4-ketoaldehydes **4**.



Scheme 3.2. Iminium ions as catalytic acceptors for EDA photoactivation

Another example of EDA complex photoactivation with an electron-poor catalyst was disclosed by Ooi and coworkers in 2020 (Scheme 3.3).^{4b} They found that electron-poor tris(pentafluorophenyl)borane (B(C₆F₅)₃) could aggregate with *N,N*-dialkylanilines to form an EDA complex, which generated the corresponding radical ions **VI** and **VII** upon irradiation. This interaction can be also be discussed in terms of frustrated Lewis pairs (FLP) undergoing a photoinduced intra-SET, thus leading to frustrated radical ions, a field of research which is recently attracting the interest of the research community.⁸ The subsequent deprotonation of **VI** then produced the α -aminoalkyl radical **VIII**, which was captured by enones **6**. The resulting species could be reduced by borane radical anion **VII** to regenerate the borane catalyst and form the desired product **7**.

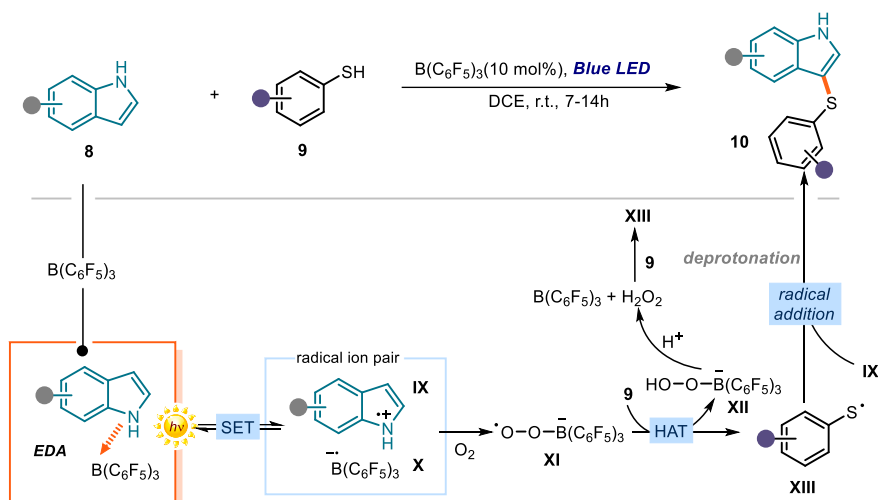
⁸ Lu, Z.; Ju, M.; Wang, Y.; Meinhardt, J. M.; Martínez Alvarado, J. I.; Villemure, E.; Terrett, J. A.; Lin, S., Regioselective aliphatic C–H functionalization using frustrated radical pairs. *Nature* **2023**, *619*, 514–520.



Scheme 3.3. $B(C_6F_5)_3$ as catalytic acceptor for EDA photoactivation, enabling coupling between tetrahydroisoquinoline **5** and enone **6**

In 2021, the Tang group described a reaction that was promoted by a catalytic amount of electron-poor $B(C_6F_5)_3$ (Scheme 3.4).^{4c} They proposed that EDA complex association occurs between $B(C_6F_5)_3$ and indole derivatives **8**, which could undergo photoinduced SET to afford radical ions **IX** and **X**. The latter borate radical anion would react with oxygen to deliver species **XI** that undergoes hydrogen atom transfer with thiol **9**, providing species **XII**. The sulfur-centered radical **XIII** could combine with radical cation **IX** to produce C-S coupled product **10**. On the other hand, species **XII** was protonated to turnover $B(C_6F_5)_3$ and produce hydrogen peroxide, which could also oxidize thiols **9** to afford another equivalent of thyl radical **XIII**.

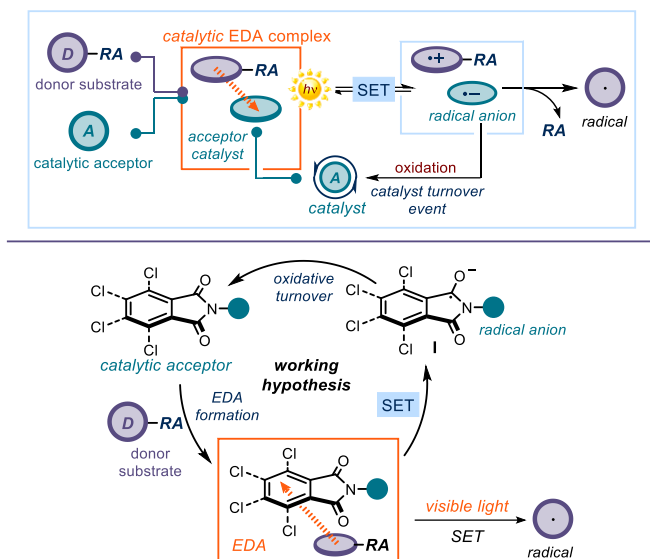
Overall, this overview highlights the limited number of acceptor catalysts available for EDA complex catalysis and the limitation in substrate scope.



Scheme 3.4. $B(C_6F_5)_3$ as catalytic acceptor for EDA photoactivation, enabling thiolation of indoles, DCE: 1,2-dichloroethylene

3.3 Target and design of the project

The current study was motivated by our interest in expanding the border of EDA complex photochemistry. The target was to develop a general EDA complex platform using an electron-acceptor organocatalyst that can generate radicals from a wide variety of electron-rich radical precursors and engage them in useful synthetic transformations (Scheme 3.5). We envisaged that phthalimides and tetrachlorophthalimides might be competent catalysts, owing to the fact that they can serve as electron-poor redox auxiliaries for stoichiometric EDA complex formation^{5,3a,3b} (see section 2.3 and 2.4 in the previous chapter for selected examples). A crucial aspect for success was the effective turnover of the catalyst via SET oxidation of the catalyst radical anion **I**, arising from the photoactivity of the progenitor EDA complex (Scheme 3.7).



Scheme 3.5. Our designed catalytic acceptor platform based on phthalimides and tetrachlorophthalimides.

3.4 Results and discussion

3.4.1 Developing a Giese addition process

We started our exploration by using cyclopentyl-1,4-dihydropyridine (DHP **11a**, Figure 3.1a) as the radical precursor because of its established ability to participate in EDA complex formation with phthalimide motifs.⁹ Initial experiments were conducted at 40 °C in dimethylformamide (DMF) with vinylsulfone **12a** as the radical trap using a blue LED emitting at 456 nm. As discussed above, the choice of suitable acceptor catalysts was informed by the tendency of phthalimides and tetrachloro phthalimides to serve as suitable electron-poor redox auxiliaries for stoichiometric EDA complex formation.^{5,3a,3b} We first tested the catalytic activity of phthalimide **A** (20 mol%), which failed to provide the target Giese addition product **13a** (entry 1, Figure 3.1b). In contrast, tetrachlorophthalimides **B** and **C** acted as effective EDA complex acceptor catalysts, affording product **13a** in high

⁹ (a) Li, Y.; Xu, R.; Chen, Y., Donor–Acceptor Complex Enables Alkoxy Radical Generation for Metal-Free C(sp³)–C(sp³) Cleavage and Allylation/Alkenylation. *Angew. Chem., Int. Ed.* **2017**, *56*, 12619–12623. (b) Marcaurrelle, L. A.; Molander, G. A., Photoredox-mediated hydroalkylation and hydroarylation of functionalized olefins for DNA-encoded library synthesis. *Chem. Sci.* **2021**, *12*, 12036–12045. (c) Elkhalfa, M.; Elbaum, M. B.; Chenoweth, D. M.; Molander, G. A., Solid-Phase Photochemical Decarboxylative Hydroalkylation of Peptides. *Org. Lett.* **2021**, *23*, 8219–8223.

yield (entries 2 and 3, respectively). These different catalytic performances can be rationalized by the higher electron-acceptor ability of catalysts **B** and **C**, as inferred by their redox properties (E_{red} (**A**) = -1.78V vs E_{red} (**B**) = -0.84V and E_{red} (**C**) = -0.86V). Cyclic voltammetric studies of the catalysts showed a well-shaped voltammogram with a reversible reduction wave for **B** and **C** (Figure 3.1c, see also the experimental section). This hints at a certain kinetic stability of the corresponding radical anion of type **I**, which can be crucial for avoiding catalyst decomposition and allowing effective catalyst turnover.

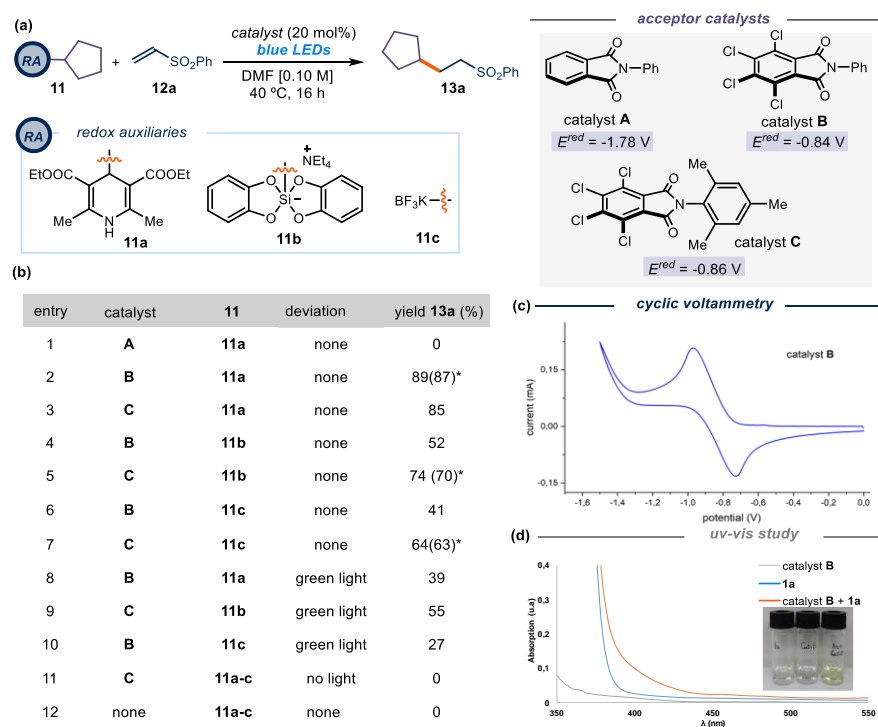


Figure 3.1. Initial explorations. (a) Model reaction and catalysts tested. (b) Optimization studies: reactions performed on a 0.1 mmol scale at 40 °C for 16 h under illumination by a Kessil lamp ($\lambda_{max} = 456$ nm, 40 W) using 1.5 equiv. of **1**. Yield determined by ^1H NMR analysis. *Yield of the isolated **13a**. (c) Cyclic voltammetric study of catalyst **B** [0.02 M] in DMF vs Ag/AgCl. (d) Optical absorption spectra, recorded in DMF in 1 mm path quartz cuvettes, of the separate reaction components and appearance of the colored EDA complex between catalyst **B** and **11a**. [1a] = 0.15 M, [B] = 0.02 M.

We then evaluated the ability of our EDA acceptor catalysts to activate electron-rich radical precursors bearing other redox auxiliary groups than DHP. We found

that silicate **11b**¹⁰ and trifluoroborate salt **11c**¹¹ could also be activated to form a cyclopentyl radical. Catalyst **C** performed better than **B** in activating **11b** and **11c**, leading to the Giese product **13a** in good yield (entries 5 and 7, respectively). These results highlight how the modular nature of the acceptor catalysts can be leveraged to optimize the activation of electronically different radical precursors.

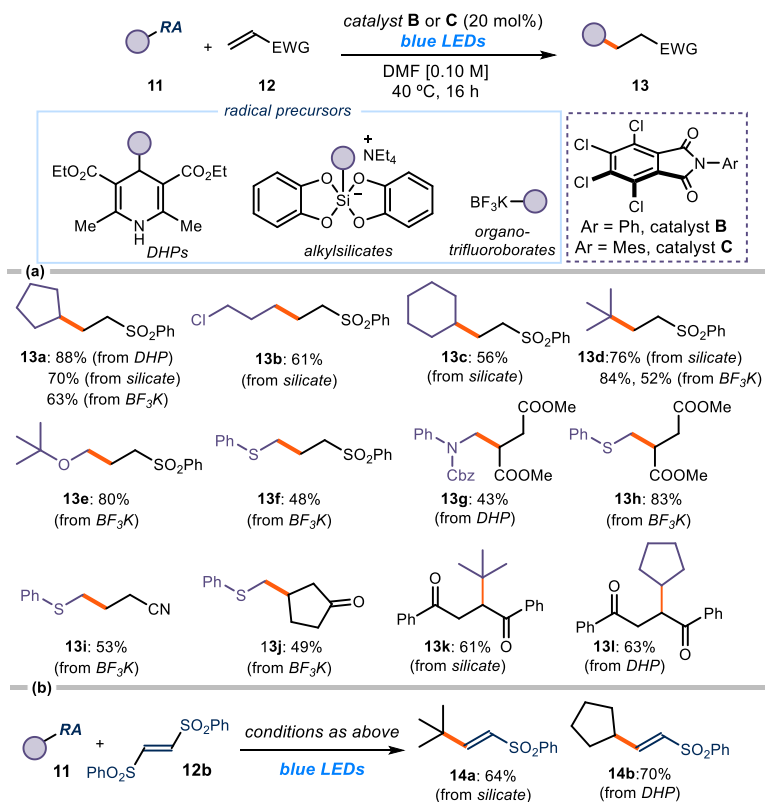
Investigations were performed to gain mechanistic insights. The formation of an EDA aggregate in the ground state was confirmed through UV/Vis spectroscopic analysis (Figure 3.1, d). After mixing catalyst **B** with substrate **11a** (both initially colorless), the solution developed a pale-yellow color, while its absorption spectrum showed a bathochromic displacement in the visible region. We have also examined the possibility that other photochemical pathways were operational in the generation of radicals, i.e. the direct excitation of catalysts **B** and **C** followed by SET activation of the substrates or the excitation of DHP **11a**. We therefore conducted the model reaction using substrates **11a**, **11b**, and **11c** under illumination by green light ($\lambda_{\text{max}} = 520 \text{ nm}$), a wavelength which cannot be absorbed by either the catalysts or the substrates (Figure 3.1d). All of these experiments led to the formation of product **13a**, albeit with diminished yields (entries 8-10). Collectively, these results are congruent with the EDA complex excitation being responsible of radical generation. Further control experiments established that light and the tetrachlorophthalide-based catalysts were essential for reactivity (entries 11 and 12, respectively).

We then evaluated the scope of the Giese addition protocol using different radical precursors **11** and electron-poor olefins **12** (Scheme 3.6). In contrast to other methods,¹² our protocol does not need stoichiometric amounts of additional reagents (e.g., bases, reductants, hydrogen-atom donors) or photoredox catalysts. The tetrachlorophthalimide-based catalyst **B** was used for the EDA complex activation of DHP radical precursors, while the mesitylene catalyst **C** proved more effective for alkylsilicates and organotrifluoroborates.

¹⁰ Corcé, V.; Chamoreau, L.-M.; Derat, E.; Goddard, J.-P.; Ollivier, C.; Fensterbank, L., Silicates as Latent Alkyl Radical Precursors: Visible-Light Photocatalytic Oxidation of Hypervalent Bis-Catecholato Silicon Compounds. *Angew. Chem., Int. Ed.* **2015**, *54*, 11414-11418.

¹¹ (a) Duan, K.; Yan, X.; Liu, Y.; Li, Z., Recent Progress in the Radical Chemistry of Alkylborates and Alkylboronates. *Adv. Synth. Catal.* **2018**, *360*, 2781-2795. (b) Corcé, V.; Ollivier, C.; Fensterbank, L., Boron, silicon, nitrogen and sulfur-based contemporary precursors for the generation of alkyl radicals by single electron transfer and their synthetic utilization. *Chem. Soc. Rev.* **2022**, *51*, 1470-1510.

¹² van Leeuwen, T.; Buzzetti, L.; Perego, L. A.; Melchiorre, P., A Redox-Active Nickel Complex that Acts as an Electron Mediator in Photochemical Giese Reactions. *Angew. Chem., Int. Ed.* **2019**, *58*, 4953-4957.

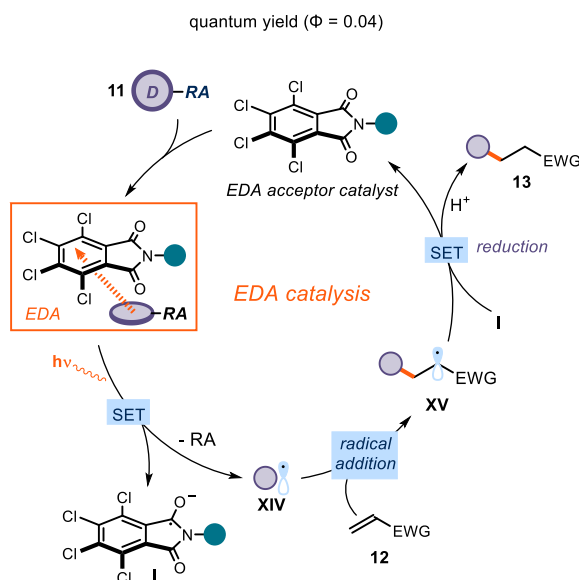


Scheme 3.6. (a) Substrate scope for the Giese reaction catalyzed by EDA acceptors. Reactions performed on a 0.2 mmol scale using 1.5 equiv. of **11**; catalyst **B** was used for DHP substrates, **C** for silicates and trifluoroborates. Yields refer to isolated products **13**. For **13b**, the cation of silicate **11d** is K⁺ rather than NEt₄⁺. For **13d**, 5 mmol scale reaction was also conducted in 52% yield. (b) Formal radical vinylation. Mes: 2,4,6-trimethylphenyl. DMF: Dimethylformamide.

Primary (product **13b**), secondary (**13a** and **13c**), tertiary (**13d**), and α -heteroatom (**13e** and **13f**) radicals were generated efficiently and trapped with vinyl sulfone **12a** in moderate to good yields. Other olefins could be used to intercept the photogenerated radicals, including dimethyl fumarate (products **13g** and **13h**), acrylonitrile (**13i**), cyclopentenone (**13j**), and dibenzoyl ethylene (**13k** and **13l**). The use of 1,2-bis(phenylsulfonyl)ethene **12b** as the radical trap led to a radical addition–elimination sequence, affording alkenylation products **14a** and **14b** in good yields (Scheme 3.6, b).

Mechanistically, we propose that the Giese reaction proceeds via a redox-neutral, closed catalytic cycle (Scheme 3.7). Photoexcitation of the EDA complex formed between the acceptor catalyst **B** or **C** and the electron-rich substrate **11** would generate the alkyl radical **XIV** along with the catalyst radical anion **I**. Interception

of **XIV** by the electron-poor olefin **12** would lead to the reactive electrophilic radical **XV**. SET reduction of **XV** by the catalyst radical anion **I** would then afford product **13** while closing the catalytic cycle. The last SET event, which is crucial for catalyst turnover, is thermodynamically feasible on the basis of the redox properties of the radical anion **I** ($E_{\text{red}} = -0.84$ V for catalyst **B**) and radical **XV** (e.g. $E_{\text{red}} = -0.54$ vs saturated calomel electrode (SCE) for the radical generated upon radical trap from fumarate).¹³ To corroborate this mechanistic proposal, we measured the quantum yield (Φ) of the reaction of **11a** and **12a** catalyzed by **B**, which was as low as 0.04 ($\lambda = 460$ nm). This result indicates that a radical-chain process is unlikely, confirming the ability of the EDA complex catalytic donor to turnover.



Scheme 3.7. Proposed mechanism of the Giese addition promoted by our catalytic acceptor organocatalysts.

3.4.2 Developing a Heck-type reaction process

One of our goals was to identify a general acceptor catalyst suitable for the design of mechanistically distinct radical processes. Specifically, we sought to integrate

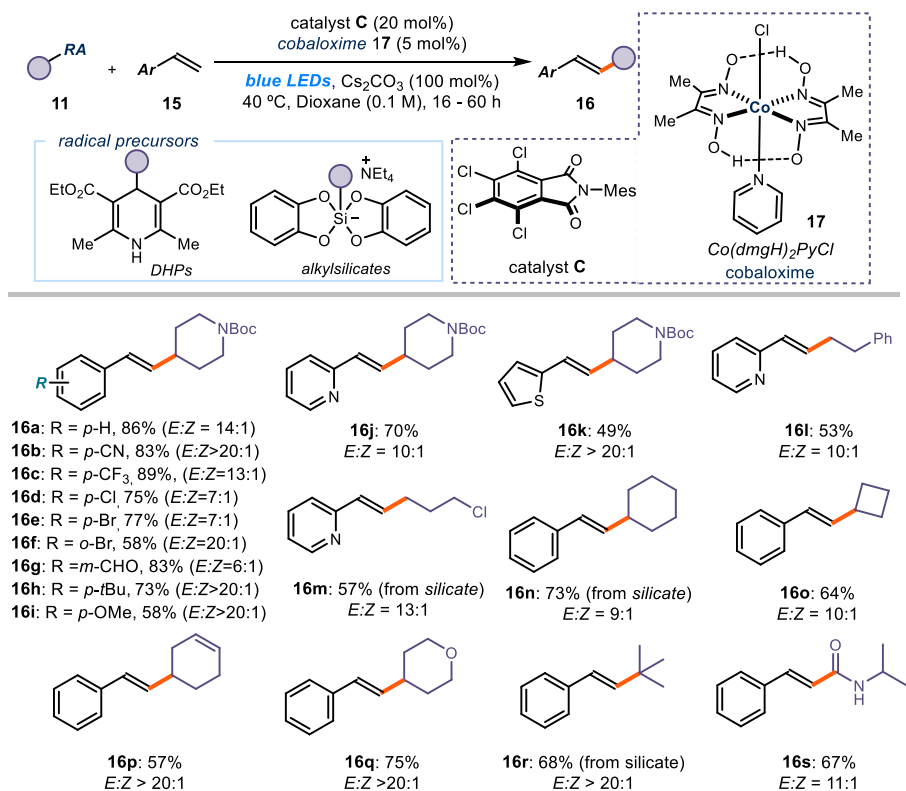
¹³ van Leeuwen, T.; Buzzetti, L.; Perego, L. A.; Melchiorre, P., A Redox-Active Nickel Complex that Acts as an Electron Mediator in Photochemical Giese Reactions. *Angew. Chem., Int. Ed.* **2019**, *58*, 4953–4957.

our EDA complex catalytic platform with a cobalt-based catalytic process. Previous literature contains few reports on the use of stoichiometric EDA complexes to generate radicals than then engage in a metal-based catalytic mechanism.¹⁴ However, to the best of our knowledge, the synergy of EDA complex catalysis and metal catalysis has not been realized. This idea was successfully implemented by combining the catalytic capabilities of the EDA complex acceptor catalyst **C** and cobaloxime catalyst **17**¹⁵ to perform the Heck-type coupling of radical precursors **11** with styrene derivatives **15** (scheme 3.8).¹⁶

¹⁴ (a) Kammer, L. M.; Badir, S. O.; Hu, R.-M.; Molander, G. A., Photoactive electron donor–acceptor complex platform for Ni-mediated C(sp³)–C(sp²) bond formation. *Chem. Sci.* **2021**, *12*, 5450–5457. (b) Li, R.-H.; Zhao, Y.-L.; Shang, Q.-K.; Geng, Y.; Wang, X.-L.; Su, Z.-M.; Li, G.-F.; Guan, W., Photocatalytic C(sp³)–O/N Cross-Couplings by NaI–PPh₃/CuBr Cooperative Catalysis: Computational Design and Experimental Verification. *ACS Catal.* **2021**, *11*, 6633–6642.

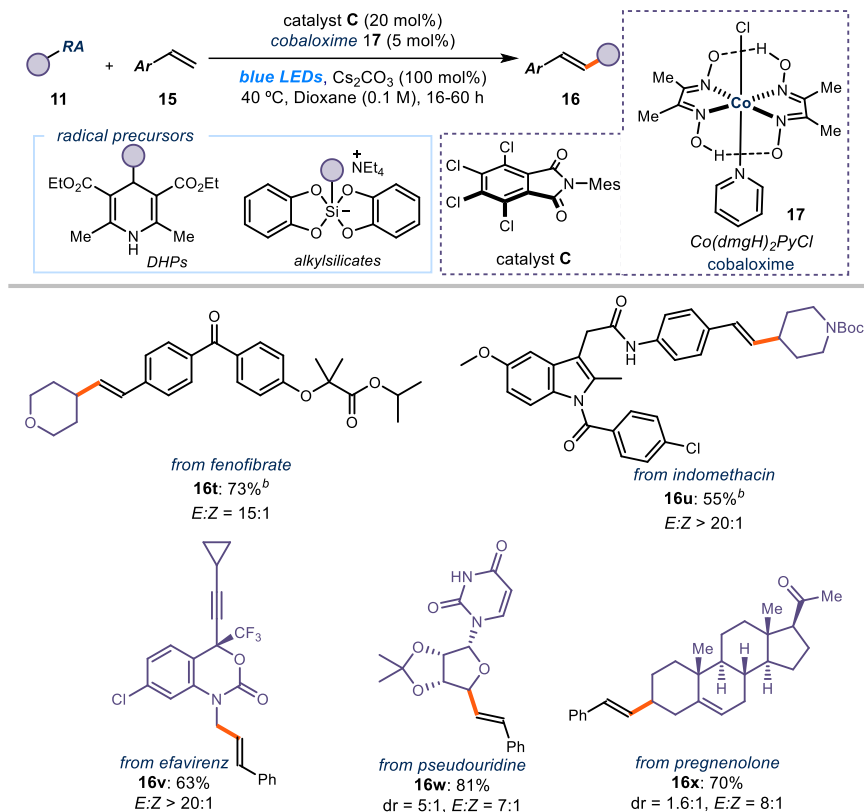
¹⁵ For selected applications of cobaloxime catalysis, see: (a) Sun, X.; Chen, J.; Ritter, T., Catalytic dehydrogenative decarboxyolefination of carboxylic acids. *Nat. Chem.* **2018**, *10*, 1229–1233. (b) U. Dighe, S.; Juliá, F.; Luridiana, A.; Douglas, J. J.; Leonori, D., A photochemical dehydrogenative strategy for aniline synthesis. *Nature* **2020**, *584*, 75–81. (c) Zhao, H.; McMillan, A. J.; Constantin, T.; Mykura, R. C.; Juliá, F.; Leonori, D., Merging Halogen-Atom Transfer (XAT) and Cobalt Catalysis to Override E2-Selectivity in the Elimination of Alkyl Halides: A Mild Route toward contra-Thermodynamic Olefins. *J. Am. Chem. Soc.* **2021**, *143*, 14806–14813. (d) Zhou, M.-J.; Zhang, L.; Liu, G.; Xu, C.; Huang, Z., Site-Selective Acceptorless Dehydrogenation of Aliphatics Enabled by Organophotoredox/Cobalt Dual Catalysis. *J. Am. Chem. Soc.* **2021**, *143*, 16470–16485.

¹⁶ A similar Heck-type process was realized by combining a photoredox catalyst and cobaloxime chemistry: Cao, H.; Jiang, H.; Feng, H.; Kwan, J. M. C.; Liu, X.; Wu, J., Photo-induced Decarboxylative Heck-Type Coupling of Unactivated Aliphatic Acids and Terminal Alkenes in the Absence of Sacrificial Hydrogen Acceptors. *J. Am. Chem. Soc.* **2018**, *140*, 16360–16367.



Scheme 3.8. Scope of the Heck-type reaction process; reactions performed on a 0.2 mmol scale using 5 equiv. of **15** and 1 equiv. of **11**. Yields refer to isolated products **16** after purification; *E/Z* ratio determined by ¹H NMR analysis of the crude mixture. For **16m**, the cation of silicate **11d** is K⁺ rather than NEt₄⁺. Boc: *tert*-Butyloxycarbonyl.

The generality of this dual catalytic protocol, which afforded products **16**, was first investigated with respect to the styrene component. Electron-poor (products **16b-g**) and electron-rich (adducts **16h** and **16i**) styrenes bearing *ortho*-, *meta*-, or *para*-substituents on the aryl ring all reacted smoothly to provide the corresponding disubstituted alkene products in moderate to good yields. Vinyl heteroarenes, bearing a pyridine (**16j**) or a thiophene (**16k**) scaffold, were competent substrates. A large variety of DHP radical precursors were amenable to this Heck-type process, but alkyl silicates could also be used. Primary (**16l** and **16m**), secondary (**16n-q**), and tertiary (**16r**) carbon-centered radicals were effectively generated and coupled with vinyl-pyridine or styrene. A carbamoyl radical could also be used effectively (product **16s**). We also demonstrated that this method is suitable for the direct functionalization of biorelevant compounds: *fenofibrate* (**16t**), *indomethacin* (**16u**), *pregnenolone* (**16v**), *pseudouridine* (**16w**), and *efavirenz* (**16x**) scaffold can be successfully decorated (Scheme 3.9).

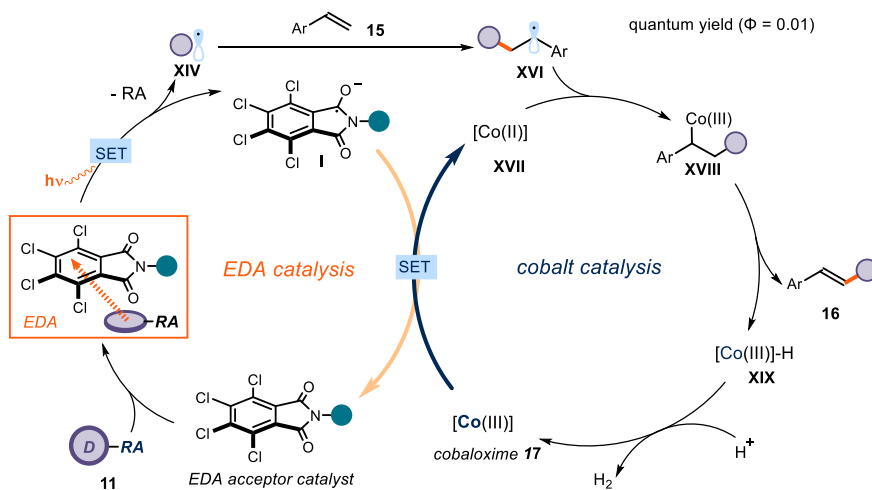


Scheme 3.9. Scope of the Heck-type process (biorelevant compounds); reactions performed on a 0.2 mmol scale using 5 equiv. of **15** and 1 equiv. of **11**. Yields refer to isolated products **16** after purification; E/Z ratio determined by ¹H NMR analysis of the crude mixture.

The proposed mechanism is depicted in Scheme 3.10. The photoactivity of the catalytic EDA complex, formed by association of the acceptor catalyst **C** with the electron-rich radical precursor **11**, would lead to the alkyl radical **XIV** and the catalyst radical anion **I**. Subsequent addition of **XIV** to styrene would furnish a stable benzylic radical intermediate **XVI**. At this juncture, the EDA complex catalytic cycle would intersect the cobaloxime cycle: the catalyst radical anion **I** would undergo SET oxidation from the Co(III) catalyst **17** ($E[\text{Co}^{\text{III}}/\text{Co}^{\text{II}}] = -0.67 \text{ V vs SCE in MeCN}$)¹⁷ to afford the Co(II) species **XVII** while turning over the EDA acceptor catalyst. The cobalt-based catalytic cycle would continue with the

¹⁷ Dempsey, J. L.; Brunschwig, B. S.; Winkler, J. R.; Gray, H. B., Hydrogen Evolution Catalyzed by Cobaloximes. *Acc. Chem. Res.* **2009**, *42*, 1995–2004.

Co(II) intermediate **XVII** intercepting the benzylic radical **XVI** to form the Co(III) intermediate **XVIII**, which is known to undergo facile β -hydride elimination.¹⁸



Scheme 3.10. Proposed mechanism for Heck-type process, with the cobalt and EDA catalytic cycles intertwined.

This step would deliver the alkene product **16** and the Co(III)–H **XIX**, which, upon reaction with either proton sources (e.g. protonated pyridine arising from DHPs) or another molecule of **XIX**, would release H₂¹⁶ and regenerate the Co(III) catalyst **17**. The quantum yield of the Heck-type reaction leading to product **16a** was as low as 0.01 ($\lambda = 460$ nm), which is congruent with the proposed dual catalytic cycle.

3.5 Conclusions

In summary, we reported that tetrachlorophthalimide-based catalysts can act as effective and general acceptors for EDA complex activation. These organocatalysts can activate a variety of radical precursors bearing different redox auxiliaries, including DHPs, silicates and trifluoroborates, which could not be activated by previous EDA catalytic protocols. Excitation with visible light granted access to alkyl radicals under mild conditions. Importantly, this EDA complex catalytic platform proved flexible enough to promote mechanistically different radical processes, including the first combination with a metal-based catalytic cycle.

¹⁸ Gridnev, A. A.; Ittel, S. D. Catalytic chain transfer in free-radical polymerizations. *Chem. Rev.* **2001**, *101*, 3611–3660.

3.6 Experimental section

General Information

The NMR spectra are available in the published manuscript¹ and are not reported in the present dissertation.

The NMR spectra were recorded at 400 MHz and 500 MHz for ¹H and 100 or 125 MHz for ¹³C. The chemical shift (δ) for ¹H and ¹³C are given in ppm relative to residual signals of the solvents (CHCl₃ @ 7.26 ppm ¹H NMR and 77.16 ppm ¹³C NMR, and tetramethylsilane @ 0 ppm). Coupling constants are given in Hertz. The following abbreviations are used to indicate the multiplicity: s, singlet; d, doublet; q, quartet; m, multiplet; bs, broad signal; app, apparent.

High resolution mass spectra (HRMS) were obtained from the ICIQ HRMS unit on MicroTOF Focus and Maxis Impact (Bruker Daltonics) with electrospray ionization. (ESI).

UV-vis measurements were carried out on a Shimadzu UV-2401PC spectrophotometer equipped with photomultiplier detector, double beam optics and D₂ and W light sources or an Agilent Cary60 spectrophotometer.

Yields refer to isolated materials of >95% purity as determined by ¹H NMR analysis.

The team of the Research Support Area at ICIQ, particularly to the NMR and the High-Resolution Mass Spectrometry Units, is thanked for their support.

Determination of *E/Z* Ratio. The *E/Z* ratio of the products was determined by ¹H NMR analysis of the crude reaction mixture through integration of diagnostic signals.

General Procedures. All reactions were set up under an argon atmosphere in oven-dried glassware. Synthesis grade solvents were used as purchased, anhydrous solvents were taken from a commercial SPS solvent dispenser. Chromatographic purification of products was accomplished using forced-flow chromatography (FC) on silica gel (35-70 mesh). For thin layer chromatography (TLC) analysis throughout this work, Merck pre-coated TLC plates (silica gel 60 GF₂₅₄, 0.25 mm) were employed, using UV light as the visualizing agent and an acidic mixture of vanillin or basic aqueous potassium permanganate (KMnO₄) stain solutions, and heat as developing agents. Organic solutions were concentrated under reduced pressure on a Büchi rotatory evaporator.

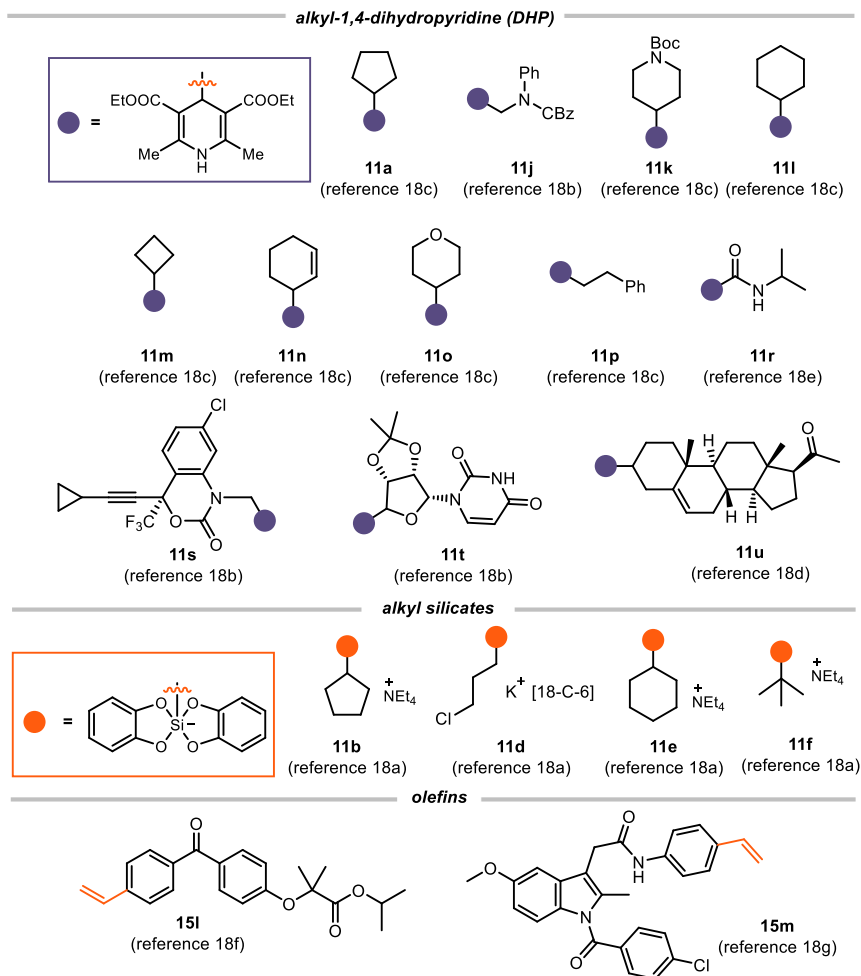
Materials. Most of the starting materials used in this study are commercial and were purchased at the highest purity available from Sigma-Aldrich, Fluka, Alfa Aesar, Fluorochem, and used as received, without further purifications.

3.6.1 Synthesis of Substrate and Catalysts

3.6.1.1 Substrate Synthesis

The following substrates were synthesized according to reported procedures (scheme 3.13).¹⁹

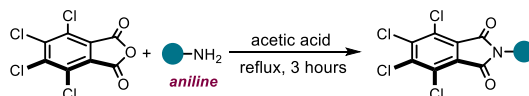
¹⁹ (a)Corcé, V.; Chamoreau, L.-M.; Derat, E.; Goddard, J.-P.; Ollivier, C.; Fensterbank, L., Silicates as Latent Alkyl Radical Precursors: Visible-Light Photocatalytic Oxidation of Hypervalent Bis-Catecholato Silicon Compounds. *Angew. Chem., Int. Ed.* **2015**, *54*, 11414–11418. (b)Crisenza, G. E. M.; Faraone, A.; Gandolfo, E.; Mazzarella, D.; Melchiorre, P., Catalytic asymmetric C–C cross-couplings enabled by photoexcitation. *Nat. Chem.* **2021**, *13*, 575–580. (c)Verrier, C.; Alandini, N.; Pezzetta, C.; Moliterno, M.; Buzzetti, L.; Hepburn, H. B.; Vega-Peñaloza, A.; Silvi, M.; Melchiorre, P., Direct Stereoselective Installation of Alkyl Fragments at the β -Carbon of Enals via Excited Iminium Ion Catalysis. *ACS Catal.* **2018**, *8*, 1062–1066. (d)Liu, X.-G.; Dong, C.-S.; Li, F.; Zhang, B., Manganese-Mediated Direct Functionalization of Hantzsch Esters with Alkyl Iodides via an Aromatization–Dearomatization Strategy. *Org. Lett.* **2021**, *23*, 4002–4007. (e)Alandini, N.; Buzzetti, L.; Favi, G.; Schulte, T.; Candish, L.; Collins, K. D.; Melchiorre, P., Amide Synthesis by Nickel/Photoredox-Catalyzed Direct Carbamoylation of (Hetero)Aryl Bromides. *Angew. Chem., Int. Ed.* **2020**, *59*, 5248–5253. (f)Liu, Z.-S.; Hua, Y.; Gao, Q.; Ma, Y.; Tang, H.; Shang, Y.; Cheng, H.-G.; Zhou, Q., Construction of axial chirality via palladium/chiral norbornene cooperative catalysis. *Nat. Cat.* **2020**, *3*, 727–733. (g)Liu, K.; Studer, A., Direct α -Acylation of Alkenes via N-Heterocyclic Carbene, Sulfinate, and Photoredox Cooperative Triple Catalysis. *J. Am. Chem. Soc.* **2021**, *143*, 4903–4909.



Scheme 3.11. Starting materials synthesized according to known procedures.

3.6.1.2 Catalysts Synthesis

General Procedure

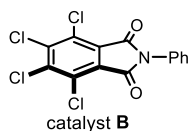


Scheme 3.12. Catalysts synthesized according to known procedures⁸.

An oven dried flask was charged with 4,5,6,7-tetrachlorophthalic anhydride (5.72 g, 20.0 mmol, 1.0 equiv.), the corresponding aniline (24.0 mmol, 1.2 equiv.) and anhydrous acetic acid (40 mL). The flask was equipped with a condenser and

placed in an oil-bath preheated to 120 °C. After 3 hours stirring, the solution was concentrated. The solid which precipitated on cooling was collected by filtration and washed first with 10 % aqueous sodium carbonate (100 mL x 3), water (100 mL x 3) and methanol (10 mL x 3). The resulting white solid was dried under reduced pressure to afford the final catalyst **B** and **C**.

Characterization

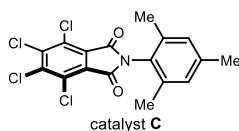


4,5,6,7-tetrachloro-2-phenylisoindoline-1,3-dione (catalyst **B**): Synthesized according to General Procedure using aniline (2.2 mL, 24.0 mmol, 1.2 equiv.). Catalyst **B** was obtained as a white solid (5.8 g, 81% yield). Melting point: 273 - 274 °C.

¹H NMR (400 MHz, CDCl₃) δ 7.52 (dd, *J* = 8.3, 6.8 Hz, 2H), 7.47 – 7.38 (m, 3H).

¹³C NMR (101 MHz, CDCl₃) δ 161.6, 139.6, 129.9, 129.3, 128.3, 127.9, 126.4, 125.6.

Matching reported literature data.²⁰



4,5,6,7-tetrachloro-2-mesitylisoindoline-1,3-dione (catalyst **C**): Synthesized according to General Procedure using 2,4,6-trimethylaniline (3.4 mL, 24.0 mmol, 1.2 equiv.). Catalyst **C** was obtained as a white solid (2.6 g, 77% yield). Melting point: 210 - 211 °C.

Melting point: 210 - 211 °C.

¹H NMR (400 MHz, CDCl₃) δ 7.00 (q, *J* = 0.7 Hz, 2H), 2.34 (s, 3H), 2.10 (s, 6H).

¹³C NMR (101 MHz, CDCl₃) δ 162.6, 140.6, 140.0, 136.3, 130.2, 129.6, 127.6, 126.4, 21.3, 18.1. Matching reported literature data.¹⁹

3.6.2 Experimental Setup

- **Set-up 1** 3D printed reactor with LED strip

For reactions performed using a blue LED strip as the light source, a 3D-printed photoreactor was used, consisting of a 9 cm diameter crystallizing dish with a 3D

²⁰ Kelterer, A.-M.; Mansha, A.; Iftikhar, F. J.; Zhang, Y.; Wang, W.; Xu, J.-H.; Grampp, G., Computational and experimental studies on the triplet states of various N-substituted 4,5,6,7-tetrachlorophthalimides. *Journal of Molecular Modeling* **2014**, *20*, 2344–2356.

printed support of 10 positions (Figure 3.2, left). A commercial 1-meter LED strip was wrapped around the crystallizing dish, while a fan was used to cool down the reactor (the reaction temperature within the reaction vessel was measured to be between 35-40 °C). Each of the positions could be used to fit a standard 16 mm diameter vial with a Teflon screw cap. Experiments at 465 nm were conducted using a 1m strip, 14.4W “LEDXON MODULAR 9009083 LED, SINGLE 5050” purchased from Farnell, catalog number 9009083. The emission spectrum of these LEDs is shown in Figure 3.2, right panel.

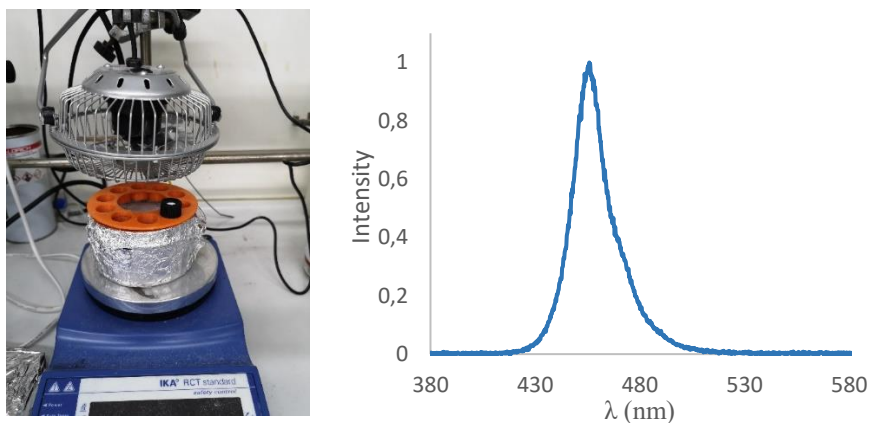


Figure 3.2. *Left panel:* Blue LEDs photoreactor used for reactions. *Right panel:* Emission spectrum of the 465 nm LED strip used in this reactor.

- **Set-up 2** *Kessil Lamp setup*

For reactions performed with a *Kessil* lamp, the irradiation set-up consisted of a 50 W *Kessil* blue LED lamp (PR160L-456, 100% intensity, 2-3 cm away – Figure 3.3) and a fan which was used to cool down the reactor (the reaction temperature within the reaction vessel was measured to be between 35-40 °C).

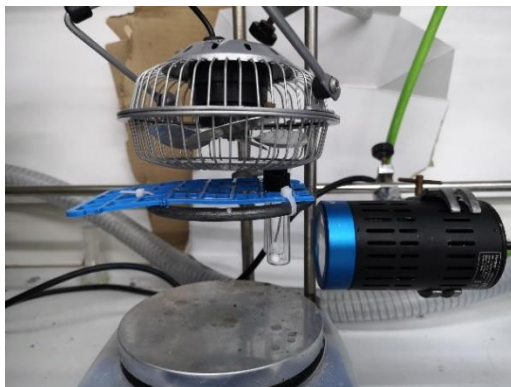


Figure 3.3: Kessil lamp set-up.

- **Set-up 3** 456nm EvoluChem™ setup

For reactions performed using an EvoluChem™ P303-30-1 LEDs (18 W, $\lambda_{\text{max}}=456$ nm, 2-3 cm away– Figure 3.4), a fan was used to cool down the reactor (the reaction temperature within the reaction vessel was measured to be between 35-40 °C, setup depicted in Figure S5).

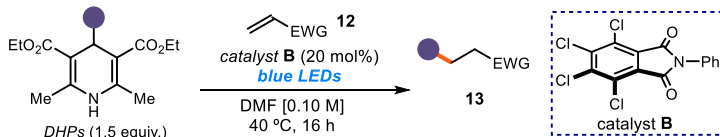


Figure 3.4: 456nm EvoluChem™ setup.

3.6.3 Giese Addition

3.6.3.4 General procedures

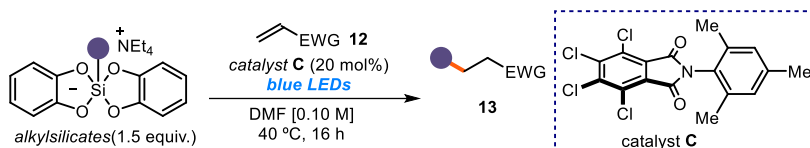
General Procedure A



Reactions with alkyl-1,4-dihydropyridines (DHPs) as radical precursors: performed using *set-up 2* in Figure 3.3.

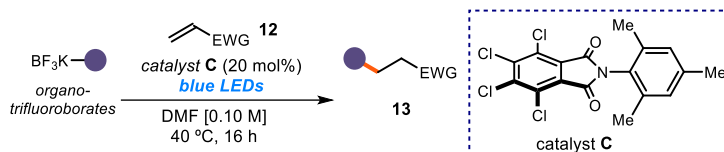
In an oven dried vial with a Teflon septum screw cap, the acceptor catalyst **B** (14.5 mg, 0.04 mmol, 0.2 equiv.), alkyl-1,4-dihydropyridine **11** (0.3 mmol, 1.5 equiv.) and the electron-poor olefin **12** (0.2 mmol, 1.5 equiv., *if solid*) were dissolved in DMF (2 mL, synthesis grade solvent). The resulting mixture was degassed with argon sparging for 60 seconds. If the electron-poor olefin **12** was *liquid*, it was added via syringe after the argon sparging. The vial was then placed in the photoreactor (Figure 3.3) and irradiated under stirring for 16 hours, unless otherwise specified. Then the solvent was evaporated and the crude mixture purified by flash column chromatography on silica gel to furnish the target product **13**.

General Procedure B



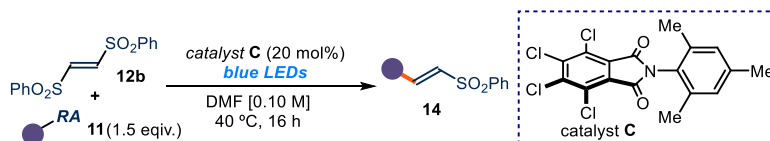
Reactions with alkylsilicates as radical precursors: performed using *set-up 1* in Figure 3.2. In an oven dried vial with a Teflon septum screw cap, acceptor catalyst **C** (16.0 mg, 0.04 mmol, 0.2 equiv.), alkylsilicates **11** (0.3 mmol, 1.5 equiv.) and the electron-poor olefin **12** (0.2 mmol, 1.0 equiv., *if solid*), were dissolved in DMF (2 mL, synthesis grade solvent). The resulting mixture was degassed with argon sparging for 60 seconds. If the electron-poor olefin **12** was *liquid*, it was added via syringe after the argon sparging. The vial was then placed in the 3D printed support photoreactor (Figure 3.2) and irradiated under stirring for 16 hours, unless otherwise specified. Then the solvent was evaporated and the crude mixture purified by flash column chromatography on silica gel to furnish the target product **13**.

General Procedure C



Reactions with organotrifluoroborates as precursors: performed using *set-up 1* in Figure 3.2. In an oven dried vial with a Teflon septum screw cap, acceptor catalyst **C** (16.0 mg, 0.04 mmol, 0.2 equiv.), organotrifluoroborates **11** (0.3 mmol, 1.5 equiv.) and the electron-poor olefin **12** (0.2 mmol, 1.0 equiv., *if solid*), were dissolved in DMF (2 mL, synthesis grade solvent). The resulting mixture was degassed with argon sparging for 60 seconds. If the electron-poor olefin **12** was *liquid*, it was added via syringe after the argon sparging. The vial was then placed in the 3D printed support photoreactor (Figure 3.2) and irradiated under stirring for 16 hours, unless otherwise specified. Then the solvent was evaporated and the crude mixture purified by flash column chromatography on silica gel to furnish the target product **13**.

General Procedure D



Reactions performed using *set-up 1* in Figure 3.2. In an oven dried vial with a Teflon septum screw cap, acceptor catalyst **C** (16.0 mg, 0.04 mmol, 0.2 equiv.), radical precursors **11** (0.3 mmol, 1.5 equiv.) and (*E*)-1,2-bis(phenylsulfonyl)ethene **12b** (61.7 mg, 0.2 mmol, 1.0 equiv), were dissolved in DMF (2 mL, synthesis grade solvent). The resulting mixture was degassed with argon sparging for 60 seconds. The vial was then placed in the 3D printed support photoreactor (Figure 3.2) and irradiated under stirring for 16 hours, unless otherwise specified. Then the solvent was evaporated and the crude mixture purified by flash column chromatography on silica gel to furnish the product **14**.

Procedure for scale-up reaction

For the scale-up reaction: in a 100 mL Schlenk tube with a Teflon septum, tertbutyl trifluoroborate (1.23 g, 6.0 mmol, 1.5equiv.), phenyl vinyl sulfone **12a** (0.84 g, 5.0 mmol, 1.0 equiv.) and catalyst **C** (0.40 g, 1.0 mmol, 0.2 equiv.) were sequentially added. Then the tube was evacuated and backfilled with argon three times followed by the addition of DMF (25 mL) via syringe. The round Schlenk flask was irradiated for 36 hours with two 50 W Kessil blue LED lamp (one PR160L-456 and one PR160L-427, 100% intensity, 4-5 cm away) (see below

Figure 2.9. Scale-up set-ups. Barton decarboxylation (left). Minisci reaction (right).

8, right). The mixture was transferred to an extraction funnel, brine (25 ml) was added and the organic layer was extracted with DCM (50×3 ml). The organic layer was dried (MgSO₄) and concentrated to dryness. The product was then purified by chromatography on silica gel (7% AcOEt in hexanes) to afford 590 mg of product **13d** (2.6 mmol, 52% yield) as a colorless oil. NMR analysis was consistent with product synthesized in the small scale process.

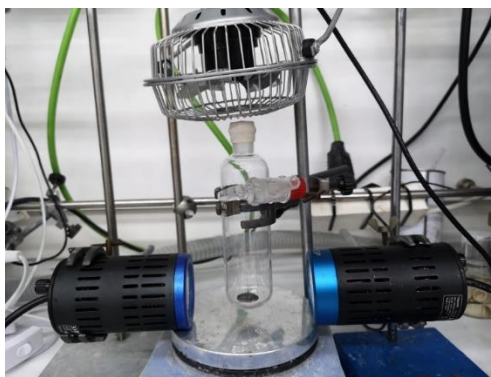
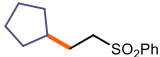


Figure 3.5: Experimental setup used for the scale-up reaction.

3.6.3.5 Characterization of Products


 **((2-Cyclopentylethyl)sulfonyl)benzene (13a):** Synthesized according to General Procedure **A**, **B** or **C** using DHP **11a** (96.5 mg, 0.3 mmol, 1.5 equiv.), silicate **11b** (137.5 mg, 0.3 mmol, 1.5 equiv.) or trifluoroborate **11c** (53.0 mg, 0.3 mmol, 1.5 equiv.), respectively, and phenyl vinyl sulfone **12a** (33.5 mg, 0.2 mmol, 1 equiv.). The crude mixture was purified by flash

column chromatography on silica gel (10% AcOEt in hexanes as eluent) to afford **13a** as a yellow oil (obtained in 87% yield (41.5 mg) from **11a**, obtained in 70% yield (33.5 mg) from **11b**, 63% yield (30.0 mg) from **11c**).

^1H NMR (400 MHz, CDCl_3) δ 7.96 – 7.84 (m, 2H), 7.70 – 7.62 (m, 1H), 7.61 – 7.51 (m, 2H), 3.14 – 3.03 (m, 2H), 1.74 – 1.66 (m, 4H), 1.64 – 1.43 (m, 4H), 1.12 – 0.98 (m, 2H).

^{13}C NMR (101 MHz, CDCl_3) δ 139.4, 133.7, 129.4, 128.2, 55.9, 38.9, 32.4, 28.7, 25.2.

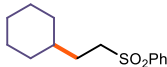
Matching reported literature data.²¹

 **((5-Chloropentyl)sulfonyl)benzene (13b)**: Synthesized according to General Procedure **B** using silicate **11d** (187.5 mg, 0.3 mmol, 1.5 equiv.) and phenyl vinyl sulfone **12a** (33.5 mg, 0.2 mmol, 1 equiv.). The crude mixture was purified by flash column chromatography on silica gel (10% AcOEt in hexanes as eluent) to afford **13b** (30.0 mg, 61% yield) as a white solid.

^1H NMR (400 MHz, CDCl_3) δ 7.97 – 7.87 (m, 2H), 7.72 – 7.63 (m, 1H), 7.62 – 7.52 (m, 2H), 3.49 (t, $J = 6.5$ Hz, 2H), 3.18 – 3.02 (m, 2H), 1.82 – 1.68 (m, 4H), 1.65 – 1.48 (m, 2H).

^{13}C NMR (101 MHz, CDCl_3) δ 139.3, 133.9, 129.5, 128.2, 56.2, 44.5, 32.0, 25.7, 22.2.

Matching reported literature data.²²

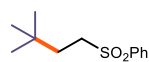
 **((2-Cyclohexylethyl)sulfonyl)benzene (13c)**: Synthesized according to General Procedure **B** using silicate **11e** (137.0 mg, 0.3 mmol, 1.5 equiv.) and phenyl vinyl sulfone **12a** (33.5 mg, 0.2 mmol, 1 equiv.). The crude mixture was purified by flash column chromatography on silica gel (10% AcOEt in hexanes as eluent) to afford **13c** (28.5 mg, 56% yield) as a yellow oil.

^1H NMR (500 MHz, CDCl_3) δ 7.92 - 7.87 (m, 2H), 7.69 - 7.61 (m, 1H), 7.60 - 7.52 (m, 2H), 3.13 - 3.05 (m, 2H), 1.70 - 1.58 (m, 7H), 1.30 - 1.24 (m, 1H), 1.20 - 1.06

²¹ Naito, T., Indium as a radical initiator in aqueous media: intermolecular alkyl radical addition to C-N and C-C bond. *Tetrahedron* **2004**, *60*, 4227–4235.

²² Horn, A.; Dussault, P. H., Synthesis of α -Cyano and α -Sulfonyl Cyclic Ethers via Intramolecular Reactions of Peroxides with Sulfone- and Nitrile-Stabilized Carbanions. *J. Org. Chem.* **2019**, *84*, 14611–14626.

(m, 3H), 0.90 - 0.80 (m, 2H). ^{13}C NMR (126 MHz, CDCl_3) δ 139.3, 133.6, 129.2, 128.0, 54.4, 36.6, 32.8, 29.6, 26.3, 26.0. Matching reported literature data.²³

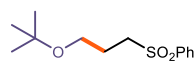


((3,3-Dimethylbutyl)sulfonyl)benzene (13d): Synthesized according to General Procedure **B** using silicate **11f** (129.5 mg, 0.3 mmol, 1.5 equiv.) or tertbutyl trifluoroborate (49.0 mg, 0.3 mmol, 1.5 equiv.) and phenyl vinyl sulfone **12a** (33.5 mg, 0.2 mmol, 1 equiv.). The crude mixture was purified by flash column chromatography on silica gel (7% AcOEt in hexanes as eluent) to afford **13d** as a colorless oil (obtained 76% yield (34.5mg) from **11f**, 84% yield (38.0 mg) from **1g**).

^1H NMR (400 MHz, CDCl_3) δ 7.92 - 7.87 (m, 2H), 7.68 - 7.62 (m, 1H), 7.60 - 7.53 (m, 2H), 3.08 - 3.02 (m, 2H), 1.62 - 1.55 (m, 2H), 0.85 (s, 9H).

^{13}C NMR (101 MHz, CDCl_3) δ 139.2, 133.6, 129.2, 128.0, 52.9, 35.6, 30.0, 28.9.

Matching reported literature data.²²



((3-(tert-Butoxy)propyl)sulfonyl)benzene (13e): Synthesized according to General Procedure **C** using 2-methoxy-2-methylpropyl trifluoroborate (58.0 mg, 0.3 mmol, 1.5 equiv.) and phenyl vinyl sulfone **12a** (33.5 mg, 0.2 mmol, 1 equiv.). The crude mixture was purified by flash column chromatography on silica gel (10% AcOEt in hexanes as eluent) to afford **13e** (41.0 mg, 80% yield) as a colorless oil.

^1H NMR (400 MHz, CDCl_3) δ 7.94 - 7.88 (m, 2H), 7.67 - 7.61 (m, 1H), 7.60 - 7.53 (m, 2H), 3.38 (t, $J = 5.9$ Hz, 2H), 3.22 - 3.15 (m, 2H), 1.95 - 1.86 (m, 2H), 1.11 (s, 9H).

^{13}C NMR (101 MHz, CDCl_3) δ 139.38, 133.7, 129.4, 128.2, 73.1, 59.4, 53.9, 27.6, 24.2.

Matching reported literature data.²²



Phenyl-(3-(phenylsulfonyl)propyl)sulfane (13f): Synthesized according to General Procedure **C** using (phenylthio)methyl trifluoroborate (69.0 mg, 0.3 mmol, 1.5 equiv.) and phenyl vinyl sulfone **12a** (33.5 mg, 0.2 mmol, 1 equiv.). The crude mixture was purified

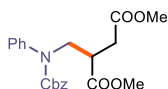
²³ Chen, X.; Luo, X.; Peng, X.; Guo, J.; Zai, J.; Wang, P., Catalyst-Free Decarboxylation of Carboxylic Acids and Deoxygenation of Alcohols by Electro-Induced Radical Formation. *Chem. Eur. J.* **2020**, *26*, 3226–3230.

by flash column chromatography on silica gel (10% AcOEt in hexanes as eluent) to afford **13f** (28.0 mg, 48% yield) as a yellow oil.

^1H NMR (500 MHz, CDCl_3) δ 7.90 – 7.84 (m, 2H), 7.69 – 7.62 (m, 1H), 7.55 (dd, $J = 8.4, 7.2$ Hz, 2H), 7.29 – 7.26 (m, 5H), 3.29 – 3.22 (m, 2H), 2.98 (t, $J = 6.9$ Hz, 2H), 2.05 – 1.97 (m, 2H).

^{13}C NMR (126 MHz, CDCl_3) δ 139.0, 134.7, 133.8, 130.4, 129.4, 129.1, 128.0, 126.8, 54.7, 32.7, 22.4.

Matching reported literature data.²⁴



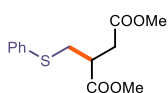
Dimethyl-2-(((benzyloxy)carbonyl)(phenyl)amino)methylsuccinate (13g): Synthesized according to General Procedure A using DHP

11j (148.0 mg, 0.3 mmol, 1.5 equiv.) and dimethyl fumarate (28.5 mg, 0.2 mmol, 1 equiv.). The crude mixture was purified by flash column chromatography on silica gel (10% AcOEt in hexanes as eluent) to afford **13g** (33.0 mg, 43% yield) as a colorless oil.

^1H NMR (400 MHz, CDCl_3) δ 7.40 - 7.34 (m, 2H), 7.33 - 7.17 (m, 8H), 5.18 - 5.06 (m, 2H), 4.10 (dd, $J = 16, 8$ Hz, 1H), 3.90 (d, $J = 12, 8$ Hz, 1H), 3.60 (s, 3H), 3.49 (s, 3H), 3.14 - 3.04 (m, 1H), 2.75 (dd, $J = 2.0, 1.2$ Hz, 1H), 2.50 (d, $J = 16, 8$ Hz, 1H).

^{13}C NMR (101 MHz, CDCl_3) δ 173.1, 171.8, 155.5, 141.1, 136.4, 129.1, 128.4, 127.9, 127.5, 127.1, 67.5, 52.0, 51.8, 51.3, 40.5, 33.3.

HRMS: calculated for $\text{C}_{21}\text{H}_{23}\text{NNaO}_6$ ($\text{M}+\text{Na}^+$): 408.1417, found 408.1409.



Dimethyl-2-((phenylthio)methyl)succinate (13h): Synthesized according to General Procedure C using (phenylthio)methyl trifluoroborate (69.0 mg, 0.3 mmol, 1.5 equiv.) and dimethyl fumarate (28.5 mg, 0.2 mmol, 1 equiv.). The crude mixture was purified by flash column chromatography on silica gel (5% AcOEt in hexanes as eluent) to afford **13h** (44.5 mg, 83% yield) as a colorless oil.

²⁴ Zhou, X.-T.; Carter, R. G., Synthesis of the C1–C26 Northern Portion of Azaspiracid-1: Kinetic versus Thermodynamic Control of the Formation of the Bis-spiroketal. *Angew. Chem., Int. Ed.* **2006**, *45*, 1787–1790.

^1H NMR (300 MHz, CDCl_3) δ 7.41 – 7.35 (m, 2H), 7.33 – 7.27 (m, 2H), 7.25 – 7.19 (m, 1H), 3.66 (s, 6H), 3.38 – 3.27 (m, 1H), 3.14 – 3.01 (m, 2H), 2.89 – 2.68 (m, 2H).

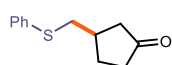
^{13}C NMR (126 MHz, CDCl_3) δ 173.5, 172.1, 135.1, 130.4, 129.2, 126.9, 52.3, 52.0, 41.3, 35.6, 34.6. Matching reported literature data.²⁵



4-(Phenylthio)butanenitrile (13i): Synthesized according to General Procedure C using (phenylthio)methyl trifluoroborate (69.0 mg, 0.3 mmol, 1.5 equiv.) and acrylonitrile (10.5 mg, 0.2 mmol, 1 equiv.). The crude mixture was purified by flash column chromatography on silica gel (7% AcOEt in hexanes as eluent) to afford **13i** (19.0 mg, 53% yield) as a colorless oil.

^1H NMR (400 MHz, CDCl_3) δ 7.42 – 7.36 (m, 2H), 7.33 (ddd, $J = 7.8, 6.8, 1.2$ Hz, 2H), 7.28 – 7.23 (m, 1H), 3.06 (t, $J = 6.9$ Hz, 2H), 2.54 (t, $J = 7.1$ Hz, 2H), 1.98 (p, $J = 7.0$ Hz, 2H).

^{13}C NMR (101 MHz, CDCl_3) δ 134.9, 130.3, 129.3, 127.0, 119.2, 32.8, 25.0, 16.1. Matching reported literature data.²⁶



3-((Phenylthio)methyl)cyclopentan-1-one (13j): Synthesized according to General Procedure C using (phenylthio)methyl trifluoroborate (69.0 mg, 0.3 mmol, 1.5 equiv.) and cyclopent-2-en-1-one (16.5 mg, 0.2 mmol, 1 equiv.). The crude mixture was purified by flash column chromatography on silica gel (5% AcOEt in hexanes as eluent) to afford **13j** (20.0 mg, 49% yield) as a colorless oil

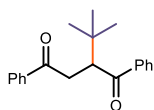
^1H NMR (400 MHz, CDCl_3) δ 7.40 – 7.34 (m, 2H), 7.29 (t, $J = 7.6$ Hz, 2H), 7.24 – 7.18 (m, 1H), 3.03 (dd, $J = 6.7, 2.8$ Hz, 2H), 2.53 – 2.43 (m, 2H), 2.39 – 2.19 (m, 3H), 2.06 – 1.94 (m, 1H), 1.76 – 1.64 (m, 1H).

^{13}C NMR (101 MHz, CDCl_3) δ 218.1, 136.1, 129.7, 129.0, 126.4, 44.5, 39.3, 38.3, 36.8, 28.8.

Matching reported literature data.²⁷

²⁶ Dou, Y.; Kouklovsky, C.; Vincent, G., Bioinspired Divergent Oxidative Cyclization from Strictosidine and Vincoside Derivatives: Second-Generation Total Synthesis of (–)-Cymoside and Access to an Original Hexacyclic-Fused Furo[3,2-b]indoline. *Chem. Eur. J.* **2020**, *26*, 17190–17194.

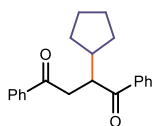
²⁷ Dou Sundararajan, G.; Prabakaran, N., A New Polymer-Anchored Chiral Catalyst for Asymmetric Michael Addition Reactions. *Org. Lett.* **2001**, *3*, 389–392.



2-(*tert*-Butyl)-1,4-diphenylbutane-1,4-dione (13k): Synthesized according to General Procedure **B** using silicate **11f** (129.5 mg, 0.3 mmol, 1.5 equiv.) and (*E*)-1,4-diphenylbut-2-ene-1,4-dione (47.5 mg, 0.2 mmol, 1 equiv.). The crude mixture was purified by flash column chromatography on silica gel (5% AcOEt in hexanes as eluent) to afford **13k** (36.0 mg, 61% yield) as a white solid.

^1H NMR (400 MHz, CDCl_3) δ 8.15 - 8.09 (m, 2H), 7.99 - 7.93 (m, 2H), 7.57 - 7.51 (m, 2H), 7.51 - 7.40 (m, 4H), 4.06 (dd, $J = 12, 4$ Hz, 1H), 3.89 (dd, $J = 16, 12$ Hz, 1H), 3.24 (dd, $J = 16, 4$ Hz, 1H), 0.99 (s, 9H). ^{13}C NMR (101 MHz, CDCl_3) δ 204.3, 199.4, 140.0, 136.7, 133.2, 132.4, 128.6, 128.5, 128.5, 128.1, 49.4, 38.8, 33.5, 28.6.

HRMS: calculated for $\text{C}_{20}\text{H}_{23}\text{O}_2$ ($\text{M}+\text{H}^+$): 295.1693, found 295.1695.

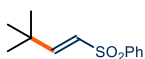


2-Cyclopentyl-1,4-diphenylbutane-1,4-dione (13l): Synthesized according to General Procedure **A** using DHP **11a** (96.5 mg, 0.3 mmol, 1.5 equiv.) and (*E*)-1,4-diphenylbut-2-ene-1,4-dione (47.5 mg, 0.2 mmol, 1 equiv.). The crude mixture was purified by flash column chromatography on silica gel (5% AcOEt in hexanes as eluent) to afford **13l** (38.5 mg, 63% yield) as a yellow oil.

^1H NMR (400 MHz, CDCl_3) δ 8.13 - 8.09 (m, 2H), 7.99 - 7.93 (m, 2H), 7.60 - 7.52 (m, 2H), 7.51 - 7.42 (m, 4H), 4.09 - 4.01 (m, 1H), 3.82 (dd, $J = 20, 12$ Hz, 1H), 3.24 (dd, $J = 16, 4$ Hz, 1H), 2.14 - 2.01 (m, 1H), 1.86 - 1.78 (m, 1H), 1.66 - 1.53 (m, 4H), 1.51 - 1.39 (m, 1H), 1.29 - 1.24 (m, 1H), 1.19 - 1.10 (m, 1H).

^{13}C NMR (101 MHz, CDCl_3) δ 204.2, 198.9, 138.2, 136.6, 133.2, 132.7, 129.2, 128.6, 128.5, 128.1, 45.5, 43.2, 40.7, 31.2, 30.6, 25.1, 24.5.

HRMS: calculated for $\text{C}_{21}\text{H}_{23}\text{O}_2$ ($\text{M}+\text{H}^+$): 307.1693, found 307.1688.

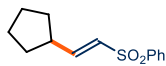


(*E*)-((3,3-Dimethylbut-1-en-1-yl)sulfonyl)benzene (14a): Synthesized according to General Procedure **D** using silicate **11f** (129.5 mg, 0.3 mmol, 1.5 equiv.) and (*E*)-1,2-bis(phenylsulfonyl)ethene **12b** (61.5 mg, 0.2 mmol, 1 equiv.). The crude mixture was purified by flash column chromatography on silica gel (5% AcOEt in hexanes as eluent) to afford **14a** (28.5 mg, 63% yield) as a yellow oil.

^1H NMR (400 MHz, CDCl_3) δ 7.88 - 7.84 (m, 2H), 7.63 - 7.57 (m, 1H), 7.55 - 7.49 (m, 2H), 6.98 (d, $J = 16$ Hz, 1H), 6.19 (d, $J = 16$ Hz, 1H), 1.07 (s, 9H).

^{13}C NMR (101 MHz, CDCl_3) δ 156.5, 140.8, 133.2, 129.3, 127.5, 126.5, 34.1, 28.3.

Matching reported literature data.²⁸



(E)-((2-Cyclopentylvinyl)sulfonyl)benzene (14b): Synthesized according to General Procedure **D** using DHP **11a** (96.5 mg, 0.3 mmol, 1.5 equiv.) and (*E*)-1,2-bis(phenylsulfonyl)ethene **12b** (61.5 mg, 0.2 mmol, 1 equiv.). The crude mixture was purified by flash column chromatography on silica gel (5% AcOEt in hexanes as eluent) to afford **14b** (33.0 mg, 70% yield) as a yellow oil.

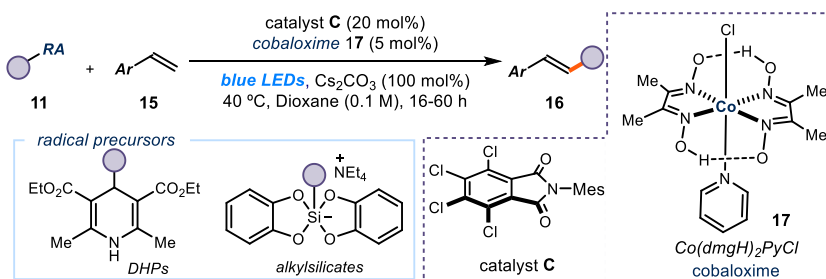
^1H NMR (400 MHz, CDCl_3) δ 7.88 - 7.84 (m, 2H), 7.63- 7.57 (m, 1H), 7.55 - 7.49 (m, 2H), 6.97 (d, $J = 12, 8$ Hz, 1H), 6.27 (dd, $J = 20, 1.2$ Hz, 1H), 2.67-2.54 (m, 1H), 1.89-1.77 (m, 2H), 1.71-1.65 (m, 2H), 1.63-1.54 (m, 2H), 1.46-1.35 (m, 2H).

^{13}C NMR (101 MHz, CDCl_3) δ 151.1, 140.9, 133.2, 129.2, 128.5, 127.5, 42.1, 32.1, 25.2.

HRMS: calculated for $\text{C}_{13}\text{H}_{17}\text{O}_2\text{S}$ ($\text{M}+\text{H}^+$): 237.0944, found 237.0935.

3.6.4. Heck-type reaction

General Procedure *E*

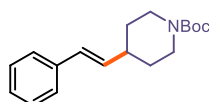


Reactions performed using *set-up 3* in Figure 3.4. To an oven dried vial with a Teflon septum screw cap, the acceptor catalyst **C** (16.0 mg, 0.04 mmol, 0.2 equiv.), the radical precursor **11** (0.2 mmol, 1.0 equiv.), cesium carbonate (32.5 mg, 0.1 mmol, 1.0 equiv), the styrene derivative **15** (1.0 mmol, 1.0 equiv., *if solid*) and $\text{Co}(\text{dmgH})_2\text{PyCl}$ (2.0 mg, 0.01 mmol, 5 mol%) were sequentially added. Then the vial was evacuated and backfilled with argon three times followed by the addition

²⁸ Delcamp, J. H.; White, M. C., Sequential Hydrocarbon Functionalization: Allylic C–H Oxidation/Vinyl C–H Arylation. *J. Am. Chem. Soc.* **2006**, *128*, 15076–15077.

of dioxane (2 mL) via syringe. If the styrene derivative **15** was *liquid*, it was added via syringe afterwards. The vial was then placed in the photoreactor (Figure 3.4) and irradiated under stirring for 16–60 hours. The solvent was evaporated and the crude mixture purified by flash column chromatography on silica gel to furnish product **16**.

3.6.4.1 Characterization of Products.

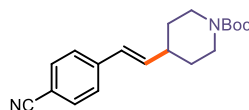


tert-Butyl-(E)-4-styrylpiperidine-1-carboxylate (16a):

Synthesized according to General Procedure **E** using DHP **11k** (87.5 mg, 0.2 mmol, 1.0 equiv.) and styrene (104.0 mg, 1.0 mmol, 5.0 equiv.). An *E/Z* ratio of 14:1 was determined by ^1H NMR analysis. The crude mixture was purified by flash column chromatography on silica gel (15% AcOEt in hexanes as eluent) to afford **16a** (49.5 mg, 86% yield) as a white solid.

^1H NMR (400 MHz, CDCl_3) δ 7.38 – 7.32 (m, 2H), 7.30 (dd, J = 10.2, 4.9 Hz, 2H), 7.23 – 7.16 (m, 1H), 6.39 (d, J = 15.9 Hz, 1H), 6.15 (dd, J = 16.0, 6.9 Hz, 1H), 4.12 (s, 2H), 2.78 (t, J = 12.2 Hz, 2H), 2.35 – 2.21 (m, 1H), 1.76 (d, J = 12.8 Hz, 2H), 1.47 (s, 9H), 1.45 – 1.32 (m, 2H). ^{13}C NMR (101 MHz, CDCl_3) δ 155.0, 137.6, 134.5, 128.7, 128.6, 127.2, 126.2, 79.5, 43.8, 39.5, 32.0, 28.6.

Matching reported literature data.²⁹



tert-Butyl-(E)-4-(4-cyanostyryl)piperidine-1-carboxylate (16b):

Synthesized according to General Procedure **E** using DHP **11k** (87.5 mg, 0.2 mmol, 1.0 equiv.) and 4-vinylbenzotrile (129.0 mg, 1.0 mmol, 5.0 equiv.). An *E/Z* ratio of >20:1 was determined by ^1H NMR analysis. The crude mixture was purified by flash column chromatography on silica gel (15% AcOEt in hexanes as eluent) to afford **16b** (52.0 mg, 83% yield) as a white solid.

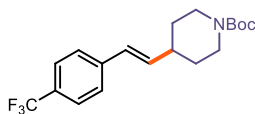
^1H NMR (400 MHz, CDCl_3) δ 7.59 (d, J = 8.4 Hz, 2H), 7.43 (d, J = 8.3 Hz, 2H), 6.41 (d, J = 16.1 Hz, 1H), 6.30 (dd, J = 16.0, 6.6 Hz, 1H), 4.16 (broad, 2H), 2.80

²⁹ Knez, D.; Coletti, N.; Iacovino, L. G.; Sova, M.; Pišlar, A.; Konc, J.; Lešnik, S.; Higgs, J.; Kamecki, F.; Mangialavori, I.; Dolšak, A.; Žakelj, S.; Trontelj, J.; Kos, J.; Binda, C.; Marder, M.; Gobec, S., Stereoselective Activity of 1-Propargyl-4-styrylpiperidine-like Analogues That Can Discriminate between Monoamine Oxidase Isoforms A and B. *J. Med. Chem.* **2020**, *63*, 1361–1387.

(t, $J = 12.1$ Hz, 2H), 2.41 – 2.28 (m, 1H), 1.78 (d, $J = 12.4$ Hz, 2H), 1.48 (s, 9H), 1.40 (ddd, $J = 16.4, 12.7, 6.6$ Hz, 2H).

^{13}C NMR (101 MHz, CDCl_3) δ 154.9, 142.1, 138.6, 132.5, 127.3, 126.7, 119.2, 110.4, 79.6, 43.7, 39.6, 31.6, 28.6.

Matching reported literature data.²⁹



***tert*-Butyl-(*E*)-4-(4-**

(trifluoromethyl)styryl)piperidine-1-carboxylate

(16c): Synthesized according to General Procedure E

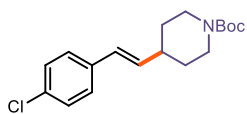
using DHP **11k** (87.5 mg, 0.2 mmol, 1.0 equiv.) and 1-(trifluoromethyl)-4-vinylbenzene (172.0 mg, 1.0 mmol, 5.0 equiv.). An *E/Z* ratio of 13:1 was determined by ^1H NMR analysis. The crude mixture was purified by flash column chromatography on silica gel (10% AcOEt in hexanes as eluent) to afford **16c** (63.5 mg, 89% yield) as a white solid.

^1H NMR (500 MHz, CDCl_3) δ 7.54 (d, $J = 8.2$ Hz, 2H), 7.43 (d, $J = 8.2$ Hz, 2H), 6.41 (d, $J = 16.0$ Hz, 1H), 6.25 (dd, $J = 16.0, 6.8$ Hz, 1H), 4.14 (s, 2H), 2.79 (t, $J = 11.3$ Hz, 2H), 2.37 – 2.27 (m, 1H), 1.77 (d, $J = 12.6$ Hz, 2H), 1.47 (s, 9H), 1.38 (ddd, $J = 17.5, 11.6, 7.5$ Hz, 2H).

^{13}C NMR (126 MHz, CDCl_3) δ 155.0, 141.1, 137.3, 129.1 (q, $J = 32.3$ Hz), 127.5, 126.3, 125.6 (q, $J = 3.7$ Hz), 124.9 (q, $J = 272.2$ Hz) 79.6, 43.9, 39.6, 31.8, 28.6.

^{19}F NMR (471 MHz, CDCl_3) δ -62.44 (s).

Matching reported literature data.²⁸



***tert*-Butyl-(*E*)-4-(4-chlorostyryl)piperidine-1-**

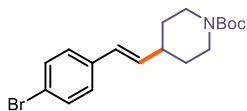
carboxylate (16d): Synthesized according to General

Procedure E using DHP **11k** (87.5 mg, 0.2 mmol, 1.0 equiv.) and 1-chloro-4-vinylbenzene (138.5 mg, 1.0 mmol, 5.0 equiv.). An *E/Z* ratio of 7:1 was determined by ^1H NMR analysis. The crude mixture was purified by flash column chromatography on silica gel (15% AcOEt in hexanes as eluent) to afford **16d** (48.5 mg, 75% yield) as a white solid.

^1H NMR (500 MHz, CDCl_3) δ 7.25 – 7.26 (m, 4H), 6.33 (dd, $J = 16.0, 1.3$ Hz, 1H), 6.12 (dd, $J = 16.0, 6.9$ Hz, 1H), 4.13 (s, 2H), 2.77 (t, $J = 13.1$ Hz, 2H), 2.34 – 2.21 (m, 1H), 1.75 (d, $J = 13.2$ Hz, 2H), 1.47 (s, 9H), 1.35 (dd, $J = 12.4, 4.3$ Hz, 2H).

^{13}C NMR (126 MHz, CDCl_3) δ 155.0, 136.2, 135.2, 132.8, 128.8, 127.5, 127.4, 79.6, 43.4, 39.5, 31.9, 28.6.

Matching reported literature data.²⁸



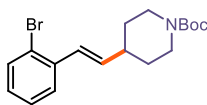
***tert*-Butyl-(*E*)-4-(4-bromostyryl)piperidine-1-carboxylate (**16e**):**

Synthesized according to General Procedure **E** using DHP **11k** (87.5 mg, 0.2 mmol, 1.0 equiv.) and 1-bromo-4-vinylbenzene (183.0 mg, 1.0 mmol, 5.0 equiv.). An *E/Z* ratio of 7:1 was determined by ¹H NMR analysis. The crude mixture was purified by flash column chromatography on silica gel (15% AcOEt in hexanes as eluent) to afford **16e** (56.5 mg, 77% yield) as a white solid.

¹H NMR (400 MHz, CDCl₃) δ 7.42 – 7.40 (m, 2H), 7.23 – 7.15 (m, 2H), 6.31 (d, *J* = 15.6 Hz, 1H), 6.13 (dd, *J* = 16.0, 6.8 Hz, 1H), 4.13 (s, 2H), 2.77 (t, *J* = 12.7 Hz, 2H), 2.26 (dtd, *J* = 14.8, 6.8, 3.4 Hz, 1H), 1.74 (d, *J* = 13.1 Hz, 2H), 1.46 (s, 9H), 1.44 – 1.30 (m, 2H).

¹³C NMR (101 MHz, CDCl₃) δ 155.0, 136.6, 135.3, 131.7, 127.7, 127.5, 120.9, 79.5, 39.51, 31.8, 28.6.

Matching reported literature data.²⁸



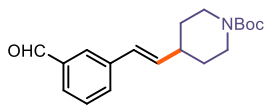
***tert*-Butyl-(*E*)-4-(2-bromostyryl)piperidine-1-carboxylate (**16f**):**

Synthesized according to General Procedure **E** using DHP **11k** (87.5 mg, 0.2 mmol, 1.0 equiv.) and 1-bromo-2-vinylbenzene (183.0 mg, 1.0 mmol, 5.0 equiv.). An *E/Z* ratio of 20:1 was determined by ¹H NMR analysis. The crude mixture was purified by flash column chromatography on silica gel (15% AcOEt in hexanes as eluent) to afford **16f** (42.5 mg, 58% yield) as a white solid.

¹H NMR (500 MHz, CDCl₃) δ 7.52 (dd, *J* = 8.0, 1.3 Hz, 1H), 7.48 (dd, *J* = 7.9, 1.7 Hz, 1H), 7.27 – 7.21 (m, 2H), 7.07 (ddd, *J* = 8.0, 7.3, 1.7 Hz, 1H), 6.72 (d, *J* = 15.8 Hz, 1H), 6.08 (dd, *J* = 15.9, 6.9 Hz, 1H), 4.14 (s, 2H), 2.80 (t, *J* = 12.4 Hz, 2H), 2.40 – 2.30 (m, 1H), 1.79 (d, *J* = 12.5 Hz, 2H), 1.47 (s, 9H), 1.46 – 1.34 (m, 2H).

¹³C NMR (101 MHz, CDCl₃) δ 155.0, 137.5, 137.4, 133.0, 128.6, 127.7, 127.6, 126.9, 123.6, 79.5, 39.6, 31.8, 28.6.

Matching reported literature data.²⁸



***tert*-Butyl-(*E*)-4-(3-formylstyryl)piperidine-1-carboxylate (**16g**):**

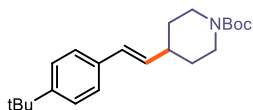
Synthesized according to General Procedure **E** using DHP **11k** (87.5 mg, 0.2 mmol, 1.0

equiv.) and 3-vinylbenzaldehyde (132.0 mg, 1.0 mmol, 5.0 equiv.). An *E/Z* ratio of 6:1 was determined by ^1H NMR analysis. The crude mixture was purified by flash column chromatography on silica gel (10% AcOEt in hexanes as eluent) to afford **16g** (42.5 mg, 58% yield) as a white solid.

^1H NMR (400 MHz, CDCl_3) δ 10.01 (s, 1H), 7.85 (t, $J = 1.8$ Hz, 1H), 7.71 (dt, $J = 7.6, 1.5$ Hz, 1H), 7.59 (dt, $J = 7.8, 1.5$ Hz, 1H), 7.46 (t, $J = 7.6$ Hz, 1H), 6.44 (d, $J = 15.8$ Hz, 1H), 6.26 (dd, $J = 16.0, 6.8$ Hz, 1H), 4.14 (s, 2H), 2.79 (t, $J = 12.8$ Hz, 2H), 2.32 (dtd, $J = 11.2, 7.3, 3.5$ Hz, 1H), 1.77 (d, $J = 13.2$ Hz, 2H), 1.47 (s, 9H), 1.45 – 1.35 (m, 2H).

^{13}C NMR (101 MHz, CDCl_3) δ 192.6, 155.0, 138.7, 136.8, 136.6, 132.2, 129.4, 128.7, 127.4, 126.9, 79.6, 43.7, 39.6, 31.8, 28.6.

HRMS: calculated for $\text{C}_{19}\text{H}_{25}\text{NNaO}_3$ ($\text{M}+\text{Na}^+$): 338.1727, found 338.1729.



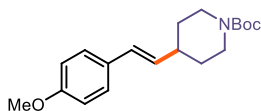
tert-Butyl-(*E*)-4-(4-(tert-butyl)styryl)piperidine-1-carboxylate (16h**):** Synthesized according to General Procedure **E** using DHP **11k** (87.5 mg, 0.2 mmol, 1.0

equiv.) and 1-(tert-butyl)-4-vinylbenzene (160.5 mg, 1.0 mmol, 5.0 equiv.). An *E/Z* ratio of >20:1 was determined by ^1H NMR analysis. The crude mixture was purified by flash column chromatography on silica gel (10% AcOEt in hexanes as eluent) to afford **16h** (50.0 mg, 73% yield) as a white solid.

^1H NMR (500 MHz, CDCl_3) δ 7.35 – 7.31 (m, 2H), 7.31 – 7.27 (m, 2H), 6.37 (d, $J = 16.0$ Hz, 1H), 6.10 (dd, $J = 16.0, 6.9$ Hz, 1H), 4.12 (s, 2H), 2.78 (t, $J = 10.6$ Hz, 2H), 2.42 – 2.30 (m, 1H), 1.75 (d, $J = 12.5$ Hz, 2H), 1.46 (d, $J = 13.0$ Hz, 9H), 1.45 – 1.34 (m, 2H), 1.31 (s, 9H).

^{13}C NMR (126 MHz, CDCl_3) δ 155.0, 150.3, 134.9, 133.8, 128.3, 125.9, 125.6, 79.5, 43.9, 39.5, 34.7, 32.0, 31.5, 28.6.

Matching reported literature data.³⁰



tert-Butyl-(*E*)-4-(4-methoxystyryl)piperidine-1-carboxylate (16i**):** Synthesized according to General Procedure **E** using DHP **11k** (87.5 mg, 0.2 mmol, 1.0

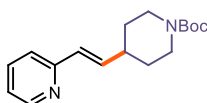
equiv.) and 1-methoxy-4-vinylbenzene (134.0 mg, 1.0 mmol, 5.0 equiv.). An *E/Z*

³⁰ Constantin, T.; Zanini, M.; Regni, A.; Sheikh Nadeem, S.; Juliá, F.; Leonori, D., Aminoalkyl radicals as halogen-atom transfer agents for activation of alkyl and aryl halides. *Science* **2020**, *367*, 1021–1026.

ratio of >20:1 was determined by ^1H NMR analysis. The crude mixture was purified by flash column chromatography on silica gel (10% AcOEt in hexanes as eluent) to afford **16i** (37.0 mg, 58% yield) as a white solid.

^1H NMR (400 MHz, CDCl_3) δ 7.32 – 7.26 (m, 2H), 6.90 – 6.84 (m, 2H), 6.35 (d, $J = 15.7$ Hz, 1H), 6.02 (dd, $J = 16.0, 6.9$ Hz, 1H), 4.14 (s, 2H), 3.82 (s, 3H), 2.80 (t, $J = 12.7$ Hz, 2H), 2.28 (dtd, $J = 14.8, 7.0, 3.2$ Hz, 1H), 1.77 (d, $J = 13.1$ Hz, 2H), 1.49 (s, 9H), 1.39 (qd, $J = 12.2, 4.3$ Hz, 2H). ^{13}C NMR (101 MHz, CDCl_3) δ 159.0, 155.0, 132.4, 130.5, 127.9, 127.3, 114.1, 79.5, 55.4, 43.9, 39.5, 32.1, 28.6.

Matching reported literature data.²⁹



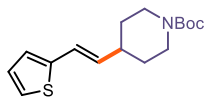
tert-Butyl-(E)-4-(2-(pyridin-2-yl)vinyl)piperidine-1-carboxylate (16j): Synthesized according to General Procedure E using DHP **11k** (87.5 mg, 0.2 mmol, 1.0 equiv.)

and 2-vinylpyridine (105.0 mg, 1.0 mmol, 5.0 equiv.). An *E/Z* ratio of 10:1 was determined by ^1H NMR analysis. The crude mixture was purified by flash column chromatography on silica gel (20% AcOEt in hexanes as eluent) to afford **16j** (40.5 mg, 70% yield) as a white solid.

^1H NMR (400 MHz, CDCl_3) δ 8.52 (d, $J = 4.9$ Hz, 1H), 7.60 (td, $J = 7.7, 1.8$ Hz, 1H), 7.23 (dt, $J = 8.0, 1.1$ Hz, 1H), 7.09 (ddd, $J = 7.5, 4.9, 1.1$ Hz, 1H), 6.68 (dd, $J = 15.8, 6.8$ Hz, 1H), 6.47 (dd, $J = 15.8, 1.4$ Hz, 1H), 4.13 (s, 2H), 2.78 (t, $J = 12.7$ Hz, 2H), 2.33 (dtdd, $J = 10.8, 6.4, 4.0, 2.0$ Hz, 1H), 1.79 (d, $J = 15.8$ Hz, 2H), 1.46 (s, 9H), 1.44 – 1.32 (m, 2H).

^{13}C NMR (101 MHz, CDCl_3) δ 155.9, 155.0, 149.6, 139.0, 136.6, 128.7, 122.0, 121.5, 79.5, 43.8, 39.3, 31.6, 28.6.

Matching reported literature data.³⁰



tert-Butyl-(E)-4-(2-(thiophen-2-yl)vinyl)piperidine-1-carboxylate (16k): Synthesized according to General Procedure E using DHP **11k** (87.5 mg, 0.2 mmol, 1.0 equiv.)

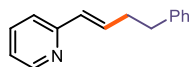
and 2-vinylthiophene (110.0 mg, 1.0 mmol, 5.0 equiv.). An *E/Z* ratio of >20:1 was determined by ^1H NMR analysis. The crude mixture was purified by flash column chromatography on silica gel (15% AcOEt in hexanes as eluent) to afford **16k** (28.8 mg, 49% yield) as a white solid.

^1H NMR (400 MHz, CDCl_3) δ 7.10 (d, $J = 5.0$ Hz, 1H), 6.94 (dd, $J = 5.1, 3.5$ Hz, 1H), 6.89 (d, $J = 3.3$ Hz, 1H), 6.55 – 6.46 (m, 1H), 6.00 (dd, $J = 15.8, 6.8$ Hz, 1H),

4.12 (s, 2H), 2.77 (t, $J = 12.6$ Hz, 2H), 2.24 (dt, $J = 10.9, 7.0, 3.6$ Hz, 1H), 1.74 (d, $J = 13.1$ Hz, 2H), 1.46 (s, 9H), 1.36 (qd, $J = 12.6, 4.7$ Hz, 2H).

^{13}C NMR (101 MHz, CDCl_3) δ 155.0, 142.9, 134.3, 127.4, 124.9, 123.6, 122.0, 79.5, 43.8, 39.3, 31.8, 28.6.

Matching reported literature data.³⁰

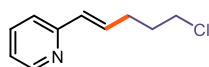


(E)-2-(4-Phenylbut-1-en-1-yl)pyridine (16l): Synthesized according to General Procedure **E** using DHP **11p** (71.5 mg, 0.2 mmol, 1.0 equiv.) and 2-vinylpyridine (105.0 mg, 1.0 mmol, 5.0 equiv.). An *E/Z* ratio of 10:1 was determined by ^1H NMR analysis. The crude mixture was purified by flash column chromatography on silica gel (10% AcOEt in hexanes as eluent) to afford **16l** (22.0 mg, 53% yield) as a colorless oil.

^1H NMR (500 MHz, CDCl_3) δ 8.55 (d, $J = 5.0$ Hz, 1H), 7.72 (dt, $J = 8.6, 4.1$ Hz, 1H), 7.37 – 7.27 (m, 3H), 7.21 (dt, $J = 14.3, 4.3$ Hz, 4H), 6.94 – 6.84 (m, 1H), 6.62 (d, $J = 15.7$ Hz, 1H), 2.92 – 2.77 (m, 2H), 2.69 – 2.56 (m, 2H).

^{13}C NMR (126 MHz, CDCl_3) δ 154.5, 141.5, 138.3, 135.0, 130.5, 128.6, 126.2, 122.2, 121.6, 35.4, 34.9.

Matching reported literature data.³¹



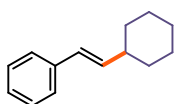
(E)-2-(5-Chloropent-1-en-1-yl)pyridine (16m): Synthesized according to General Procedure **E** using silicate **11d** (125.0 mg, 0.2 mmol, 1.0 equiv.) and 2-vinylpyridine (105.0 mg, 1.0 mmol, 5.0 equiv.). An *E/Z* ratio of 13:1 was determined by ^1H NMR analysis. The crude mixture was purified by flash column chromatography on silica gel (10% AcOEt in hexanes as eluent) to afford **16m** (20.5 mg, 57% yield) as a white solid.

^1H NMR (500 MHz, CDCl_3) δ 8.53 (d, $J = 3.9$ Hz, 1H), 7.62 (td, $J = 7.7, 1.8$ Hz, 1H), 7.23 (dt, $J = 7.9, 1.1$ Hz, 1H), 7.11 (ddd, $J = 7.5, 4.8, 1.1$ Hz, 1H), 6.72 (dt, $J = 15.7, 7.1$ Hz, 1H), 6.54 (dt, $J = 15.6, 1.5$ Hz, 1H), 3.60 (t, $J = 6.5$ Hz, 2H), 2.44 (qd, $J = 7.1, 1.5$ Hz, 2H), 2.02 – 1.95 (m, 2H).

^{13}C NMR (126 MHz, CDCl_3) δ 155.6, 149.4, 136.8, 134.0, 131.0, 122.0, 121.5, 44.5, 31.8, 30.0.

³¹ Wen, L.; Yue, Z.; Zhang, H.; Chong, Q.; Meng, F., Cu-Catalyzed Enantioselective Boron Addition to N-Heteroaryl-Substituted Alkenes. *Org Lett.* **2017**, *19*, 6610–6613.

Matching reported literature data.³¹

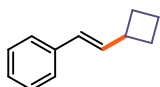


(E)-(2-Cyclohexylvinyl)benzene (16n): Synthesized according to General Procedure **E** using DHP **11l** (67.0 mg, 0.2 mmol, 1.0 equiv.) and styrene (104.0 mg, 1.0 mmol, 5.0 equiv.). An *E/Z* ratio of 9:1 was determined by ¹H NMR analysis. The crude mixture was purified by flash column chromatography on silica gel (2% AcOEt in hexanes as eluent) to afford **16n** (27.0 mg, 73% yield) as a colorless oil.

¹H NMR (500 MHz, CDCl₃) δ 7.38 – 7.32 (m, 2H), 7.28 (t, *J* = 7.7 Hz, 2H), 7.20 – 7.14 (m, 1H), 6.34 (d, *J* = 16.0 Hz, 1H), 6.18 (dd, *J* = 16.0, 7.0 Hz, 1H), 2.13 (dtd, *J* = 11.3, 7.4, 3.8 Hz, 1H), 1.85 – 1.74 (m, 4H), 1.71 – 1.65 (m, 1H), 1.38 – 1.28 (m, 3H), 0.87 (dd, *J* = 15.7, 9.0 Hz, 2H).

¹³C NMR (126 MHz, CDCl₃) δ 138.2, 137.0, 128.6, 127.4, 126.9, 126.1, 41.3, 33.1, 26.3, 26.2.

Matching reported literature data.³²

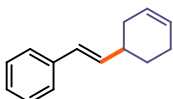


(E)-(2-Cyclobutylvinyl)benzene (16o): Synthesized according to General Procedure **E** using DHP **11m** (61.5 mg, 0.2 mmol, 1.0 equiv.) and styrene (104.0 mg, 1.0 mmol, 5.0 equiv.). An *E/Z* ratio of 10:1 was determined by ¹H NMR analysis. The crude mixture was purified by flash column chromatography on silica gel (2% AcOEt in hexanes as eluent) to afford **16o** (20.0 mg, 64% yield) as a colorless oil.

¹H NMR (400 MHz, CDCl₃) δ 7.39 – 7.32 (m, 2H), 7.29 (ddd, *J* = 7.8, 6.8, 1.2 Hz, 2H), 7.23 – 7.15 (m, 1H), 6.40 – 6.25 (m, 2H), 3.17 – 3.05 (m, 1H), 2.24 – 2.12 (m, 2H), 2.03 – 1.78 (m, 4H).

¹³C NMR (126 MHz, CDCl₃) δ 137.9, 135.4, 128.6, 127.7, 127.0, 126.1, 38.9, 28.9, 18.7.

Matching reported literature data.³²



(E)-(2-(Cyclohex-3-en-1-yl)vinyl)benzene (16p): Synthesized according to General Procedure **E** using DHP **11n** (66.5 mg, 0.2 mmol, 1.0 equiv.) and styrene (104.0 mg,

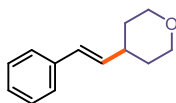
³² Cao, H.; Jiang, H.; Feng, H.; Kwan, J. M. C.; Liu, X.; Wu, J., Photo-induced Decarboxylative Heck-Type Coupling of Unactivated Aliphatic Acids and Terminal Alkenes in the Absence of Sacrificial Hydrogen Acceptors. *J. Am. Chem. Soc.* **2018**, *140*, 16360–16367.

1.0 mmol, 5.0 equiv.). An *E/Z* ratio of >20:1 was determined by ^1H NMR analysis. The crude mixture was purified by flash column chromatography on silica gel (2% AcOEt in hexanes as eluent) to afford **16p** (21.0 mg, 57% yield) as a colorless oil.

^1H NMR (400 MHz, CDCl_3) δ 7.40 – 7.33 (m, 2H), 7.32 – 7.27 (m, 2H), 7.22 – 7.17 (m, 1H), 6.40 (d, $J = 15.9$ Hz, 1H), 6.24 (dd, $J = 15.9, 7.2$ Hz, 1H), 5.71 (d, $J = 2.2$ Hz, 2H), 2.50 – 2.39 (m, 1H), 2.26 – 2.09 (m, 3H), 2.01 – 1.91 (m, 1H), 1.90 – 1.82 (m, 1H), 1.61 – 1.49 (m, 1H).

^{13}C NMR (101 MHz, CDCl_3) δ 138.0, 135.9, 128.6, 128.1, 127.2, 127.0, 126.2, 126.1, 37.3, 31.5, 28.9, 25.0.

Matching reported literature data.³³



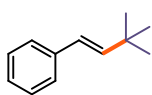
(E)-4-Styryltetrahydro-2H-pyran (16q): Synthesized according to General Procedure **E** using DHP **11n** (67.5 mg, 0.2 mmol, 1.0 equiv.) and styrene (104.0 mg, 1.0 mmol, 5.0 equiv.).

An *E/Z* ratio of >20:1 was determined by ^1H NMR analysis. The crude mixture was purified by flash column chromatography on silica gel (2% AcOEt in hexanes as eluent) to afford **16q** (28.5 mg, 75% yield) as a colorless oil.

^1H NMR (400 MHz, CDCl_3) δ 7.38 – 7.33 (m, 2H), 7.33 – 7.27 (m, 2H), 7.24 – 7.18 (m, 1H), 6.39 (d, $J = 16.1$ Hz, 1H), 6.16 (dd, $J = 16.0, 6.8$ Hz, 1H), 4.01 (ddd, $J = 11.8, 4.6, 2.0$ Hz, 2H), 3.47 (td, $J = 11.6, 2.2$ Hz, 2H), 2.38 (ddd, $J = 20.3, 11.8, 6.3$ Hz, 1H), 1.81 – 1.66 (m, 2H), 1.64 – 1.57 (m, 2H).

^{13}C NMR (101 MHz, CDCl_3) δ 137.7, 134.8, 128.7, 128.4, 127.2, 126.2, 67.9, 38.5, 32.8.

Matching reported literature data.³²



(E)-(3,3-Dimethylbut-1-en-1-yl)benzene (16r): Synthesized according to General Procedure **E** using silicate **11f** (86.5 mg, 0.2 mmol, 1.0 equiv.) and styrene (104.0 mg, 1.0 mmol, 5.0 equiv.).

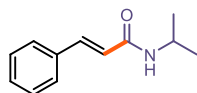
An *E/Z* ratio of >20:1 was determined by ^1H NMR analysis. The crude mixture was purified by flash column chromatography on silica gel (2% AcOEt in hexanes as eluent) to afford **16r** (22.0 mg, 68% yield) as a colorless oil.

^1H NMR (400 MHz, CDCl_3) δ 7.40 – 7.34 (m, 2H), 7.33 – 7.26 (m, 2H), 7.21 – 7.15 (m, 1H), 6.34 – 6.21 (m, 2H), 1.12 (s, 9H).

³³ Zhang, Y.-L.; Yang, L.; Wu, J.; Zhu, C.; Wang, P., Vinyl Sulfonium Salts as the Radical Acceptor for Metal-Free Decarboxylative Alkenylation. *Org Lett.* **2020**, *22*, 7768–7772.

^{13}C NMR (101 MHz, CDCl_3) δ 142.0, 138.2, 128.6, 126.9, 126.2, 124.7, 33.5, 29.8.

Matching reported literature data.³²



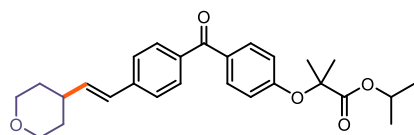
(E)-N-Isopropyl-4-phenylbut-3-enamide (16s):

Synthesized according to General Procedure E using DHP **11r** (67.5 mg, 0.2 mmol, 1.0 equiv.) and styrene (104.0 mg, 1.0 mmol, 5.0 equiv.). An *E/Z* ratio of 11:1 was determined by ^1H NMR analysis. The crude mixture was purified by flash column chromatography on silica gel (15% AcOEt in hexanes as eluent) to afford **16s** (27.0 mg, 67% yield) as a white solid.

^1H NMR (500 MHz, CDCl_3) δ 7.63 (d, J = 15.6 Hz, 1H), 7.54 – 7.48 (m, 2H), 7.41 – 7.35 (m, 3H), 6.37 (d, J = 15.6 Hz, 1H), 5.48 (s, 1H), 4.31 – 4.20 (m, 1H), 1.25 (d, J = 6.5 Hz, 6H).

^{13}C NMR (126 MHz, CDCl_3) δ 165.1, 140.9, 135.1, 129.7, 128.9, 127.9, 121.2, 41.7, 23.0.

Matching reported literature data.³⁴



(E)-2-Methyl-2-(4-(4-(2-(tetrahydro-2H-pyran-4-yl)vinyl)benzoyl)phenoxy)propanoate (16t):

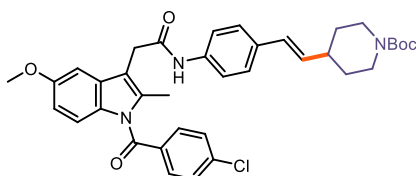
Synthesized according to General Procedure E using DHP **11n** (67.5 mg, 0.2 mmol, 1.0 equiv.) and styrene derivative **15l** (211.5 mg, 0.6 mmol, 3.0 equiv.). An *E/Z* ratio of 15:1 was determined by ^1H NMR analysis. The crude mixture was purified by flash column chromatography on silica gel (10% AcOEt in hexanes as eluent) to afford **16t** (63.5 mg, 73% yield) as a white solid.

^1H NMR (500 MHz, CDCl_3) δ 7.76 – 7.69 (m, 4H), 7.45 – 7.42 (m, 2H), 6.88 – 6.84 (m, 2H), 6.44 (d, J = 16.0 Hz, 1H), 6.30 (dd, J = 16.0, 6.7 Hz, 1H), 5.09 (p, J = 6.3 Hz, 1H), 4.07 – 3.99 (m, 2H), 3.48 (td, J = 11.7, 2.1 Hz, 2H), 2.43 (ddt, J = 11.1, 7.0, 4.1 Hz, 1H), 1.77 – 1.69 (m, 2H), 1.66 (s, 6H), 1.62 (dd, J = 11.9, 4.5 Hz, 2H), 1.20 (d, J = 6.3 Hz, 6H).

^{13}C NMR (126 MHz, CDCl_3) δ 195.2, 173.4, 159.6, 141.5, 137.4, 136.7, 132.1, 131.0, 130.5, 127.7, 125.9, 117.3, 79.5, 69.5, 67.8, 38.7, 32.6, 29.8, 21.7.

HRMS: calculated for $\text{C}_{27}\text{H}_{33}\text{O}_5$ ($\text{M}+\text{H}^+$): 437.2323, found 437.2307.

³⁴ Zhang, K.-Q.; Deng, Q.-F.; Luo, J.; Gong, C.-L.; Chen, Z.-G.; Zhong, W.; Hu, S.-Q.; Wang, H.-F., Multifunctional Ag(I)/CAAA-Amidphos Complex-Catalyzed Asymmetric [3 + 2] Cycloaddition of α -Substituted Acrylamides. *ACS Catal.* **2021**, *11*, 5100–5107.



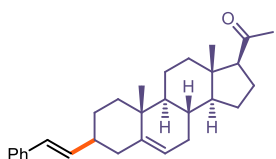
tert-Butyl-(E)-4-(4-(2-(1-(4-chlorobenzoyl)-5-methoxy-2-methyl-1H-indol-3-yl)acetamido)styryl)piperidine-1-carboxylate (16u): Synthesized

according to General Procedure E using DHP **11k** (87.5 mg, 0.2 mmol, 1.0 equiv.) and styrene derivative **15m** (275.5 mg, 0.6 mmol, 3.0 equiv.). An *E/Z* ratio of >20:1 was determined by ^1H NMR analysis. The crude mixture was purified by flash column chromatography on silica gel (30% AcOEt in hexanes as eluent) to afford **16u** (70.5 mg, 55% yield) as a white solid.

^1H NMR (400 MHz, CDCl_3) δ 7.73 – 7.65 (m, 2H), 7.54 – 7.47 (m, 2H), 7.38 – 7.32 (m, 2H), 7.29 (s, 1H), 7.15 (d, $J = 8.5$ Hz, 2H), 6.95 (d, $J = 2.5$ Hz, 1H), 6.87 (d, $J = 9.0$ Hz, 1H), 6.72 (dd, $J = 9.1, 2.5$ Hz, 1H), 6.31 (d, $J = 11.7$ Hz, 1H), 5.41 (dd, $J = 11.6, 10.0$ Hz, 1H), 4.11 – 4.02 (m, 2H), 3.81 (s, 5H), 2.77 – 2.59 (m, 3H), 2.46 (s, 3H), 1.63 (d, $J = 13.4$ Hz, 2H), 1.45 (s, 9H), 1.40 – 1.32 (m, 2H).

^{13}C NMR (126 MHz, CDCl_3) δ 168.3, 168.1, 156.4, 154.8, 139.8, 136.7, 136.5, 136.0, 134.0, 133.5, 131.3, 131.0, 130.1, 129.3, 129.1, 127.6, 120.0, 115.2, 112.5, 112.3, 100.7, 79.4, 55.8, 43.4, 35.1, 33.3, 32.0, 28.5, 13.3.

HRMS: calculated for $\text{C}_{37}\text{H}_{40}\text{ClN}_3\text{NaO}_5$ ($\text{M}+\text{Na}^+$): 664.2549, found 664.2560.



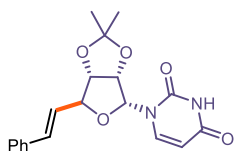
1-((3S,8S,9S,10R,13S,14S,17S)-10,13-Dimethyl-3-(E-styryl)-2,3,4,7,8,9,10,11,12,13,14,15,16,17-tetradecahydro-1H-cyclopenta[a]phenanthren-17-yl)ethan-1-one (16v): Synthesized according to

General Procedure E using DHP **11u** (110.5 mg, 0.2 mmol, 1.0 equiv.) and styrene (104.0 mg, 1.0 mmol, 5.0 equiv.). An *E/Z* ratio of 8:1 was determined by ^1H NMR analysis. The crude mixture was purified by flash column chromatography on silica gel (10% AcOEt in hexanes as eluent) to afford **16v** (dr = 1.6:1, 56.5 mg, 70% yield) as a white solid.

^1H NMR (500 MHz, CDCl_3) δ 7.43 – 7.26 (m, 4.37H), 7.22 – 7.16 (m, 1.05H), 6.46 – 6.37 (m, 0.78H), 6.36 – 6.29 (m, 0.86H), 5.34 (dq, $J = 5.2, 2.7, 2.0$ Hz, 1.00H), 2.68 – 2.60 (m, 1.27H), 2.54 (td, $J = 9.0, 6.5$ Hz, 1.24H), 2.13 (s, 1.85H), 2.12 (s, 2.20H), 2.24 – 1.87 (m, 10.69H), 1.75 – 1.13 (m, 16.03H), 1.05 (s, 2.34H), 1.02 (s, 1.26H), 0.64 (s, 1.06H), 0.64 (s, 1.89H).

^{13}C NMR (126 MHz, CDCl_3) δ 209.8, 209.8, 142.6, 140.5, 138.3, 138.0, 136.0, 134.2, 129.4, 128.6, 128.6, 127.9, 127.0, 126.9, 126.1, 126.1, 121.3, 119.9, 63.9, 57.2, 57.2, 50.5, 50.3, 44.2, 43.1, 39.4, 39.2, 39.1, 37.9, 37.6, 37.2, 37.1, 34.5, 32.0, 32.0, 31.97, 31.93, 31.7, 29.0, 28.1, 24.7, 24.6, 23.0, 21.1, 20.92, 19.6, 19.6, 13.4, 13.4.

HRMS: calculated for $\text{C}_{29}\text{H}_{39}\text{O}$ ($\text{M}+\text{H}^+$): 403.2995, found 403.3004.



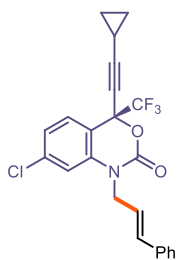
1-((3a*S*,4*R*,6*S*,6a*S*)-2,2-Dimethyl-6-((*E*)-styryl)tetrahydrofuro [3,4-*d*][1,3]dioxol-4-yl)pyrimidine-2,4(1*H*,3*H*)-dione (16w): Synthesized according to General Procedure **E** using DHP **11t** (101.0

mg, 0.2 mmol, 1.0 equiv.) and styrene (104.0 mg, 1.0 mmol, 5.0 equiv.). An *E/Z* ratio of 7:1 was determined by ^1H NMR analysis. The crude mixture was purified by flash column chromatography on silica gel (25% AcOEt in hexanes as eluent) to afford **16w** (diastereomers, *dr* = 5:1, 57.5 mg, 81% yield) as a white solid.

^1H NMR (400 MHz, CDCl_3) δ 9.15 (s, 1H), 7.48 – 7.26 (m, 7H), 6.68 (d, J = 16.1 Hz, 1H), 6.31 (dd, J = 15.9, 7.8 Hz, 1H), 5.74 (dd, J = 8.1, 2.0 Hz, 1H), 5.66 (d, J = 1.8 Hz, 1H), 5.08 (dd, J = 6.4, 1.9 Hz, 1H), 4.86 (dd, J = 6.4, 4.3 Hz, 1H), 4.71 (ddd, J = 7.7, 4.3, 1.1 Hz, 1H), 1.61 (s, 3H), 1.37 (s, 3H).

^{13}C NMR (101 MHz, CDCl_3) δ 163.4, 150.1, 142.6, 136.1, 134.1, 128.7, 128.7, 128.4, 127.0, 126.9, 125.9, 114.8, 102.7, 94.9, 89.1, 85.0, 84.6, 27.3, 25.5.

HRMS: calculated for $\text{C}_{19}\text{H}_{20}\text{N}_2\text{NaO}_5$ ($\text{M}+\text{Na}^+$): 379.1264, found 379.1258.



(*S*)-7-Chloro-1-cinnamyl-4-(cyclopropylethynyl)-4-(trifluoromethyl)-1,4-dihydro-2*H*-benzo[*d*][1,3]oxazin-2-one (16x): Synthesized according to General Procedure **E** using DHP **11s** (116.0 mg, 0.2 mmol, 1.0 equiv.) and styrene (104.0 mg, 1.0 mmol, 5.0 equiv.). An *E/Z* ratio of >20:1 was determined by ^1H NMR analysis. The crude mixture was purified by flash column chromatography on silica gel (15% AcOEt in hexanes as eluent) to afford **16x** (54.5 mg, 63% yield) as a white solid.

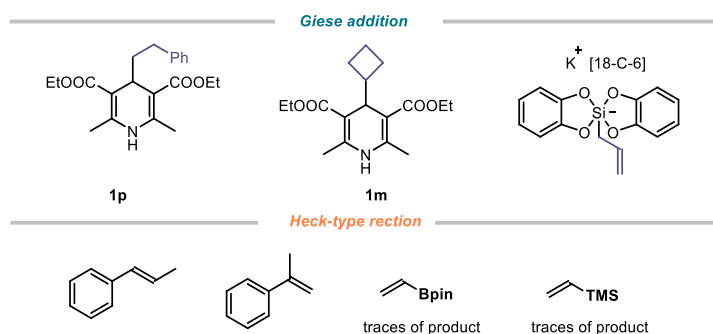
^1H NMR (400 MHz, CDCl_3) δ 7.59 – 7.51 (m, 1H), 7.42 – 7.27 (m, 5H), 7.25 – 7.22 (m, 1H), 6.98 (d, J = 8.8 Hz, 1H), 6.58 (dt, J = 16.1, 1.7 Hz, 1H), 6.18 (dt, J = 16.1, 5.6 Hz, 1H), 4.79 – 4.59 (m, 2H), 1.40 (tt, J = 8.3, 5.1 Hz, 1H), 0.99 – 0.78 (m, 4H).

^{13}C NMR (101 MHz, CDCl_3) δ 148.2, 136.0, 135.4, 133.4, 131.6, 129.1, 128.8, 128.3, 126.6, 122.1, 117.8, 115.8, 95.8, 77.4, 66.4, 46.9, 8.94, 8.91, -0.5.

^{19}F NMR (376 MHz, CDCl_3) δ -80.20.

HRMS: calculated for $\text{C}_{23}\text{H}_{17}\text{ClF}_3\text{NNaO}_2$ ($\text{M}+\text{Na}^+$): 454.0792, found 454.0800.

3.6.4 Unsuccessful Substrates



Scheme 3.13: Unsuccessful substrates that offered poor yields (ranging from 0 to <20%)

3.6.5 Mechanistic Studies

3.6.5.1. Control reactions with green light

For the reactions performed under green light irradiation, an EvoluChem™ P303-30-1 LEDs (18 W, $\lambda_{\text{max}}=520$ nm, 2-3 cm away) was used. The reaction temperature was controlled by a fan (T internal to the vial was measured to be between 35 °C and 40 °C - the setup is depicted in Figure 3.6).

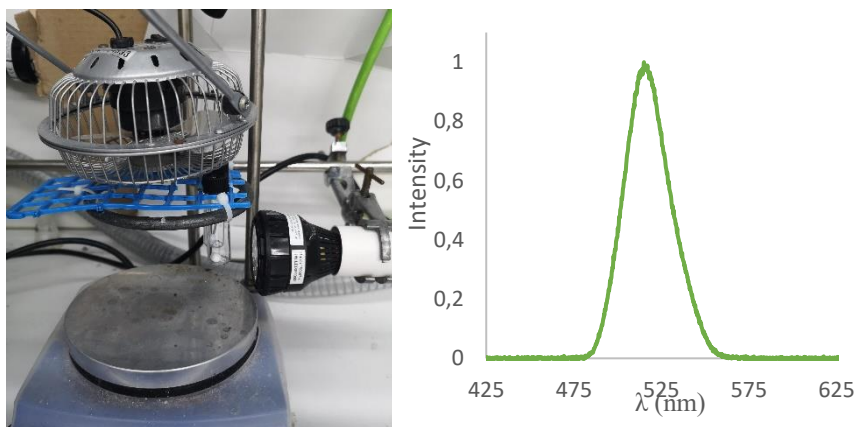


Figure 3.6: Reaction set-up for green light irradiation.

3.6.5.2 UV-Vis measurements

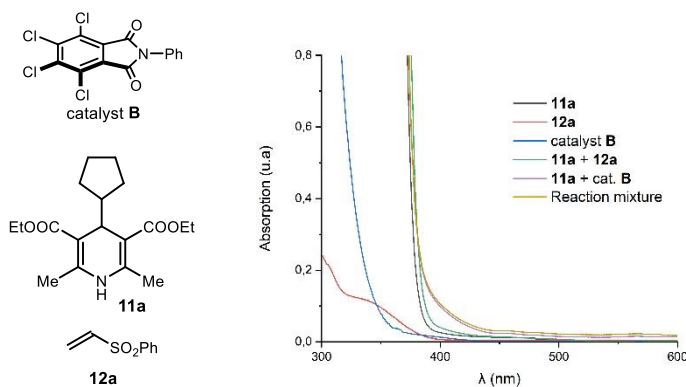


Figure 3.7: Optical absorption spectra, recorded in DMF in 1 cm path quartz cuvettes using a Shimadzu 2401PC UV-vis spectrophotometer, and visual appearance of the separate reaction components and of the colored EDA complex between catalyst **B** and **11a**. [**11a**] = 0.15 M, [**12a**] = 0.10 M [catalyst **B**] = 0.02 M.

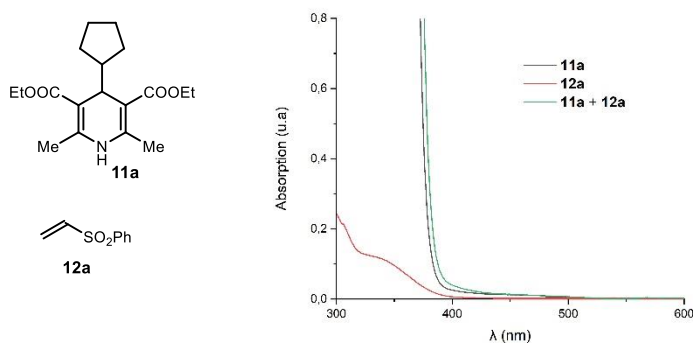


Figure 3.8: Optical absorption spectra, recorded in DMF in 1 cm path quartz cuvettes using a Shimadzu 2401PC UV-vis spectrophotometer, and visual appearance of the substrates **11a**, **12a** and of their mixture. [**11a**] = 0.15 M, [**12a**] = 0.10 M.

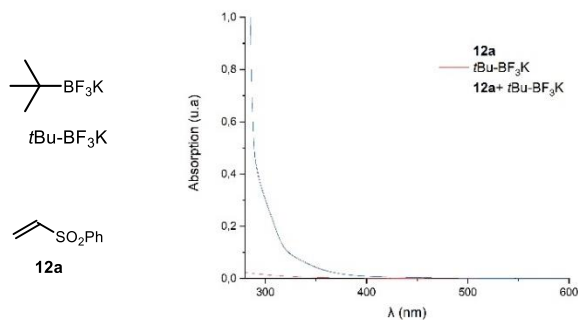


Figure 3.9: Optical absorption spectra, recorded in DMF in 1 cm path quartz cuvettes using a Shimadzu 2401PC UV-vis spectrophotometer, and visual appearance of the substrates *t*Bu-BF₃K, **12b** and of their mixture. [*t*Bu-BF₃K] = 0.15 M, [**12b**] = 0.10 M.

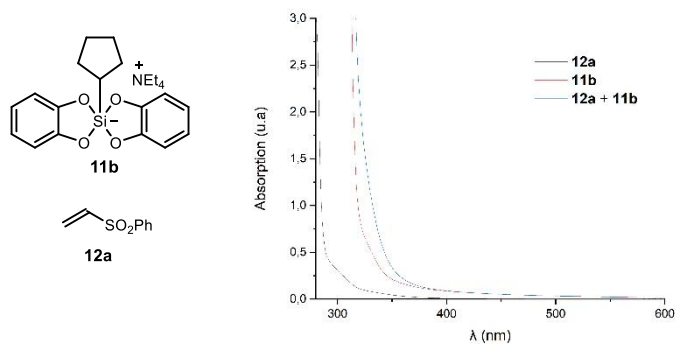


Figure 3.10: Optical absorption spectra, recorded in DMF in 1 cm path quartz cuvettes using a Shimadzu 2401PC UV-vis spectrophotometer, and visual appearance of the substrates **12a**, **11b** and of their mixture. [**11b**] = 0.15 M, [**12a**] = 0.10 M.

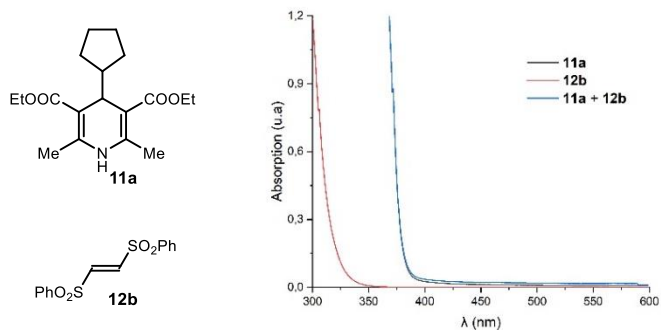


Figure 3.11: Optical absorption spectra, recorded in DMF in 1 cm path quartz cuvettes using a Shimadzu 2401PC UV–vis spectrophotometer, and visual appearance of the substrates **11a**, **12b** and of their mixture. [**11a**] = 0.15 M, [**12b**] = 0.10 M.

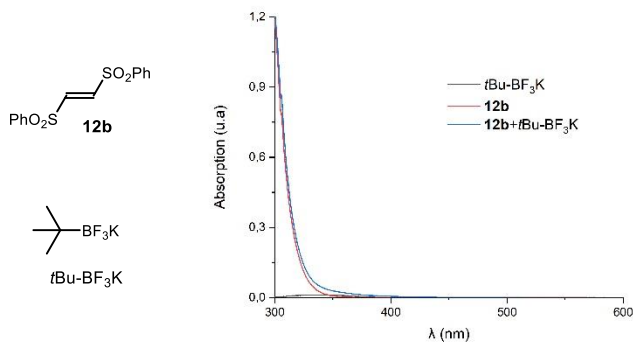


Figure 3.12: Optical absorption spectra, recorded in DMF in 1 cm path quartz cuvettes using a Shimadzu 2401PC UV–vis spectrophotometer, and visual appearance of the substrates *t*Bu-BF₃K, **2b** and of their mixture. [*t*Bu-BF₃K] = 0.15 M, [**2b**] = 0.10 M.

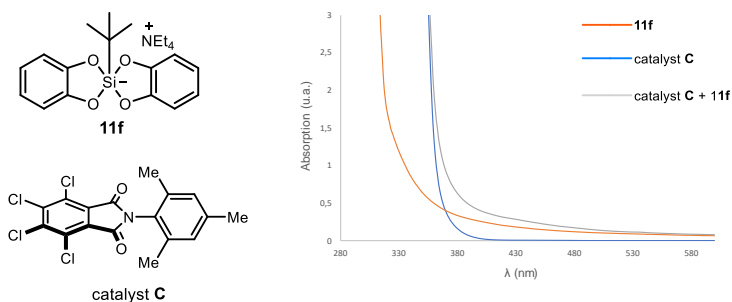


Figure 3.13: Optical absorption spectra, recorded in DMF in 1 cm path quartz cuvettes using a Shimadzu 2401PC UV–vis spectrophotometer, and visual appearance of the separate reaction components and of the colored EDA complex between catalyst **C** and silicate **11b**. [**11b**] = 0.15 M, [catalyst **C**] = 0.02 M.

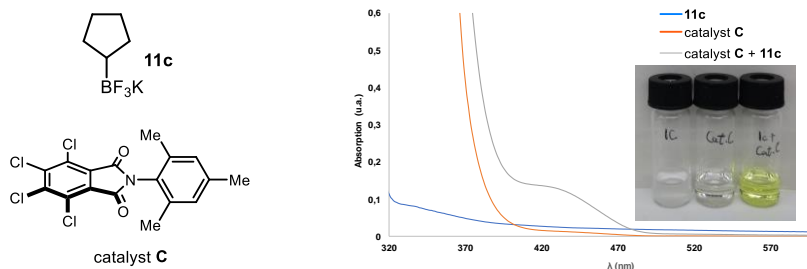


Figure 3.14: Optical absorption spectra, recorded in DMF in 1 cm path quartz cuvettes using a Shimadzu 2401PC UV-vis spectrophotometer, and visual appearance of the separate reaction components and of the colored EDA complex between catalyst **C** and trifluoroborate salt **1c**. $[1c] = 0.15$ M, $[\text{catalyst C}] = 0.02$ M.

3.6.5.3 Cyclic Voltammetry Measurements

For all cyclic voltammetry (CV) measurements, a glassy carbon disk electrode (diameter 3 mm) was used as the working electrode. A silver wire coated with AgCl immersed in a 3.5 M aqueous solution of KCl and separated from the analyte by a fritted glass disk was employed as the reference electrode. A Pt wire counter-electrode completed the electrochemical setup. The scan rate used in each CV experiment is indicated case by case.

Potentials are quoted with the following notation: E_p^C refers to the cathodic peak potential, E_p^A refers to the anodic peak potential, while the E^{red} value describes the electrochemical properties of the referred compound.

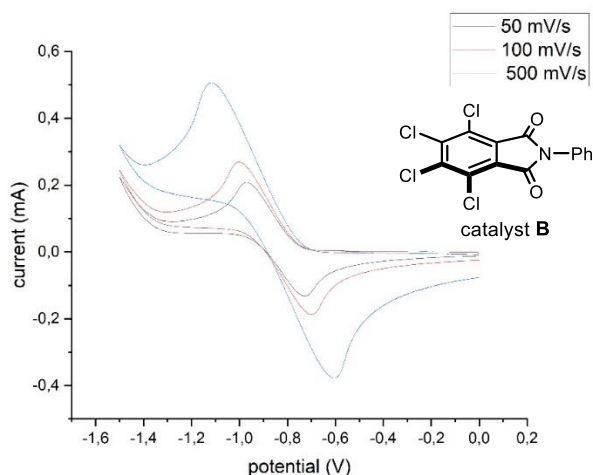


Figure 3.15: Cyclic voltammogram for catalyst **B** [0.02 M] in [0.1 M] TBAPF₆ in DMF. Measurement started by reduction from 0 to -2.0 V, followed by oxidation from -2.0 V to 0, and finishing at 0 V. Glassy carbon electrode working electrode, Ag/AgCl (KCl 3.5 M) reference electrode, Pt wire auxiliary electrode. Two irreversible peaks observed increasing with sweep rate.

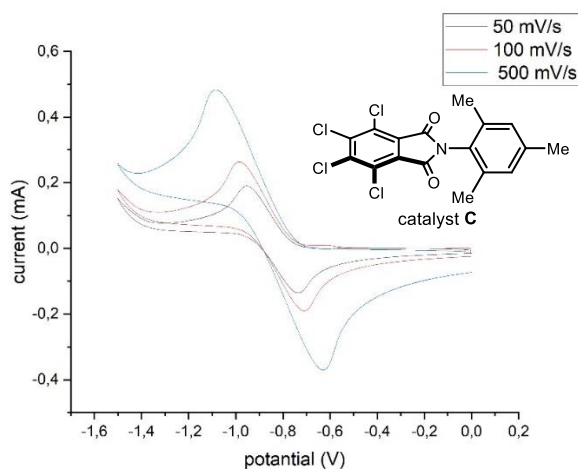


Figure 3.16: Cyclic voltammogram for catalyst **C** [0.02 M] in [0.1 M] TBAPF₆ in DMF. Measurement started by reduction from 0 to -2.0 V, followed by oxidation from -2.0 V to 0, and finishing at 0 V. Glassy carbon electrode working electrode, Ag/AgCl (KCl 3.5 M) reference electrode, Pt wire auxiliary electrode. Two irreversible peaks observed increasing with sweep rate.

3.6.5.4 Quantum Yield Determination

Experimental Setup

The experiments for the quantum yield determination were conducted under illumination by a 460 nm high-power single LED (setup depicted in Figure 3.17), using an aluminum block on a 3D-printed holder, fitted with a 460 nm high-power single LED. The irradiance was fixed at 60 ± 2 mW/cm², as controlled by an external power supply and measured using a photodiode light detector at the start of each reaction. This setup secured a reliable irradiation while keeping a distance of 1 cm between the reaction vessel and the light source.



Figure 3.17: high-power single LED setup

General Procedure F for quantum yield determinations.

A ferrioxalate actinometer solution was prepared by following the Hammond variation of the Hatchard and Parker procedure outlined in the Handbook of Photochemistry.²³ The ferrioxalate actinometer solution measures the decomposition of ferric ions to ferrous ions, which are complexed by 1,10-phenanthroline and monitored by UV/Vis absorbance at 510 nm. The moles of iron-phenanthroline complex formed are related to moles of photons absorbed. The following solutions were prepared and stored in a dark laboratory (red light):

1. Potassium ferrioxalate solution: 294.8 mg of potassium ferrioxalate (commercially available from Alfa Aesar) and 139 μ L of sulfuric acid (96%) were added to a 50 mL volumetric flask, and filled to the mark with water (HPLC grade).
2. Phenanthroline solution: 0.2% by weight of 1,10-phenanthroline in water (100 mg in 50 mL volumetric flask).

3. Buffer solution: 2.47 g of NaOAc and 0.5 mL of sulfuric acid (96%) were added to a 50 mL volumetric flask and filled to the mark with water (HPLC grade).

The actinometry measurements were done as follows:

5. 1 mL of the actinometer solution was added to a 16 mm diameter vial. The vial was placed into an aluminum block on a 3D-printed holder, fitted with a 460 nm high-power single LED (Figure 3.17). The solution was irradiated at 460 nm. This procedure was repeated 4 times, quenching the solutions after different time intervals.
6. Then 1 mL of the model reaction following General Procedure A, B or E was placed in the irradiation set up and irradiated for different irradiation times.
7. After irradiation, the actinometer solutions were removed and placed in a 10 mL volumetric flask containing 0.5 mL of 1,10-phenanthroline solution and 2 mL of buffer solution. These flasks were filled to the mark with water (HPLC grade).
8. The UV-Vis spectra of the complexed actinometer samples were recorded for each time interval. The absorbance of the complexed actinometer solution was monitored at 510 nm.

The moles of Fe^{2+} formed for each sample is determined using Beers' Law (Eq. 1):

$$\text{Mols of Fe(II)} = V_1 \times V_3 \times \Delta A(510 \text{ nm}) / 10^3 \times V_2 \times l \times \epsilon(510 \text{ nm}) \quad (\text{Eq. 1})$$

where V_1 is the irradiated volume (1 mL), V_2 is the aliquot of the irradiated solution taken for the determination of the ferrous ions (1 mL), V_3 is the final volume after complexation with phenanthroline (10 mL), l is the optical path-length of the irradiation cell (1 cm), $\Delta A(510 \text{ nm})$ is the optical difference in absorbance between the irradiated solution and the one stored in the dark, $\epsilon(510 \text{ nm})$ is the extinction coefficient the complex $\text{Fe}(\text{phen})_3^{2+}$ at 510 nm ($11100 \text{ L mol}^{-1} \text{ cm}^{-1}$). The moles of Fe^{2+} formed (x) are plotted as a function of time (t). The slope of this line was correlated to the moles of incident photons by unit of time (q_0) by the use of the following Equation 2:

$$\Phi(\lambda) = dx/dt \cdot q_0 / [1 - 10^{-A(\lambda)}] \quad (\text{Eq. 2})$$

where dx/dt is the rate of change of a measurable quantity (spectral or any other property), the quantum yield (Φ) for Fe^{2+} at 458 nm is $1.1 \cdot 10^{-A(\lambda)}$ is the ratio of absorbed photons by the solution, and $A(\lambda)$ is the absorbance of the actinometer at the wavelength used to carry out the experiments (460 nm). The absorbance at 460 nm $A(460)$ was measured using a Shimadzu 2401PC UV-Vis spectrophotometer in a 10 mm path quartz cuvette.

The moles of product formed for the model reaction were determined by GC measurement (FID detector) using 1,3,5-trimethoxybenzene as internal standard. The moles of product per unit of time are related to the number of photons absorbed.

The photons absorbed are correlated to the number of incident photons by the use of Equation 1. According to this, if we plot the moles of product (y) versus the moles of incident photons ($q_0 n, p \cdot dt$), the slope is equal to: $\Phi \cdot (1 - 10^{-A(460 \text{ nm})})$, where Φ is the quantum yield to be determined and $A(460 \text{ nm})$ is the absorption of the reaction under study. $A(460 \text{ nm})$ was measured using a Shimadzu 2401PC UV-Vis spectrophotometer in 10 mm path quartz.

*Quantum Yield of the Giese addition to vinylsulfone **12a** using DHP **11a** catalyzed by **B***

The quantum yield has been determined following general procedure **F**. The actinometer solution was irradiated for 3 sec, 6 sec, 9 sec, and 12 sec. The model reaction was prepared according to General Procedure **A** and each reaction mixture was irradiated for 52min, 60 min, 90 min, 140 min. The absorbance at 460 nm of the non-complexed actinometer solution was measured to be 0.186. An absorbance of 0.064 was determined for the model reaction mixture (1:4 dilution). Plot of mols of Fe^{2+} formed vs irradiation time and plot of mols of incident photons vs mols of product formed were depicted as Figure 3.18 and Figure 3.19, respectively.

The quantum yield (Φ)_{cat.} of the photochemical transformation was measured to be **0.04**.

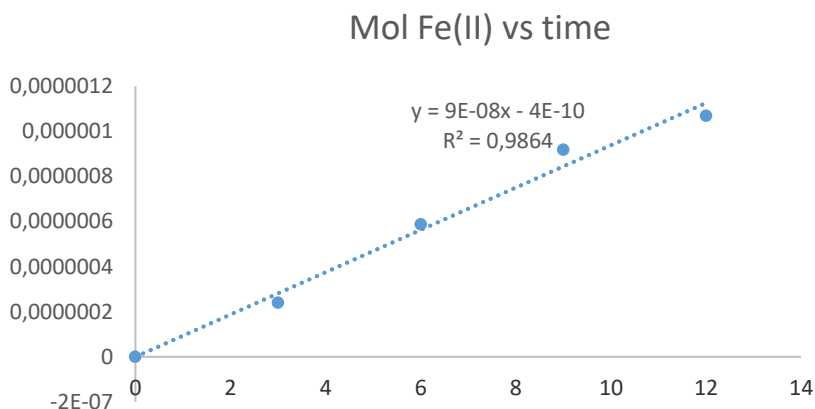


Figure 3.18: Plot of moles of Fe^{2+} formed vs irradiation time. Slope of the line correlates to the moles of incident photons by unit of time.

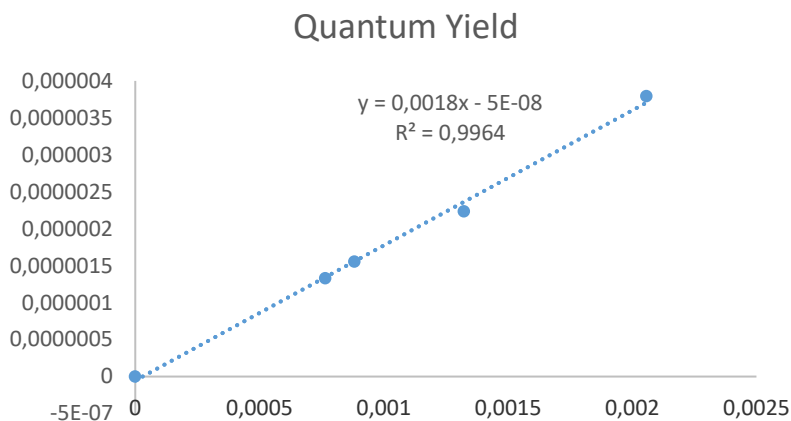


Figure 3.19: Plot of moles of incident photons vs moles of product formed. Slope of the line correlates to quantum yield of the photochemical transformation.

*Quantum yield of the Giese addition to vinylsulfone **12a** using silicate **11f** catalyzed by **C***

The quantum yield has been determined following general procedure **F**. The actinometer solution was irradiated for 3 sec, 6 sec, 9 sec, and 12 sec. The model reaction was prepared according to General Procedure **B** and each reaction mixture was irradiated for 15min, 30 min, 45 min, 63 min. The absorbance at 460 nm of the non-complexed actinometer solution was measured to be 0.144. An absorbance of 0.09 was determined for the model reaction mixture (1:4 dilution). Plot of mols of Fe^{2+} formed vs irradiation time and plot of mols of incident photons vs mols of product formed were depicted as Figure 3.20 and Figure 3.21, respectively.

The quantum yield (Φ)_{cat.} of the photochemical transformation was measured to be **0.03**.

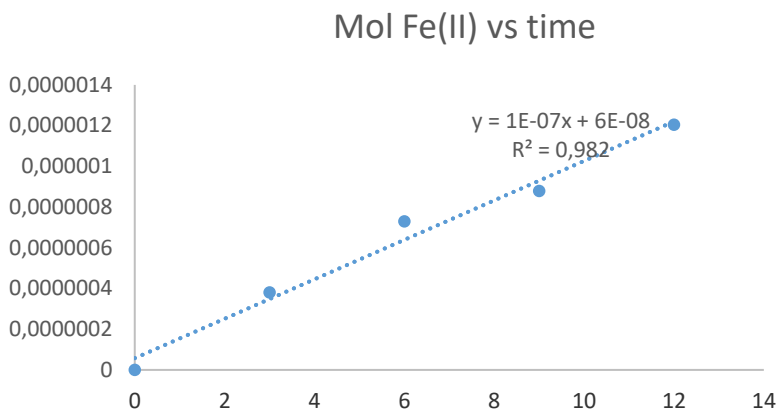


Figure 3.20: Plot of mols of Fe^{2+} formed vs irradiation time. Slope of the line correlates to the moles of incident photons by unit of time.

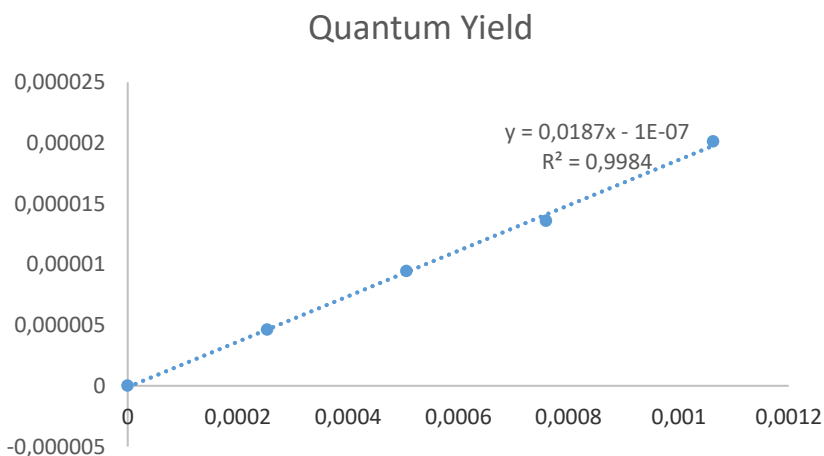


Figure 3.21: Plot of mols of incident photons vs mols of product formed. Slope of the line correlates to quantum yield of the photochemical transformation.

Quantum yield of the Heck-type reaction using styrene and DHP 11k catalyzed by C

The quantum yield has been determined following general procedure **F**. The actinometer solution was irradiated for 1 sec, 3 sec, and 9 sec. The model reaction was prepared with 0.9 mL dioxane and 0.1 mL water instead of 1 mL dioxane according to General Procedure **E** and each reaction mixture was irradiated for 90 min, 150 min, 210 min, 270 min. The absorbance at 460 nm of the non-

complexed actinometer solution was measured to be 0.139. An absorbance of 0.037 was determined for the model reaction mixture (1:4 dilution). Plot of mols of Fe^{2+} formed vs irradiation time and plot of mols of incident photons vs mols of product formed were depicted as Figure 3.22 and Figure 3.23, respectively.

The quantum yield (Φ)_{cat.} of the photochemical transformation was measured to be **0.01**.

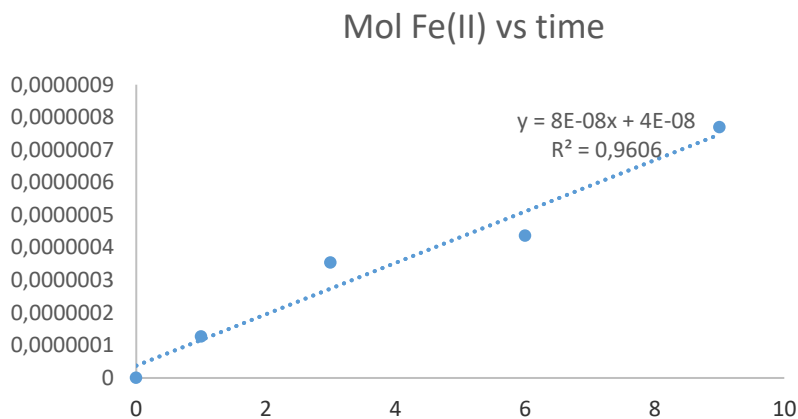


Figure 3.22: Plot of mols of Fe^{2+} formed vs irradiation time. Slope of the line correlates to the moles of incident photons by unit of time.

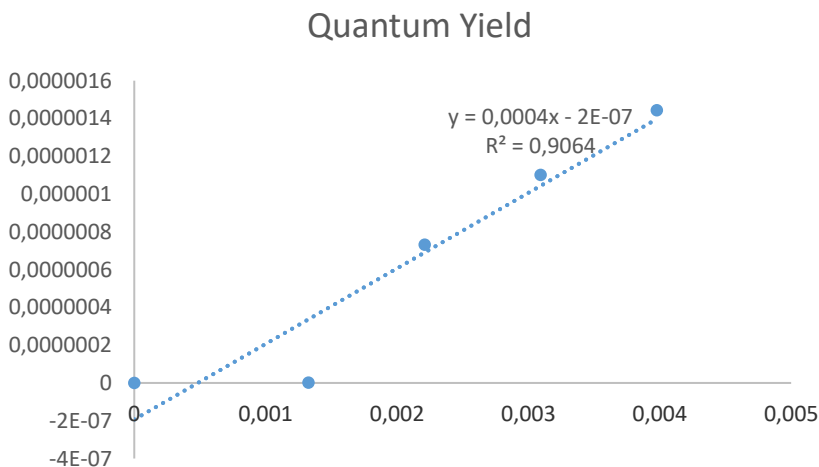


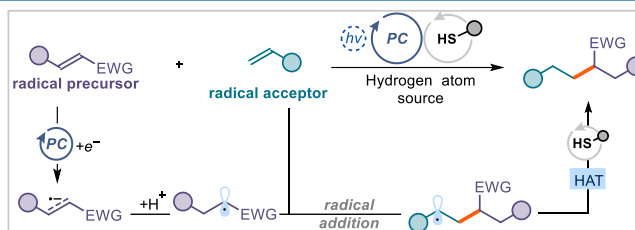
Figure 3.23: Plot of mols of incident photons vs mols of product formed. Slope of the line correlates to quantum yield of the photochemical transformation.

Chapter IV

Reductive cross-coupling of olefins via a radical path

Target

To develop a new system for the reductive cross-coupling of neutral olefins with electron-poor olefins, the latter serving as radical precursors.



Tool

Using a photoredox catalyst to reduce electron-poor olefins and generate radicals, which are then captured by neutral olefins to deliver another radical. By means of hydrogen atom transfer (HAT) catalysis, the ensuing radical is then reduced to afford olefin cross-coupling products.¹

4.1 Introduction

Olefins are versatile feedstock for chemical synthesis that can be transformed to install various functional groups.² Illustrative examples of olefin reactions are

¹ The project discussed in this chapter was conducted in collaboration with Igor Dmitriev. I was involved in the discovery and optimization of the reactions and investigated the scope. I also conducted mechanistic studies. This work is still in progress and we are about to submit the resulting scientific manuscript for publication.

² Selected reviews: (a) Qi, X.; Diao, T. Nickel-Catalyzed Dicarbofunctionalization of Alkenes. *ACS Catal.* **2020**, *10*, 8542–8556. (b) Badir, S. O.; Molander, G. A. Developments in Photoredox/ Nickel Dual-Catalyzed 1,2-Difunctionalizations. *Chem.* **2020**, *6*, 1327–1339. (c) Dhungana, R. K.; Sapkota, R. R.; Niroula, D.; Giri, R. Walking Metals: Catalytic Difunctionalization of Alkenes at Nonclassical Sites. *Chem. Sci.* **2020**, *11*, 9757–9774. (d) Lan, X. W.; Wang, N. X.; Xing, Y. Recent Advances in Radical Difunctionalization of Simple Alkenes. *Eur. J. Org. Chem.* **2017**, *2017*, 5821–5851. (e) McDonald, R. I.; Liu, G.; Stahl, S. S. Palladium (II)-Catalyzed Alkene Functionalization via Nucleopalladation: Stereochemical Pathways and Enantioselective Catalytic Applications. *Chem. Rev.* **2011**, *111*, 2981–3019. (f) Cheung, K. P. S.; Sarkar, S.; Gevorgyan, V. Visible Light-Induced Transition Metal Catalysis. *Chem. Rev.* **2022**, *122*, 1543–1625.

displayed in Figure 4.1, which details how epoxides, cyclopropanes, aldehydes, carboxylic acids, and alkanes can be readily prepared.

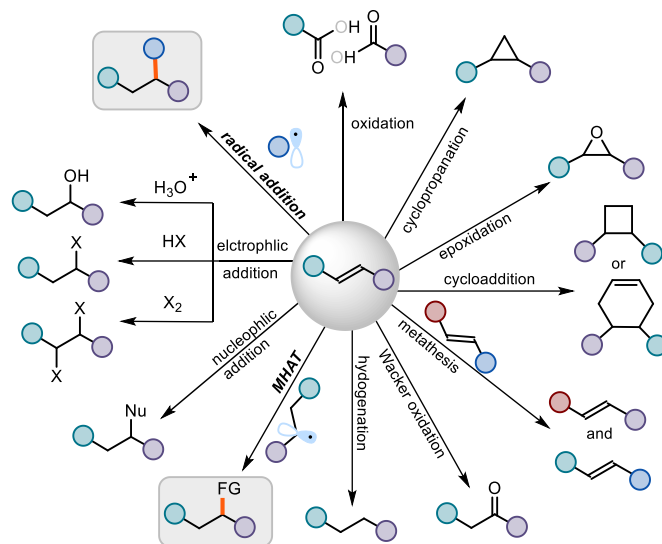
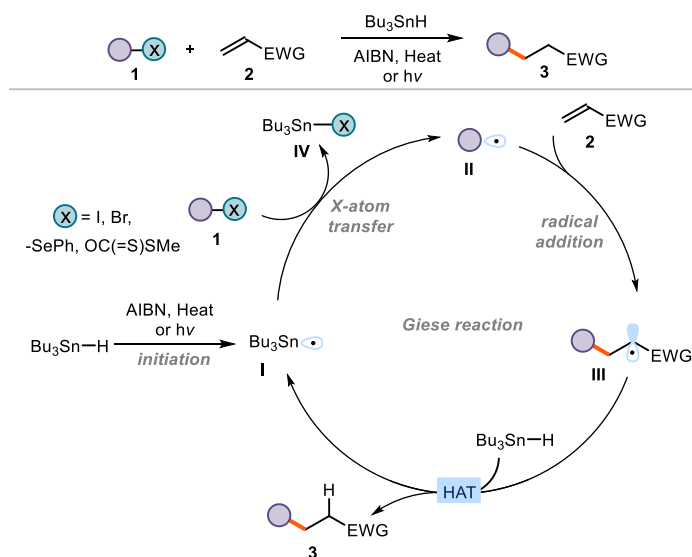


Figure 4.5. Olefin reaction map

Also radical-based reactions with olefins are well-established. A first example is the radical addition to olefins, a process known as the Giese reaction.³ In this chemistry, electron-poor olefins act as radical acceptors. In early studies (Scheme 4.1), toxic tin reagents were used to initiate the process. The tin reagent either reacted with azobisisobutyronitrile (AIBN) under heating condition or underwent homolytic cleavage via ultraviolet (UV) irradiation to afford tin radical **I**. The resulting radical **I** would then abstract an atom (often a halogen, X) or group from the radical precursors **1** (e.g., alkyl halides, alkyl Barton ester) to generate the alkyl radical **II**, which could be trapped by electron-poor olefin **2** to provide another electrophilic radical **III**. In the last step, radical **III** abstracted a hydrogen atom from tin hydride to deliver the C-C coupling product **3** and another alkyl-tin radical **I**, which propagated a radical chain process. Giese reactions are useful to form new C-C bonds, complementing organometallic conjugate addition processes. However,

³ (a) Giese, B., Formation of C-C Bonds by Addition of Free Radicals to Alkenes. *Angew. Chem., Int. Ed.* **1983**, *22*, 753-764; (b) Giese, B.; Horler, H.; Leising, M., Umpolungsreaktionen mit dem Malonyl-Radikal. *Chem. Ber.* **1986**, *119*, 444-452.

the high toxicity of the tin reagents, along with the harsh conditions required, stimulated research to identify milder and more sustainable methods.⁴



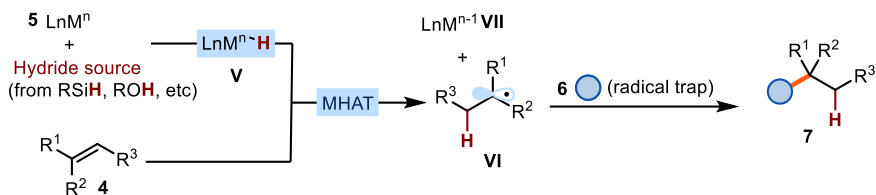
Scheme 4.6. Mechanism of the tin-hydride-mediated Giese reactions

Another relevant radical-based reaction involving olefins is based on metal-hydride hydrogen atom transfer (MHAT).⁵ In this manifold (Scheme 4.2), electron-rich or neutral olefins are generally used. First, the metal catalyst **5** (e.g. Fe, Co, Mn and Pd) reacts with a hydride source, which usually comes from silanes or alcohol solvents, producing the corresponding metal-hydride species **V**. Then olefin **4** could undergo MHAT with metal-hydride **V** to afford the alkyl radical **VI** and the reduced state of the metal catalyst **VII**. The resulting alkyl radical **VI** is then

⁴ (a) Gant Kanegusuku, A. L.; Roizen, J. L., Recent Advances in Photoredox-Mediated Radical Conjugate Addition Reactions: An Expanding Toolkit for the Giese Reaction. *Angew. Chem., Int. Ed.* **2021**, *60*, 21116-21149; (b) Kitcatt, D. M.; Nicolle, S.; Lee, A.-L., Direct decarboxylative Giese reactions. *Chem. Soc. Rev.* **2022**, *51*, 1415-1453.

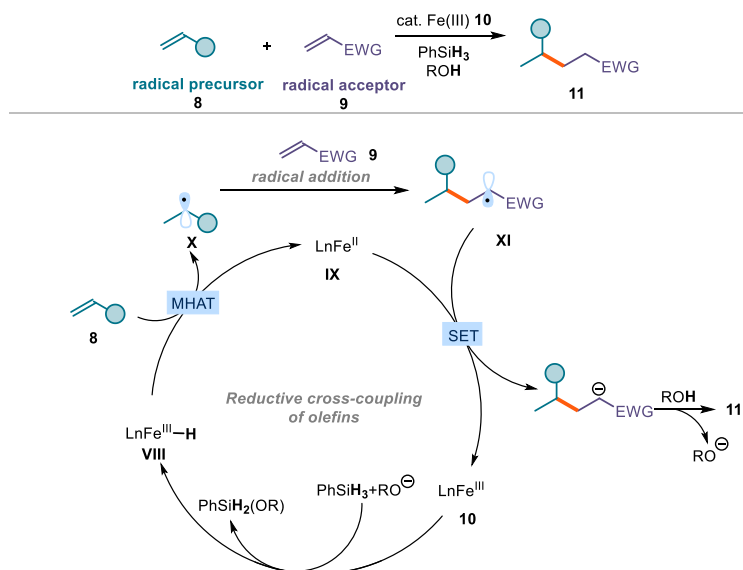
⁵ (a) Shevick, S. L.; Wilson, C. V.; Kotesova, S.; Kim, D.; Holland, P. L.; Shenvi, R. A., Catalytic hydrogen atom transfer to alkenes: a roadmap for metal hydrides and radicals. *Chem. Sci.* **2020**, *11*, 12401-12422; Green, S. A.; Crossley, S. W. M.; Matos, J. L. M.; Vázquez-Céspedes, S.; Shevick, S. L.; (b) Shenvi, R. A., The High Chemofidelity of Metal-Catalyzed Hydrogen Atom Transfer. *Acc. Chem. Res.* **2018**, *51*, 2628-2640; (c) Crossley, S. W. M.; Obradors, C.; Martinez, R. M.; Shenvi, R. A., Mn-, Fe-, and Co-Catalyzed Radical Hydrofunctionalizations of Olefins. *Chem. Rev.* **2016**, *116*, 8912-9000; (d) Jana, S.; Mayerhofer, V. J.; Teskey, C. J., Photo- and Electrochemical Cobalt Catalyzed Hydrogen Atom Transfer for the Hydrofunctionalisation of Alkenes. *Angew. Chem., Int. Ed.* e202304882; (f) Wu, J.; Ma, Z., Metal-hydride hydrogen atom transfer (MHAT) reactions in natural product synthesis. *Org. Chem. Front.* **2021**, *8*, 7050-7076.

intercepted by a trap **6** to forge a new bond and deliver the desired product **7**. Finally, the metal complex **VII** is regenerated by external oxidants or a reaction intermediate (not shown in Figure 4.2).



Scheme 4.2. Metal-hydride hydrogen atom transfer (MHAT)

One representative MHAT process was reported by the Baran group (Scheme 4.3).⁶ They developed a reductive cross-coupling of olefins enabled by Fe-catalyzed MHAT. In the proposed mechanism, electron-rich or electron-neutral olefins **8** first underwent MHAT with Fe(III)-hydride **VIII** to provide alkyl radicals **X** and the Fe^{II} complex **IX**.

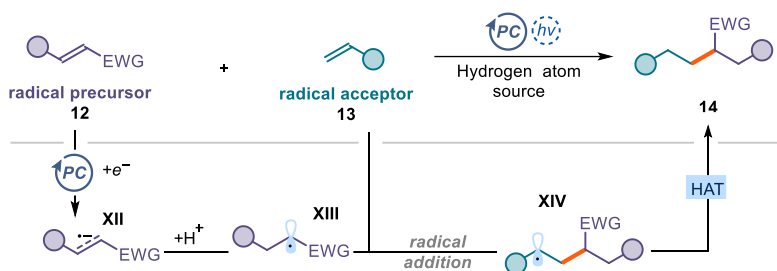


Scheme 4.3. Reductive cross-coupling of olefins enabled by Fe-catalyzed MHAT

⁶ (a) Lo, J. C.; Yabe, Y.; Baran, P. S., A Practical and Catalytic Reductive Olefin Coupling. *J. Am. Chem. Soc.* **2014**, *136*, 1304-1307; (b) Lo, J. C.; Gui, J.; Yabe, Y.; Pan, C.-M.; Baran, P. S., Functionalized olefin cross-coupling to construct carbon-carbon bonds. *Nature* **2014**, *516*, 343-348.

The Fe(III)-hydride **VIII** complex was formed by reaction of the Fe^{III} catalyst **10** with phenylsilanes. The alkyl radical **X** was then captured by the electron-poor olefin **9** to generate an electrophilic radical **XI**, which was reduced by Fe^{II} **IX** to turnover the iron catalyst while delivering the olefin-coupling product **11**. In this protocol, electron-poor olefins served as radical acceptors while electron-rich or neutral olefins as the radical precursors. Overall, an olefin reductive cross-coupling was achieved.

The process developed by Baran was synthetically appealing since it combined two olefins, which are readily available at a low cost and with a degree of diversity, to access *sp*³-hybridized products. Inspired by this work, and because of our interest in photoredox chemistry, we wondered if we could achieve a mechanistically distinct approach for the reductive cross-coupling of two olefins (Scheme 4.4). Specifically, we surmised that an excited photocatalyst could reduce an electron-poor olefins **12** to form a radical anion **XII**, which upon protonation would deliver a carbon radical α to an electron-drawing group (EWG). This radical **XIII** could then be intercepted by an electron-rich or electron-neutral olefins **13** via a radical addition path. Eventually, the ensuing radical **XIV** would be reduced by an external hydrogen donor via a hydrogen atom transfer (HAT) path to afford the desired olefin cross-coupling product **14**.



Scheme 4.4. Our working hypothesis for the reductive cross-coupling of two olefins

This transformation would offer a complementary strategy to the olefin cross-coupling developed by Baran, as the two olefins would play opposite roles in the two processes. As a result, products with different connectivity, arising from complementary disconnections, will be available.

This chapter details the successful realization of this idea. We report the design, development, synthetic implementation and mechanistic study of the reductive coupling of olefins, based on the use of electron-poor olefins as radical precursors.

In the following section, relevant methods to generate radicals from electron-poor olefins, which could engage in subsequent transformations, are discussed.

4.2 Electron-poor olefins as radical precursors

To obtain radicals from electron-poor olefins, the most conventional method is to reduce them to form the corresponding radical anions. Typically, this required the use of electrochemical systems or super stoichiometric reducing agents, such as SmI_2 or dissolved metals.⁷ However, these protocols often have practicality problems, including over-reduction, reductive dimerization, poor functional group compatibility, and limited reaction scope. To pursue a more practical and sustainable approach, a catalytic reductive system which operates under mild conditions is desirable. Visible-light photoredox catalysis⁸ has recently been proven as a useful tool for the generation of radicals, including olefin radical anions. Pioneering works⁹ have confirmed the feasibility for photoredox catalysis to achieve selective reduction of electron-poor olefins, although these photochemical methods are currently limited to specific olefins or require harsh UV-light irradiation. Recently, a few research groups¹⁰ reported the photoreduction of the

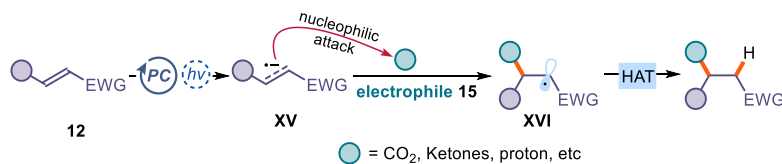
⁷ (a) R. Engels, H. J. Schäfer, Cathodic Acylation of Aryl Olefins. *Angew. Chem., Int. Ed.* **1978**, *17*, 460-460; (b) M. Fruianu, M. Marchetti, G. Melloni, G. Sanna, R. Seeber, Electrochemical reduction of 1,1-diaryl-substituted ethenes in dimethylformamide. *J. Chem. Soc., Perkin Trans.* **1994**, *2*, 2039-2044; (c) R. G. Janssen, M. Motevalli, Electroreductive coupling of vinylpyridines and vinylquinolines: radical anion-substrate cycloaddition. *Chem. Commun.*, **1998**, 539-540; (d) A. Dahlén, G. Hilmersson, Selective reduction of carbon-carbon double and triple bonds in conjugated olefins mediated by $\text{SmI}_2/\text{H}_2\text{O}/\text{amine}$ in THF. *Tetrahedron Lett.* **2003**, *44*, 2661-2664; (e) A. Baba, M. Yasuda, Y. Nishimoto, Partial Reduction of Enones, Styrenes, and Related Systems. In *Comprehensive Organic Synthesis II*, **2014**, 1673-740; (f) J. Yang, G. A. Felton, N. L. Bauld, M. J. Krische, Chemically induced anion radical cycloadditions: intramolecular cyclobutane formation of bis(enones) via homogeneous electron transfer. *J. Am. Chem. Soc.* **2004**, *126*, 1634-1635.

⁸ (a) Shaw, M. H.; Twilton, J.; MacMillan, D. W. C. Photoredox Catalysis in Organic Chemistry. *J. Org. Chem.* **2016**, *81*, 6898-6926. (b) Romero, N.; Nicewicz, D. Organic Photoredox Catalysis. *Chem. Rev.* **2016**, *116*, 10075-10166. (c) Matsui, J. K.; Lang, S. B.; Heitz, D. R.; Molander, G. A. Photoredox-mediated routes to radicals: the value of catalytic radical generation in synthetic methods development, *ACS Catal.* **2017**, *7*, 2563-2575.

⁹ (a) K. Mizuno, M. Ikeda, Y. Otsuji, Dual Regioselectivity in the Photoallylation of Electron-Deficient Alkenes by Allylic Silanes. *Chem. Lett.* **1988**, *17*, 1507-1510; (b) G. Pandey, S. Hajra, A Novel Photosystem for Harvesting Visible Light to Drive Photoinduced Electron Transfer (PET) Reductions: β -Activation of α,β -Unsaturated Ketones for Radical Cyclizations. *Angew. Chem. Int. Ed.* **1994**, *33*, 1169-1171.

¹⁰ Selected examples: (a) M. L. Czyz, M. S. Taylor, T. H. Horngren, A. Polyzos, Reductive Activation and Hydrofunctionalization of Olefins by Multiphoton Tandem Photoredox

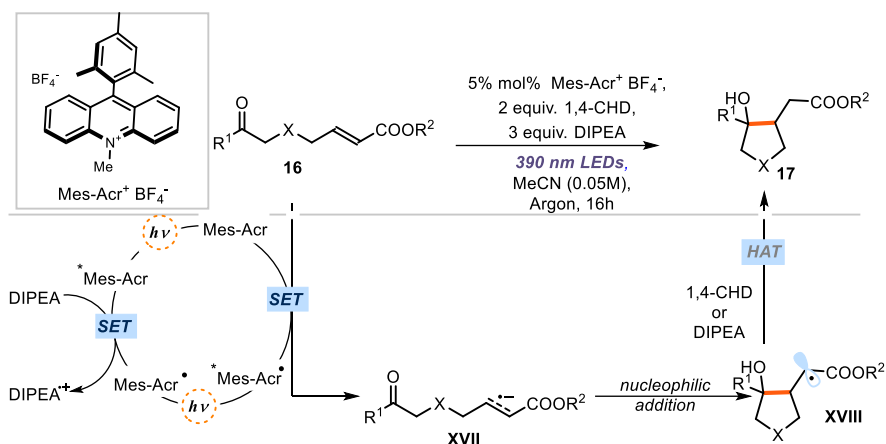
conjugated olefins **12** to the corresponding radical anions **XV** under visible-light irradiation (Scheme 4.5). The reaction of the resulting radical anion **XV** occurred at the anion site and did not capitalize on the radical reactivity. Specifically, **XV** underwent nucleophilic addition to electrophiles **15** to deliver radical **XVI**, which then engaged in subsequent steps. Overall, the new bond was formed at the β position of the EWG group.



Scheme 4.5. Photoreduction of electron-poor olefins and subsequent transformations with electrophiles **15**.

One representative example was reported the Nicewicz group in 2022 (Scheme 4.6).^{10b} In this study, the excited photocatalyst (^{*}Mes-Acr) was quenched by *N,N*-diisopropylethylamine (DIPEA), leading to the photocatalyst radical state (Mes-Acr). This species was excited by a second photon to reach the excited state (^{*}Mes-Acr), which could reduce the C-C double bond of substrate **16**, affording the radical anion **XVII**. **XVII** underwent an intramolecular nucleophilic addition to furnish radical **XVIII**, which was reduced by cyclohexa-1,4-diene (1,4-CHD) or DIPEA, delivering the final product **17**.

Catalysis. *ACS Catal.* **2021**, *11*, 5472-5480 (b) N. J. Venditto, Y. S. Liang, R. K. El Mokadem, D. A. Nicewicz, Ketone-Olefin Coupling of Aliphatic and Aromatic Carbonyls Catalyzed by Excited-State Acridine Radicals. *J. Am. Chem. Soc.* **2022**, *144*, 11888-11896; (c) T. Ju et al., Dicarboxylation of alkenes, allenes and (hetero)arenes with CO₂ via visible-light photoredox catalysis. *Nat. Catal.* **2021**, *4*, 304-311; (d) Kang, W.-J.; Li, B.; Duan, M.; Pan, G.; Sun, W.; Ding, A.; Zhang, Y.; Houk, K. N.; Guo, H., Discovery of a Thioxanthone-TfOH Complex as a Photoredox Catalyst for Hydrogenation of Alkenes Using *p*-Xylene as both Electron and Hydrogen Sources. *Angew. Chem. Int. Ed.* **2022**, *61*, e202211562.



Scheme 4.6. Ketone–olefin coupling enabled by photoreduction of arylates.

Reactions also can occur at the radical sites of the radical anions of type **XV**. In this way, electron-poor olefins are used as radical precursors. The following subchapters detail this reactivity, which can be classified depending on the type of reactive radical generated: β -radicals or α -radicals, with respect to the EWG group.

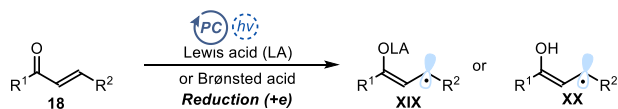
4.2.1 β -Radicals from electron-poor olefins

In the realm of radical processes, electron-poor olefins generally act as radical acceptors (to trap radicals). In contrast, there are few protocols where they served as radical precursors, which are however limited to specific α,β -unsaturated olefins (e.g. enones, modified acrylamides, and acrylates). This reductive strategy generates radicals **XIX** or **XX** that are in β position with respect to an EWG group (Scheme 4.7a).¹¹ One representative example came from the Yoon group,^{11b,11d}

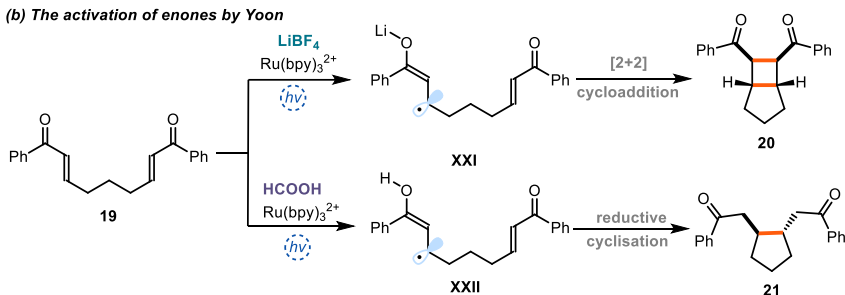
¹¹ See some selected examples: (a) Ischay, M. A.; Anzovino, M. E.; Du, J.; Yoon, T. P., Efficient Visible Light Photocatalysis of [2+2] Enone Cycloadditions. *J. Am. Chem. Soc.* **2008**, *130*, 12886-12887. (b) Du, J.; Yoon, T. P., Crossed Intermolecular [2+2] Cycloadditions of Acyclic Enones via Visible Light Photocatalysis. *J. Am. Chem. Soc.* **2009**, *131*, 14604-14605. (c) Du, J.; Espelt, L. R.; Guzei, I. A.; Yoon, T. P., Photocatalytic reductive cyclizations of enones: Divergent reactivity of photogenerated radical and radical anion intermediates. *Chem. Sci.* **2011**, *2*, 2115-2119. (d) Betori, R. C.; Scheidt, K. A., Reductive Arylation of Arylidene Malonates Using Photoredox Catalysis. *ACS Catal.* **2019**, *9* (11), 10350-10357. (f) Betori, R. C.; McDonald, B. R.; Scheidt, K. A., Reductive annulations of arylidene malonates with unsaturated electrophiles using photoredox/Lewis acid cooperative catalysis. *Chem. Sci.* **2019**, *10*, 3353-3359. (f) Kong, M.; Tan, Y.; Zhao, X.; Qiao, B.; Tan, C.-H.; Cao, S.; Jiang, Z., Catalytic Reductive Cross Coupling and Enantioselective Protonation of Olefins to Construct Remote Stereocenters for Azaarenes. *J. Am. Chem. Soc.* **2021**, *143*, 4024-4031. (g) Li, Y.; Han, C.; Wang, Y.; Huang, X.;

describing the intramolecular cyclization of enones (Scheme 4.7b). More specifically, enone **19** could undergo single-electron transfer (SET) reduction to deliver the β -radical **XXI** under Lewis acid activation, or β -radical **XXII** under Brønsted acid activation. These radicals then engaged in intramolecular addition to afford products **20** or **21**, respectively.

(a) Carbonyl compounds activation by Lewis acid or Brønsted acid



(b) The activation of enones by Yoon

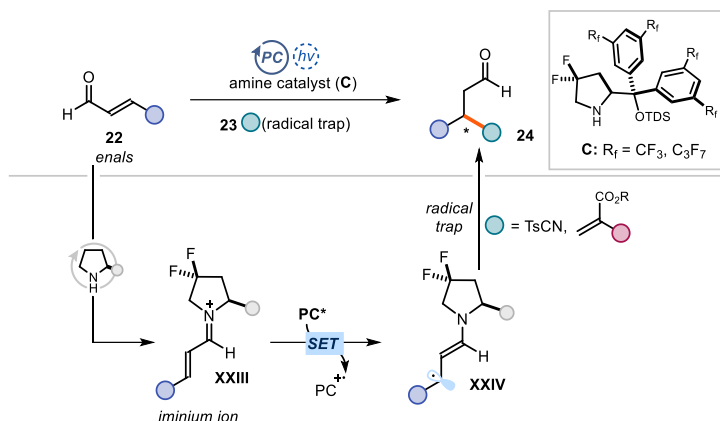


Scheme 4.7. (a) Generation of β -carbon radicals via photoreduction of electron-poor olefins enabled by Lewis acid or Brønsted acid activation; (b) activation of enones to generate β -carbon radicals reported by Yoon.

Recently, our research group developed the asymmetric β -functionalization of aliphatic enals combining amine catalysis and photoredox chemistry (Scheme 4.8).¹²

Zhao, X.; Qiao, B.; Jiang, Z., Catalytic Asymmetric Reductive Azaarylation of Olefins via Enantioselective Radical Coupling. *J. Am. Chem. Soc.* **2022**, *144*, 7805-7814. (h) Yuan, W.; Zhou, Z.; Gong, L.; Meggers, E., Asymmetric alkylation of remote C(sp³)-H bonds by combining proton-coupled electron transfer with chiral Lewis acid catalysis. *Chem. Comm.* **2017**, *53*, 8964-8967. (i) Zhou, Z.; Li, Y.; Han, B.; Gong, L.; Meggers, E., Enantioselective catalytic β -amination through proton-coupled electron transfer followed by stereocontrolled radical-radical coupling. *Chem. Sci.* **2017**, *8*, 5757-5763; (j) Huang, X.; Luo, S.; Burghaus, O.; Webster, R. D.; Harms, K.; Meggers, E., Combining the catalytic enantioselective reaction of visible-light-generated radicals with a by-product utilization system. *Chem. Sci.* **2017**, *8*, 7126-7131; see also ref. 10b.

¹² Berger, M.; Ma, D.; Baumgartner, Y.; Wong, T. H.-F.; Melchiorre, P., Stereoselective conjugate cyanation of enals by combining photoredox and organocatalysis. *Nat. Catal.* **2023**, *6*, 332-338.



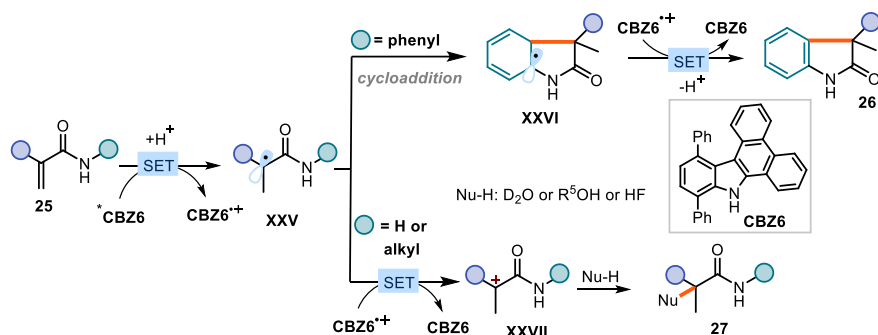
Scheme 4.8. The generation of β -radicals via SET reduction of enals enabled by amine catalysis

In this case, the chiral amine catalyst **C** activated enals **22** to provide the ground-state electron-poor iminium ion **XXIII**, which was reduced by an external excited photocatalyst (PC^*) to form the β -radical **XXIV**. This radical was intercepted by the radical trap **23** (e.g. tosyl cyanide or acrylate) to afford the chiral product **24** with high stereocontrol.

4.2.2 α -Radicals from electron-poor olefins

Few examples have been reported for the generation of radicals at the α position of EWG groups, achieved by SET reduction of electron-poor olefins.¹³ The first example was reported in 2020 by the Kang group^{13a,b} (Scheme 4.9), establishing the formation of α -position radical from α -substituted acrylamides **25** under photoreducing conditions. Photocatalyst **CBZ6** was used to reduce acrylamides **25** under acidic condition, yielding the α -position radical **XXV** upon protonation of the radical anion (not shown). When **25** was a phenyl-substituent (green circle in Scheme 4.9), this radical could cyclize to form radical **XXVI**, which was oxidized by the **CBZ6** radical cation to deliver the final product **26**.

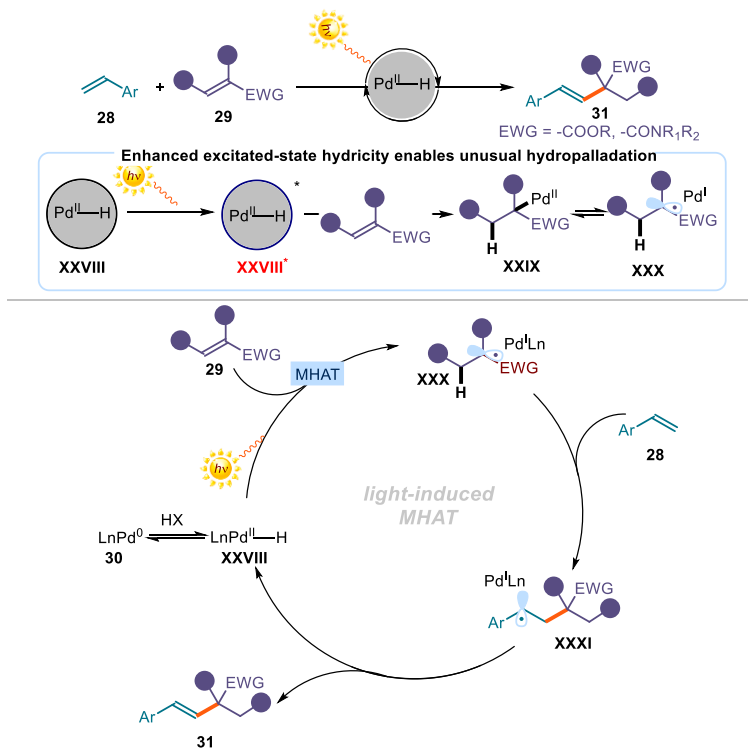
¹³ (a) Luan, Z.-H.; Qu, J.-P.; Kang, Y.-B., Discovery of Oxygen α -Nucleophilic Addition to α,β -Unsaturated Amides Catalyzed by Redox-Neutral Organic Photoreductant. *J. Am. Chem. Soc.* **2020**, *142*, 20942-20947; (b) Cai, X.-P.; Han, B.-H.; Cen, F.-T.; Qu, J.-P.; Kang, Y.-B., Endo/Exo-Controllable Photocyclization by EnT-SET-Switch. *Org. Lett.* **2023**, *25*, 2863-2867; (c) Sarkar, S.; Ghosh, S.; Kurandina, D.; Noffel, Y.; Gevorgyan, V., Enhanced Excited-State Hydricity of Pd-H Allows for Unusual Head-to-Tail Hydroalkenylation of Alkenes. *J. Am. Chem. Soc.* **2023**, *145*, 12224-12232.



Scheme 4.9. The generation of α -position radicals from photoreduction of acrylamides enabled by **CBZ6**.

When **25** was substituted with an alkyl group or H (green circle in Scheme 4.9), radical **XXV** was first oxidized by the **CBZ6** radical cation to produce cation **XXVII**, which was then attacked by nucleophiles (e.g. D_2O , alcohols, and HF) to form product **27**.

Recently, another strategy to generate α -position radicals upon olefin reduction was reported by Gevorgyan,^{13c} who developed an unusual head-to-tail hydroalkenylation of styrene **28** (Scheme 4.8). In this chemistry, a Pd(0) species **30** and a Brønsted acid (HX) could react to afford a palladium-hydride **XXVIII** upon oxidative addition, which was unable to undergo MHAT with electron-poor olefins **29** in the ground state. It was proposed that light irradiation could bring **XXVIII** to the excited state **XXVIII***, which increased its hydricity, promoting an unusual hydropalladation of **29** to provide intermediate **XXIX**. A Pd–C bond homolysis led to the hybrid Pd(I) alkyl radical **XXX**, which was captured by styrene **28** to deliver another Pd(I) alkyl radical **XXXI**. Upon β -H elimination, the final product **31** was formed while regenerating the palladium-hydride species **XXVIII**. This protocol offered a novel pathway to generate α -radicals from electron-poor olefins, which complemented the previous MHAT strategy. However, the electron-poor olefins were mainly limited to acrylates and acrylamides, while only styrene could be used as the radical trap.



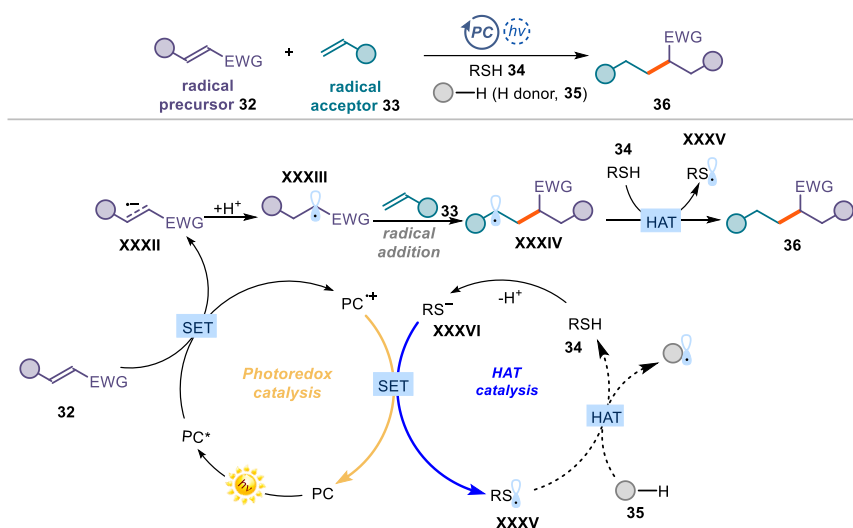
Scheme 4.10. Generation of α -radicals from acrylates and acrylamides enabled by photoinduced MHAT

Overall, the reported methodologies have established the feasibility to form radicals from electron-poor olefins using photoredox catalysis, although the examples remained sparse and limited in scope.

4.3 Target and design of the project

The current study was motivated by our interest in generating radicals by using photoredox chemistry. The target was to develop a photocatalytic strategy to generate radicals from a variety of electron-poor olefins and react them with electron-neutral or electron-rich olefins (Scheme 4.11). Specifically, this new methodology could realize the reductive coupling of two olefins capitalizing on their different electronic properties. We envisaged that electron-poor olefins **32** would be more prone to SET reduction by an excited photocatalyst (PC^*) than the electron-neutral or electron-rich olefins **33**. We reasoned that the ensuing radical anion **XXXII** would require a protonation to afford the target α -radical **XXXIII**. We considered thiols **34** as suitable compounds, as they can act both as a proton

source and hydrogen atom transfer (HAT) reagents.^{14,15} Our choice was also informed by the fact that a HAT process between radical **XXXIII** and thiol **34** is polar-mismatched.^{14b} Then, the α -radical **XXXIII** could be trapped by the acceptor olefin **33** to generate another radical **XXXIV**. This latter radical, being nucleophilic in nature, would be polarity-matched with the thiol **34**.



Scheme 4.11. Design plan for the reductive olefin coupling using the combination of photoredox and HAT catalysis.

The resulting abstraction of a hydrogen atom would therefore be feasible, leading to the reductive olefin coupling product **36** and thiyl radical **XXXV**. Meanwhile, thiol **34** or thiolate **XXXVI** could be oxidized by the oxidized photocatalyst (PC) while giving the thiyl radical **XXXV**. This system

¹⁴ See some reviews about thiyl radical in HAT: (a) Dénès, F.; Pichowicz, M.; Povie, G.; Renaud, P., Thiyl Radicals in Organic Synthesis. *Chem. Rev.* **2014**, *114*, 2587-2693; (b) Capaldo, L.; Ravelli, D.; Fagnoni, M., Direct Photocatalyzed Hydrogen Atom Transfer (HAT) for Aliphatic C–H Bonds Elaboration. *Chem. Rev.* **2022**, *122*, 1875-1924; (c) Patehebieke, Y., An overview on disulfide-catalyzed and -cocatalyzed photoreactions. *Beilstein J. Org. Chem.* **2020**, *16*, 1418-1435.

¹⁵ See some selected examples using thiols as HAT reagent: (a) Wang, Y.; Carder, H. M.; Wendlandt, A. E., Synthesis of rare sugar isomers through site-selective epimerization. *Nature* **2020**, *578*, 403-408; (b) Loh, Y. Y.; Nagao, K.; Hoover, A. J.; Hesk, D.; Rivera, N. R.; Colletti, S. L.; Davies, I. W.; MacMillan, D. W. C., Photoredox-catalyzed deuteration and tritiation of pharmaceutical compounds. *Science* **2017**, *358*, 1182-1187; (c) Margrey, K. A.; Nicewicz, D. A., A General Approach to Catalytic Alkene Anti-Markovnikov Hydrofunctionalization Reactions via Acridinium Photoredox Catalysis. *Acc. Chem. Res.* **2016**, *49*, 1997-2006; (d) Erchinger, J. E.; Hoogesteger, R.; Laskar, R.; Dutta, S.; Hümpel, C.; Rana, D.; Daniluc, C. G.; Glorius, F., EnT-Mediated N–S Bond Homolysis of a Bifunctional Reagent Leading to Aliphatic Sulfonyl Fluorides. *J. Am. Chem. Soc.* **2023**, *145*, 2364-2374.

could use either a stoichiometric thiol or a catalytic thiol and a different hydrogen atom donor **35** (e.g. γ -terpinene or cyclohexadiene) in the presence of catalytic thiol acting as the HAT catalyst. In the latter case, the generated thiyl radical **XXXV** may abstract a hydrogen atom from H donor **35** to turnover the thiol catalytic cycle.

4.4 Results and discussion

We started our exploration by using dimethyl fumarate **32a** as the radical precursor and styrene **33a** as the radical acceptor. The experiments were performed in 1,2-dichloroethane (DCE) as solvent in the presence of γ -terpinene as H donor (2.0 equiv.) and thiophenol (20 mol.%) as the HAT catalyst. Irradiation was provided by an EvoluChem lamp (λ_{\max} = 450-455 nm).

Table 4.1. Optimization studies.

	photocatalysts	HAT catalysts	H donor	entry	PC	deviation	yield (%) ^a
		 HAT A	 H donor I (1,3-Cyclohexadiene)	1	a	-	95 (83)
				2	b	-	13
		 HAT B	 H donor II (γ -terpinene)	3	a	HAT B	
				4	a	HAT C	18
		 HAT C		5	a	H donor I	83
				6 ^b	a	No H donor	6
				7	a	No HAT catalyst	0
				8	a	No light	0
				9	-	-	0
				10 ^c	a	TEMPO	0

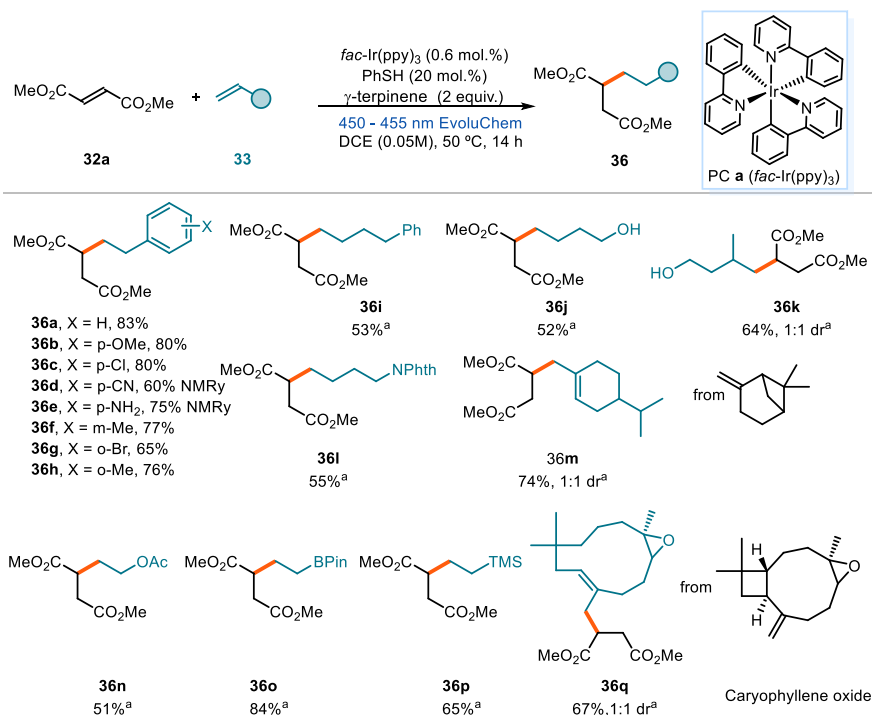
Reactions performed on a 0.1 mmol scale using 1 equiv. of styrene **33a** and 1.5 equiv. of dimethyl fumarate **32a** under illumination by a 450 - 455 nm EvoluChem. ^aYield of **36a** determined by GC-FID analysis of the crude reaction mixture using 1,3,5-trimethoxybenzene as the internal standard. Yields of isolated **36a** are reported in parentheses. ^b Performed using 2 equiv. of HAT **A**. ^c Using 1.5 equiv. of TEMPO.

First, we tested the highly reducing photoredox catalysts **a** and **b**. The iridium-based photocatalyst **a** delivered the reductive coupling product **36a** in better yield (entries 1-2). Different H donors and HAT catalysts were screened (entries 3-5), which identified γ -terpinene as the best performing H donor and thiophenol **A** as the best HAT catalyst (20 mol%). When using stoichiometric thiophenol **A** in the absence of additional H donors (entry 6), product **36a** was obtained in low amount

because of competitive thiol-ene and sulfa-Michael processes. Control experiments established that the presence of H donor, HAT catalyst, light and photocatalyst was essential for reactivity (entries 7-9). When adding the radical scavenger TEMPO under the best reaction conditions, the reactivity was completely inhibited, suggesting that a radical path was operative.

4.4.1 Generality of the protocol

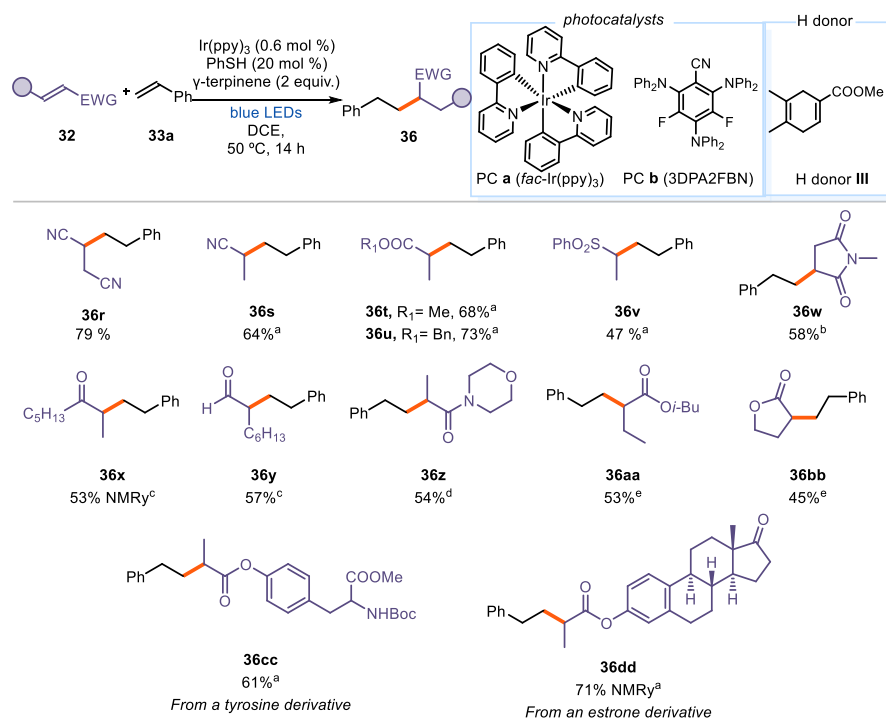
With the optimized conditions in hand (entry 1 in table 4.1), we investigated the scope of the radical acceptor olefins using fumarate **32a** as the radical precursor (Scheme 4.12). Styrenes with different substitution at the *para*-position afforded the coupling products **36b-e** in satisfying yield. Also *ortho* and *meta*-substituted styrenes were competent substrates (adducts **36f-h**). Non-activated terminal olefins bearing aliphatic substituents were suitable for this cross-coupling process, affording the corresponding products **36i-36l** in good yields.



Scheme 4.12. Substrate scope of the acceptor olefins. Reactions performed on a 0.2 mmol scale; yields refer to the isolated products **36**. ^aPerformed using PC **a** (0.3 mol.%), an excess of **33** (3 equiv.), HAT **C** (20 mol.%) and γ -terpinene (1 equiv.); N-Phth: phthalimide; Ac: acetyl; Bpin: bis(pinacolato)boron; TMS: trimethylsilyl.

A variety of functional groups were well tolerated, including a free alcohol (adduct **36j** and **36k**). When β -pinene was used as the substrate, the ring-opening product **36m** was obtained in good yield, which supported the intermediacy of a radical in the process. Electron-rich (vinyl acetate) and heteroatom functionalized olefins were also reactive under our reaction conditions, affording products **36n-36p**. Our methodology was also suitable for the late-stage functionalization of pharmaceuticals bearing an olefin moiety (*Caryophyllene oxide*, adduct **36r**).

Next, we evaluated the scope of the reductive olefin cross-coupling protocol reacting different electron-poor olefins with styrene **33a** (Scheme 4.13). Fumaronitrile could be used as radical precursor to afford product **36r** in high yield.

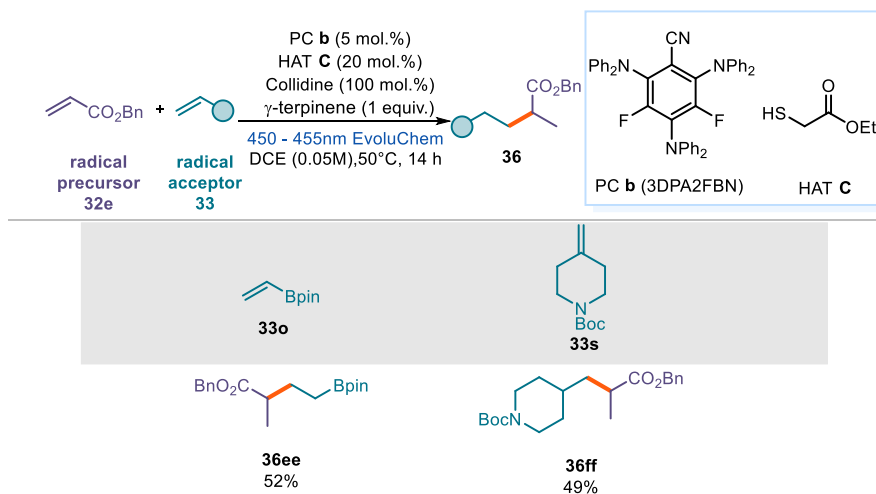


Scheme 4.13. Substrate scope of the electron-poor olefins as the radical precursors. Reactions performed on a 0.2 mmol scale using PC **a** (0.6 mol.%), PhSH (20 mol. %) and γ -terpinene (3.0 equiv.); yields refer to isolated products **36**. ^aPerformed using PC **b** (5.0 mol.%), and 2,4,6-collidine (100 mol.%); ^bPerformed using PC **a** (0.6 mol.%), HAT **B** (20 mol.%) and H donor **III** (2 equiv.); ^cPerformed using PC **b** (5.0 mol.%), HAT **B** (20 mol.%) and H donor **III** (3 equiv.); ^dPerformed using PC **a** (1.5 mol.%), HAT **B** (20 mol.%) and H donor **III** (3 equiv.); ^ePerformed using PC **a** (1.5 mol. %), Cs₂CO₃(100 mol.%), and ACN (0.05 M). Ph: phenyl; Bn: benzyl; *i*-Bu: isobutyl.

We found that the addition of a weak base (2,4,6-collidine) was useful to react less activated electron-poor olefins: acrylonitrile, acrylate and vinylsulfone delivered the corresponding products **36s-v** in moderate to good yield.

Using the optimal conditions (with and w/o base), we noticed that the reactions of *N*-methyl maleimide, methyl vinyl ketone, enal, and acrylamide were plagued by the formation of the corresponding reduced products. We surmised that this undesired path arose from the ability of the electrophilic radical **XXXIII** (Scheme 4.10) to abstract a hydrogen atom from the H donor (γ -terpinene), thus leading to the reduced byproduct. To bypass this side reaction, we used a more acidic thiol (HAT **B**) and a more electrophilic H donor (H donor **III**). Under those conditions, the target products **36w-z** were obtained in decent yields. This protocol was also effective for internal and cyclic acrylates (adducts **36aa-bb**). Furthermore, bio-relevant molecule-derived acrylates were applied to our coupling method (**36cc-dd**).

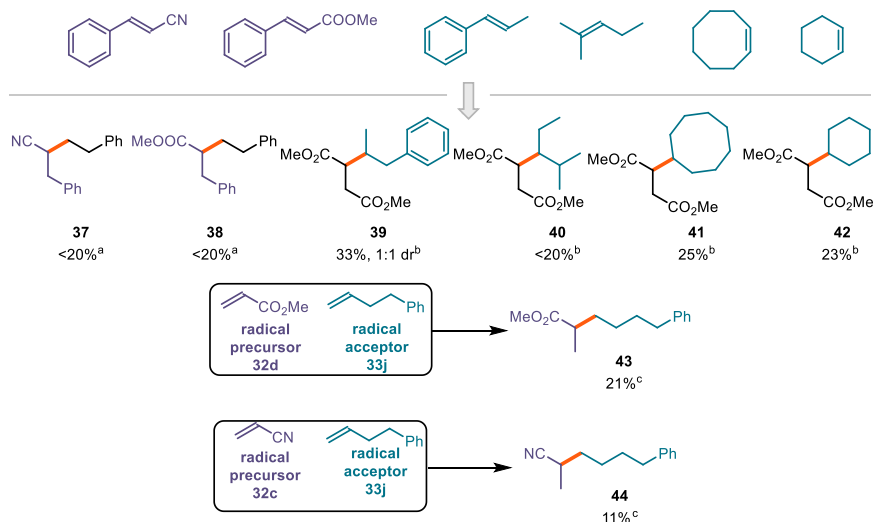
To expand the utility of our methodology (Scheme 4.14), we also investigated the reactivity of less activated electron-poor olefins (e.g., benzyl acrylate) and other radical acceptor olefins than styrenes, which delivered adducts **36ee** and **36ff** in moderate yield.



Scheme 4.14. Expanding the substrate scope. Reactions performed on a 0.2 mmol scale; yields refer to isolated products **36**.

Some substrates were not suitable for our methodology. These limitations in scope are depicted in Scheme 4.15. β -Phenyl substituted electron-poor olefins delivered the cross-coupling products **37** and **38** only in low yield (< 20%), mainly because of a competitive [2+2] photocycloaddition path (among two olefins, formed in ~

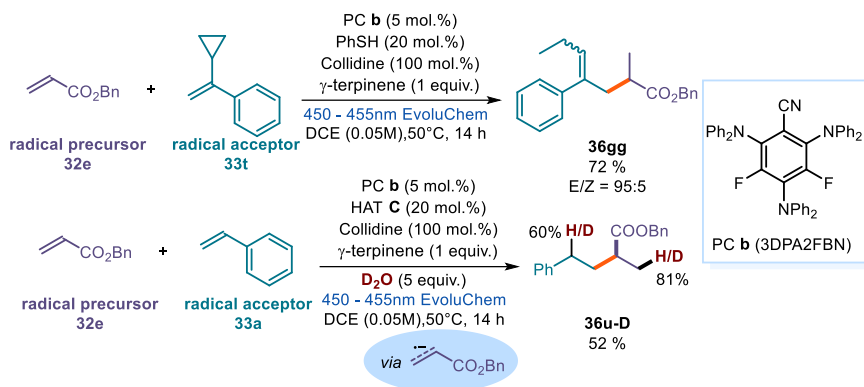
60% yield). For the radical acceptor olefins, internal olefins (products **39-42**) were poorly reactive, probably because of steric hindrance. More challenging coupling partner (**32c** and **33j**, **32b** and **33j**) were tested, but all offered the desired product in low yield (**43** and **44**).



Scheme 4.15. Moderately successful and unsuccessful substrates. Reactions performed on a 0.2 mmol scale. ^aPerformed using PC **b** (5.0 mol.%), PhSH (20 mol. %) and γ -terpinene (3.0 equiv.); ^bPerformed using PC **a** (0.3 mol.%), HAT **C** (20 mol. %) and γ -terpinene (1.0 equiv.); ^cPerformed using PC **b** (5.0 mol.%), HAT **C** (20 mol. %), 2,4,6-collidine (100 mol.%) and γ -terpinene (1.0 equiv.); yields determined by ¹H NMR analysis of the crude reaction mixtures using dibromomethane as the internal standard.

4.4.2 Mechanistic investigations

A radical probe experiment was performed using a cyclopropyl-containing olefin **33**, which provided the ring-opening product **36gg** in good yield (Scheme 4.16). This result further indicated that a radical was generated from the electron-poor olefin and then trapped by another olefin.



Scheme 4.16. Mechanistic studies: radical probe and deuterium labeling experiments

Also D_2O was subjected to the reaction conditions, yielding the deuterated product **36u-D** in 52% and with 81% of deuterium incorporation at β position and/or 60% at benzylic position. This hinted that the electron-poor olefins were reduced and protonated to form the α -EWG radical and thiols quench the radical **XXXIV** (Scheme 4.11).

We also conducted Stern–Volmer quenching studies of the excited photocatalyst **PC-a** using fumarate **32a** as the quencher (Figure 4.2). Experimentally, a 1.5×10^{-6} M solution of **PC-a** in thoroughly degassed DCE was used.

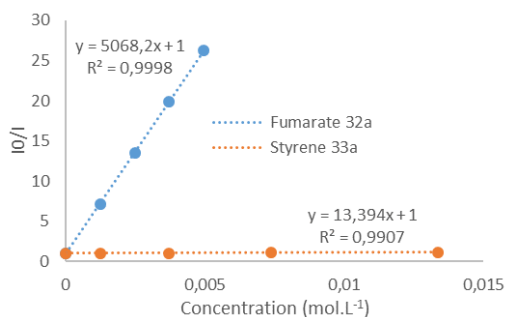


Figure 4.2. Stern–Volmer luminescence quenching studies of *fac*-Ir(ppy)₃ with dimethyl fumarate **32a** and styrene **33a**.

PC-a displayed an emission maximum at 513 nm when excited with 440 nm light (see experimental section). Sequential addition of a solution of **32a** caused a decrease in emission intensity. The Stern–Volmer plot was constructed (orange line in Figure 4.2), which showed a linear correlation between I_0/I and **[32a]**. From this data, a Stern–Volmer constant $K_{SV} = 5068.2 \text{ M}^{-1}$ was determined. A quenching constant $k_q = 2.7 \cdot 10^9 \text{ M}^{-1}\cdot\text{s}^{-1}$ was calculated considering the lifetime of **PC-a** in

the excited state (1.9 μs).¹⁶ Styrene **33a** was much less effective at quenching than fumarate **32a** (orange line in Figure 4.2 for styrene **33a**, see also experimental section for quenching studies with other components). This observation supported our proposed mechanism that the excited photocatalyst is quenched by the electron-poor electron olefins.

4.5 Conclusions

In summary, we have developed a photoredox protocol to reduce electron-poor olefins and generate α -EWG radicals. Our method encompasses a variety of olefins as radical precursors, including unsaturated ester, carbonyl, amide, cyano and sulfone. The generated radicals were coupled with styrenes and non-activated olefins. Overall, a reductive cross-coupling of two olefins was achieved. We also highlighted how the method's high functional group tolerance could be advantageous for the radical functionalization of substrates bearing different functional groups, including free hydroxyl and amide groups, and for applications in the late-stage elaboration of biorelevant compounds. Mechanistic experiments, including Stern-Volmer quenching study, supported our proposal.

¹⁶ Wu, Y.; Kim, D.; Teets, T. S. "Photophysical Properties and Redox Potentials of Photosensitizers for Organic Photoredox Transformations" *Synlett* **2022**, *33*, 1154.

4.6 Experimental section

General Information

The NMR spectra were recorded at 400 MHz and 500 MHz for ^1H and 100 or 125 MHz for ^{13}C . The chemical shift (δ) for ^1H and ^{13}C are given in ppm relative to residual signals of the solvents (CHCl_3 @ 7.26 ppm ^1H NMR, CDCl_3 @ 77.16 ppm ^{13}C NMR, and tetramethylsilane @ 0 ppm). Coupling constants are given in Hertz. The following abbreviations are used to indicate the multiplicity: s, singlet; d, doublet; q, quartet; m, multiplet; bs, broad signal; app, apparent.

High resolution mass spectra (HRMS) were obtained from the ICIQ HRMS unit on MicroTOF Focus and Maxis Impact (Bruker Daltonics) with electrospray ionization. (ESI).

UV-vis measurements were carried out on a Shimadzu UV-2401PC spectrophotometer equipped with photomultiplier detector, double beam optics and D₂ and W light sources or an Agilent Cary60 spectrophotometer.

Isolated yields refer to materials of >95% purity as determined by ^1H NMR analysis.

The team of the Research Support Area at ICIQ, particularly the NMR and the High-Resolution Mass Spectrometry Units, is thanked for their support.

General Procedures. All reactions were set up under an argon atmosphere in oven-dried glassware. Synthesis grade solvents were used as purchased; anhydrous solvents were taken from a commercial SPS solvent dispenser. Chromatographic purification of products was accomplished using forced-flow chromatography (FC) on silica gel (230-400 mesh). For thin layer chromatography (TLC) analysis throughout this work, Merck pre-coated TLC plates (silica gel 60 GF₂₅₄, 0.25 mm) were employed, using UV light as the visualizing agent and an acidic mixture of vanillin, basic aqueous potassium permanganate (KMnO_4) or phosphomolybdic acid (PMA, ethanol solution) as stain solutions, and heat as developing agents. Organic solutions were concentrated under reduced pressure on a Büchi rotatory evaporator.

Materials. Most of the starting materials used in this study are commercial and were purchased at the highest purity available from Sigma-Aldrich, Fluka, Alfa Aesar, Fluorochem, TCI, and used as received, without further purifications.

Photocatalyst **b** (3DPA2FBN) and H donor III were synthesized according to the reported procedure.^{17,18}

4.6.1 Experimental Setup

All reactions performed using an EvoluChem™ P303-30-1 LEDs (18 W, $\lambda_{\text{max}}=450-455$ nm, 0.5-1 cm away– Figure 4.3), a fan was used to cool down the reactor (the reaction temperature within the reaction vessel was measured to be between 45-55 °C, setup depicted in Figure 4.3).



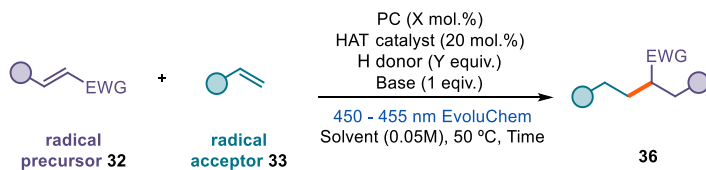
Figure 4.3: Photoreactor.

4.6.2 General procedures

Stock solution preparation of *fac*-Ir(ppy)₃: To an oven-dried 2-dram vial, 4.0 mg of *fac*-Ir(ppy)₃ were added. The vial was sealed with a septum, evacuated and backfilled with argon three times, and 4.0 ml of degassed DCE were added. The resulting suspension was sonicated for 10-15 minutes until complete dissolution and used the same day as prepared.

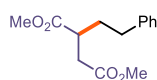
¹⁷ Askey, H. E.; Grayson, J. D.; Tibbetts, J. D.; Turner-Dore, J. C.; Holmes, J. M.; Kociok-Kohn, G.; Wrigley, G. L.; Cresswell, A. J., Photocatalytic Hydroaminoalkylation of Styrenes with Unprotected Primary Alkylamines. *J. Am. Chem. Soc.* **2021**, *143*, 15936-15945.

¹⁸ Agudo, R.; Roiban, G.-D.; Reetz, M. T., Achieving Regio- and Enantioselectivity of P450-Catalyzed Oxidative CH Activation of Small Functionalized Molecules by Structure-Guided Directed Evolution. *ChemBioChem* **2012**, *13*, 1465-1473.



To an oven dried vial with a Teflon septum screw cap, containing a dry Teflon stir bar, photocatalyst, photocatalyst (if 3DPA2FBN), olefin substrates **32** and **33** (if solid) and bases (if solid and needed) were added. The vial was sealed with a Teflon septum screw cap, evacuated and backfilled with argon three times, and the solvent was added. Then photocatalyst stock solution (if *fac*-Ir(ppy)₃), HAT catalyst, H donor, olefin substrates **32** and **33** (if liquid) and bases (if liquid and needed) were added sequentially. The vial was then placed in the photoreactor (Figure 4.3) and irradiated under stirring for 6 hours (if radical acceptors are styrenes) or 14 hours, unless otherwise specified. Then the solvent was evaporated and the crude mixture purified by flash column chromatography on silica gel to furnish the target product **36**.

4.6.3 Characterization of Products

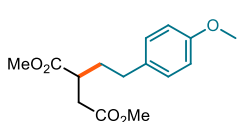


dimethyl 2-phenethylsuccinate (36a): Synthesized according to General Procedure (*fac*-Ir(ppy)₃ (0.8 mg, 0.6 mol. %), PhSH (4.1 μL, 0.04 mmol, 20 mol. %) and γ -terpinene (64.1 μL, 0.4 mmol, 2 equiv.)) using dimethyl fumarate **32a** (43.2 mg, 0.3 mmol, 1.5 equiv.) and styrene **33a** (22.9 μL, 0.2 mmol, 1 equiv.). The crude mixture was purified by flash column chromatography on silica gel (10% EtOAc in hexanes as eluent) to afford **36a** (41.7 mg, 83% yield) as a light-yellow oil.

¹H NMR (500 MHz, CDCl₃) δ 7.30 – 7.26 (m, 2H), 7.21 – 7.17 (m, 2H), 7.17 – 7.16 (m, 1H), 3.71 (s, 3H), 3.67 (s, 3H), 2.94 – 2.87 (m, 1H), 2.77 (dd, *J* = 16.5, 9.1 Hz, 1H), 2.69 – 2.58 (m, 2H), 2.49 (dd, *J* = 16.5, 5.3 Hz, 1H), 2.00 (dddd, *J* = 13.7, 9.4, 7.8, 6.5 Hz, 1H), 1.83 (dddd, *J* = 13.7, 9.4, 6.8, 6.0 Hz, 1H).

¹³C NMR (126 MHz, CDCl₃) δ 175.3, 172.3, 141.2, 128.6, 128.5, 126.2, 52.0, 51.9, 40.9, 36.0, 33.7, 33.3.

Matching reported literature data.¹⁹



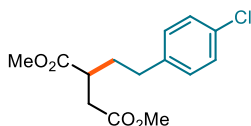
dimethyl 2-(4-methoxyphenethyl)succinate (36b):

Synthesized according to General Procedure (*fac*-Ir(ppy)₃ (0.8 mg, 0.6 mol. %), PhSH (4.1 μL, 0.04 mmol, 20 mol. %) and γ-terpinene (64.1 μL, 0.4 mmol, 2 equiv.)) using dimethyl fumarate **32a** (43.2 mg, 0.3 mmol, 1.5 equiv.) and 4-methoxystyrene **33b** (26.6 μL, 0.2 mmol, 1 equiv.). The crude mixture was purified by flash column chromatography on silica gel (10% EtOAc in hexanes as eluent) to afford **36b** (44.8 mg, 80% yield) as a light-yellow oil.

¹H NMR (500 MHz, CDCl₃) δ 7.10 – 7.06 (m, 2H), 6.84 – 6.80 (m, 2H), 3.78 (s, 3H), 3.70 (s, 3H), 3.66 (s, 3H), 2.87 (dddd, *J* = 9.2, 7.7, 6.0, 5.2 Hz, 1H), 2.75 (dd, *J* = 16.5, 9.2 Hz, 1H), 2.62 – 2.52 (m, 2H), 2.47 (dd, *J* = 16.5, 5.2 Hz, 1H), 1.95 (dddd, *J* = 13.7, 9.2, 7.8, 6.7 Hz, 1H), 1.78 (dddd, *J* = 13.7, 9.2, 6.9, 6.0 Hz, 1H).

¹³C NMR (126 MHz, CDCl₃) δ 175.3, 172.4, 158.1, 133.2, 129.4, 114.0, 55.4, 52.0, 51.9, 40.8, 36.0, 33.9, 32.4.

HRMS: (ESI⁺) calculated for C₁₅H₂₀NaO₅⁺ [*M*+Na⁺]: 303.1203, found 303.1210.



dimethyl 2-(4-chlorophenethyl)succinate (36c):

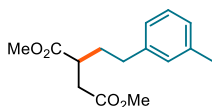
Synthesized according to General Procedure (*fac*-Ir(ppy)₃ (0.8 mg, 0.6 mol. %), PhSH (4.1 μL, 0.04 mmol, 20 mol. %) and γ-terpinene (64.1 μL, 0.4 mmol, 2 equiv.)) using dimethyl fumarate **32a** (43.2 mg, 0.3 mmol, 1.5 equiv.) and 4-chlorostyrene **33c** (25.4 μL, 0.2 mmol, 1 equiv.). The crude mixture was purified by flash column chromatography on silica gel (9% to 11% EtOAc in hexanes as eluent) to afford **36c** (45.8 mg, 80% yield) as a colorless oil.

¹H NMR (500 MHz, CDCl₃) δ 7.26 – 7.22 (m, 2H), 7.11 – 7.08 (m, 2H), 3.70 (s, 3H), 3.66 (s, 3H), 2.86 (ddt, *J* = 8.9, 7.9, 5.6 Hz, 1H), 2.75 (dd, *J* = 16.5, 8.9 Hz, 1H), 2.66 – 2.53 (m, 2H), 2.47 (dd, *J* = 16.5, 5.4 Hz, 1H), 1.96 (dddd, *J* = 13.7, 9.4, 8.0, 6.3 Hz, 1H), 1.79 (dddd, *J* = 13.7, 9.5, 6.8, 5.8 Hz, 1H).

¹³C NMR (126 MHz, CDCl₃) δ 175.1, 172.2, 139.6, 132.0, 129.9, 128.7, 52.1, 52.0, 40.8, 36.0, 33.5, 32.7.

¹⁹ Fini, F.; Beltrani, M.; Mancuso, R.; Gabriele, B.; Carfagna, C., Selective Aryl α-Diimine/Palladium-Catalyzed Bis-Alkoxy- carbonylation of Olefins for the Synthesis of Substituted Succinic Diesters. *Adv. Synth. Catal.* **2015**, *357*, 177-184.

HRMS: (ESI⁺) calculated for C₁₄H₁₇ClNaO₄⁺ [M+Na⁺]: 307.0708, found 307.0711.



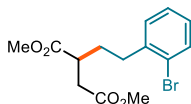
dimethyl 2-(3-methylphenethyl)succinate (36f):

Synthesized according to General Procedure (*fac*-Ir(ppy)₃ (0.8 mg, 0.6 mol. %), PhSH (4.1 μL, 0.04 mmol, 20 mol. %) and γ-terpinene (64.1 μL, 0.4 mmol, 2 equiv.)) using dimethyl fumarate **32a** (43.2 mg, 0.3 mmol, 1.5 equiv.) and 3-methylstyrene **33f** (26.6 μL, 0.2 mmol, 1 equiv.). The crude mixture was purified by flash column chromatography on silica gel (6% to 9% EtOAc in hexanes as eluent) to afford **36f** (40.7 mg, 77% yield) as a yellowish oil.

¹H NMR (500 MHz, CDCl₃) δ 7.19 – 7.15 (m, 1H), 7.03 – 6.95 (m, 3H), 3.72 (s, 3H), 3.67 (s, 3H), 2.93 – 2.87 (m, 1H), 2.77 (dd, *J* = 16.5, 9.2 Hz, 1H), 2.65 – 2.54 (m, 2H), 2.49 (dd, *J* = 16.5, 5.2 Hz, 1H), 2.33 (s, 3H), 1.98 (dddd, *J* = 13.7, 9.5, 7.7, 6.6 Hz, 1H), 1.82 (dddd, *J* = 13.7, 9.5, 6.8, 6.0 Hz, 1H).

¹³C NMR (126 MHz, CDCl₃) δ 175.3, 172.4, 141.1, 138.1, 129.3, 128.5, 127.0, 125.5, 52.0, 51.9, 41.0, 36.0, 33.8, 33.3, 21.5.

HRMS: (ESI⁺) calculated for C₁₅H₂₀NaO₄⁺ [M+Na⁺]: 287.1254, found 287.1264.



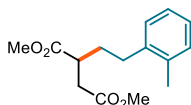
dimethyl 2-(2-bromophenethyl)succinate (36g):

Synthesized according to General Procedure (*fac*-Ir(ppy)₃ (0.8 mg, 0.6 mol. %), PhSH (4.1 μL, 0.04 mmol, 20 mol. %) and γ-terpinene (64.1 μL, 0.4 mmol, 2 equiv.)) using dimethyl fumarate **32a** (43.2 mg, 0.3 mmol, 1.5 equiv.) and 2-bromostyrene **33g** (25.1 μL, 0.2 mmol, 1 equiv.). The crude mixture was purified by flash column chromatography on silica gel (8% EtOAc in hexanes as eluent) to afford **36g** (43.1 mg, 65% yield) as a yellowish oil.

¹H NMR (500 MHz, CDCl₃) δ 7.52 – 7.50 (m, 1H), 7.25 – 7.19 (m, 2H), 7.08 – 7.03 (m, 1H), 3.73 (s, 3H), 3.68 (s, 3H), 2.97 – 2.91 (m, 1H), 2.80 (dd, *J* = 16.6, 9.2 Hz, 1H), 2.79 – 2.69 (m, 2H), 2.53 (dd, *J* = 16.6, 5.3 Hz, 1H), 1.95 (dddd, *J* = 13.6, 10.3, 7.5, 6.1 Hz, 1H), 1.88 – 1.80 (m, 1H).

¹³C NMR (126 MHz, CDCl₃) δ 175.1, 172.4, 140.5, 133.0, 130.5, 128.0, 127.7, 124.4, 52.1, 52.0, 41.0, 35.9, 33.7, 32.1.

HRMS: (ESI⁺) calculated for C₁₄H₁₇BrNaO₄⁺ [M+Na⁺]: 351.0202, found 351.0214.

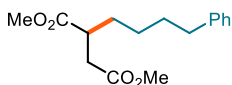
**dimethyl 2-(2-methylphenethyl)succinate (36h):**

Synthesized according to General Procedure (*fac*-Ir(ppy)₃ (0.8 mg, 0.6 mol. %), PhSH (4.1 μL, 0.04 mmol, 20 mol. %) and γ -terpinene (64.1 μL, 0.4 mmol, 2 equiv.)) using dimethyl fumarate **32a** (43.2 mg, 0.3 mmol, 1.5 equiv.) and 2-methylstyrene **33h** (25.9 μL, 0.2 mmol, 1 equiv.). The crude mixture was purified by flash column chromatography on silica gel (6% to 9% EtOAc in hexanes as eluent) to afford **36h** (40.1 mg, 76% yield) as a colorless oil.

¹H NMR (500 MHz, CDCl₃) δ 7.15 – 7.09 (m, 4H), 3.73 (s, 3H), 3.68 (s, 3H), 2.95 (ddt, J = 8.9, 7.7, 5.6 Hz, 1H), 2.80 (dd, J = 16.5, 8.9 Hz, 1H), 2.68 – 2.54 (m, 2H), 2.51 (dd, J = 16.6, 5.5 Hz, 1H), 2.29 (s, 3H), 1.92 (dddd, J = 13.6, 10.6, 7.7, 6.1 Hz, 1H), 1.84 – 1.73 (m, 1H).

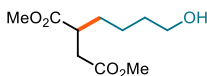
¹³C NMR (126 MHz, CDCl₃) δ 175.2, 172.4, 139.4, 135.9, 130.4, 128.9, 126.4, 126.2, 52.0, 51.9, 41.3, 36.0, 32.5, 30.8, 19.2.

HRMS: (ESI⁺) calculated for C₁₅H₂₀NaO₄⁺ [M+Na⁺]: 287.1254, found 287.1256.

**dimethyl-2-(4-phenylbutyl)succinate (36 i):** Synthesized according to General Procedure (*fac*-Ir(ppy)₃ (0.4 mg, 0.3 mol. %), HAT **C** (Ethyl thioglycolate, 4.4 μL, 0.04 mmol, 20 mol. %) and γ -terpinene (32.0 μL, 0.2 mmol, 1 equiv.)) using dimethyl fumarate **32a** (28.8 mg, 0.2 mmol, 1 equiv.) and 4-Phenyl-1-butene **33i** (90.1 μL, 0.6 mmol, 3 equiv.). The crude mixture was purified by flash column chromatography on silica gel (3% EtOAc in hexanes as eluent) to afford **36i** (29.5 mg, 53 % yield) as a colorless oil.

¹H NMR (400 MHz, CDCl₃) δ 7.33 – 7.26 (m, 2H), 7.22 – 7.15 (m, 3H), 3.72 (s, 3H), 3.69 (s, 3H), 2.91 – 2.81 (m, 1H), 2.73 (dd, J = 16.5, 9.3 Hz, 1H), 2.66 – 2.58 (m, 2H), 2.44 (dd, J = 16.5, 5.1 Hz, 1H), 1.73 – 1.56 (m, 4H), 1.43 – 1.30 (m, 2H).

¹³C NMR (101 MHz, CDCl₃) δ 175.6, 172.6, 142.4, 128.5, 128.4, 125.9, 51.9, 51.9, 41.2, 35.9, 35.7, 31.8, 31.2, 26.6.

**dimethyl-2-(4-hydroxybutyl)succinate (36 j):** Synthesized according to General Procedure (*fac*-Ir(ppy)₃ (0.4 mg, 0.3 mol. %), HAT **C** (Ethyl thioglycolate, 4.4 μL, 0.04 mmol, 20 mol. %) and γ -terpinene (32.0 μL, 0.2 mmol, 1 equiv.)) using dimethyl fumarate **32a** (28.8 mg, 0.2 mmol, 1 equiv.) and 3-Buten-1-ol **33j** (51.6 μL, 0.6 mmol, 3 equiv.). The crude

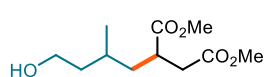
crude mixture was purified by flash column chromatography on silica gel (3% EtOAc in hexanes as eluent) to afford **36j** (29.5 mg, 53 % yield) as a colorless oil.

mixture was purified by flash column chromatography on silica gel (50% EtOAc in hexanes as eluent) to afford **36j** (22.7 mg, 52 % yield) as a colorless oil.

^1H NMR (400 MHz, CDCl_3) δ 3.72 (s, 3H), 3.69 (s, 3H), 3.65 (t, $J = 6.4$ Hz, 2H), 2.93 – 2.84 (m, 1H), 2.74 (dd, $J = 16.5, 9.1$ Hz, 1H), 2.49 (d, $J = 5.3$ Hz, 1H), 1.78 – 1.65 (m, 2H), 1.58 (dtdd, $J = 14.7, 6.0, 4.7, 2.1$ Hz, 3H), 1.46 – 1.41 (m, 1H).

^{13}C NMR (101 MHz, CDCl_3) δ 175.4, 172.5, 62.6, 52.0, 51.9, 41.2, 35.9, 32.5, 31.7, 23.3.

HRMS: (ESI $^+$) calculated for $\text{C}_{10}\text{H}_{18}\text{NaO}_5^+$ [$\text{M}+\text{Na}^+$]: 241.1046, found 241.1043.



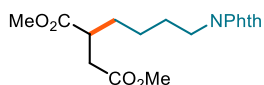
dimethyl 2-(4-hydroxy-2-methylbutyl)succinate

(36k): Synthesized according to General Procedure (*fac*-Ir(ppy) $_3$ (0.4 mg, 0.3 mol. %), PhSH (4.1 μL , 0.04 mmol, 20 mol. %) and γ -terpinene (32.1 μL , 0.2 mmol, 1 equiv.)) using dimethyl fumarate **32a** (28.8 mg, 0.3 mmol, 1.0 equiv.) and 3-methyl-3-buten-1-ol **33k** (60.8 μL , 0.6 mmol, 3 equiv.). The crude mixture was purified by flash column chromatography on silica gel (17% to 50% EtOAc in hexanes as eluent) to afford **36k** (29.9 mg, 64% yield, 1:1 dr) as a colorless oil.

^1H NMR (500 MHz, CDCl_3 , mixture of diastereomers) δ 3.68 (s, 6H), 3.72 – 3.59 (m, 4H), 3.65 (s, 3H), 3.65 (s, 3H), 2.96 – 2.87 (m, 2H), 2.69 (dd, $J = 16.5, 8.7$ Hz, 1H), 2.66 (dd, $J = 16.7, 9.3$ Hz, 1H), 2.44 (dd, $J = 16.6, 5.0$ Hz, 1H), 2.42 (dd, $J = 16.5, 5.7$ Hz, 1H), 1.71 (ddd, $J = 13.9, 9.4, 4.8$ Hz, 1H), 1.66 – 1.49 (m, 5H), 1.47 – 1.34 (m, 3H), 1.21 (ddd, $J = 13.5, 8.8, 5.4$ Hz, 1H), 0.93 (d, $J = 6.5$ Hz, 3H), 0.90 (d, $J = 6.5$ Hz, 3H).

^{13}C NMR (126 MHz, CDCl_3 , mixture of diastereomers) δ 175.8, 175.8, 172.5, 172.4, 60.7, 60.6, 52.0, 52.0, 51.9, 51.9, 39.8, 39.4, 39.4, 39.3, 39.2, 39.2, 36.8, 35.9, 27.6, 27.4, 19.6, 19.6.

HRMS: (ESI $^+$) calculated for $\text{C}_{11}\text{H}_{20}\text{NaO}_5^+$ [$\text{M}+\text{Na}^+$]: 255.1203, found 255.1205.



dimethyl 2-(4-(1,3-dioxoisindolin-2-

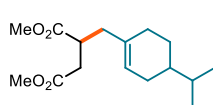
yl)butyl)succinate (36l): Synthesized according to General Procedure (*fac*-Ir(ppy) $_3$ (0.4 mg, 0.3 mol. %), HAT C (Ethyl thioglycolate, 4.4 μL , 0.04 mmol, 20 mol. %) and γ -terpinene (32.0 μL , 0.2 mmol, 1 equiv.)) using dimethyl fumarate **32a** (28.8 mg, 0.2 mmol, 1 equiv.) and 2-(but-3-en-1-yl)isoindoline-1,3-dione **33l** (120.7 mg, 0.6 mmol, 3 equiv.). The crude mixture was purified by flash column chromatography on silica

gel (40% EtOAc in hexanes as eluent) to afford **36l** (38.2 mg, 55 % yield) as a white solid.

$^1\text{H NMR}$ (500 MHz, CDCl_3) δ 7.83 (dd, $J = 5.4, 3.0$ Hz, 2H), 7.71 (dd, $J = 5.5, 3.0$ Hz, 2H), 3.68 – 3.65 (m, 8H), 2.83 (dddd, $J = 9.2, 7.5, 6.2, 5.2$ Hz, 1H), 2.71 (dd, $J = 16.6, 9.1$ Hz, 1H), 2.42 (dd, $J = 16.6, 5.2$ Hz, 1H), 1.73 – 1.65 (m, 3H), 1.60 – 1.51 (m, 1H), 1.35 (p, $J = 8.5$ Hz, 2H).

$^{13}\text{C NMR}$ (101 MHz, CDCl_3) δ 175.3, 172.4, 168.5, 134.0, 132.2, 123.3, 51.9, 51.9, 41.1, 37.7, 35.9, 31.4, 28.4, 24.3.

HRMS: (ESI⁺) calculated for $\text{C}_{18}\text{H}_{21}\text{NNaO}_6^+$ [$\text{M}+\text{Na}^+$]: 370.1261, found 370.1265.

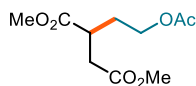


dimethyl 2-((4-isopropylcyclohex-1-en-1-yl)methyl)succinate (36m): Synthesized according to General Procedure (*fac*-Ir(ppy)₃ (0.4 mg, 0.3 mol. %), PhSH (4.1 μL , 0.04 mmol, 20 mol. %) and γ -terpinene (32.1 μL , 0.2 mmol, 1 equiv.)) using dimethyl fumarate **32a** (28.8 mg, 0.3 mmol, 1.0 equiv.) and (-)-beta-pinene **33m** (93.7 μL , 0.6 mmol, 3 equiv.). The crude mixture was purified by flash column chromatography on silica gel (6% EtOAc in hexanes as eluent) to afford **36m** (41.9 mg, 74% yield, 1:1 dr) as a colorless oil.

$^1\text{H NMR}$ (500 MHz, CDCl_3 , mixture of diastereomers) δ 5.43 – 5.39 (m, 2H), 3.67 (s, 3H), 3.66 (s, 3H), 3.65 (s, 6H), 3.02 – 2.95 (m, 2H), 2.64 (dd, $J = 16.9, 9.5$ Hz, 1H), 2.61 (dd, $J = 16.9, 9.8$ Hz, 1H), 2.41 (dd, $J = 16.9, 4.8$ Hz, 1H), 2.40 (dd, $J = 16.9, 5.0$ Hz, 1H), 2.36 – 2.28 (m, 2H), 2.11 – 2.03 (m, 2H), 2.03 – 1.88 (m, 6H), 1.79 – 1.64 (m, 4H), 1.48 – 1.39 (m, 2H), 1.23 – 1.12 (m, 4H), 0.88 – 0.84 (m, 12H).

$^{13}\text{C NMR}$ (126 MHz, CDCl_3 , mixture of diastereomers) δ 175.6, 175.5, 172.8, 172.7, 134.0, 133.9, 124.8, 124.7, 51.9, 51.9, 51.8, 51.8, 40.5, 40.2, 40.1, 40.0, 39.8, 39.6, 35.4, 35.1, 32.3, 32.3, 29.1, 29.1, 28.6, 28.5, 26.5, 26.4, 20.1, 20.0, 19.8, 19.8.

HRMS: (ESI⁺) calculated for $\text{C}_{16}\text{H}_{26}\text{NaO}_4^+$ [$\text{M}+\text{Na}^+$]: 305.1723, found 305.1728.

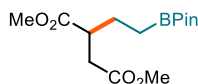


dimethyl 2-(2-acetoxyethyl)succinate (36n): Synthesized according to General Procedure (*fac*-Ir(ppy)₃ (0.4 mg, 0.3 mol. %), HAT C (Ethyl thioglycolate, 4.4 μL , 0.04 mmol, 20 mol. %) and γ -terpinene (32.0 μL , 0.2 mmol, 1 equiv.)) using dimethyl fumarate **32a** (28.8 mg, 0.2 mmol, 1 equiv.) and vinyl acetate **33n** (55.3 μL , 0.6 mmol, 3 equiv.). The crude mixture was purified by flash column chromatography on silica gel (10% EtOAc in hexanes as eluent) to afford **36n** (23.7 mg, 51 % yield) as a colorless oil.

¹H NMR (400 MHz, CDCl₃) δ 4.11 (t, *J* = 6.3 Hz, 2H), 3.71 (s, 3H), 3.68 (s, 3H), 3.02 – 2.93 (m, 1H), 2.76 (dd, *J* = 16.6, 8.7 Hz, 1H), 2.51 (dd, *J* = 16.7, 5.6 Hz, 1H), 2.07 – 1.98(m, 4H), 1.90 – 1.8 (m, 1H).

¹³C NMR (101 MHz, CDCl₃) δ 174.7, 172.1, 171.0, 62.0, 52.2, 52.0, 38.4, 35.7, 30.6, 21.0.

HRMS: (ESI⁺) calculated for C₁₀H₁₆NaO₆⁺ [M+Na⁺]: 255.0839, found 255.0838.

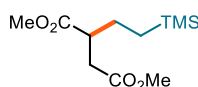


dimethyl-2-(2-(4,4,5,5-tetramethyl-1,3,2-dioxaborolan-2-yl)ethyl)succinate (36o) : Synthesized according to General Procedure (*fac*-Ir(ppy)₃ (0.4 mg, 0.3 mol. %), HAT C (Ethyl thioglycolate, 4.4 μL, 0.04 mmol, 20 mol. %) and γ-terpinene (32.0 μL, 0.2 mmol, 1 equiv.)) using dimethyl fumarate **32a** (28.8 mg, 0.2 mmol, 1 equiv.) and vinylboronic acid pinacol ester **33o** (101.8 μL, 0.6 mmol, 3 equiv.). The crude mixture was purified by flash column chromatography on silica gel (20% EtOAc in hexanes as eluent) to afford **36o** (50.4 mg, 84 % yield) as a colorless oil.

¹H NMR (500 MHz, CDCl₃) δ 3.69 (s, 3H), δ 3.67 (s, 3H), 2.83 (dddd, *J* = 9.6, 7.5, 6.5, 4.7 Hz, 1H), 2.71 (dd, *J* = 16.6, 9.7 Hz, 1H), 2.44 (dd, *J* = 16.6, 4.8 Hz, 1H), 1.79 – 1.69 (m, 1H), 1.69 – 1.62 (m, 1H), 1.24 (s, 12H), 0.77 (d, *J* = 8.0 Hz, 2H).

¹³C NMR (126 MHz, CDCl₃) δ 175.5, 172.6, 83.3, 51.8, 43.1, 35.7, 29.8, 26.6, 24.9.

HRMS: (ESI⁺) calculated for C₁₄H₂₅NaO₆B⁺ [M+Na⁺]: 322.1673, found 322.1664.

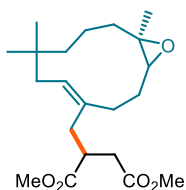


dimethyl-2-(2-(trimethylsilyl)ethyl)succinate (36p): Synthesized according to General Procedure (*fac*-Ir(ppy)₃ (0.4 mg, 0.3 mol. %), HAT C (Ethyl thioglycolate, 4.4 μL, 0.04 mmol, 20 mol. %) and γ-terpinene (32.0 μL, 0.2 mmol, 1 equiv.)) using dimethyl fumarate **32a** (28.8 mg, 0.2 mmol, 1 equiv.) and vinyltrimethylsilane **33p** (87.9 μL, 0.6 mmol, 3 equiv.). The crude mixture was purified by flash column chromatography on silica gel (2% EtOAc in hexanes as eluent) to afford **36p** (32.0 mg, 65 % yield) as a colorless oil.

¹H NMR (400 MHz, CDCl₃) δ 3.70 (s, 3H), 3.67 (s, 3H), 2.87 – 2.78 (m, 1H), 2.71 (dd, *J* = 16.3, 9.3 Hz, 1H), 2.45 (dd, *J* = 16.3, 5.0 Hz, 1H), 1.68 – 1.58 (m, 1H), 1.56 – 1.48 (m, 1H), 0.51 – 0.41 (m, 2H), -0.02 (s, 9H).

¹³C NMR (126 MHz, CDCl₃) δ 175.5, 172.7, 51.9, 51.8, 44.0, 35.4, 26.6, 13.7, -1.7.

HRMS: (ESI⁺) calculated for C₁₁H₂₂NaO₄Si⁺ [M+Na⁺]: 269.1180, found 269.1177.



dimethyl

2-(((11R,Z)-7,7,11-trimethyl-12-

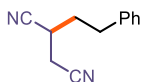
oxabicyclo[9.1.0]dodec-4-en-4-yl)methyl)succinate (**36q**):

Synthesized according to General Procedure (*fac*-Ir(ppy)₃ (0.4 mg, 0.3 mol. %), HAT C (Ethyl thioglycolate, 4.4 μL, 0.04 mmol, 20 mol. %) and γ -terpinene (32.1 μL, 0.2 mmol, 1 equiv.)) using dimethyl fumarate **32a** (28.8 mg, 0.3 mmol, 1.0 equiv.) and (–)-Caryophyllene oxide **33q** (132.2 mg, 0.6 mmol, 3 equiv.). The crude mixture was purified by flash column chromatography on silica gel (6% to 20% EtOAc in hexanes as eluent) to afford **36q** (48.8 mg, 67% yield, 1:1 dr) as a colorless oil and (–)-Caryophyllene oxide (88.6 mg, 0.4 mmol).

¹H NMR (500 MHz, CDCl₃, mixture of diastereomers) δ 5.35 (dd, J = 11.3, 2.4 Hz, 1H), 5.30 (dd, J = 11.3, 2.5 Hz, 1H), 3.70 (s, 3H), 3.65 (s, 3H), 3.64 (s, 3H), 3.64 (s, 3H), 2.93 (dddd, J = 8.9, 8.2, 6.6, 5.7 Hz, 1H), 2.89 – 2.83 (m, 1H), 2.74 (dd, J = 6.8, 1.8 Hz, 1H), 2.72 (dd, J = 6.8, 2.1 Hz, 1H), 2.70 (dd, J = 16.8, 8.9 Hz, 1H), 2.59 (dd, J = 16.8, 9.5 Hz, 1H), 2.56 (dd, J = 13.8, 8.5 Hz, 1H), 2.43 (dd, J = 16.7, 5.7 Hz, 1H), 2.43 (dd, J = 16.9, 4.6 Hz, 1H), 2.37 – 2.27 (m, 3H), 2.23– 2.14 (m, 3H), 2.13 – 2.07 (m, 2H), 2.05 – 1.91 (m, 5H), 1.67 – 1.57 (m, 2H), 1.51 – 1.34 (m, 4H), 1.23 – 1.12 (m, 4H), 1.15 (s, 6H), 0.92 (d, J = 0.6 Hz, 3H), 0.91 (d, J = 0.6 Hz, 3H), 0.84 (s, 3H), 0.83 (s, 3H), 0.80 – 0.73 (m, 4H).

¹³C NMR (126 MHz, CDCl₃, mixture of diastereomers) δ 175.3, 174.8, 172.5, 172.3, 134.1, 134.0, 127.9, 127.4, 62.8, 62.8, 62.7, 62.7, 52.2, 52.0, 51.9, 51.8, 40.8, 40.8, 40.3 (2C), 38.5, 38.5, 37.4, 37.2, 35.8, 35.5, 34.8, 34.7, 33.2, 33.2, 31.0, 30.6, 29.6, 29.6, 28.3 (2C), 24.6, 24.5, 18.5, 18.4, 18.0 (2C).

HRMS: (ESI⁺) calculated for C₂₁H₃₄NaO₅⁺ [$M+Na^+$]: 389.2298, found 389.2308.



2-phenethylsuccinonitrile (36r): Synthesized according to General Procedure (*fac*-Ir(ppy)₃ (0.8 mg, 0.6 mol. %), PhSH (4.1 μL, 0.04 mmol, 20 mol. %) and γ -terpinene (64.1 μL, 0.4 mmol, 2

equiv.)) using fumaronitrile **32b** (23.4 mg, 0.3 mmol, 1.5 equiv.) and styrene **33a** (22.9 μL, 0.2 mmol, 1 equiv.). The crude mixture was purified by flash column chromatography on silica gel (10% EtOAc in hexanes as eluent) to afford **36r** (29.1 mg, 79% yield) as a light-yellow oil.

¹H NMR (500 MHz, CDCl₃) δ 7.36 – 7.31 (m, 2H), 7.28 – 7.24 (m, 1H), 7.24 – 7.19 (m, 2H), 2.97 (ddd, J = 13.7, 8.2, 5.2 Hz, 1H), 2.87 – 2.76 (m, 2H), 2.75 – 2.65 (m, 2H), 2.20 – 2.10 (m, 1H), 2.06 (dtd, J = 13.5, 8.2, 5.2 Hz, 1H).

^{13}C NMR (126 MHz, CDCl_3) δ 138.8, 129.0, 128.5, 127.0, 118.7, 115.4, 33.2, 32.8, 27.7, 21.2.

Matching reported literature data.²⁰

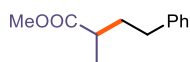


2-methyl-4-phenylbutanenitrile (36s): Synthesized according to General Procedure (3DPA2FBN (6.4 mg, 5.0 mol. %), PhSH (4.1 μL , 0.04 mmol, 20 mol. %), 2,4,6-collidine (26.4 μL , 0.2 mmol, 1 equiv.) and γ -terpinene (96.2 μL , 0.6 mmol, 3 equiv.)) using acrylonitrile **32c** (13.1 μL , 0.2 mmol, 1 equiv.) and styrene **33a** (68.7 μL , 0.6 mmol, 3 equiv.). The crude mixture was purified by flash column chromatography on silica gel (2% EtOAc in hexanes as eluent) to afford **36s** (20.4 mg, 64% yield) as a colorless oil.

^1H NMR (500 MHz, CDCl_3) δ 7.33 – 7.28 (m, 2H), 7.24 – 7.18 (m, 3H), 2.88 (ddd, $J = 14.3, 9.1, 5.4$ Hz, 1H), 2.80 – 2.71 (m, 1H), 2.64 – 2.53 (m, 1H), 1.99 – 1.92 (m, 1H), 1.84 (dddd, $J = 13.6, 9.1, 7.5, 5.5$ Hz, 1H), 1.34 (d, $J = 7.1$ Hz, 3H).

^{13}C NMR (126 MHz, CDCl_3) δ 140.2, 128.7, 128.5, 126.5, 122.1, 35.8, 33.3, 24.9, 18.1.

Matching reported literature data.²¹



methyl-2-methyl-4-phenylbutanoate (36t): Synthesized according to General Procedure (3DPA2FBN (6.4 mg, 5.0 mol. %), PhSH (4.1 μL , 0.04 mmol, 20 mol. %), 2,4,6-collidine (26.4 μL , 0.2 mmol, 1 equiv.) and γ -terpinene (96.2 μL , 0.6 mmol, 3 equiv.)) using methyl acrylate **32d** (18.1 μL , 0.2 mmol, 1 equiv.) and styrene **33a** (68.7 μL , 0.6 mmol, 3 equiv.). The crude mixture was purified by flash column chromatography on silica gel (2% EtOAc in hexanes as eluent) to afford **36t** (26.1 mg, 68% yield) as a colorless oil.

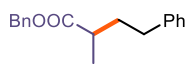
^1H NMR (400 MHz, CDCl_3) δ 7.31 – 7.27 (m, 2H), 7.22 – 7.16 (m, 3H), 3.68 (s, 3H), 2.62 (t, $J = 8.0$ Hz, 2H), 2.54 – 2.44 (m, 1H), 2.09 – 1.96 (m, 1H), 1.79 – 1.68 (m, 1H), 1.20 (d, $J = 7.0$ Hz, 3H).

^{13}C NMR (101 MHz, CDCl_3) δ 177.1, 141.7, 128.5, 128.5, 126.0, 51.6, 39.0, 35.5, 33.6, 17.2.

²⁰ Zhang, Y.; Han, Y.; Zhu, S.; Qing, F.-L.; Xue, X.-S.; Chu, L., Light-Induced Divergent Cyanation of Alkynes Enabled by Phosphorus Radicals. *Angew. Chem., Int. Ed.* **2022**, *61*, e202210838.

²¹ Gaspar, B.; Carreira, E. M., Mild Cobalt-Catalyzed Hydrocyanation of Olefins with Tosyl Cyanide. *Angew. Chem., Int. Ed.* **2007**, *46*, 4519-4522.

Matching reported literature data.³



benzyl-2-methyl-4-phenylbutanoate (36u): Synthesized according to General Procedure (3DPA2FBN (6.4 mg, 5.0 mol. %), PhSH (4.1 μ L, 0.04 mmol, 20 mol. %), 2,4,6-collidine (26.4 μ L, 0.2 mmol, 1 equiv.) and γ -terpinene (96.2 μ L, 0.6 mmol, 3 equiv.)) using benzyl acrylate **32e** (30.6 μ L, 0.2 mmol, 1 equiv.) and styrene **33a** (68.7 μ L, 0.6 mmol, 3 equiv.). The crude mixture was purified by flash column chromatography on silica gel (2% EtOAc in hexanes as eluent) to afford **36u** (39.2 mg, 73% yield) as a colorless oil. ¹H NMR (500 MHz, CDCl₃) δ 7.38 – 7.35 (m, 4H), 7.35 – 7.31 (m, 1H), 7.28 – 7.25 (m, 2H), 7.20 – 7.16 (m, 1H), 7.15 – 7.11 (m, 2H), 5.13 (s, 2H), 2.60 (t, J = 8.0 Hz, 2H), 2.56 – 2.52 (m, 1H), 2.08 – 1.99 (m, 1H), 1.78 – 1.71 (m, 1H), 1.22 (d, J = 7.0 Hz, 3H).

¹³C NMR (126 MHz, CDCl₃) δ 176.4, 141.7, 136.3, 128.7, 128.5, 128.5, 128.3, 128.2, 126.0, 66.2, 39.2, 35.5, 33.5, 17.2.

Matching reported literature data.²²



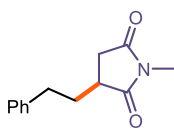
((4-phenylbutan-2-yl)sulfonyl)benzene (36v): Synthesized according to General Procedure (3DPA2FBN (6.4 mg, 5.0 mol. %), PhSH (4.1 μ L, 0.04 mmol, 20 mol. %), 2,4,6-collidine (26.4 μ L, 0.2 mmol, 1 equiv.) and γ -terpinene (96.2 μ L, 0.6 mmol, 3 equiv.)) using phenyl vinyl sulfone **32f** (33.6 mg, 0.2 mmol, 1 equiv.) and styrene **33a** (68.7 μ L, 0.6 mmol, 3 equiv.). The crude mixture was purified by flash column chromatography on silica gel (2% EtOAc in hexanes as eluent) to afford **36v** (25.8 mg, 47% yield) as a white solid.

¹H NMR (400 MHz, CDCl₃) δ 7.90 – 7.84 (m, 2H), 7.69 – 7.63 (m, 1H), 7.59 – 7.53 (m, 2H), 7.32 – 7.26 (m, 2H), 7.25 – 7.19 (m, 1H), 7.15 – 7.10 (m, 2H), 3.05 (dtd, J = 13.7, 6.8, 3.8 Hz, 1H), 2.84 (ddd, J = 14.3, 9.4, 5.3 Hz, 1H), 2.62 (ddd, J = 13.9, 9.0, 7.4 Hz, 1H), 2.34 (dddd, J = 13.4, 9.4, 7.4, 3.8 Hz, 1H), 1.82 – 1.68 (m, 1H), 1.34 (d, J = 6.9 Hz, 3H).

²² Ren, W.; Wang, M.; Guo, J.; Zhou, J.; Chu, J.; Shi, Y.; Shi, Y., Pd-Catalyzed Regioselective Branched Hydrocarboxylation of Terminal Olefins with Formic Acid. *Org. Lett.* **2022**, *24*, 886-891.

^{13}C NMR (101 MHz, CDCl_3) δ 140.1, 137.2, 133.6, 129.1, 128.9, 128.5, 128.3, 126.3, 59.1, 32.4, 30.7, 13.2.

Matching reported literature data.²³



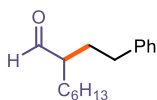
1-methyl-3-phenethylpyrrolidine-2,5-dione (36w):

Synthesized according to General Procedure (3DPA2FBN (6.4 mg, 5.0 mol. %), HAT **B** (3,5-bis(trifluoromethyl)benzenethiol, 6.7 μL , 0.04 mmol, 20 mol. %), and H donor **1** (methyl 4,5-dimethylcyclohexa-1,4-diene-1-carboxylate, 64.0 μL , 0.4 mmol, 2 equiv.)) using *N*-Methylmaleimide **32g** (22.2 mg, 0.2 mmol, 1 equiv.) and styrene **33a** (68.7 μL , 0.6 mmol, 3 equiv.). The crude mixture was purified by flash column chromatography on silica gel (20% EtOAc in hexanes as eluent) to afford **36w** (25.2 mg, 58% yield) as a white solid.

^1H NMR (300 MHz, CDCl_3) δ 7.32 – 7.26 (m, 2H), 7.24 – 7.15 (m, 3H), 2.97 (s, 3H), 2.88 – 2.65 (m, 4H), 2.44 – 2.35 (m, 1H), 2.27 (dtt, $J = 11.8, 7.0, 2.3$ Hz, 1H), 1.82 (dtd, $J = 13.6, 8.7, 6.3$ Hz, 1H).

^{13}C NMR (101 MHz, CDCl_3) δ 180.0, 176.7, 140.4, 128.7, 128.6, 126.5, 39.3, 34.6, 33.2, 33.1, 24.9.

Matching reported literature data.²⁴



2-phenethyloctanal (36y): Synthesized according to General

Procedure (3DPA2FBN (6.4 mg, 5.0 mol. %), HAT **B** (3,5-bis(trifluoromethyl)benzenethiol, 6.7 μL , 0.04 mmol, 20 mol. %), and H donor **1** (methyl 4,5-dimethylcyclohexa-1,4-diene-1-carboxylate, 96.0 μL , 0.6 mmol, 3 equiv.)) using *trans*-2-Octenal **32i** (89.5 μL , 0.6 mmol, 3 equiv.) and styrene **33a** (22.9 μL , 0.2 mmol, 1 equiv.). The crude mixture was purified by flash column chromatography on silica gel (25% DCM in hexanes as eluent) to afford **36y** (26.5 mg, 57% yield) as a colorless oil.

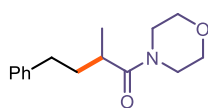
²³ Schoenebeck, F.; Murphy, J. A.; Zhou, S.-z.; Uenoyama, Y.; Miclo, Y.; Tuttle, T., Reductive Cleavage of Sulfones and Sulfonamides by a Neutral Organic Super-Electron-Donor (S.E.D.) Reagent. *J. Am. Chem. Soc.* **2007**, *129*, 13368-13369.

²⁴ Sharma, S.; Han, S. H.; Jo, H.; Han, S.; Mishra, N. K.; Choi, M.; Jeong, T.; Park, J.; Kim, I. S., Rhodium-Catalyzed Vinylic C–H Functionalization of Enol Carbamates with Maleimides. *Eur. J. Org. Chem.* **2016**, *2016*, 3611-3618.

^1H NMR (500 MHz, CDCl_3) δ 9.60 (d, $J = 2.9$ Hz, 1H), 7.31 – 7.27 (m, 2H), 7.22 – 7.15 (m, 3H), 2.68 – 2.55 (m, 2H), 2.29 (ttd, $J = 8.1, 5.4, 2.8$ Hz, 1H), 2.01 – 1.93 (m, 1H), 1.79 – 1.71 (m, 1H), 1.69 – 1.63 (m, 1H), 1.53 – 1.45 (m, 1H), 1.31 – 1.25 (m, 9H), 0.89 – 0.86 (m, 3H).

^{13}C NMR (126 MHz, CDCl_3) δ 205.3, 141.6, 128.6, 128.5, 126.2, 51.4, 33.4, 31.7, 30.6, 29.4, 29.0, 27.0, 22.7, 14.1.

Matching reported literature data.²⁵



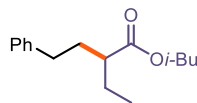
2-methyl-1-morpholino-4-phenylbutan-1-one (36z):

Synthesized according to General Procedure (3DPA2FBN (6.4 mg, 5.0 mol. %), HAT **B** (3,5-bis(trifluoromethyl)benzenethiol, 6.7 μL , 0.04 mmol, 20 mol. %), 2,4,6-collidine (26.4 μL , 0.2 mmol, 1 equiv.), and H donor **1** (methyl 4,5-dimethylcyclohexa-1,4-diene-1-carboxylate, 96.0 μL , 0.6 mmol, 3 equiv.)) using 4-Acryloylmorpholine **32j** (25.2 μL , 0.2 mmol, 1 equiv.) and styrene **33a** (68.7 μL , 0.6 mmol, 3 equiv.). The crude mixture was purified by flash column chromatography on silica gel (25% EtOAc in hexanes as eluent) to afford **36z** (26.7 mg, 58% yield) as a colorless oil.

^1H NMR (500 MHz, CDCl_3) δ 7.30 – 7.26 (m, 2H), 7.20 – 7.14 (m, 3H), 3.69 – 3.61 (m, 4H), 3.58 (t, $J = 4.8$ Hz, 2H), 3.37 – 3.28 (m, 2H), 2.69 – 2.56 (m, 3H), 2.09 – 2.01 (m, 1H), 1.74 – 1.67 (m, 1H), 1.14 (d, $J = 6.8$ Hz, 3H).

^{13}C NMR (126 MHz, CDCl_3) δ 174.9, 141.8, 128.6, 128.5, 126.1, 67.2, 66.8, 45.9, 42.1, 35.5, 34.1, 33.5, 17.6.

Matching reported literature data.²⁶



isobutyl-2-ethyl-4-phenylbutanoate (36aa):

Synthesized according to General Procedure (3DPA2FBN (6.4 mg, 5.0 mol. %), %), PhSH (4.1 μL , 0.04 mmol, 20 mol. %), Cs_2CO_3 (32.6 mg, 0.2 mmol, 1 equiv.) and γ -terpinene (96.2 μL , 0.6 mmol, 3 equiv.) using Isobutyl trans-2-butenoate **32k** (32.0 μL , 0.2 mmol, 1 equiv.) and styrene **33a** (68.7 μL , 0.6 mmol, 3 equiv.). The crude mixture was purified by flash column

²⁵ Capacci, A. G.; Malinowski, J. T.; McAlpine, N. J.; Kuhne, J.; MacMillan, D. W. C., Direct, enantioselective α -alkylation of aldehydes using simple olefins. *Nat. Chem.* **2017**, *9*, 1073-1077.

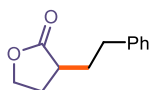
²⁶ Ling, J.; Bruneau-Voisine, A.; Journot, G.; Evano, G., Copper-Catalyzed Carbonylative Cross-Coupling of Alkyl Iodides and Amines. *Chem. Eur. J.* **2022**, *28*, e202201356.

chromatography on silica gel (1% EtOAc in hexanes as eluent) to afford **36aa** (26.3 mg, 53% yield) as a light-yellow oil.

^1H NMR (400 MHz, CDCl_3) δ 7.31 – 7.26 (m, 2H), 7.20 – 7.16 (m, 3H), 3.89 (dd, $J = 6.6, 0.9$ Hz, 2H), 2.68 – 2.51 (m, 2H), 2.34 (ddd, $J = 10.5, 9.0, 5.2$ Hz, 1H), 2.05 – 1.89 (m, 2H), 1.77 (ddd, $J = 6.7, 5.0, 2.5$ Hz, 1H), 1.68 – 1.55 (m, 2H), 0.96 (d, $J = 6.7$ Hz, 6H), 0.91 (d, $J = 7.4$ Hz, 3H).

^{13}C NMR (101 MHz, CDCl_3) δ 176.2, 141.9, 128.5, 128.5, 126.0, 70.5, 47.1, 33.9, 33.9, 27.9, 25.6, 19.3, 11.8.

HRMS: (ESI⁺) calculated for $\text{C}_{16}\text{H}_{24}\text{NaO}_2^+$ [$\text{M}+\text{Na}^+$]: 271.1669, found 271.1667.

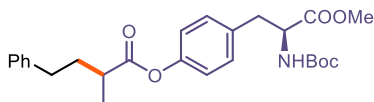


3-phenethyldihydrofuran-2(3H)-one (36bb): Synthesized according to General Procedure (3DPA2FBN (6.4 mg, 5.0 mol. %), PhSH (4.1 μL , 0.04 mmol, 20 mol. %), Cs_2CO_3 (32.6 mg, 0.2 mmol, 1 equiv.) and γ -terpinene (96.2 μL , 0.6 mmol, 3 equiv.) using 2-Furanone **32i** (14.2 μL , 0.2 mmol, 1 equiv.) and styrene **33a** (68.7 μL , 0.6 mmol, 3 equiv.). The crude mixture was purified by flash column chromatography on silica gel (1% EtOAc in hexanes as eluent) to afford **36bb** (17.1 mg, 45% yield) as a light-yellow oil.

^1H NMR (500 MHz, CDCl_3) δ 7.32 – 7.28 (m, 2H), 7.24 – 7.19 (m, 3H), 4.35 (td, $J = 8.8, 2.8$ Hz, 1H), 4.17 (ddd, $J = 9.8, 9.1, 6.7$ Hz, 1H), 2.81 (ddd, $J = 14.7, 9.1, 6.0$ Hz, 1H), 2.72 (ddd, $J = 13.8, 8.8, 7.1$ Hz, 1H), 2.49 (ddt, $J = 10.2, 8.9, 4.4$ Hz, 1H), 2.38 (dddd, $J = 12.5, 8.7, 6.7, 2.8$ Hz, 1H), 2.28 – 2.20 (m, 1H), 1.96 (dtd, $J = 12.5, 10.0, 8.5$ Hz, 1H), 1.77 (dtd, $J = 13.9, 8.9, 5.9$ Hz, 1H).

^{13}C NMR (126 MHz, CDCl_3) δ 179.4, 140.8, 128.6, 128.5, 126.3, 66.5, 38.5, 33.4, 32.1, 28.9.

Matching reported literature data.²⁷



4-((S)-2-((tert-butoxycarbonyl)amino)-3-methoxy-3-oxopropyl)phenyl (S)-2-methyl-4-phenylbutanoate (36cc):

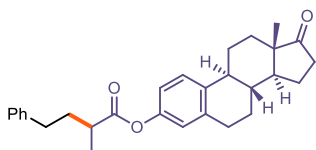
Synthesized according to General Procedure (3DPA2FBN (6.4 mg, 5.0 mol. %), PhSH (4.1 μL , 0.04 mmol, 20 mol. %), 2,4,6-collidine (26.4 μL , 0.2 mmol, 1 equiv.) and γ -terpinene (96.2 μL , 0.6 mmol, 3 equiv.) using (S)-4-(2-((tert-

²⁷ Miao, P.; Li, R.; Lin, X.; Rao, L.; Sun, Z., Visible-light induced metal-free cascade Wittig/hydroalkylation reactions. *Green Chemistry* **2021**, *23* (4), 1638-1641.

butoxycarbonyl)amino)-3-methoxy-3-oxopropyl)phenyl acrylate **32m** (30.6 μ L, 0.2 mmol, 1 equiv.) and styrene **33a** (68.7 μ L, 0.6 mmol, 3 equiv.). The crude mixture was purified by flash column chromatography on silica gel (5% to 10% EtOAc in hexanes as eluent) to afford **36cc** (55.6 mg, 61% yield, mixture of diastereomers) as a colorless oil.

$^1\text{H NMR}$ (500 MHz, CDCl_3) δ 7.33 – 7.28 (m, 2H), 7.24 – 7.19 (m, 3H), 7.17 – 7.12 (m, 2H), 7.02 – 6.99 (m, 2H), 4.99 (d, $J = 8.3$ Hz, 1H), 4.62 – 4.54 (m, 1H), 3.71 (s, 3H), 3.15 – 3.02 (m, 2H), 2.77 – 2.67 (m, 3H), 2.19 – 2.11 (m, 1H), 1.89 – 1.82 (m, 1H), 1.43 (s, 9H), 1.34 (d, $J = 7.0$ Hz, 3H).

$^{13}\text{C NMR}$ (126 MHz, CDCl_3) δ 175.1, 172.3, 155.2, 150.0, 141.6, 133.7, 130.4, 128.6, 128.6, 126.2, 121.7, 80.2, 54.5, 52.4, 39.3, 37.8, 35.5, 33.6, 28.4, 17.2.



(8R,9S,13S,14S)-13-methyl-17-oxo-7,8,9,11,12,13,14,15,16,17-decahydro-6H-cyclopenta[a]phenanthren-3-yl 2-methyl-4-phenylbutanoate (36dd): Synthesized according

to General Procedure (3DPA2FBN (6.4 mg, 5.0 mol. %), PhSH (4.1 μ L, 0.04 mmol, 20 mol. %), 2,4,6-collidine (26.4 μ L, 0.2 mmol, 1 equiv.) and γ -terpinene (96.2 μ L, 0.6 mmol, 3 equiv.)) using (8R,9S,13S,14S)-13-methyl-17-oxo-7,8,9,11,12,13,14,15,16,17-decahydro-6H-cyclopenta[a]phenanthren-3-yl acrylate **32n** (64.9 mg, 0.2 mmol, 1 equiv.) and styrene **33a** (68.7 μ L, 0.6 mmol, 3 equiv.). The crude mixture was purified by flash column chromatography on silica gel (9% EtOAc in hexanes as eluent) to afford **36dd** (54.5 mg, 90% purity, 57% yield) as a colorless oil. To obtain an analytically pure sample, preparative HPLC has been performed.

$^1\text{H NMR}$ (500 MHz, CDCl_3) δ 7.32 – 7.27 (m, 3H), 7.24 – 7.19 (m, 3H), 6.85 (dd, $J = 8.4, 2.6$ Hz, 1H), 6.81 – 6.78 (m, 1H), 2.94 – 2.89 (m, 2H), 2.78 – 2.67 (m, 3H), 2.51 (ddd, $J = 18.9, 8.8, 0.9$ Hz, 1H), 2.45 – 2.38 (m, 1H), 2.29 (td, $J = 10.6, 3.8$ Hz, 1H), 2.20 – 2.11 (m, 2H), 2.09 – 1.95 (m, 3H), 1.86 (dddd, $J = 13.7, 8.6, 7.3, 6.1$ Hz, 1H), 1.69 – 1.39 (m, 6H), 1.34 (d, $J = 7.0$ Hz, 3H), 0.92 (s, 3H).

$^{13}\text{C NMR}$ (126 MHz, CDCl_3) δ 220.9, 175.4, 148.8, 141.6, 138.1, 137.4, 128.6, 126.5, 126.1, 121.6, 118.8, 50.5, 48.0, 44.3, 39.2, 38.1, 36.0, 35.6, 33.6, 31.6, 29.5, 26.4, 25.9, 21.7, 17.2, 13.9.



benzyl-2-methyl-4-(4,4,5,5-tetramethyl-1,3,2-dioxaborolan-2-yl)butanoate(36ee): Synthesized according

to General Procedure (3DPA2FBN (6.4 mg, 5.0 mol. %), HAT C (Ethyl thioglycolate, 4.4 μ L, 0.04 mmol, 20 mol. %), 2,4,6-collidine (26.4 μ L, 0.2 mmol, 1 equiv.) and γ -terpinene (32.0 μ L, 0.2 mmol, 1 equiv.)) using benzyl acrylate **32e** (30.6 μ L, 0.2 mmol, 1 equiv.) and vinylboronic acid pinacol ester **33o** (101.8 μ L, 0.6 mmol, 3 equiv.). The crude mixture was purified by flash column chromatography on silica gel (2% acetone in hexanes as eluent) to afford **36ee** (33.1 mg, 52% yield) as a yellow oil.

$^1\text{H NMR}$ (400 MHz, CDCl_3) δ 7.39 – 7.27 (m, 5H), 5.10 (s, 2H), 2.51 – 2.43 (m, 1H), 1.79 (dq, $J = 13.6, 7.8$ Hz, 1H), 1.58 – 1.52 (m, 1H), 1.23 (s, 12H), 1.16 (d, $J = 7.0$ Hz, 3H), 0.78 (t, $J = 8.3$ Hz, 2H).

$^{13}\text{C NMR}$ (101 MHz, CDCl_3) δ 176.7, 136.4, 128.6, 128.1, 128.1, 83.2, 66.0, 41.6, 28.2, 24.9, 24.9, 16.8.



tert-butyl-4-(3-(benzyloxy)-2-methyl-3-oxopropyl)piperidine-1-carboxylate (36ff): Synthesized

according to General Procedure (3DPA2FBN (6.4 mg, 5.0 mol. %), HAT C (Ethyl thioglycolate, 4.4 μ L, 0.04 mmol, 20 mol. %), 2,4,6-collidine (26.4 μ L, 0.2 mmol, 1 equiv.) and γ -terpinene (32.0 μ L, 0.2 mmol, 1 equiv.)) using benzyl acrylate **32e** (30.6 μ L, 0.2 mmol, 1 equiv.) and tert-butyl 4-methylenepiperidine-1-carboxylate **33s** (118.4 μ L, 0.6 mmol, 3 equiv.). The crude mixture was purified by flash column chromatography on silica gel (10% EtOAc in hexanes as eluent) to afford **36ff** (35.4 mg, 49% yield) as a colorless oil.

$^1\text{H NMR}$ (500 MHz, CDCl_3) δ 7.40 – 7.30 (m, 5H), 5.18 – 5.06 (m, 2H), 4.02 (s, 2H), 2.66 – 2.38 (m, 3H), 1.69 – 1.52 (m, 3H), 1.44 (s, 9H), 1.35 – 1.28 (m, 2H), 1.16 (d, $J = 6.9$ Hz, 3H), 1.06 – 0.99 (m, 2H).

$^{13}\text{C NMR}$ (126 MHz, CDCl_3) δ 176.7, 154.9, 136.2, 128.7, 128.3, 79.4, 66.2, 40.8, 36.9, 33.9, 32.0, 29.8, 28.6, 17.8.

HRMS: (ESI⁺) calculated for $\text{C}_{21}\text{H}_{31}\text{NNaO}_4^+$ [$\text{M}+\text{Na}^+$]: 384.2145, found 384.2140.

4.6.4 Mechanistic experiments

4.6.4.1 Stern-Volmer Quenching Studies

First, the absorption spectra of *fac*-Ir(ppy)₃ (**PC**) was recorded in order to establish appropriate concentration and excitation wavelength. The spectra was recorded using a Shimadzu 2401PC UV–vis spectrophotometer and 10 mm path quartz cuvette. The **PC** concentration of 1.5 μ M in DCE, and excitation wavelength of

440 nm were chosen for Stern-Volmer studies based on these results (absorbance value of 0.1 at 440 nm in these conditions).

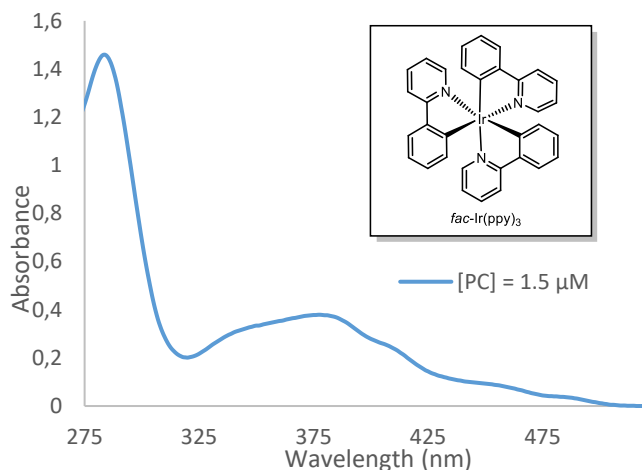


Figure 4.4: Absorption spectrum of **PC** (1.5 μM in DCE).

The emission spectra was recorded in a Fluorolog Horiba Jobin Yvon spectrofluorimeter equipped with a photomultiplier detector, a double monochromator, and a 350W xenon light source. 2 mL of a 1.5 μM solution of **PC** in thoroughly degassed DCE were placed in a 10x10 mm light path quartz fluorescence cuvette equipped with Silicone/PTFE 3.2 mm septum under an argon atmosphere. The excitation wavelength was fixed at 440 nm (incident light slit regulated to 1.5 nm), while the emission signal was acquired from 455 nm to 650 nm (emission light slit regulated to 1.5 nm).

A 0.5 M solution of dimethyl fumarate **32a** in DCE was prepared, and 5 μL of this stock solution were added to the solution of the catalyst. The addition of this solution was repeated four consecutive times. After each addition, an absorption spectrum and an emission spectrum of the solution were recorded. The results shown in Figure 4.5 indicate that dimethyl fumarate **32a** quenches the excited state of the catalyst **PC**. No change in the absorption spectra of the solution was observed during the addition of **32a**.

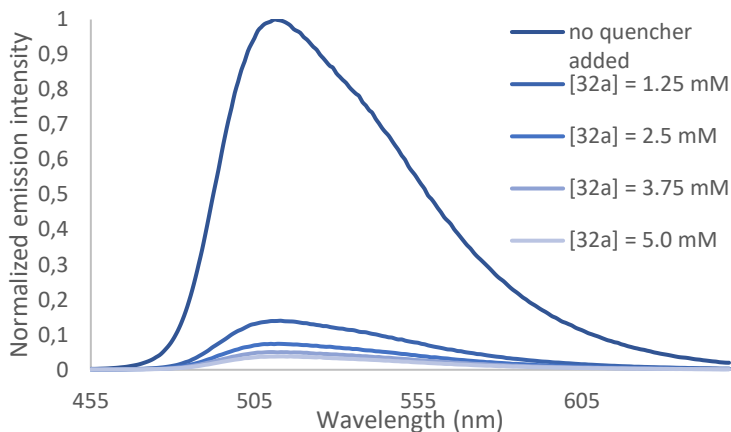


Figure 4.5: Quenching of the emission of **PC** ($1.5 \mu\text{M}$ in DCE) in the presence of increasing amounts of **32a**.

The Stern-Volmer plot, reported in Figure S21, shows a linear correlation between the concentration of **1a** and the ratio I^0/I . On the basis of the Stern-Volmer equation $I_0/I = 1 + K_{SV}[Q]$, we calculated a Stern-Volmer quenching constant $K_{SV} = 5.07 \cdot 10^3 \text{ M}^{-1}$. A 0.5 M solution of styrene **33a** in DCE was prepared, and portions of this stock solution were added to the solution of the catalyst. The addition of this solution was repeated five consecutive times. After each addition, an absorption spectrum and an emission spectrum of the solution were recorded.

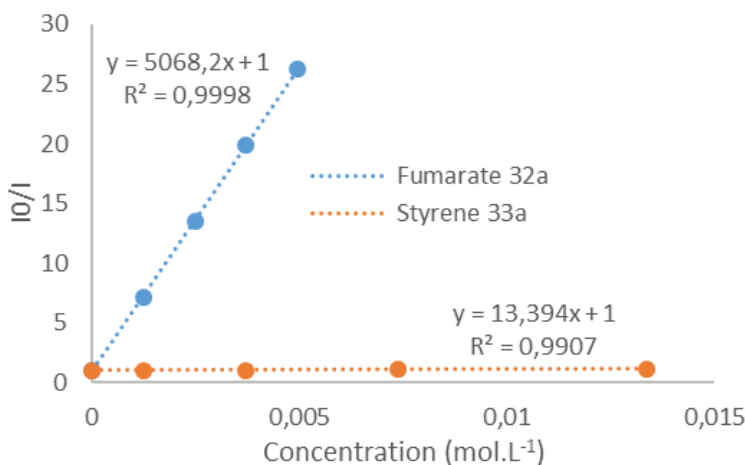
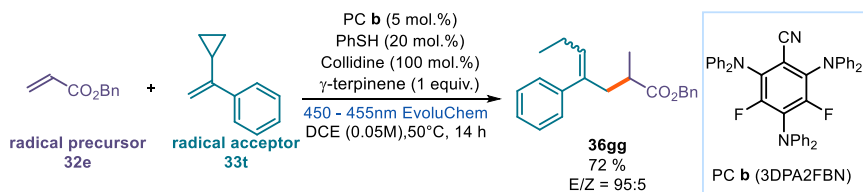


Figure 4.6: Stern-Volmer quenching plot using **32a** and **33a** as a quencher.

No change in the absorption spectra of the solution was observed during the addition of **33a**. Stern-Volmer plot is reported in Figure 20. A much smaller Stern-Volmer constant was calculated in this case ($K_{SV} = 13.3 \text{ M}^{-1}$).

4.6.4.2 Radical clock and deuterium labelling experiments

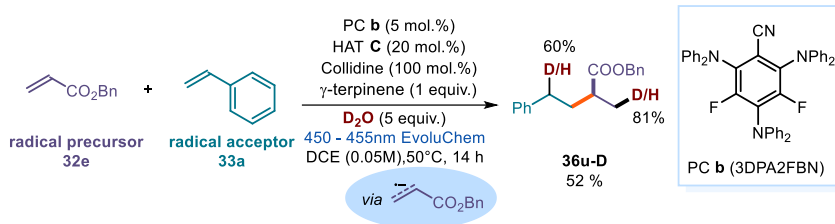


The above radical clock experiment was performed according to General Procedure (3DPA2FBN (6.4 mg, 5.0 mol. %), PhSH (4.1 μL , 0.04 mmol, 20 mol. %), 2,4,6-collidine (26.4 μL , 0.2 mmol, 1 equiv.) and γ -terpinene (96 μL , 0.6 mmol, 3 equiv.)) using benzyl acrylate **32e** (30.6 μL , 0.2 mmol, 1 equiv.) and α -cyclopropylstyrene **33t** (90.0 μL , 0.6 mmol, 3 equiv.). The crude mixture was purified by flash column chromatography on silica gel (2% EtOAc in hexanes as eluent) to afford **36gg** (44.7 mg, 72% yield, 95:5 Z/E) as a colorless oil.

¹H NMR (500 MHz, CDCl_3 , major) δ 7.39 – 7.28 (m, 7H), 7.25 – 7.21 (m, 1H), 7.14 – 7.10 (m, 2H), 5.46 (t, $J = 7.4$, 1H), 5.04 (s, 2H), 2.81 (ddq, $J = 13.4$, 6.9, 1.1 Hz, 1H), 2.49 – 2.40 (m, 1H), 2.39 (ddq, $J = 13.4$, 7.4, 0.8 Hz, 1H), 1.97 – 1.84 (m, 2H), 1.13 (d, $J = 6.9$ Hz, 3H), 0.90 (t, $J = 7.5$ Hz, 3H).

¹³C NMR (126 MHz, CDCl_3 , major) δ 176.3, 140.3, 137.4, 136.3, 131.9, 128.7, 128.6, 128.2, 128.2, 126.8, 66.1, 43.4, 38.2, 22.4, 16.8, 14.7.

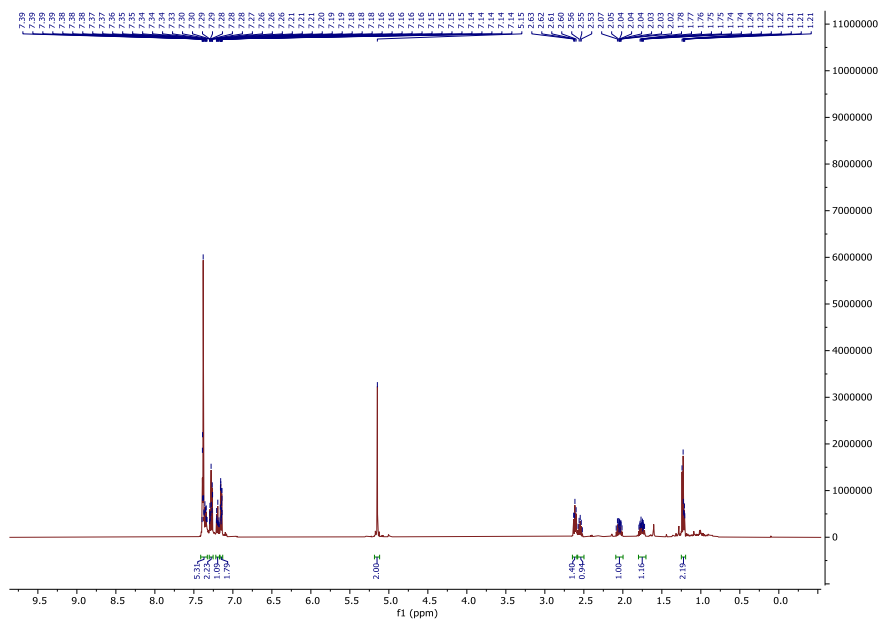
HRMS: (ESI⁺) calculated for $\text{C}_{21}\text{H}_{24}\text{NaO}_2^+$ [$\text{M}+\text{Na}^+$]: 331.1669, found 331.1670.



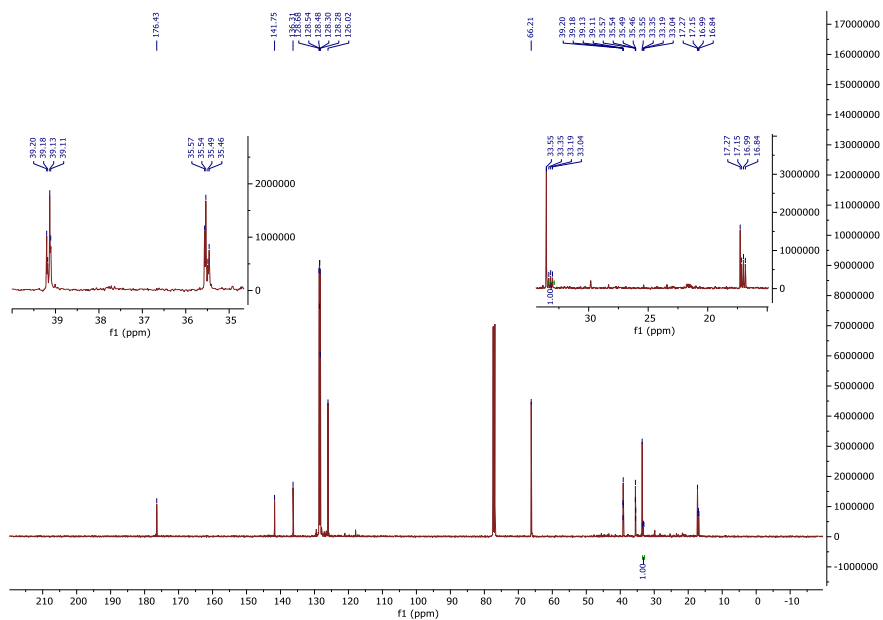
To an oven dried vial with a Teflon septum screw cap, containing a dry Teflon stir bar, 3DPA2FBN (6.4 mg, 5.0 mol. %) was added. The vial was sealed with a Teflon

septum screw cap, evacuated and backfilled with argon three times, and the solvent was added. Then PhSH (4.1 μL , 0.04 mmol, 20 mol. %), 2,4,6-collidine (26.4 μL , 0.2 mmol, 1 equiv.), γ -terpinene (96 μL , 0.6 mmol, 3 equiv.), benzyl acrylate **32e** (30.6 μL , 0.2 mmol, 1 equiv.), styrene **33a** (68.7 μL , 0.6 mmol, 3 equiv.) and **D₂O** (18.1 μL , 1.0 mmol, 5 equiv.) were added sequentially. The vial was then placed in the photoreactor (Figure 4.3) and irradiated under stirring for 14 hours. Then the solvent was evaporated and the crude mixture purified by flash column chromatography on silica gel (2% EtOAc in hexanes as eluent) to furnish the target product **36u-D** (27.9 mg, 52% yield) as a colorless oil.

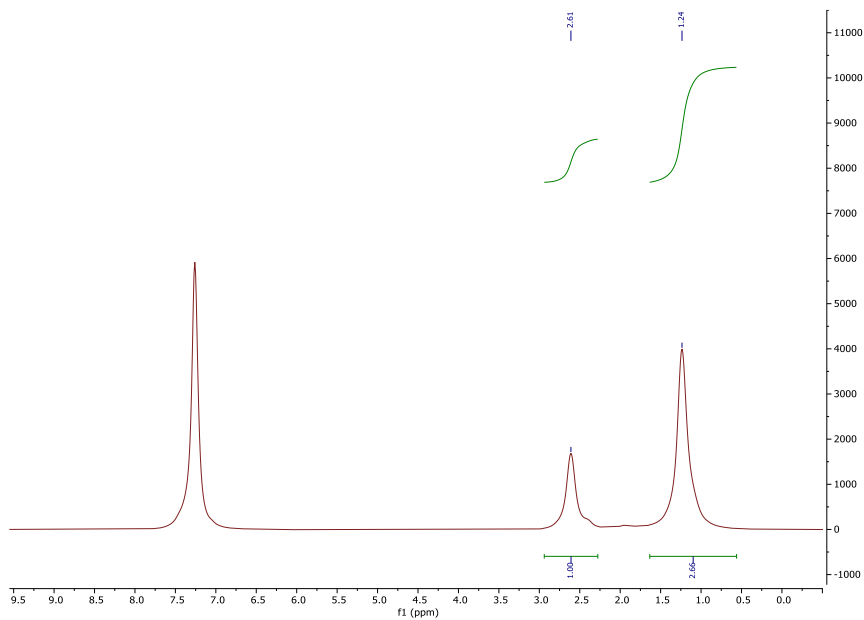
^1H NMR (500 MHz, CDCl_3) δ 7.41 – 7.33 (m, 5H), 7.30 – 7.25 (m, 2H), 7.22 – 7.17 (m, 1H), 7.15 (ddt, $J = 7.7, 1.4, 0.7$ Hz, 2H), 5.15 (s, 2H), 2.62 – 2.60 (m, 1.4H), 2.58 – 2.50 (m, 1H), 2.09 – 2.00 (m, 1H), 1.79 – 1.72 (m, 6.1 Hz, 1H), 1.25 – 1.19 (m, 2.19H).



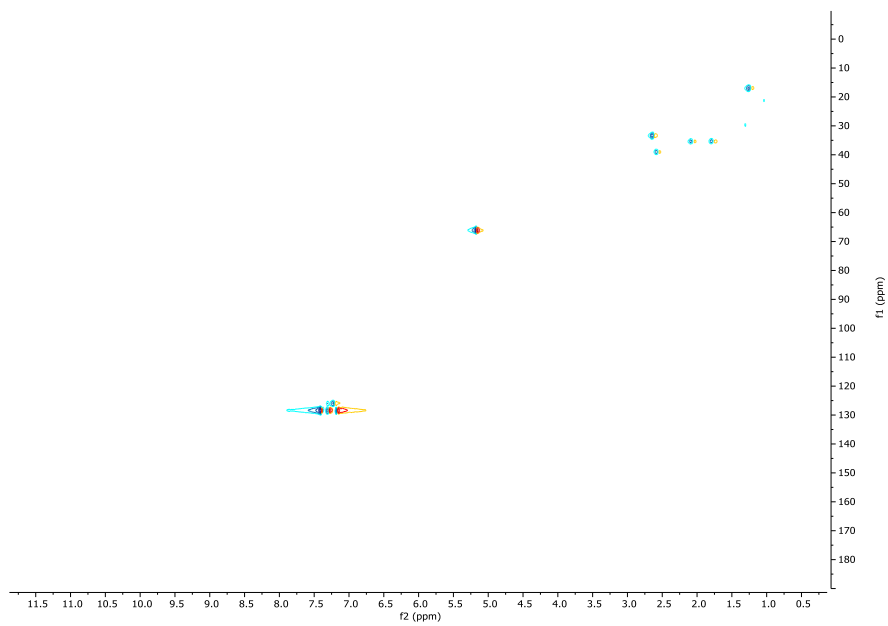
^{13}C NMR (126 MHz, CDCl_3) δ 176.43, 141.75, 136.31, 128.68, 128.54, 128.48, 128.30, 128.28, 126.02, 66.21, 39.20 – 39.11, 35.57 – 35.46, 33.55, 33.19 (t, $J = 19.5$ Hz), 17.27, 16.99 (t, $J = 19.5$ Hz).



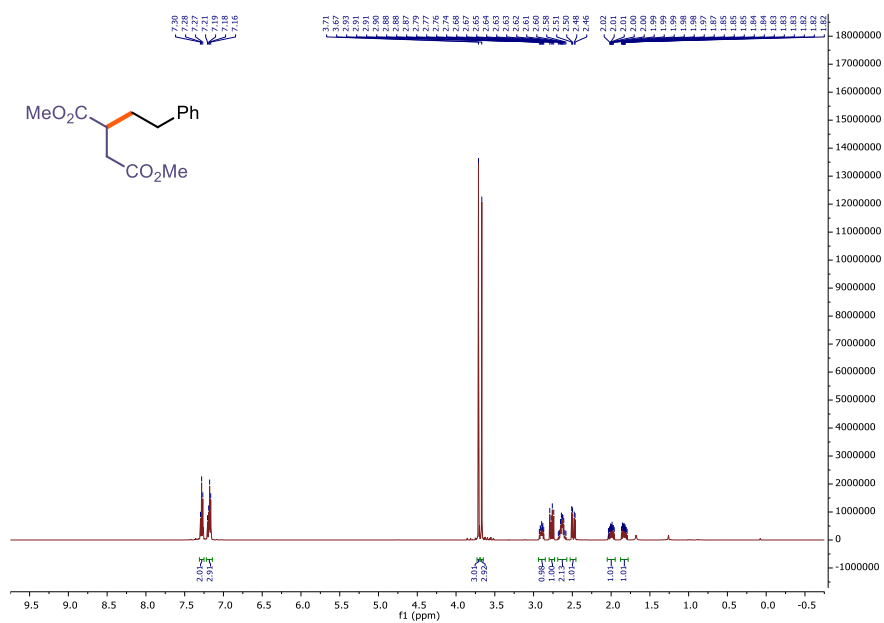
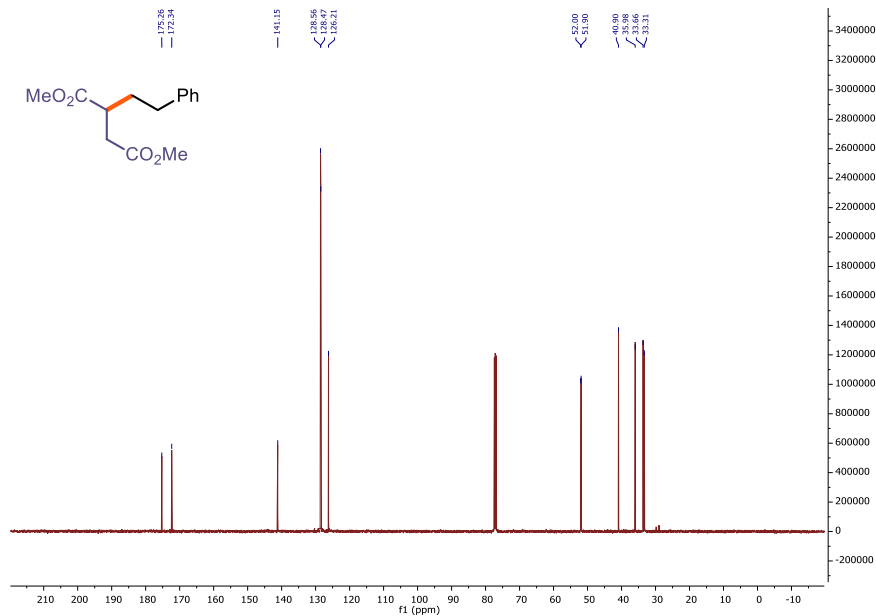
²H NMR (77 MHz, CDCl₃) δ 2.61 (s, 1D), 1.24 (s, 2.66D).



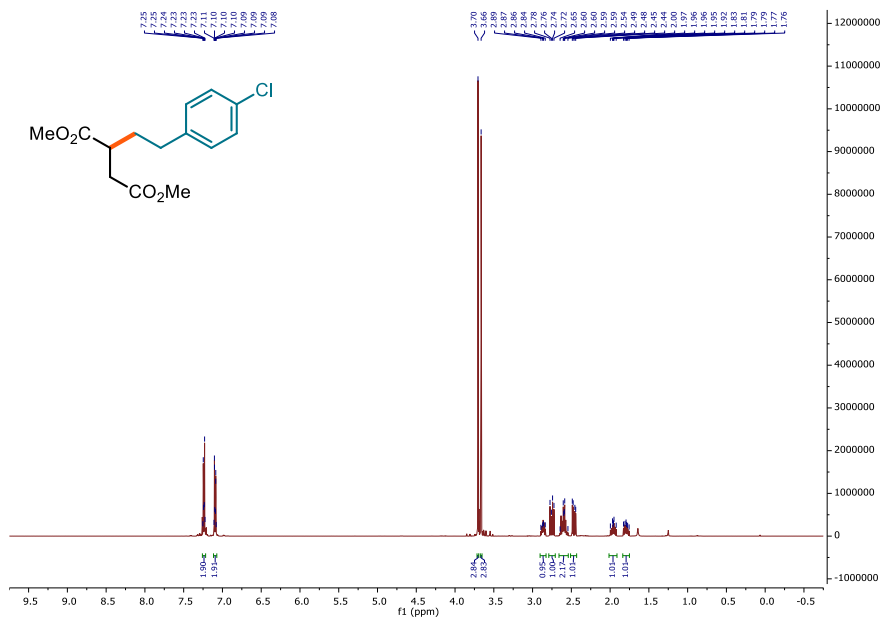
HSQC



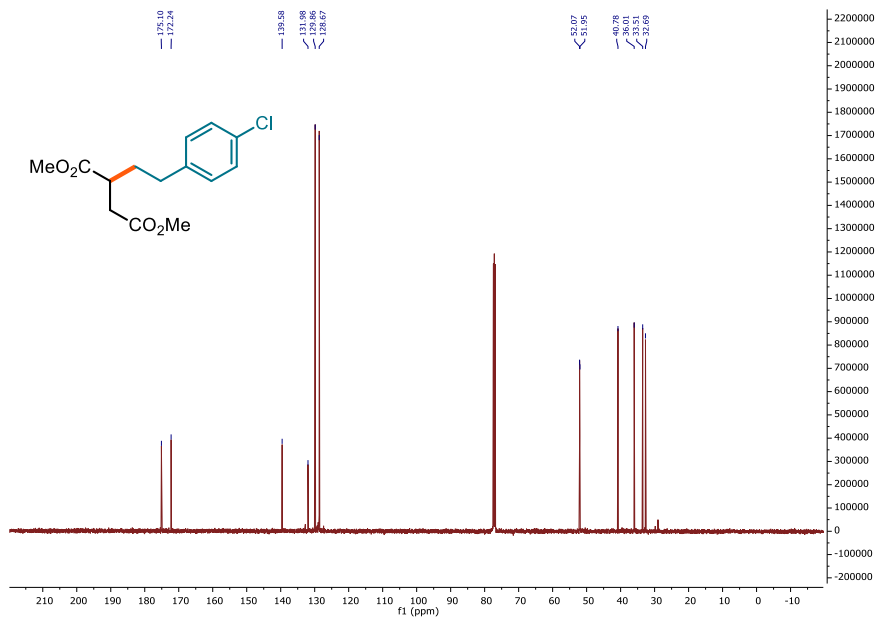
4.6.5. NMR spectra

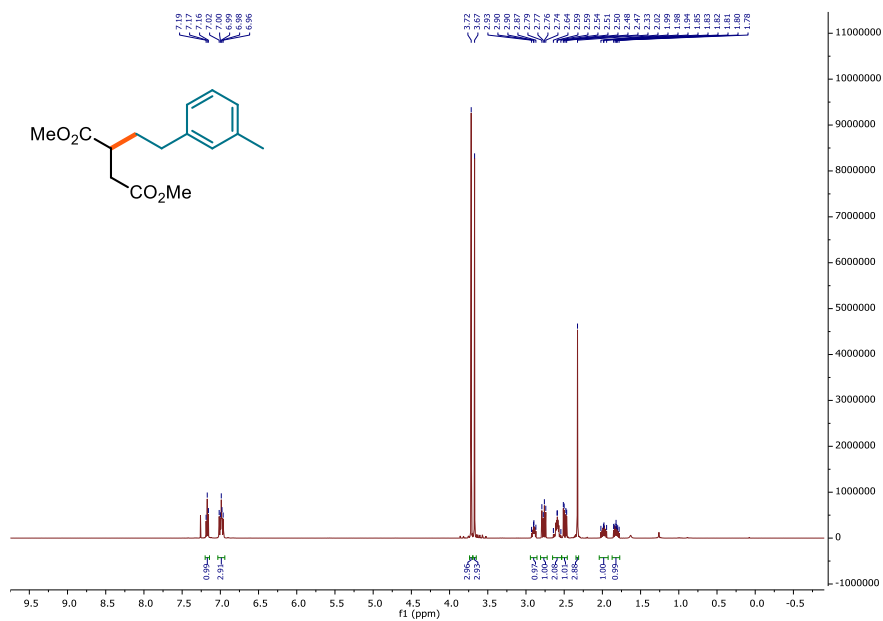
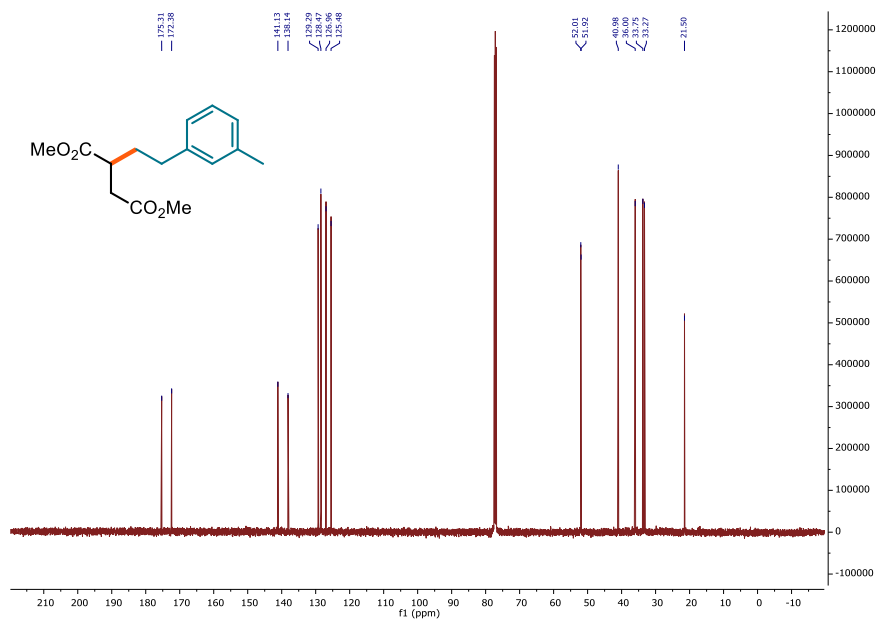
¹H NMR (500 MHz, CDCl₃) of **36a**¹³C NMR (126 MHz, CDCl₃) of **36a**

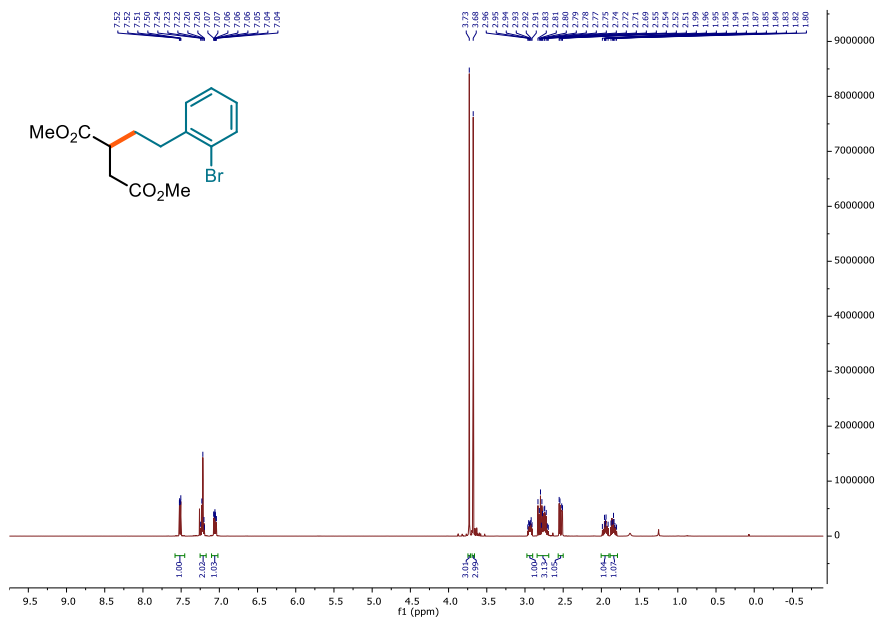
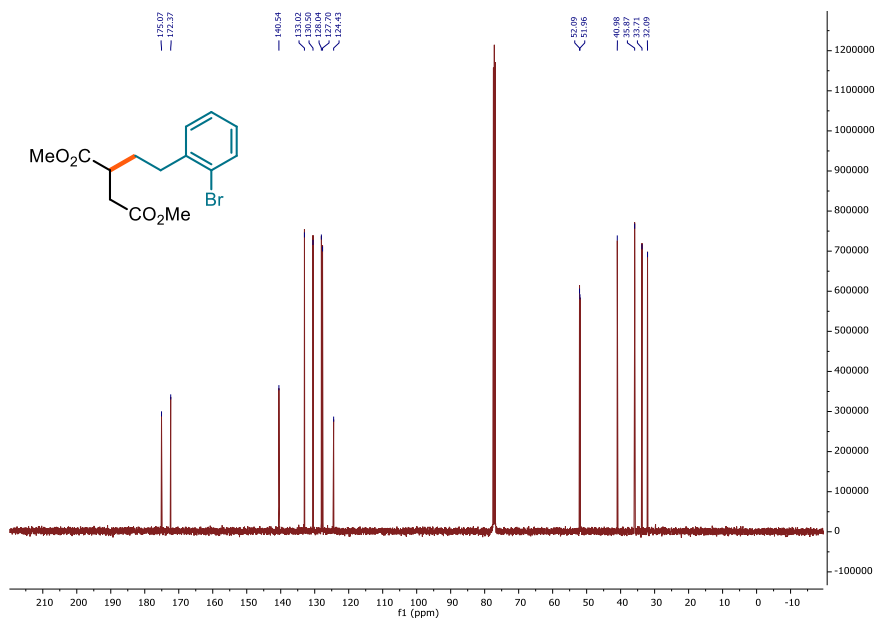
^1H NMR (500 MHz, CDCl_3) of **36c**

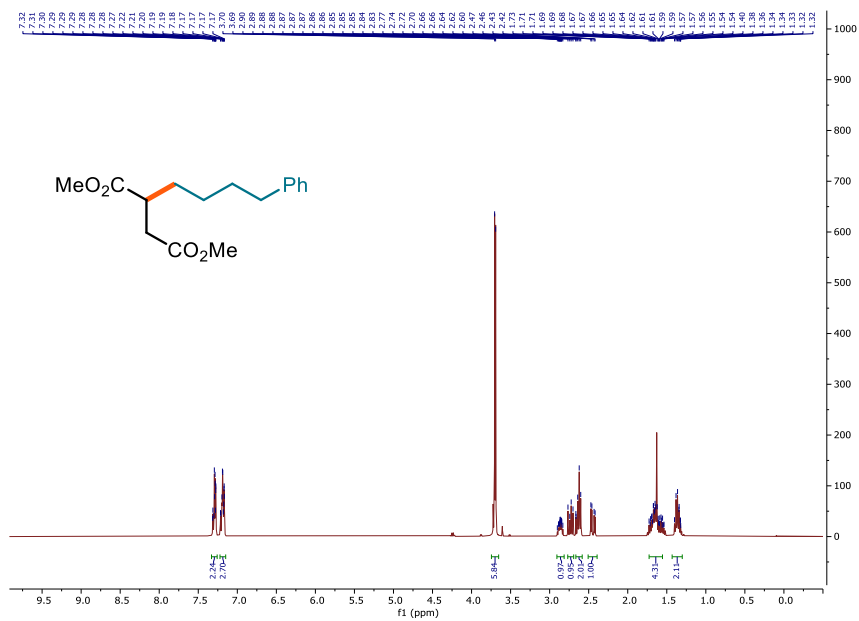
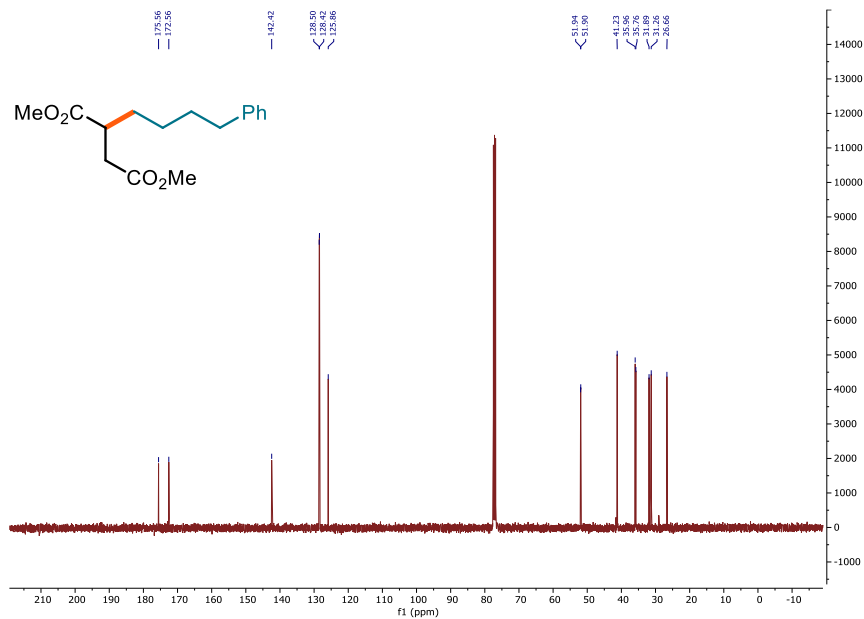


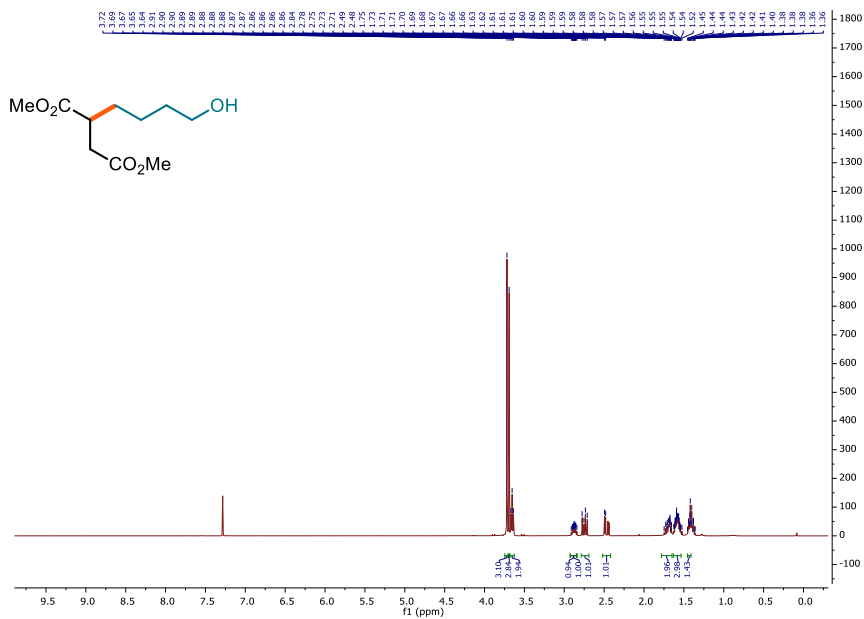
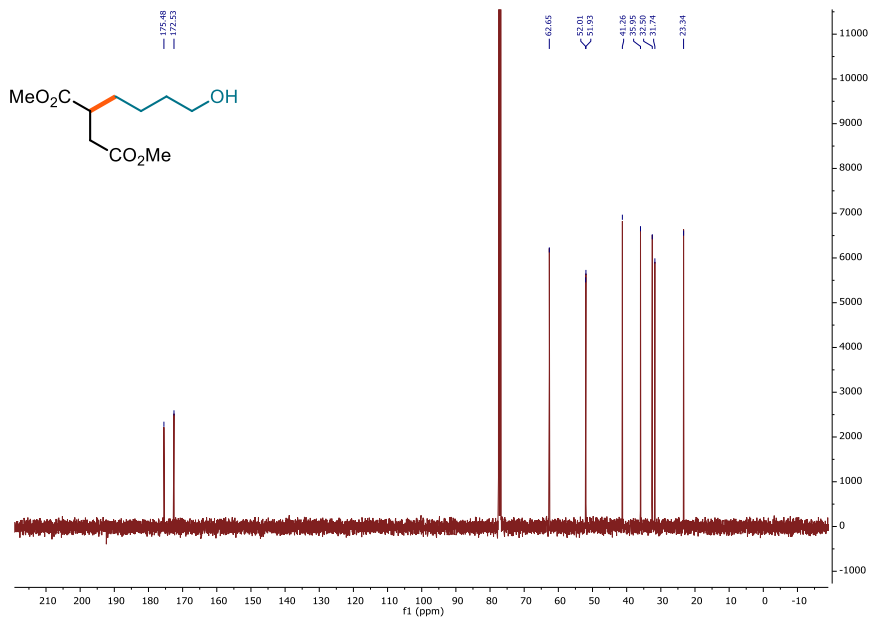
^{13}C NMR (126 MHz, CDCl_3) of **36c**

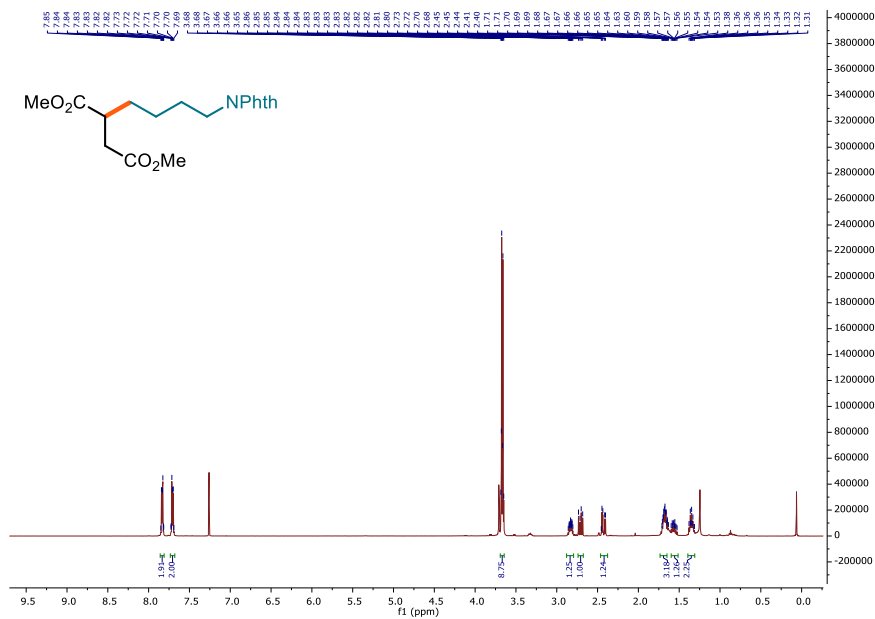
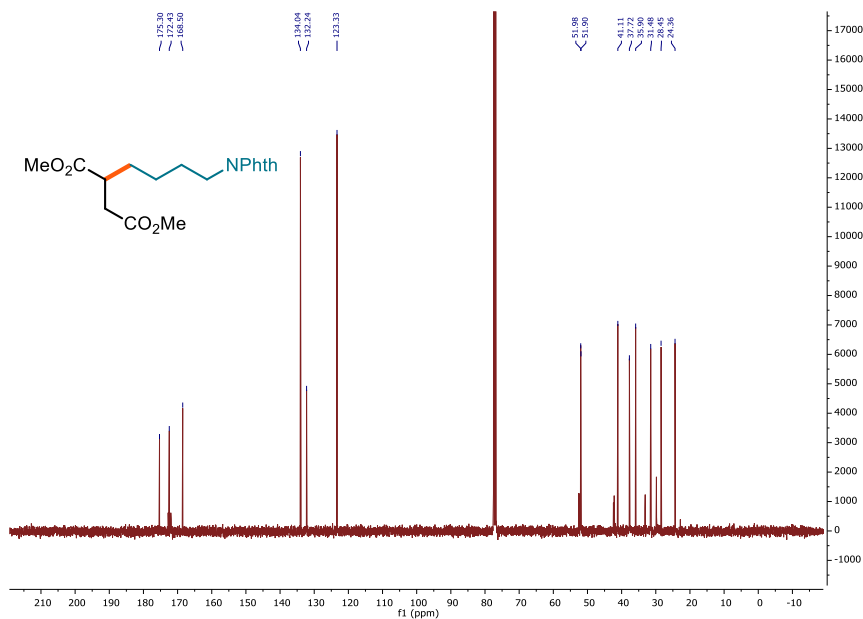


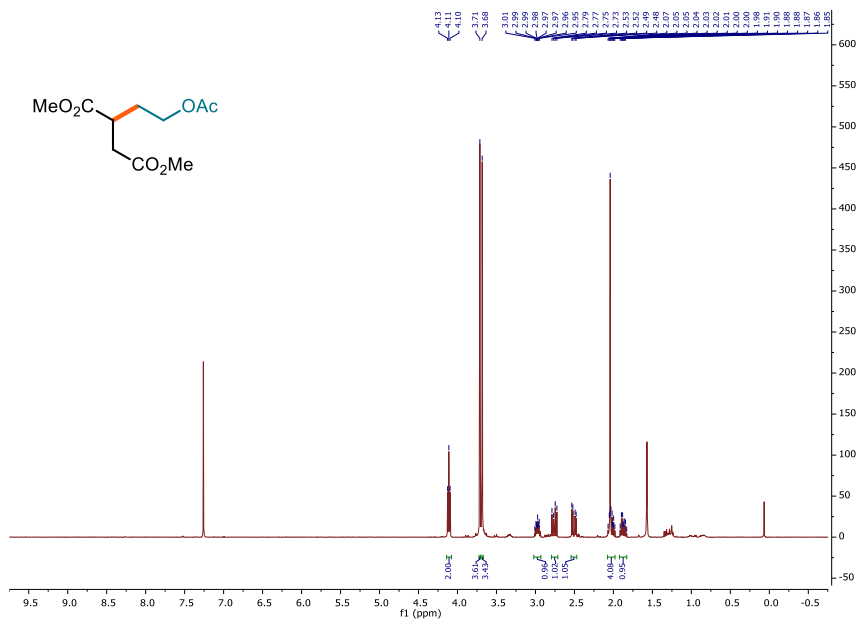
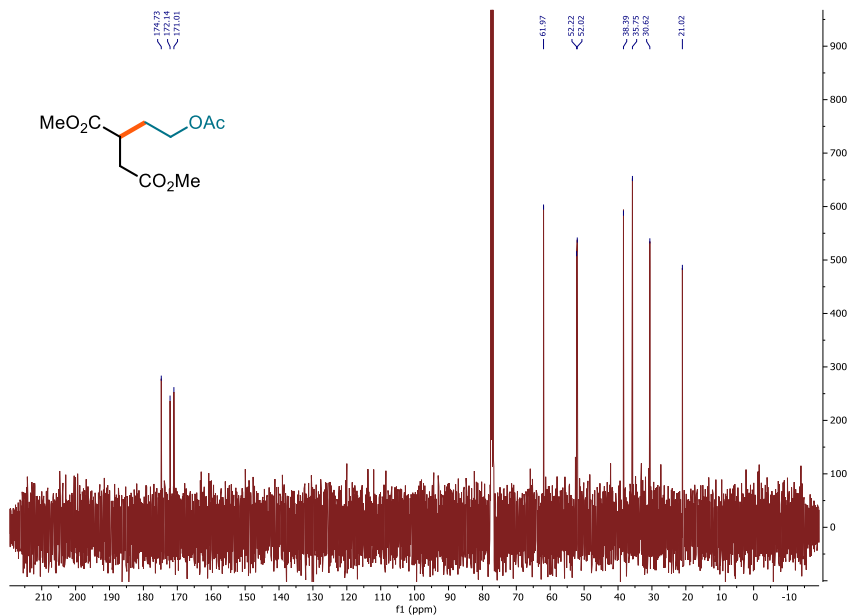
^1H NMR (500 MHz, CDCl_3) of **36f** ^{13}C NMR (126 MHz, CDCl_3) of **36f**

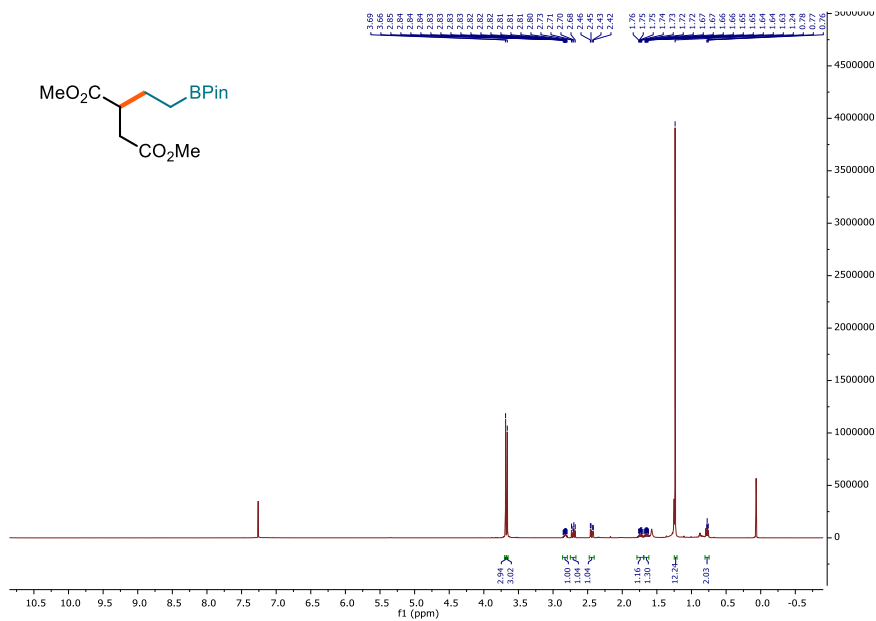
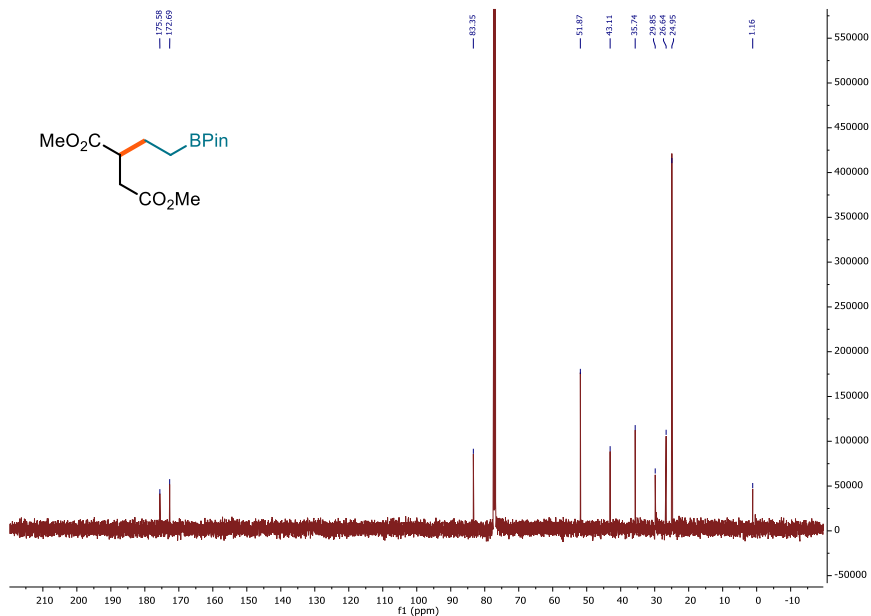
^1H NMR (500 MHz, CDCl_3) of **36g** ^{13}C NMR (126 MHz, CDCl_3) of **36g**

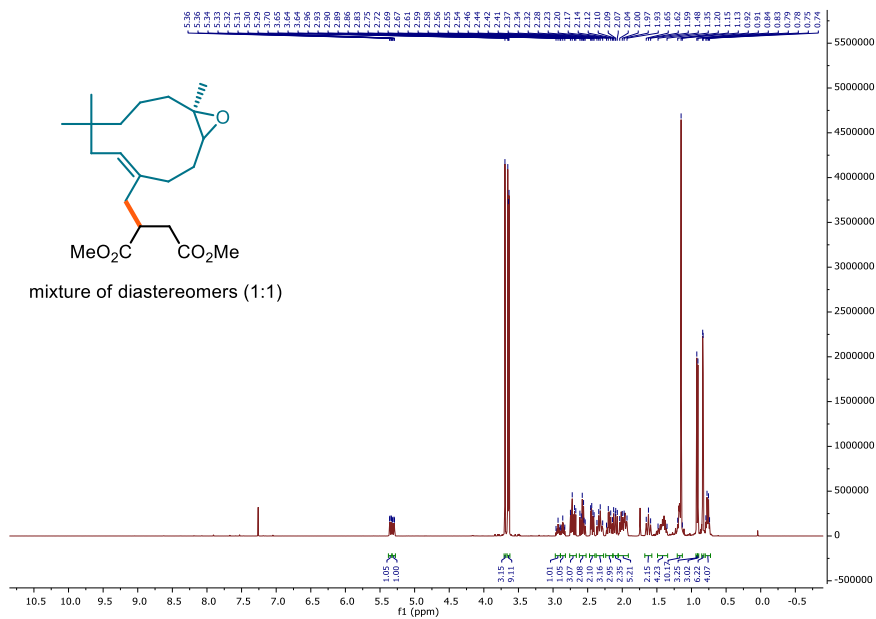
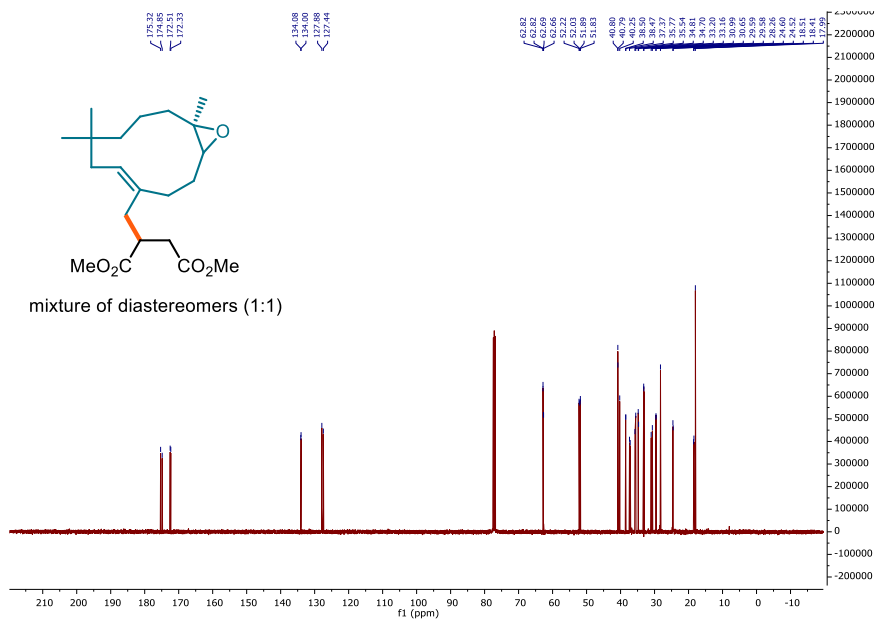
¹H NMR (500 MHz, CDCl₃) of **36i**¹³C NMR (101 MHz, CDCl₃) of **36i**

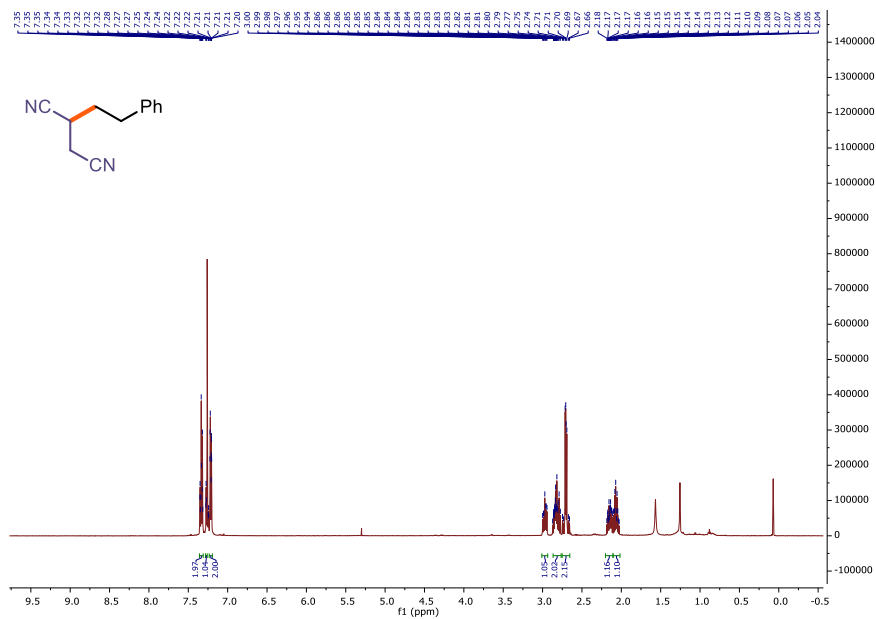
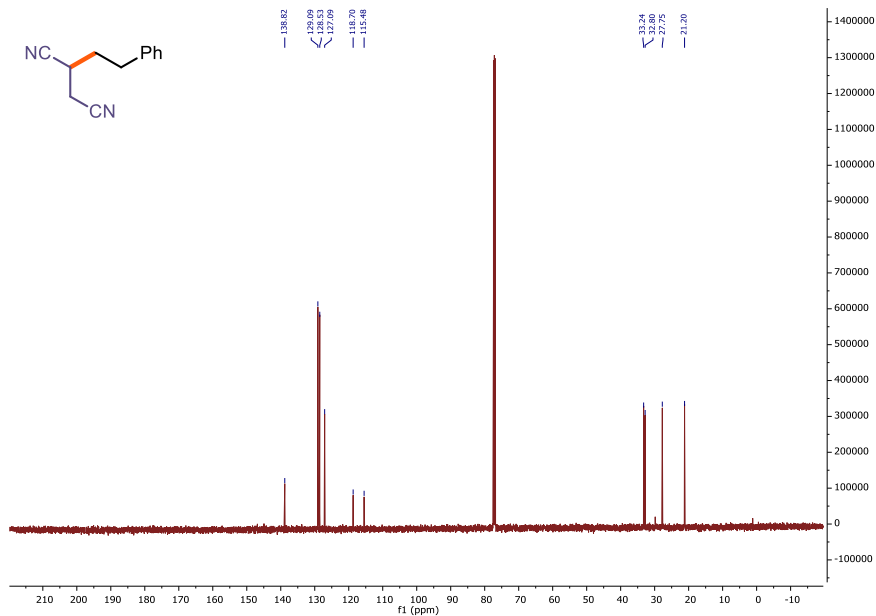
^1H NMR (400 MHz, CDCl_3) of **36j** ^{13}C NMR (101 MHz, CDCl_3) of **36j**

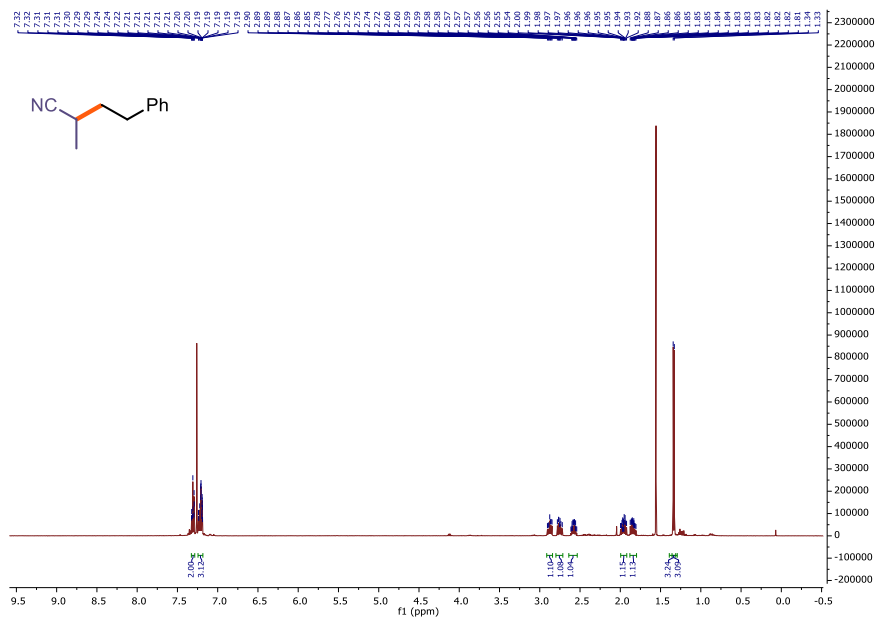
^1H NMR (500 MHz, CDCl_3) of **361** ^{13}C NMR (101 MHz, CDCl_3) of **361**

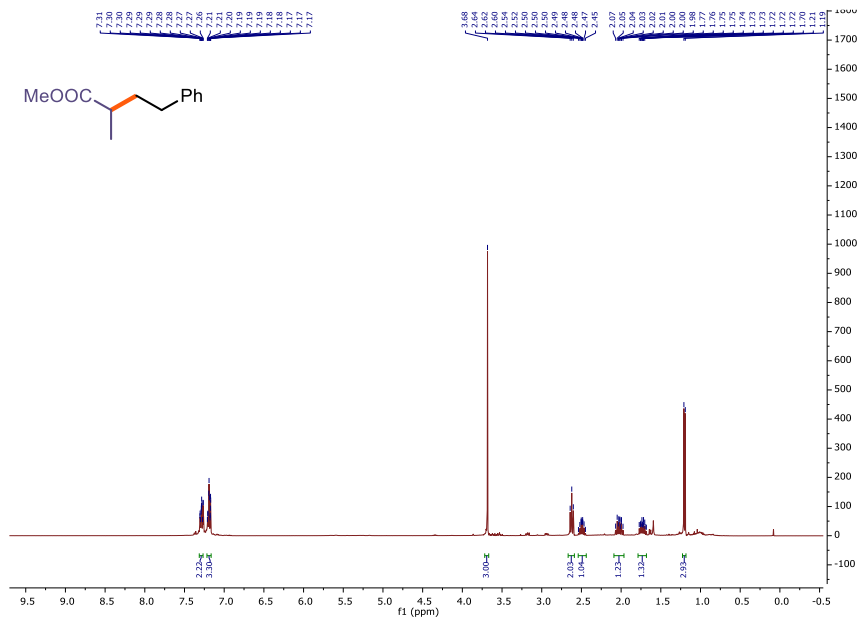
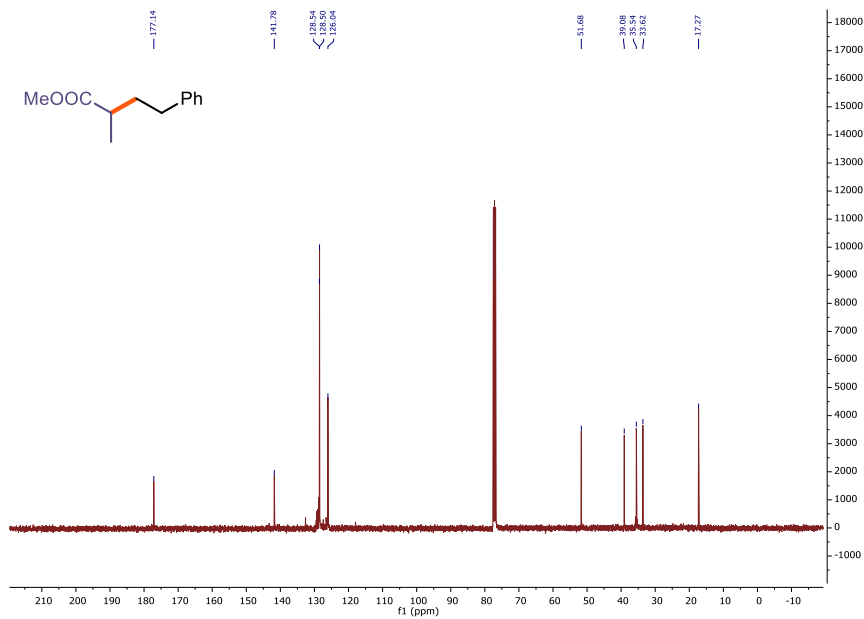
^1H NMR (400 MHz, CDCl_3) of **36n** ^{13}C NMR (101 MHz, CDCl_3) of **36n**

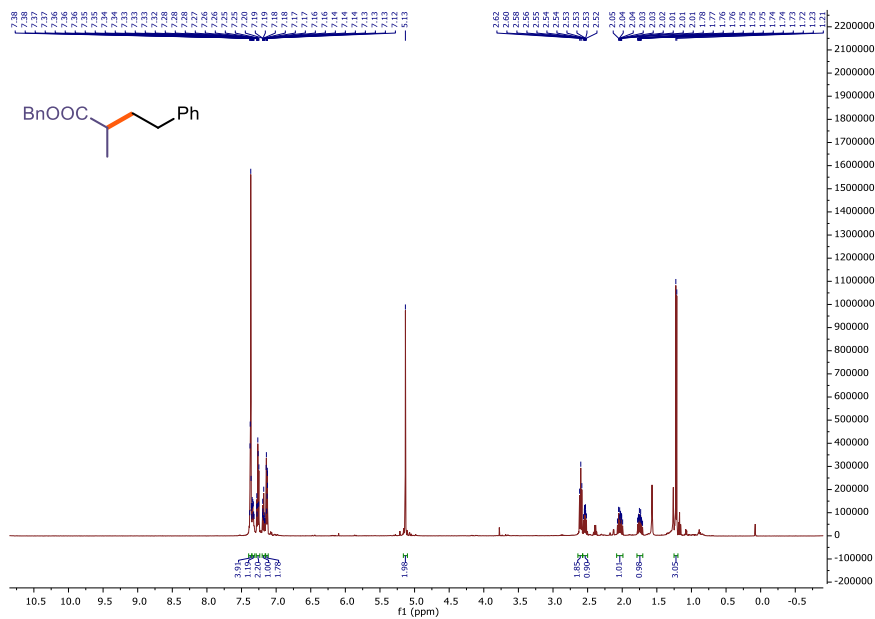
^1H NMR (500 MHz, CDCl_3) of **36o** ^{13}C NMR (126 MHz, CDCl_3) of **36o**

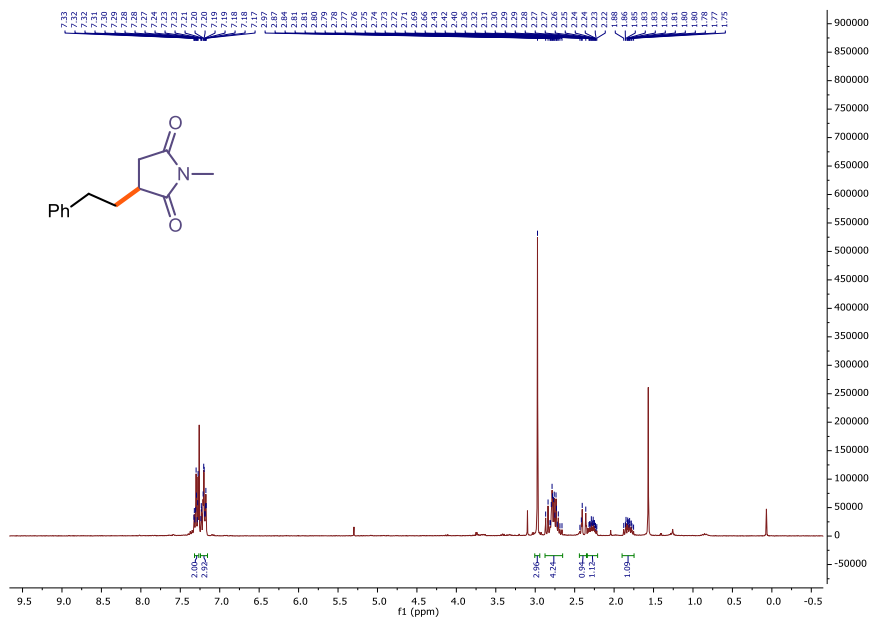
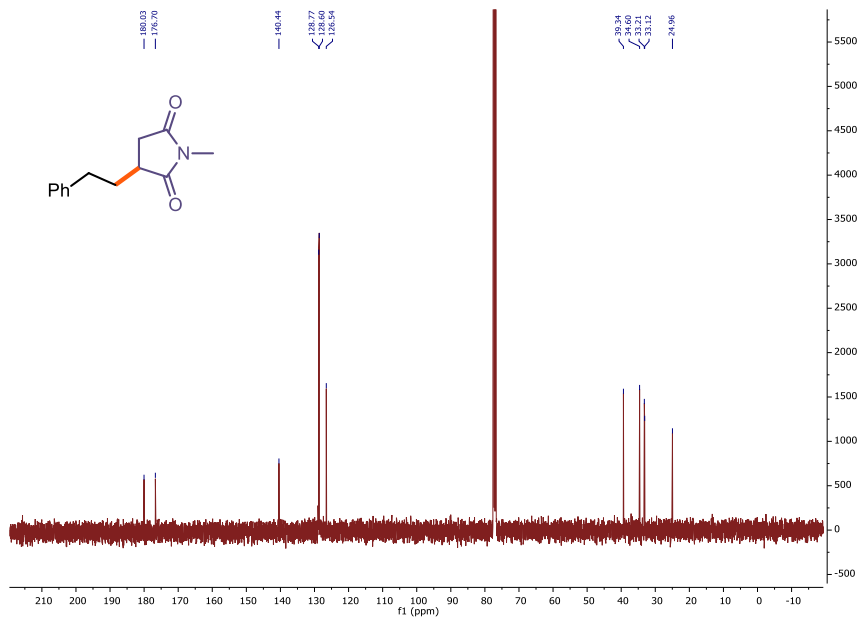
^1H NMR (500 MHz, CDCl_3) of **36r** ^{13}C NMR (126 MHz, CDCl_3) of **36r**

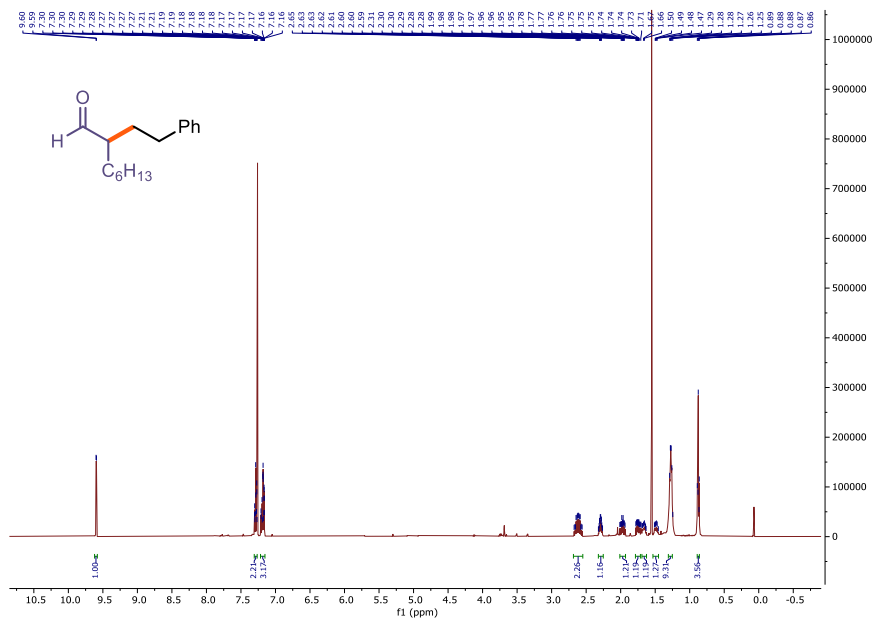
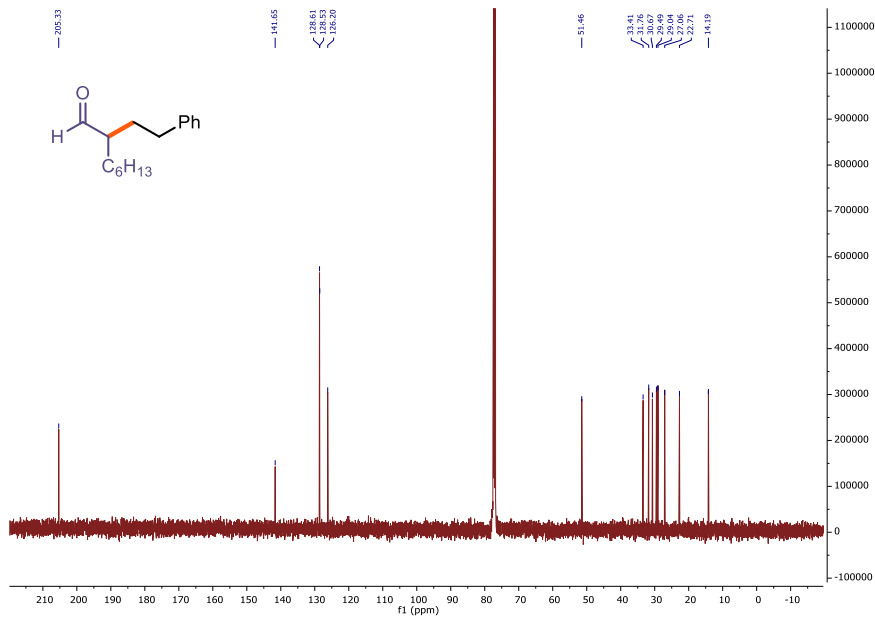
^1H NMR (500 MHz, CDCl_3) of **36s** ^{13}C NMR (126 MHz, CDCl_3) of **36s**

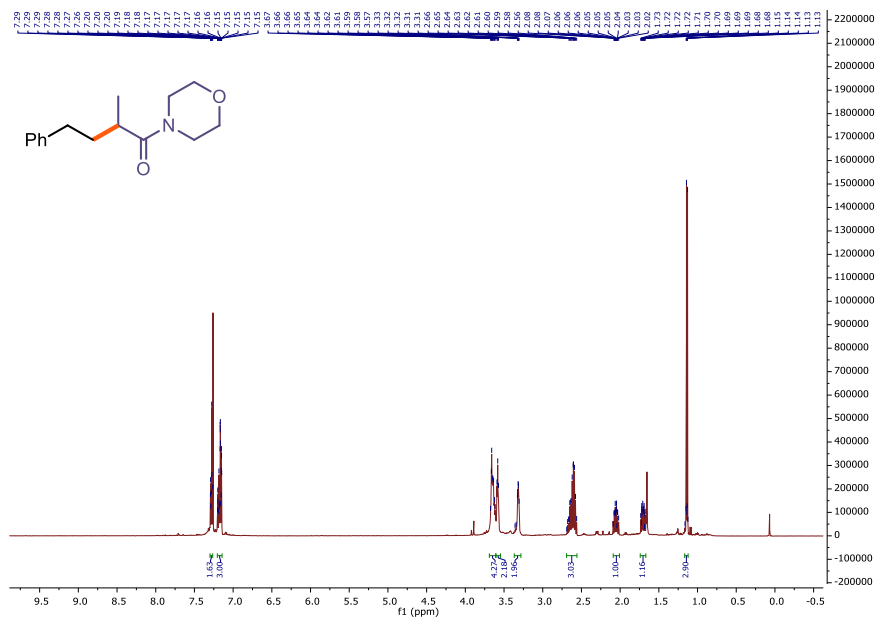
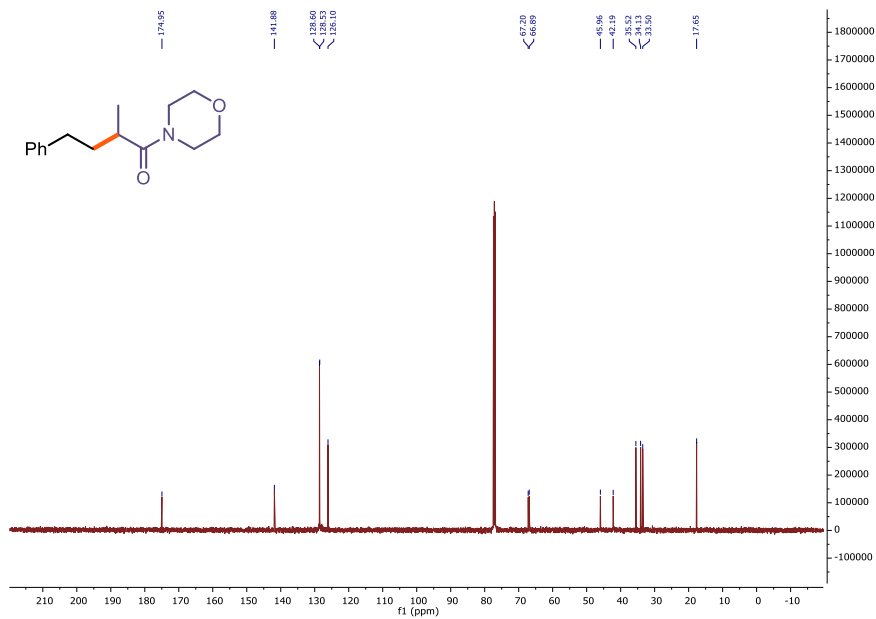
^1H NMR (500 MHz, CDCl_3) of **36t**

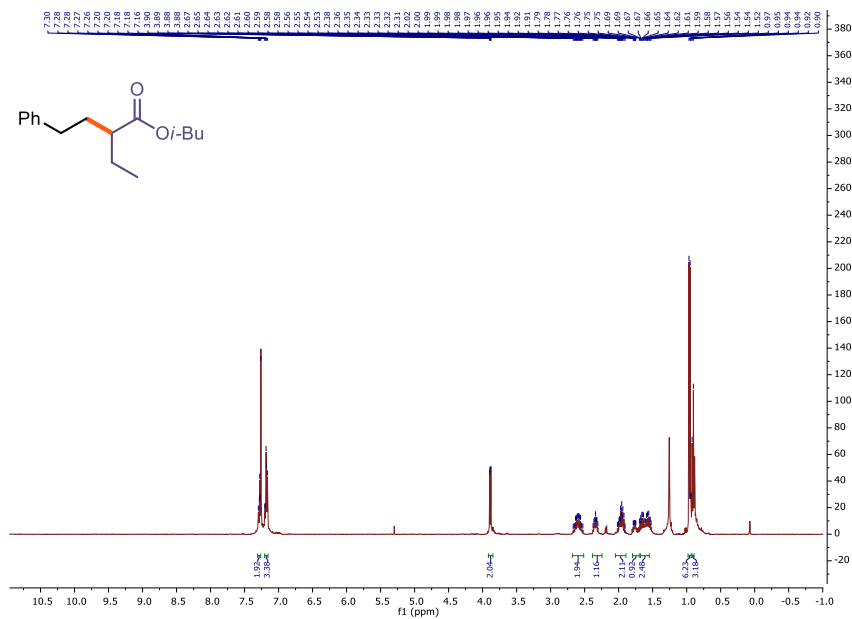
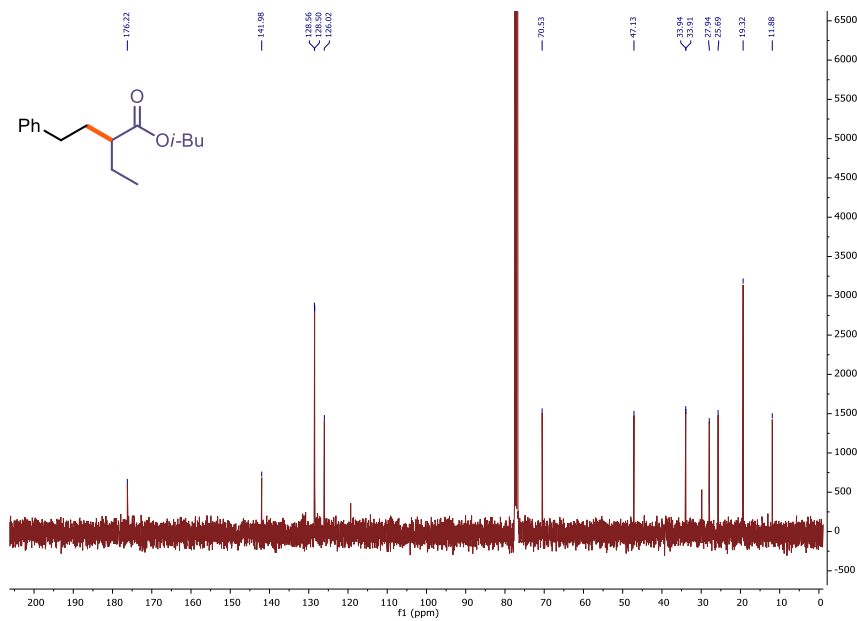
^1H NMR (400 MHz, CDCl_3) of **36u** ^{13}C NMR (101 MHz, CDCl_3) of **36u**

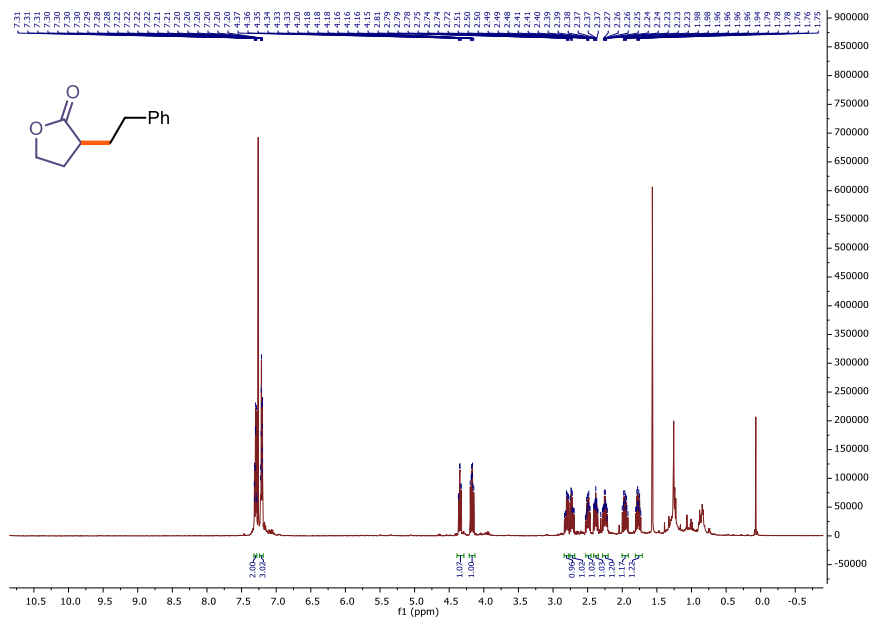
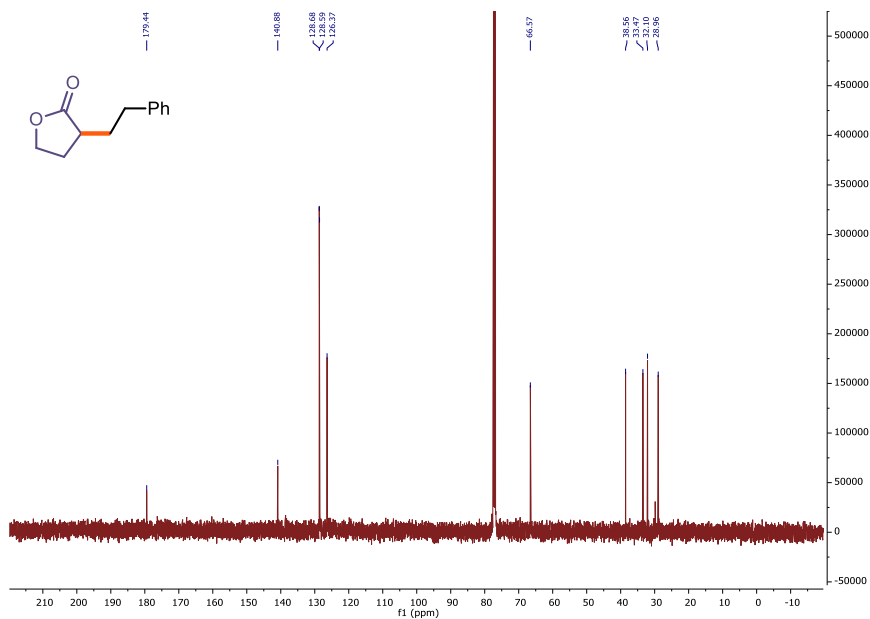
^1H NMR (500 MHz, CDCl_3) of **36v**

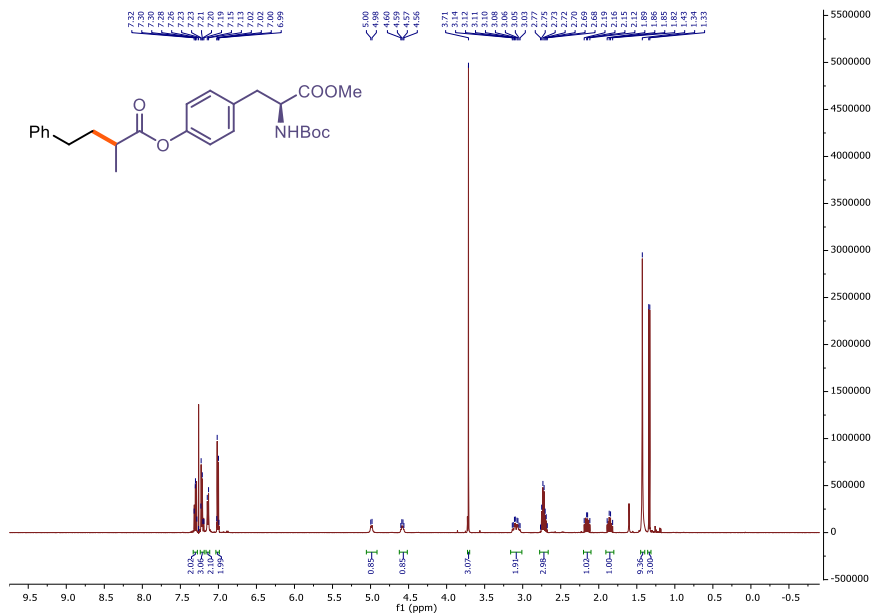
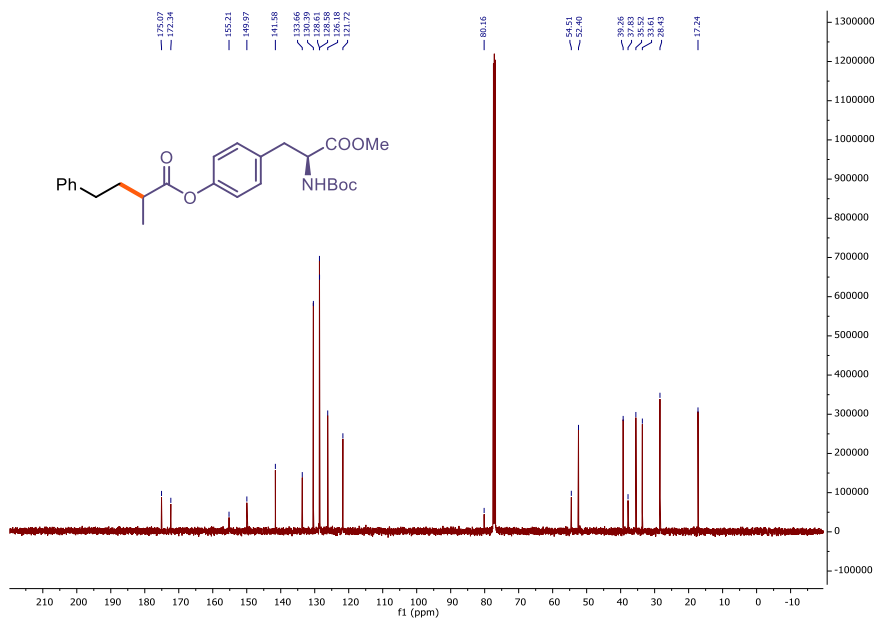
^1H NMR (300 MHz, CDCl_3) of **36x** ^{13}C NMR (101 MHz, CDCl_3) of **36x**

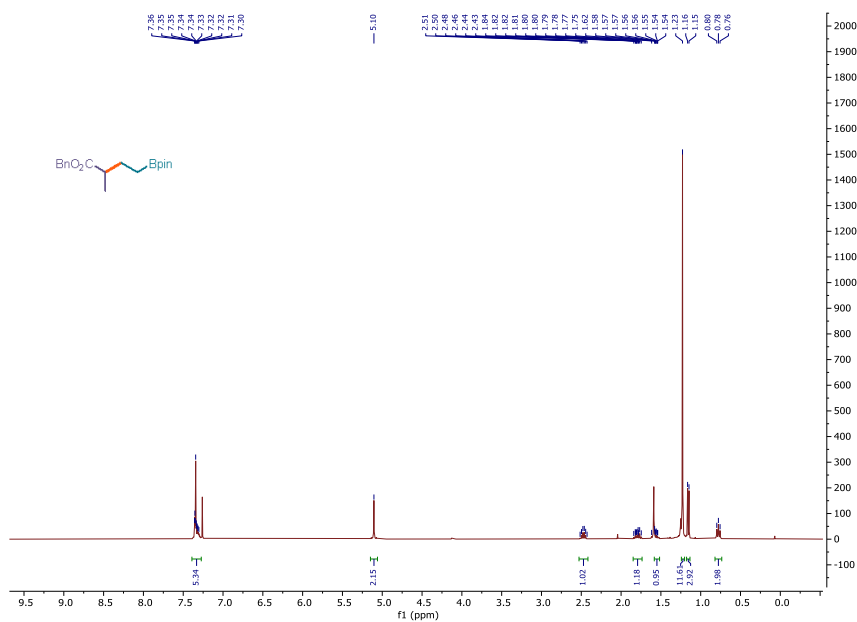
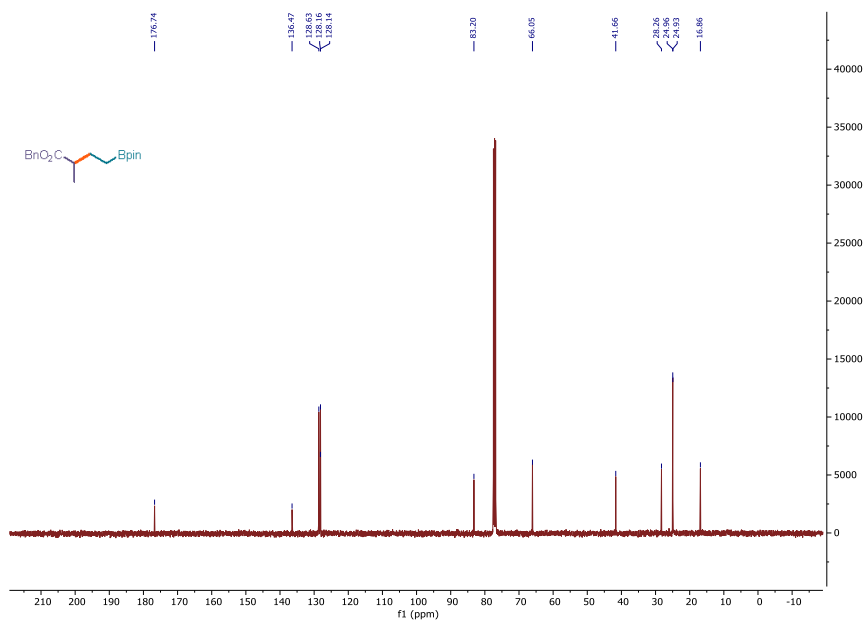
^1H NMR (500 MHz, CDCl_3) of **36z** ^{13}C NMR (126 MHz, CDCl_3) of **36z**

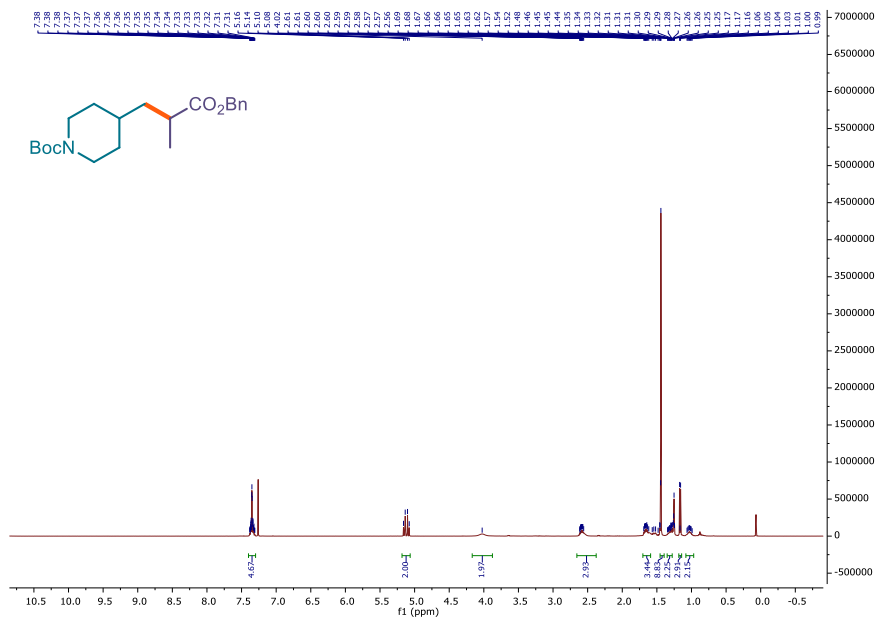
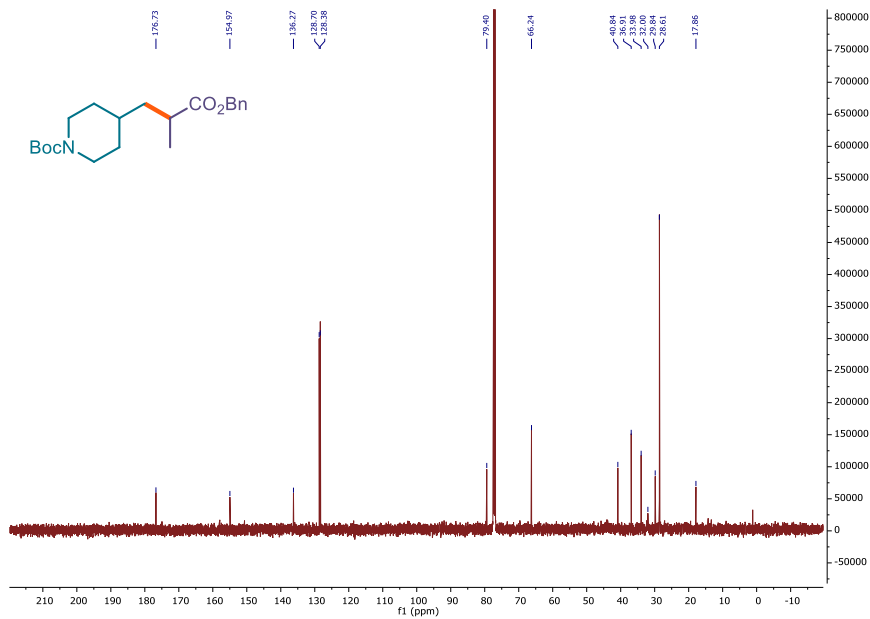
^1H NMR (500 MHz, CDCl_3) of **36aa** ^{13}C NMR (126 MHz, CDCl_3) of **36aa**

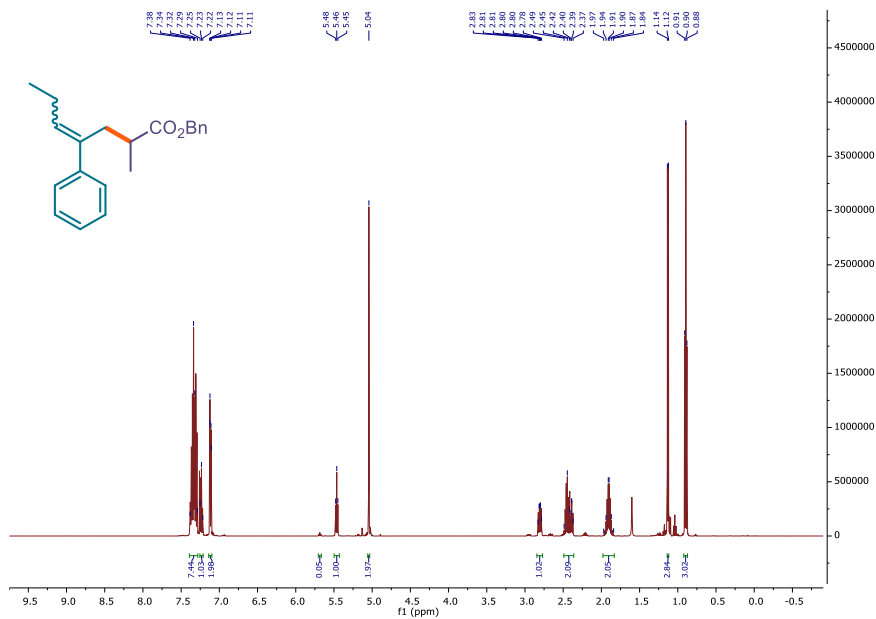
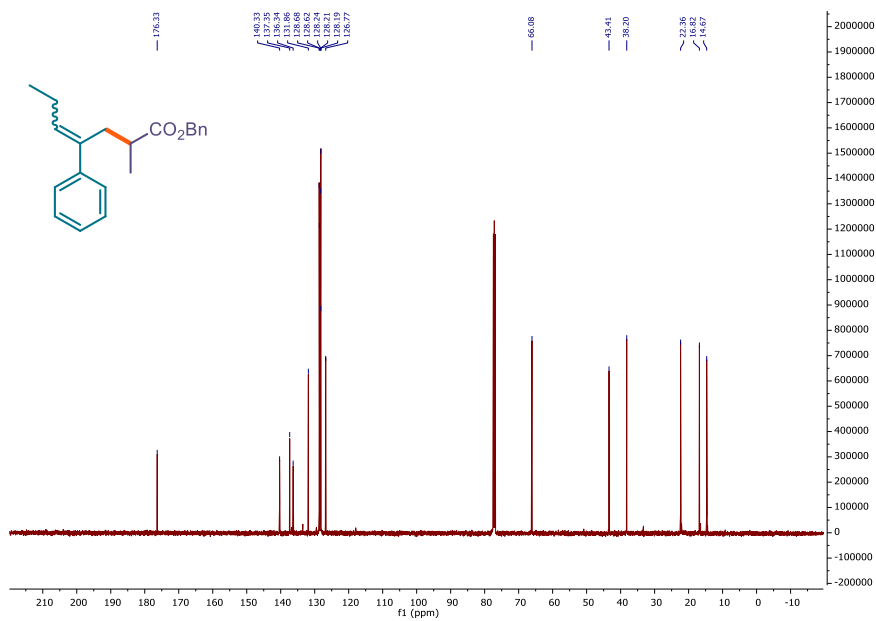
^1H NMR (400 MHz, CDCl_3) of **36bb** ^{13}C NMR (101 MHz, CDCl_3) of **36bb**

^1H NMR (500 MHz, CDCl_3) of **36cc** ^{13}C NMR (126 MHz, CDCl_3) of **36cc**

^1H NMR (500 MHz, CDCl_3) of **36dd** ^{13}C NMR (126 MHz, CDCl_3) of **36dd**

^1H NMR (500 MHz, CDCl_3) of **36ff** ^{13}C NMR (101 MHz, CDCl_3) of **36ff**

^1H NMR (400 MHz, CDCl_3) of **36gg** ^{13}C NMR (101 MHz, CDCl_3) of **36gg**

^1H NMR (500 MHz, CDCl_3) of **36jj** ^{13}C NMR (126 MHz, CDCl_3) of **36jj**

Chapter V

General Conclusions

The work carried out in this doctoral thesis has highlighted how different photochemical activation manifolds can be used to generate radicals and design new catalytic processes.

In chapter II, it was shown that dithiocarbamates and xanthogenates were used as catalytic donors in the formation of photoactive electron donor-acceptor (EDA) complexes with a variety of radical precursors. Excitation with visible light triggered the generation of open-shell intermediates under mild conditions, including non-stabilized carbon radicals and nitrogen-centered radicals. The modular nature of the organocatalysts offered a versatile EDA complex catalytic platform for developing mechanistically distinct radical reactions, including redox neutral and net-reductive processes. Mechanistic investigations supported the hypothesis that a closed catalytic cycle is operational, highlighting the ability of the organic catalysts to turnover and iteratively drive each catalytic cycle.

Chapter III detailed that tetrachlorophthalimide-based catalysts can act as effective and general acceptors for EDA complex activation. These organocatalysts permitted the activation of a variety of radical precursors bearing different redox auxiliaries, including 1,2-dihydropyridines (DHPs), silicates and trifluoroborates, which could not be activated by previous EDA catalytic protocols. Excitation with visible light granted access to alkyl radicals under mild conditions. Importantly, this EDA complex catalytic platform proved flexible enough to promote mechanistically different radical processes, including the first combination with a metal-based catalytic cycle.

In chapter IV, we detailed the discovery of a photochemical reductive cross-coupling of olefins based on photoredox catalysis in concert with hydrogen atom transfer (HAT). It was found that electron-poor olefins can be reduced to form radicals, which were then coupled with electron-rich and neutral olefins. Our method encompassed a variety of olefins as radical precursors, including unsaturated esters, carbonyls, amides, cyano and sulfone, and radical acceptors, such as styrenes and non-activated olefins. Further mechanistic experiments, including including Stern-Volmer quenching study, supported our proposed mechanism.